



**HAL**  
open science

# Mechanisms of biogenesis and maintenance of the outer membrane of Gram-negative bacteria

Luis Orenday Tapia

► **To cite this version:**

Luis Orenday Tapia. Mechanisms of biogenesis and maintenance of the outer membrane of Gram-negative bacteria. Microbiology and Parasitology. Université Paul Sabatier - Toulouse III, 2022. English. NNT : 2022TOU30206 . tel-04157577

**HAL Id: tel-04157577**

**<https://theses.hal.science/tel-04157577v1>**

Submitted on 10 Jul 2023

**HAL** is a multi-disciplinary open access archive for the deposit and dissemination of scientific research documents, whether they are published or not. The documents may come from teaching and research institutions in France or abroad, or from public or private research centers.

L'archive ouverte pluridisciplinaire **HAL**, est destinée au dépôt et à la diffusion de documents scientifiques de niveau recherche, publiés ou non, émanant des établissements d'enseignement et de recherche français ou étrangers, des laboratoires publics ou privés.



# THÈSE

En vue de l'obtention du  
**DOCTORAT DE L'UNIVERSITÉ DE TOULOUSE**  
Délivré par l'Université Toulouse 3 - Paul Sabatier

---

Présentée et soutenue par  
**Luis ORENDAY TAPIA**

Le 23 septembre 2022

**Mécanismes de biogenèse et de maintenance de la membrane  
externe de bactéries Gram-négatives**

---

Ecole doctorale : **BSB - Biologie, Santé, Biotechnologies**

Spécialité : **MICROBIOLOGIE**

Unité de recherche :

**LMGM - Laboratoire de Microbiologie et Génétique Moléculaires**

Thèse dirigée par  
**Raffaele IEVA et Cécile ALBENNE**

Jury

Mme Alessandra POLISSI, Rapporteur  
M. Peter VAN ULSEN, Rapporteur  
M. Romé VOULHOUX, Examinateur  
M. Raffaele IEVA, Directeur de thèse  
Mme Cécile ALBENNE, Co-directrice de thèse  
Mme Gwennaele FICHANT, Présidente

## Acknowledgments

This manuscript is the fruit of several years of work. It all started by the acceptance of my master's degree internship and it continued for some years after being granted with a PhD contract from the French Ministry. The first persons I want to thank is of course Raffaele Ieva and Cécile Albenne, as they trusted in me for this project over the years. They taught me scientific rigor, organization skills and of course they transmitted me passion for research that allowed me to get through.

We passed by many moments during these years and many good and bad experiences in the team Ieva. I am very happy to have shared these many moments with such wonderful people: Anne always with a smile and willing to discuss about life and love; Violette standing for her impeccable methods of purification and scientific rigor; Yassin always offering his help and open to discuss about science; Yiying, a very nice and hardworking person; Haoxiang, a very gentle and smart person; Jelena, a savage and free soul with whom I could talk hours about Paganini; Doriane, an excellent and brilliant human being; and Cyril that would go crazy while doing his mitopreps listening to "interesting" music. I want to thank all of you, because you made me grow in science, but also as a person in our escapades in Bordeaux, at the beach, at the barbecue, playing pétanque, drinking a beer or eating at the restaurant.

I want to thank also the people from other teams in our institute, mainly PhD students that understood the duality of the sacrifice and the pleasure of our job. Sometimes in a coffee break, sometimes in a bar, sometimes in a trip, but we always spent such a wonderful moment together. Unluckily for us, Covid time came and our lives changed, as for many other people. We were lucky enough to continue to work at the lab in summer (sometimes without our PIs) and the lab became this mix of a scientific summer camp and work place, where we worked and at the same time, we were able to chill and enjoy the weather. Thus, it was born the Apéro Clandestin society, a group that aimed to continue our lives during pandemics. The list of members included many people and it continued even after Covid time: Micka, Nathalie, Come, Marie, Claudie, Alix, Cyril, Hicham, Ahmed, Clair, Dylan, Charlotte, among others. Today I am pleased to say that some of these people have become true friends over the years. Some became like an extended family and others became part of the most prolific dynasty of the lab: the Batista dynasty, starting with Manon, my godmother and Alix, my goddaughter and followed by Claudie and Romane.

And how could I forget the seminars? A tradition that started longtime ago with Alexandre: each Thursday night we met at the local pub and discuss about science and

life (with a couple of beers of course). The main result was that every Friday he had, as we like to call it, a trash Friday (vendredi poubelle). At the Dubliners (the name of the pub) we would meet with other people, such as Paulo, Carine, Emilie, Jade, Cécilia, Maxime, Lud, Clémence, Moises, Raul, Gabriel and of course many members from the Apéro Clandestin group.

In this same bar I gave the first Spanish lesson to Cécilia. After the years, she became one of the most important persons in my life during my PhD with her joie-de-vivre, her determination and her intelligence. I cannot think my PhD without her and I want to thank her for everything she taught me and for making me travel in life and love.

I had been very lucky, as I made great friendships with people during this time: Marie, one of the most amiable persons since the day I met her, with a positive attitude or a nice comment to cheer your day, but somehow direct and honest without being rude (a rare and magical power); Nathalie that always amazed how easy she figured out things just with a gaze and found the right words to say with a warm heart (sometimes I wondered if you could read my mind); Come that was always willing to help with personal and professional stuff and tried to better things in people (take a look at our skin!); Sarah that had time to discuss about life and support me in difficult times; Pinette that has a nice and warm soul. Thanks to Gabriel a good company to talk and party; to Raul, a trustworthy friend with a golden heart; to Sasha that I was able to witness her way into the French life; to Jade with whom we shared many adventures; to Laura, one of my oldest friends in France with who I could share many experiences over time; and to Manon, because I was able to become not only his friend, but also her godson and she became a bit a part of my extended family in France.

I would like to end this list by thanking Micka, my oldest friend in France and without a doubt, my brother. We started our master's degree in 2016 without knowing that after finishing our studies, we will have not only a PhD degree, but also a friendship for life. Today, I cannot imagine all these 6 years without his presence, his friendship and his support. I can only think of him as my biggest and most constant support during the past years and without him this PhD would have been very different.

Finally, I would like to thank my family that supported me during all my expatriation to France and continues to support me in my futures projects. Gracias a ustedes.

Thank you all for your kind words, your support, your savoir-faire, for inviting me a beer or a meal, for inviting me to spend Christmas and Easter together, for playing cards and caps with me, for teaching me how to purify proteins or make a particular cloning, for your corrections in my reports, for teaching me scientific rigor, for having a drink with me,

for cheering me up, for going in a trip together, for coming to Mexico with me, for spending Covid lockdown together, for going to a concert together, for making me laugh and cry, for your precious time, for all your love and your friendship. Thank you for being there! Merci ! ¡Gracias!

## Remerciements

Ce manuscrit est le résultat de plusieurs années de travail. Tout a commencé quand j'ai commencé mon projet avec un stage de master que j'ai poursuivi après l'obtention d'un contrat doctoral du ministère français. Les premières personnes que je tiens à remercier sont bien sûr Raffaele Ieva et Cécile Albenne, car ils m'ont fait confiance pour ce projet au fil des ans. Ils m'ont appris la rigueur scientifique, le sens de l'organisation et bien sûr ils m'ont transmis la passion pour la recherche qui m'a permis de m'en sortir.

Nous sommes passés par de nombreux moments durant ces années et de nombreuses bonnes et mauvaises expériences au sein de l'équipe Ieva. Je suis très heureux d'avoir partagé ces nombreux moments avec des personnes aussi merveilleuses : Anne toujours souriante et prête à discuter de la vie et de l'amour ; Violette qui se bat pour ses méthodes irréprochables de purification avec une grande rigueur scientifique ; Yassin toujours partant pour aider et ouvert à la discussion scientifique ; Yiyi, une personne très gentille et travailleuse ; Haoxiang, une personne très sympa et intelligente ; Jelena une âme sauvage et libre avec qui je pourrais parler des heures de Paganini ; Doriane comme un excellent et brillant être humain ; et Cyril qui devenait fou pendant la préparation de ses mitopreps en écoutant de la musique « intéressante ». Je tiens à vous remercier tous, car vous m'avez fait grandir en science, mais aussi en tant que personne dans nos escapades à Bordeaux, à la plage, au barbecue, mais aussi pendant qu'on jouait à la pétanque, quand on partageait un coup ou un bon repas.

Je tiens également à remercier les personnes des autres équipes de notre institut, principalement des doctorants qui comprennent la dualité de la vie de thèse avec les sacrifices et les plaisirs de notre métier. Parfois pendant la pause-café, parfois dans un bar, parfois en voyage, mais toujours un beau moment de partage. Malheureusement pour nous, la Covid est arrivée et nos vies ont changées, comme pour beaucoup d'autres personnes. Nous avons eu la chance de continuer à travailler au laboratoire en été (parfois sans les chefs) et le laboratoire est devenu ce mélange de colonie scientifique d'été et un lieu de travail, où on travaillait et en même temps, on pouvait se détendre et profiter du beau temps. Ainsi, la société d'Apéro Clandestin est née, un groupe qui visait à continuer nos vies pendant la pandémie. Les membres étaient nombreux et le groupe a continué même après les nombreux confinements : Micka, Nathalie, Côme, Marie, Claudie, Alix, Cyril, Hicham, Ahmed, Clair, Dylan, Charlotte, entre autres. Aujourd'hui, je suis heureux de dire que certaines de ces personnes sont devenues de véritables amis au fil des ans. Certains sont devenus comme une famille d'adoption et d'autres sont devenus membres de la dynastie la plus prolifique du labo : la dynastie Batista, en

commençant par Manon, ma marraine et Alix, ma filleule et suivie par Claudie et Romane.

Et comment je pourrais oublier les séminaires ? Une tradition qui a commencé il y a longtemps avec Alexandre : chaque jeudi soir, on sortait au bar et discussions de la science et de la vie (avec quelques bières, bien sûr). Le résultat principal était que tous les vendredis on avait ce qu'on appelait un vendredi poubelle. Au Dubliners (le nom du bar), on rencontrait des gens comme Paulo, Carine, Emilie, Jade, Cécilia, Maxime, Lud, Clémence, Moises, Raul, Gabriel et bien sûr de nombreux membres du groupe d'Apéro Clandestin.

Et c'était dans ce même bar que j'ai donné le premier cours d'espagnol à Cécilia. Après les années, elle est devenue l'une des personnes les plus importantes de ma vie pendant ma thèse avec sa joie de vivre, sa détermination et son intelligence. Je ne peux pas imaginer ma thèse sans elle et je tiens à la remercier pour tout ce qu'elle m'a appris et pour m'avoir fait voyager dans la vie et dans l'amour.

J'ai eu beaucoup de chance, car j'ai fait de grandes amitiés avec des gens pendant ma thèse : Marie, l'une des personnes les plus aimables depuis le jour où je l'ai rencontrée, avec une attitude positive ou un commentaire gentil pour requinquer la journée, mais elle pourrait aussi dire des choses d'une certaine manière directe et honnête sans être impolie (un pouvoir assez rare et magique) ; Nathalie, qui m'a toujours surpris avec la facilité avec laquelle elle comprenait les choses avec un simple regard et trouvait les mots justes à dire avec un cœur chaleureux (parfois je me demandais si tu pouvais lire dans mes pensées) ; Come, qui était toujours prêt à aider avec des trucs personnels et professionnels et qui essayait d'améliorer les choses chez les gens (regardez notre peau, par exemple !) ; Sarah qui avait le temps de discuter de la vie et de me soutenir dans des moments compliqués ; Pinette qui a une âme belle et chaleureuse. Merci à Gabriel pour sa bonne compagnie pour discuter et faire la fête ; à Raul, un ami digne de confiance avec un cœur en or ; à Sasha que j'ai pu témoigner son développement en France au cours des années ; à Jade avec qui on a partagé de nombreuses aventures ; à Laura, une de mes plus anciennes amies en France avec qui j'ai pu partager de nombreuses expériences au fil du temps ; et à Manon, parce que j'ai pu devenir non seulement son amie, mais aussi son filleul et qui fait un peu partie de ma famille élargie en France.

Je voudrais terminer cette liste en remerciant Micka, mon plus vieil ami en France et sans aucun doute mon frère. Nous avons commencé notre master en 2016 sans savoir qu'à la fin de nos études, nous aurions non seulement un doctorat, mais aussi une amitié

à vie. Aujourd'hui, je ne peux pas imaginer toutes ces 6 années sans sa présence, son amitié et son soutien. Je ne peux que le considérer comme mon soutien le plus important et le plus constant au cours des dernières années et sans lui, ce doctorat aurait été très différent.

Enfin, je tiens à remercier ma famille qui m'a soutenu durant toute mon expatriation en France et qui continue de me soutenir dans mes projets futurs. Gracias a ustedes.

Merci à tous pour vos gentils mots, votre soutien, votre savoir-faire, de m'avoir invité une bière ou à un repas, de m'avoir invité à passer Noël et Pâques ensemble, d'avoir joué aux cartes et aux caps avec moi, de m'avoir appris à purifier des protéines ou faire un clonage particulier, pour vos corrections dans mes rapports, de m'avoir appris la rigueur scientifique, d'avoir bu un verre avec moi, de m'avoir remonté le moral, d'être parti en voyage ensemble, d'être venu au Mexique avec moi, d'avoir passé le confinement Covid ensemble, d'être allé à un concert ensemble, de m'avoir fait rire et pleurer, pour votre temps précieux, pour tout votre amour et votre amitié. Merci d'avoir été là ! Thank you!  
¡Gracias!



## Abstract

Gram-negative bacteria encompass many multidrug resistant pathogens. Their multilayered envelope is formed by an inner membrane (IM), an outer membrane (OM), and a separating periplasm containing the peptidoglycan (PG). The OM forms a semipermeable barrier that prevents the entry of numerous chemicals. Lipoproteins and integral OM proteins (OMPs) are crucial, structural components of the OM permeability barrier. These proteins also mediate the exchange of nutrients, the excretion of toxic molecules and the interactions with the surrounding environment. The OM contains lipopolysaccharide (LPS) in the external leaflet and phospholipids in the internal one. All OM components are synthesized in the cytosol or at the IM and are delivered to the OM by specific transport pathways. Among these, the  $\beta$ -barrel assembly machinery (BAM) complex folds OMPs into  $\beta$ -barrel structures, inserting them into the OM. The assembly of some OMPs requires the poorly understood activity of the translocation and assembly module (TAM). The accumulation of unfolded OMPs in the periplasm triggers activation of the  $\sigma^E$ -mediated envelope stress response.  $\sigma^E$  regulates a number of genes enhancing the levels of BAM subunits. Whereas many envelope biogenesis pathways have been described in the last decades, little is known about how these processes are coordinated during the life cycle of the cell.

This PhD project aimed at studying the regulation of BAM by determining all BAM interactions in the envelope of the enterobacterium *Escherichia coli*. We setup a quantitative proteomic approach to analyze the BAM complex purified upon mild-solubilization of the cell envelope. The identified BAM putative interactors include the envelope proteins DolP/YraP and TamB that were further studied.

DolP is a poorly characterized lipoprotein upregulated upon activation of the envelope stress response. It consists of two bacterial OsmY and nodulation (BON) domains, a protein fold of ill-defined function. Although DolP was implicated in preserving the OM permeability barrier, the molecular function of DolP and the reason of its upregulation during envelope stress were unknown. We demonstrated that DolP localized at the OM and makes direct contact to the central and catalytic subunit of the BAM complex, BamA. This interaction was mapped at the N-terminal BON domain of DolP. We obtained important clues concerning the physiological role of the BAM-DolP interaction. We showed that increased levels of BamA enhance the OM permeability and this detrimental effect is opposed by DolP. From a mechanistic point of view, our results revealed that DolP is required for proper folding of BamA in the OM thus supporting efficient OMP biogenesis. We speculate that upon activation of the envelope stress response, upregulation of BAM requires DolP for efficient *de novo* assembly of its central subunit BamA into the OM.

Finally, we explored the interaction between BAM and TamB, the IM component of the TAM module. TamB contains a large periplasmic domain and was known to form a complex with the OMP TamA, a homolog of BamA. By performing pull-down of TamB we confirmed that this protein is a *bona fide* interactor of the BAM complex. Furthermore, our data suggest that the C-terminal segment of TamB plays an important role in stabilizing this complex. These results provide a molecular explanation concerning how BAM and TAM may cooperate during OMP biogenesis forming a larger complex.

By characterizing novel interactions of the BAM complex, these results contribute to identify potential targets for the development of antibacterials that can hinder the biogenesis of the envelope permeability barrier of Gram-negative bacteria.

## Résumé

Les bactéries Gram-négatives comptent de nombreux agents pathogènes multirésistants. Leur enveloppe multicouche est composée d'une membrane interne (IM) et d'une membrane externe (OM) séparées par le périplasma contenant le peptidoglycane (PG). L'OM forme une barrière semi-perméable qui empêche l'entrée de nombreux produits chimiques. Les lipoprotéines et les protéines intégrales de l'OM (OMPs) sont des composants cruciaux de l'OM impliqués dans l'échange de nutriments, la sécrétion de molécules toxiques et l'interaction avec l'environnement. L'OM contient des lipopolysaccharides (LPS) dans le feuillet externe et des phospholipides dans le feuillet interne. Tous les composants de l'OM sont synthétisés dans le cytosol ou au niveau de l'IM et sont acheminés vers l'OM par des voies de transport spécifiques. Parmi celles-ci, le complexe BAM ( *$\beta$ -barrel assembly machinery*) replie et insère les OMPs dans l'OM. L'assemblage de certaines OMPs nécessite le module de translocation et d'assemblage (TAM) dont l'activité demeure mal comprise. L'accumulation d'OMPs dépliées dans le périplasma déclenche l'activation de la réponse au stress de l'enveloppe médiée par  $\sigma^E$ . Le facteur  $\sigma^E$  régule un certain nombre de gènes, augmentant le niveau des sous-unités de BAM. Alors que les voies de biogénèse de l'enveloppe ont été bien décrites ces dernières décennies, la manière dont ces processus sont coordonnés au cours du cycle cellulaire reste peu connue.

Ce projet de thèse visait à étudier la régulation du complexe BAM en identifiant ses interactions dans l'enveloppe de l'entérobactérie *Escherichia coli*. Nous avons mis en place une approche de protéomique quantitative visant à décrire l'interactome de BAM une fois purifié et solubilisé. Parmi les interactants putatifs de BAM identifiés, on trouve les protéines de l'enveloppe DolP/YraP et TamB qui ont été étudiées au cours de cette thèse.

DolP est une lipoprotéine mal caractérisée, régulée positivement lors de l'activation de la réponse au stress de l'enveloppe. Elle est constituée de deux domaines *bacterial OsmY and nodulation* (BON), caractérisés par un repliement conservé mais dont la fonction est mal définie. Il était établi que DolP contribue au maintien de la barrière de perméabilité de l'OM mais les bases moléculaires de sa fonction et le lien avec la réponse au stress demeuraient incompris. Nous avons démontré que DolP est localisée au niveau de l'OM et qu'elle interagit directement avec la sous-unité centrale et catalytique du complexe BAM, BamA. Cette interaction a été localisée au niveau du domaine BON N-terminal de DolP. Nous avons aussi apporté des éléments nouveaux sur le rôle physiologique de l'interaction BAM-DolP. En effet, nous avons montré que des niveaux accrus de BamA augmentent la perméabilité de l'OM et que cet effet néfaste est contré par DolP. D'un point de vue mécanistique, nos résultats ont révélé que DolP est nécessaire pour le repliement correct de BamA dans l'OM, favorisant ainsi une biogénèse efficace des OMPs. Nos données suggèrent que lors de l'activation de la

réponse au stress de l'enveloppe, la production accrue de BAM nécessite DoIP qui assure le repliement correct de BamA dans l'OM.

Enfin, nous avons exploré l'interaction entre BAM et TamB, le composant de l'IM du module TAM. TamB contient un large domaine connu pour former un complexe avec TamA, une OMP homologue à BamA. Nous avons confirmé par *pull-down* que TamB interagit avec BAM. De plus, nos données suggèrent que le segment C-terminal de TamB joue un rôle clé dans la stabilisation de ce complexe. Nos résultats apportent des données moléculaires sur la façon dont BAM et TAM coopèrent pendant la biogenèse des OMPs, via la formation d'un plus grand complexe.

En caractérisant de nouvelles interactions impliquant BAM, nos résultats contribuent à identifier des cibles potentielles pour le développement d'antibactériens qui pourraient entraver la barrière de perméabilité de l'enveloppe des bactéries Gram-négatives.

## Table of content

|  |    |
|--|----|
| <b>Abstract</b> .....  | 1  |
| <b>Résumé</b> .....  | 3  |
| <b>Table of content</b> .....  | 5  |
| <b>Abreviation list</b> .....  | 10 |
| <b>Introduction</b> .....  | 12 |
| 1 Several Gram-negative bacteria represent a major concern in public health. ....                | 12 |
| 2 Biogenesis of the Gram-negative bacterial envelope components.....                             | 16 |
| 2.1 Protein biogenesis and targeting from ribosome to the secretory pathways .....               | 17 |
| 2.2 Secretion of substrates via Sec and TAT.....   | 19 |
| 2.2.1 The Sec translocon .....   | 19 |
| 2.2.2 The Twin-Arginine translocation (TAT) pathway .....  | 20 |
| 2.3 Biogenesis of lipoproteins at the IM.....  | 21 |
| 2.4 Integral outer membrane proteins (OMPs) .....  | 22 |
| 2.5 Biogenesis and transport of membrane phospholipids .....                                     | 23 |
| 2.5.1 The Mammalian Cell Export (MCE) domain-containing systems to transport phospholipids ..... | 25 |
| 2.5.2 The AmsA-like superfamily.....   | 27 |
| 2.6 Lipopolysaccharide (LPS).....  | 28 |
| 2.7 Remodeling of the bacterial envelope during cell division.....                               | 29 |
| 2.7.1 PG remodeling and penicillin-binding proteins (PBP) .....                                  | 29 |
| 2.7.2 Remodeling of the bacterial envelope during cell division.....                             | 30 |
| 3 Biogenesis of the OM .....   | 33 |
| 3.1 Export of lipoproteins to the OM .....   | 33 |
| 3.1.1 The Localization of lipoproteins (LOL) pathway .....                                       | 33 |
| 3.1.2 Lipoprotein topology in the OM.....  | 34 |
| 3.2 Biogenesis of OMPs from the IM to the OM .....   | 35 |
| 3.2.1 The periplasmic journey of OMPs to the OM .....  | 35 |

|       |   |    |
|-------|---|----|
| 3.2.2 | The BAM-Sec holotranslocon supercomplex.....  | 37 |
| 3.2.3 | The BAM complex.....  | 37 |
| 3.2.4 | Mechanism of biogenesis.....  | 39 |
| 3.2.5 | Assembly of some OMPs not only depends on BAM.....  | 44 |
| 3.3   | LPS biogenesis and transport to the OM.....   | 45 |
| 4     | Transport of substrates across the bacterial envelope.....  | 47 |
| 4.1   | An overview of secretion systems in <i>E. coli</i> .....  | 47 |
| 4.1.1 | One-step secretion systems.....   | 47 |
| 4.1.2 | Two-step secretion systems.....   | 50 |
| 5     | Homeostasis of the Gram-negative bacterial envelope.....  | 54 |
| 5.1   | The Rcs response for PG homeostasis, LPS damages and BAM function.....                                    | 54 |
| 5.2   | The Cpx response for lipoprotein homeostasis.....   | 57 |
| 5.3   | The $\sigma^E$ response for OMPs and LPS homeostasis.....   | 58 |
| 5.4   | DolP is a poorly characterized factor upregulated by the $\sigma^E$ response.....                         | 60 |
|       | <b>Work objective</b> .....   | 63 |
|       | <b>Results</b> .....  | 64 |
| 1     | Affinity-purification of the BAM complex for quantitative proteomics analyses.....                        | 64 |
| 1.1   | SILAC-based strategy used for the BAM interactomic analysis.....  | 64 |
| 1.2   | Choice of the purification method of the BAM complex.....   | 66 |
| 1.3   | The detergent used for solubilization of membranes has an impact on the stability of the BAM complex..... | 69 |
| 1.4   | Yield of the BAM complex from cells grown on minimal medium.....  | 70 |
| 1.5   | SILAC-based analysis of the BAM interactome.....  | 72 |
| 1.6   | Interactome of the BAM complex.....   | 75 |
| 2     | DolP is a putative interactor of the BAM complex.....   | 77 |
| 2.1   | DolP is an OM lipoprotein.....  | 77 |
| 2.2   | DolP is required for OM integrity.....  | 79 |
| 3     | Characterization of the interaction between DolP and the BAM complex.....                                 | 83 |
| 3.1   | DolP and the BAM complex interact <i>in vivo</i> .....  | 83 |

|     |   |            |
|-----|---|------------|
| 3.2 | DolP – BAM interaction is detergent-sensitive .....                                 | 85         |
| 3.3 | DolP and the BAM complex can be purified separately .....                           | 86         |
| 3.4 | Soluble DolP can be expressed in the cytosol and purified.....                      | 88         |
| 3.5 | DolP and the BAM complex interact <i>in vitro</i> .....                             | 89         |
| 3.6 | BamA is efficiently co-purified with DolP when both proteins are overproduced ..... | 93         |
| 3.7 | DolP interacts with OM-assembled BamA .....   | 94         |
| 4   | Characterization of DolP interactors by crosslinking approaches.....                | 96         |
| 4.1 | Chemical crosslinking of DolP did not permit to detect BAM subunits .....           | 96         |
| 4.2 | Site-directed photocrosslinking of DolP .....                                       | 98         |
| 4.3 | Identification of Bpa-crosslink proteins by MALDI-TOF MS .....                      | 101        |
|     | OmpA.....   | 103        |
|     | Pal.....  | 105        |
|     | DolP-DolP intramolecular crosslink .....  | 106        |
| 4.4 | Identification of Bpa-crosslink products by immunodetection.....                    | 108        |
| 4.5 | BON 1 interacts directly with BamA.....   | 110        |
| 5   | DolP is necessary for proper folding and activity of BamA.....                      | 113        |
| 5.1 | OmpA is not required for DolP function .....  | 113        |
| 5.2 | Overproduction of BamA causes a detrimental effect that is opposed by DolP .....    | 114        |
| 5.3 | DolP promotes proper folding of BamA .....  | 116        |
| 5.4 | DolP contributes to promote BamA activity.....                                      | 119        |
| 6   | Molecular characterization of DolP to promote OM homeostasis.....                   | 121        |
| 6.1 | Both BON domains of DolP are necessary for the proper function of the protein..     | 121        |
| 6.2 | Strategy for mutagenesis of DolP .....  | 124        |
| 6.3 | Mutations on DolP affect its ability to promote OM integrity .....                  | 126        |
| 6.4 | Mutations on DolP may affect its recruitment to the division septum .....           | 129        |
| 7   | TamB is a putative interactor of the BAM complex .....                              | 133        |
| 7.1 | TamB interacts with the BAM complex <i>in vivo</i> .....                            | 134        |
| 7.2 | The C-terminus of TamB is critical for the interaction with the BAM complex.....    | 135        |
|     | <b>Conclusions and perspectives .....</b>   | <b>139</b> |

|   |     |
|---|-----|
| <b>Materials and Methods</b> .....                                      | 142 |
| 1 Plasmid construction .....  | 142 |
| 2 Cell cultures .....   | 143 |
| 2.1 Bacterial culture .....   | 143 |
| 2.2 Lambda red recombination.....                                       | 143 |
| 2.3 Excision of antibiotic resistance.....                              | 144 |
| 2.4 Preparation of electro competent cells.....                         | 144 |
| 2.5 Preparation of chemical competent cells .....                       | 145 |
| 2.6 P1 transduction .....   | 145 |
| 2.7 Spot test assay.....  | 146 |
| 2.8 SILAC labeling .....  | 146 |
| 2.9 $\beta$ -galactosidase assay .....                                  | 146 |
| 2.10 Fluorescence microscopy and analysis .....                         | 147 |
| 3 Cell fractionation.....   | 147 |
| 3.1 Preparation of crude envelope fraction .....                        | 147 |
| 3.2 Cell fractionation by sucrose gradients .....                       | 147 |
| 3.3 Preparation of spheroplasts.....                                    | 148 |
| 4 Protein purification.....   | 148 |
| 4.1 Ni-NTA affinity native purification.....                            | 148 |
| 4.2 IgG-affinity native purification .....                              | 149 |
| 4.3 Protein purification scale-up using FPLC automate .....             | 149 |
| 5 Analyses of protein-protein interaction.....                          | 150 |
| 5.1 Chemical crosslink .....  | 150 |
| 5.2 Site-specific photocrosslinking .....                               | 150 |
| 5.3 <i>In vitro</i> reconstitution of protein-protein interaction ..... | 151 |
| 6 Protein analyses.....   | 151 |
| 6.1 SDS-PAGE .....  | 151 |
| 6.2 Blue Native (BN)-PAGE .....   | 152 |
| 6.3 Western blot.....   | 152 |



|     |   |            |
|-----|---|------------|
| 6.4 | Heat-modifiability assay .....  | 153        |
| 7   | Mass spectrometry analyses .....  | 153        |
| 7.1 | SILAC NanoLC ESI MS-MS analysis .....   | 153        |
| 7.2 | MALDI-TOF MS .....  | 154        |
| 7.3 | Fragmentation of crosslink products by NanoLC-MS/MS.....                        | 154        |
| 8   | Bioinformatic analysis of DoIP/YraP sequences in $\gamma$ -proteobacteria ..... | 155        |
| 9   | Strains.....  | 155        |
| 10  | Plasmids .....  | 156        |
|     | <b>Bibliography</b> .....   | <b>160</b> |

## Abbreviation list

|          |   |
|----------|---|
| ABC      | ATP-binding cassette                                      |
| AMR      | Antimicrobial resistance                                  |
| ATP      | Adenosine triphosphate                                    |
| BAM      | $\beta$ -barrel assembly machinery                        |
| BN-PAGE  | Blue native-polyacrylamide gel electrophoresis            |
| Bpa      | para-benzoylphenylalanine                                 |
| CDP-DAG  | Cytidine diphosphate diacylglycerol                       |
| CL       | Cardiolipin   |
| cryoEM   | Cryogenic electron microscopy                             |
| DAG      | Diacylglycerol  |
| DDM      | n-dodecyl- $\beta$ -D-maltoside                           |
| EDTA     | Ethylenediaminetetraacetic acid                           |
| ESI      | Electrospray ionization                                   |
| ESR      | Extracytoplasmic stress responses                         |
| G3P      | Glyceraldehyde 3-phosphate                                |
| HTL      | Holo-translocon   |
| IM       | Inner membrane  |
| IPTG     | Isopropyl $\beta$ -D-1-thiogalactopyranoside              |
| Kdo      | 3-deoxy-manno-oct-2-ulosonic acid                         |
| LB       | Lysogenic broth   |
| LOL      | Localization of lipoproteins                              |
| LPA      | Lysophosphatidic acid                                     |
| LPS      | Lipopolysaccharide  |
| LPT      | Lipopolysaccharide translocation                          |
| LSB      | Lauryl sulfobetaine                                       |
| MALDI    | Matrix-assisted laser desorption/ionization               |
| MCE      | Mammalian cell export                                     |
| MDR      | Multidrug resistance                                      |
| MES      | 2-(N-morpholino)ethanesulfonic acid                       |
| MOPS     | 3-morpholinopropane-1-sulfonic acid                       |
| MS       | Mass spectrometry   |
| Ni-NTA   | Nickel-nitrilotriacetic acid                              |
| OM       | Outer membrane  |
| OMP      | Integral outer membrane protein                           |
| ONPG     | o-nitrophenyl- $\beta$ -D-galactoside                     |
| PA       | Phosphatidic acid   |
| PBP      | Penicillin-binding proteins                               |
| PG       | Peptidoglycan   |
| PGP      | Phosphatidylglycerol phosphate                            |
| PhE      | Phosphatidylethanolamine                                  |
| PhG      | Phosphatidylglycerol                                      |
| PMF      | Proton motif force  |
| POTRA    | Polypeptide transport associated                          |
| PPIase   | Parvulin-like peptidyl-prolyl isomerase                   |
| PS       | Phosphatidylserine  |
| SDS-PAGE | Sodium dodecyl sulfate-polyacrylamide gel electrophoresis |

|       |  |
|-------|--|
| SILAC | Stable isotope labeling by amino acids in cell culture |
| SRP   | Signal recognition particle                            |
| TAM   | Translocation and assembly module                      |
| TAT   | Twin-arginine translocation                            |
| TCA   | Trichloroacetic acid                                   |
| TEV   | Tobacco etch virus                                     |
| TOF   | Time of flight   |
| uOMP  | Unfolded integral outer membrane protein               |
| WT    | Wild type  |

## Introduction

### 1 Several Gram-negative bacteria represent a major concern in public health.

Bacteria are prokaryotic organisms that play many beneficial roles in ecology, food industry, and pharmacology, but that can also be pathogenic to humans. They possess several environment-adaptation, defense and attack mechanisms via which they successfully colonize their niches. These mechanisms are torn to perfection thanks to their ability of fast growing, which facilitates evolutionary adaptation. Some bacteria can also adapt by reducing their growth rate, which helps them to persist to adverse conditions (Kussell et al., 2005).

The use of antibiotics as a therapeutic treatment to fight against bacteria begun relatively recently in the history of human medicine. Indeed in 1928 Alexander Fleming provided a key contribution to the discovery of antibiotics, identifying penicillin, extracted from the fungus *Penicillium rubens* (Houbraken et al., 2011). Since then, many other antibiotics have been discovered in nature or chemically synthesized. Antibiotics belong to several classes according to their chemical structure and bacterial targets, including  $\beta$ -lactams, sulfonamides, macrolides, aminoglycosides, quinolones and glycopeptides. The use of antibiotics in modern medicine is essential for public health, as they are needed for treating diseases caused by pathogens or to prevent infections in hospitalized patients that undergo surgeries or other medical procedures. Diagnosis of these infections requires a rapid antibiotic intervention. As the identification of the precise infecting pathogen requires time, these infectious diseases are often treated with broad-spectrum antibiotics. This strategy, however, favors as a side-effect the development of bacteria that can resist to these antibiotics (Pruden, 2018).

When bacteria are able to neutralize the activity of antibiotics while growing in relatively normal conditions, they develop a process which is called antimicrobial resistance (AMR) ("New report calls for urgent action to avert antimicrobial resistance crisis," n.d.). Furthermore, some bacteria can develop resistance to not only one, but also several antibiotics and this process is called multidrug resistance (MDR). The development and spread of MDR bacteria can be facilitated by several environmental factors, such as the excessive use of antibiotics for food industry, the abuse of antibiotics for treating diseases, hospitalization of patients carrying MDR bacteria, etc. (Prestinaci et al., 2015). This has created a major concern in public health, therefore it is necessary to find alternatives to cure people and fight against MDR bacteria (Dadgostar, 2019).

The World Health Organization (WHO) estimates that at least 700,000 people die each year due to MDR bacterial diseases. According to the WHO commission, if no action is taken, we will face more than 10 million death per year by 2050 ("New report calls for urgent action to

avert antimicrobial resistance crisis," n.d.). This dramatic scenario marks an unprecedented urge for the study of essential processes in bacterial physiology that will help the identification of new inhibitory molecules that can be used as antibiotics.

Recent clinical reports have identified a group of bacteria that seems to be recurrent in developing MDR. This group is named ESKAPE, to allude to the fact that these bacteria "escape" from being treated with antibiotics and their strong prevalence in their hosts. The ESKAPE acronym stands for *Enterococcus faecium*, *Staphylococcus aureus*, *Klebsiella pneumoniae*, *Acinetobacter baumannii*, *Pseudomonas aeruginosa* and *Enterobacter spp* (Rice, 2008; Santajit and Indrawattana, 2016). The study of essential processes in these organisms has attracted a great deal of attention these last years and they have become important model organisms in the research of new drugs.

Bacteria are traditionally divided in two major groups: Gram-positive and Gram-negative bacteria (Megrian et al., 2020). This classification was originated by the Gram staining test, in which after coloration with Crystal Violet some bacteria were capable to retain this color even after treatment with ethanol used as a decolorant. Bacteria that retained the color were then called Gram-positive, while the ones that lost coloration were Gram-negative as a result for the staining. The retention or loss of this dye depends on specific features of the morphology of the bacterial envelope.

Most (but not all) Gram-positive bacteria contain a single membrane surrounded by a thick layer of peptidoglycan (PG), a complex molecule composed of sugars and crosslinking peptides that serves as a cell-structuring wall, conferring protection against adverse osmotic conditions and serving as a platform for the attachment of appendices on the cell surface. Gram-negative bacteria contain an inner and an outer membrane (IM and OM, respectively), separated by a thin PG layer in the separating periplasm (Fig. 1). Crystal Violet initially colors both types of bacteria. The subsequent use of solvents dissolves the bacterial membranes. The dye leaks out the thin PG layer of Gram-negative bacteria but is retained by the dehydrated thick PG layer of Gram-positive bacteria.

The OM is essential for the cell and it serves as first line of interaction with the extracellular environment. Additionally, the OM is asymmetric and contains a molecule called lipopolysaccharide (LPS) in the external leaflet of the OM, while phospholipids are in the internal leaflet. LPS is molecule composed of a lipid moiety (lipid A) and polysaccharides that protect bacteria. The LPS of some bacteria can act as an endotoxin, increasing the toxicity of these bacteria. The presence of this molecule prevents the entry of some toxic molecules, including small hydrophobic compounds and detergents. In fact, the LPS molecules form a packed layer thanks to the presence of multiple (4-7) acyl chains and salt bridges between the

polar head of the lipid A moiety and divalent cations. These properties confer mechanical stability to the OM contributing to form an effective permeability barrier.

Notably, from the ESKAPE group, four out of six bacteria are Gram-negative, which possess mechanisms that permits them to grow even in the presence of noxious molecules.

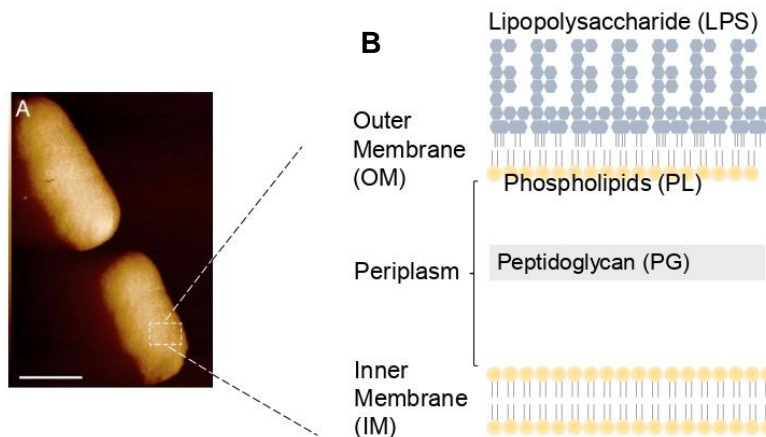


**Figure 1. The Gram-negative bacterial envelope.** **A.** Atom force microscopy (AFM) of *E. coli* cells, adapted from Benn et al., 2021. **B.** Scheme of the Gram-negative bacterial envelope. LPS: lipopolysaccharide; OM: outer membrane; PL: phospholipids; PG: peptidoglycan; IM: inner membrane.

Two types of proteins can be found at the OM of Gram-negative bacteria: OM lipoproteins and integral outer membrane proteins (OMPs). These peripheral proteins perform several functions including the import of nutrients, the export of virulence factors, the attachment to surfaces or the activation of efflux pumps to get rid of noxious molecules (Ranova et al., 2018). Some machineries at the OM are responsible for critical processes, such as the biogenesis of LPS molecules in the external leaflet of the OM, or act as stress response sensors to promote envelope homeostasis. The study of these machineries will help developing new antibiotics that can interfere with processes related to biogenesis and maintenance of the envelope. Other alternatives include the use of bacterial viruses to cure infections, known as bacteriophage therapy (Broncano-Lavado et al., 2021; Hart et al., 2019b; Imai et al., 2019; Luther et al., 2019; Mulani et al., 2019).

In this manuscript introduction, we will focus on the study of processes that drive biogenesis and homeostasis of the OM, as it is a critical component for cell viability. We will present how the OM building blocks are first synthesized and then transported across the envelope to reach the OM. Finally, we will present processes that promote envelope homeostasis and their

regulation. We will apply special emphasis to studies of these processes in the model organisms *Escherichia coli* (a member of  $\gamma$ -proteobacteria). *E. coli* is closely related to important enterobacterial pathogens (*Klebsiella*, *Shigella* species) as well as to dreaded pathogens such as *Yersinia pestis*. Furthermore, the vast literature on this microorganisms and the availability of numerous experimental tools to study its physiology, make *E. coli* an ideal model organisms to investigate the regulation of an essential and evolutionarily conserved process such as the biogenesis of the Gram-negative bacterial envelope.

## 2 Biogenesis of the Gram-negative bacterial envelope components

The Gram-negative bacterial envelope is composed by two membranes (Fig. 2). In this chapter, we introduce the biogenesis of the building blocks of bacterial envelope, focusing mostly on the components of the OM, including membrane proteins, phospholipids, and LPS. Finally, this chapter ends with an overview of remodeling of the bacterial envelope during cell division.

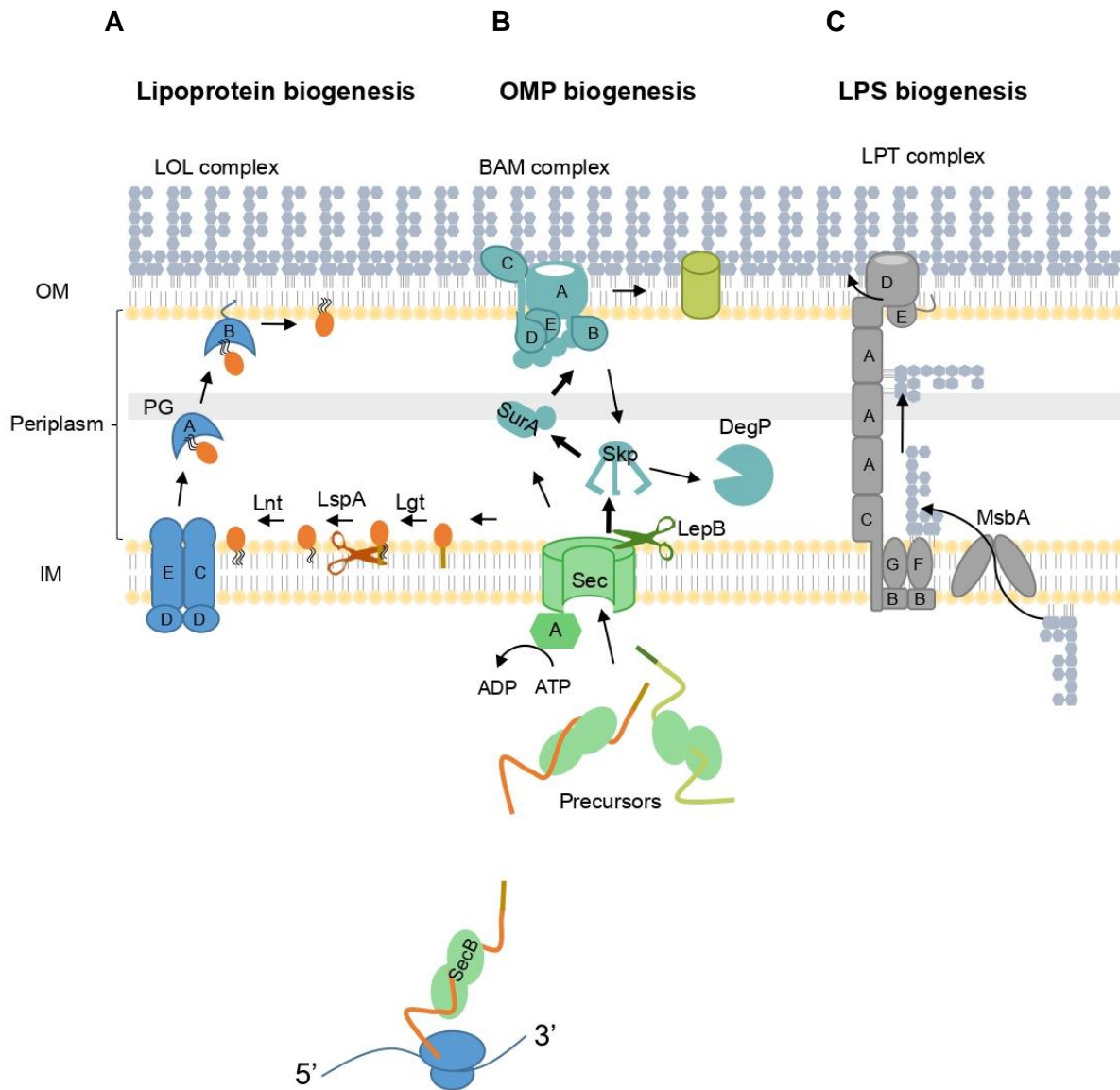


**Figure 2. Biogenesis of components of the OM.** After synthesis of secretory proteins by ribosomes in the cytoplasm, these proteins are taken to the Sec translocase by cytosolic chaperones, such as SecB. Translocation of the substrate is energized by the ATPase SecA. After translocation, the signal peptide at the N-termini of secretory proteins is cleaved by LepB (also known as signal peptidase, SPase I) or LspA (SPase II). **A.** The LOL pathway. When a secretory protein contains a lipobox motif at its signal peptide, this signal peptide is retained to the IM and the precursor is matured by the integration of acyl chains by Lgt at a conserved Cys. The signal peptide is then cleaved by LspA (SPase II) and another acyl chain is transferred by



Lnt. If the protein possesses a retention signal, it stays at the IM, otherwise it is recognized by the LOL pathway that exports precursors to the OM via the IM subcomplex (LolCDE), the periplasmic partner LolA and the OM receptor LolB. **B.** The OMP biogenesis pathway. When the secretory protein contains a C-terminal motif called a  $\beta$ -signal, this precursor is taken to the BAM complex to be assembled into the OM. Periplasmic chaperone molecules such as Skp, SurA and DegP assure the delivery to BAM and act as quality checkpoints to prevent aberrant OMP biogenesis. **C.** The LPS biogenesis pathway. After synthesis of lipid A-core oligosaccharide at the cytoplasmic leaflet of the IM, it is flipped by MsbA to the periplasmic leaflet. Then, LPS is transported to the OM along the the LPT pathway via the IM subcomplex LptBCFG, the periplasmic partner LptA and the OM subcomplex LptDE. LOL: localization of lipoproteins BAM:  $\beta$ -barrel assembly machinery; LPT: lipopolysaccharide transport.

## 2.1 Protein biogenesis and targeting from ribosome to the secretory pathways

Envelope components, such as membrane proteins, have to be first synthesized in the cytoplasm to be further transported across the bacterial envelope. Several studies have aimed at understanding the process of export and nowadays we understand that transport of these components is mediated by protein machineries.

More than four decades ago, studies on secretory pathways of eukaryotic cells led to the signal hypothesis according to which secreted proteins were synthesized as precursors containing an N-terminal extension that permitted the subsequent export to their mature form to the endoplasmic reticulum. The detailed mechanisms were demonstrated in the following years. Günter Blobel, who first proposed the signal hypothesis, received the Nobel prize in Physiology in 1999 because of this work (Blobel and Dobberstein, 1975; Simon, 2018). Soon after the formulation of the signal hypothesis, similar N-terminal signals were found in bacteria for secreted proteins, like the maltose binding protein or arabinose binding protein (Randall et al., 1978). In bacteria, these extensions are called signal (or leader) sequences or signal peptides. Today, more than 40 years after the discovery of these N-terminal extensions, we continue to discover the components, the regulation and mechanisms by which these protein transport machineries function.

Signal peptides are often located at the N-termini of protein precursors and they are essential for protein export in bacteria. They typically consist of 20 to 25 residues, containing an N-terminal domain, a hydrophobic central core, and a C-terminal domain. This C-terminal domain serves as a recognition sequence for the removal of the signal peptide by a peptidase (Heijne, 1983). In Gram-negative bacteria, the majority of proteins that contain a signal peptide are translocated via the Sec translocon and few are recognized by other machineries.

In *E. coli*, the Sec translocon is composed by a core complex SecYEG that permits the translocation of substrates from the cytoplasm to the periplasm through the IM. SecYEG

requires other ancillary proteins that promote function to assure the translocation of secretory proteins across the membrane and that provide the energy required for the process of translocation and release (Oswald et al., 2021).

All cellular proteins are synthesized in the cytoplasm by ribosomes and they may have different fates: they can remain at the cytoplasm as soluble proteins. If they possess N-terminal cleavable signal peptides or other targeting signals such as hydrophobic regions that can ultimately function as membrane-anchoring segments, they can be targeted to the bacterial envelope via a co-translational or post-translational translocation mechanism. During translation, a highly hydrophobic signal peptide promotes the recruitment of a signal recognition particle (SRP) at the signal peptide to be taken in the vicinity of the membrane (Akopian et al., 2013). By this mean, the ribosome associates with the membrane in the proximity of the Sec translocon via the receptor FtsY. From there, the protein continues its synthesis and is co-translationally translocated via the Sec complex. The translocation process is possible because the ribosome provides energy and there is some evidence that suggests chaperones molecules may assist in this process (Crane and Randall, 2017; Steinberg et al., 2018). Another mechanism of co-translational translocation is possible by the recognition of the insertase YidC. (Steinberg et al., 2018). YidC can independently insert small peptide sequences in the membrane, but it was suggested that it could also cooperate with SecYEG for translocation of inner membrane proteins (Kumazaki et al., 2014; Steinberg et al., 2018).

The second type of translocation consists of the delivery of already synthesized proteins to the Sec complex, post-translationally (Fig. 2). The precursor must stay unfolded to cross the membrane, and they acquire their tertiary structure after being translocated, at their final destination in the envelope. Chaperone molecules in the cytoplasm prevent aggregation of these precursors until they are delivered to the Sec translocase. The ATPase SecA is one of these and can work in cooperation with the chaperone SecB (Castanié-Cornet et al., 2014). SecA also serves as a targeting factor to take precursors to the Sec translocon. Evidence suggests that the signal peptide delays the folding of mature domains and this permits the recognition by the chaperone SecB (Beena et al., 2004).

To promote transport of secretory proteins an energy source is required. The proton gradient across the inner membrane that is generally established by respiratory chain complexes generates a potential of energy called Proton Motif Force (PMF). Energization via PMF and ATP hydrolysis is required for the functioning of the Sec translocon *in vivo*. The ATPase SecA interacts with the core subunit SecY and it provides energy to the transport process by the hydrolysis of ATP during translocation of precursors (Keramisanou et al., 2006; Knyazev et al., 2018; Lill et al., 1989; Tsirigotaki et al., 2017). SecA can form dimers and 50% is free in the

cytoplasm, whereas 50% is associated with the membrane (Cabelli et al., 1991; Crane and Randall, 2017). However, SecA has been identified forming complexes with ribosomes and this suggest it interacts with nascent substrates. This leads to the hypothesis that SecA has a double role: one in which SecA is free at the cytoplasm and can carry substrates after synthesis to permit their translocation via the posttranslational pathway (Steinberg et al., 2018) and another in which it participates during post-translational translocation to efficiently channel them through SecYEG by associating to a SRP (Huber et al., 2011).

The other chaperone SecB has shown to form homooligomers composed by a dimer of dimers in *E. coli*. When SecB homooligomerizes, it creates an hydrophobic surface by the addition of  $\beta$ -strands of two molecules in each of the two faces of the homooligomer (Murén et al., 1999; Smith et al., 1996; Suo et al., 2015; Topping et al., 2001). Thanks to this arrangement, the surface of the homooligomer can arrange precursor proteins. Depending of the size, the homooligomer can carry one or several precursors (Lecker et al., 1989). SecB can bind to SecA and form a complex and their interaction is enhanced when SecA is in complex with the translocon (Hartl et al., 1990).

The gene *secB* is not essential and other chaperones (such as DnaJ/K) can substitute its function. Thus it was suggested that the role of SecB is to prevent aggregation or premature folding and to promote the correct engaging of secretory proteins with the translocon (Crane and Randall, 2017).

## 2.2 Secretion of substrates via Sec and TAT

### *2.2.1 The Sec translocon*

Once secretory proteins reach the membrane, they are exported by the SecYEG translocon. The Sec core subunit SecY is a transmembrane  $\alpha$ -helical protein comprising 10 transmembrane segments arranged in two cluster domains disposed as a clamp. SecE consists of two transmembrane  $\alpha$ -helical segments and it engages SecY externally. It has been shown that *in vitro* SecYE is sufficient to promote translocation of substrates into proteoliposomes (Akimaru et al., 1991). SecYE is conserved in prokaryotes, eukaryotes and archaea, whereas SecG is not. Studies from the group of Tokuda show SecG may invert its localization from the cytoplasm to the periplasmic space (Nagamori et al., 2002; Nishiyama et al., 1996, 1996; Sugai et al., 2007). When the complex is not active, the protein SecG can block the pore of SecY suggesting a regulation of the translocation activity (Tanaka et al., 2015). *In vitro* analyses have shown that SecG may play a role in energizing the complex in *E. coli* and helping to maintain the homeostasis of the complex by regulating protein translocation (Crane and Randall, 2017; Tanaka et al., 2015).

Current knowledge on the function of the core of the SecYEG translocon relies on biochemical and structural analyses of the complex isolated from different organisms (Berg et al., 2004; Egea and Stroud, 2010; Mitra et al., 2005; Tanaka et al., 2015; Tsukazaki et al., 2008). Two mechanisms can be mediated by the SecYEG translocon: translocation of the secretory protein across the membrane via a central polypeptide transport channel and insertion of transmembrane segments via a lateral gate that forms between the  $\alpha$ -helices 2 and 7 in each moiety of the SecY clamp (Egea and Stroud, 2010; Tanaka et al., 2015). The translocon in its idle conformation is closed by a plug domain of SecY, which is displaced upon entry of the signal peptide to unlock the transport activity of the channel, suggesting a dynamic behavior of the complex to promote translocation (Hizlan et al., 2012).

Other ancillary proteins assist the process of protein secretion by SecYEG (Komar et al., 2016). These accessory subunits include SecD, SecF, YajC and the insertase YidC. Together, they form the Sec-Holotranslocon (HTL).

YajC is a small protein that can form homooligomers *in vitro* with an N-terminal domain buried in the membrane (Fang and Wei, 2011) and can associated to SecDF. SecD and SecF form a multi- $\alpha$ -helical span membrane complex that can conduct protons. The SecDF complex has been linked to energy harnessing from the PMF supporting steps of the protein transport by SecYEG (Collinson, 2019; Crane and Randall, 2017). The inner membrane insertase YidC can associate with SecYEG via the SecDFYajC subcomplex to promote the insertion of some transmembrane segments of the secretory proteins. This complex may also associate with ribosomes for the co-translational translocation (Carlson et al., 2019; Duong, 2014).

### 2.2.2 *The Twin-Arginine translocation (TAT) pathway*

As described previously, the conserved Sec translocon is a machinery that permits the translocation of unfolded substrates through the IM. Some secretory proteins need to acquire cofactors and fold in the cytoplasm before being secreted. These proteins follow a different translocation pathway where proteins are transported in a folded state: the Twin-Arginine Translocation or TAT pathway. The TAT pathway is conserved among bacteria, plant mitochondria and chloroplasts. Generally, fewer proteins are translocated via this pathway compared to the Sec (Palmer and Berks, 2012).

Secretory proteins that follow the TAT pathway contain an N-terminal signal peptide recognized by TAT and that contains two consecutive Arginines (R-R motif) in the N-terminal region (thus the name of this transport system). The translocon recognizes this motif and translocates different types of substrates, including lipoproteins. In *E. coli*, the translocon is

composed by three subunits TatA, B and C. In some organisms, only TatA and TatC are present (Palmer and Berks, 2012). TatBC function as a receptor that recognizes the R-R motif at the signal peptide of secretory proteins. Then, TatA is recruited to the TatBC subcomplex and it homooligomerizes in a PMF-dependent manner. This polymerization of TatA occurs at the surroundings of the secretory proteins to translocate, adapting to its size up to 70 Å. Then, the substrate crosses by the pore of the polymer of TatA, while the signal peptide remains attached to TatC. After full translocation, the signal peptide is proteolytically removed (Palmer and Berks, 2012).

By integrative approaches, the structure of the TAT translocon has been partially solved. TatA is observed as a big polymer that may vary in copy numbers to create pores of different sizes. TatBC subcomplex can form an integral IM complex that contains approx. 6-8 copies of each protein (Bolhuis et al., 2001). Analysis by fluorescence microscopy suggests the presence of subunits TatBC permits the clustering of approximately 25 molecules of TatA, while their deletion allows clustering of only 4 molecules of TatA (Leake et al., 2008). This suggests TatBC subcomplex may influence the ability of TatA to form homooligomers, probably linked to their role to promote translocation (Palmer and Berks, 2012). The precise mechanisms by which TAT translocates proteins across the IM are still not fully understood as we lack the structure of the active TAT complex.

After transport of substrates by either the Sec translocon or the TAT pathway, the signal peptide of proteins is cleaved by the activity of the signal peptidases. Signal peptidase I (SPase I or LepB) functions at the periplasmic face of the cytoplasmic membrane and uses a Serine/Lysine catalytic mechanism (Tschantz et al., 1993; Wolfe et al., 1983; Zimmermann et al., 1982) that handles signal peptides imported by the Sec translocon and by the TAT pathway (Lüke et al., 2009). After cleavage, the mature protein is addressed to the periplasm or taken by periplasmic chaperones. The signal peptide remains in the membrane, where it can be degraded (Auclair et al., 2012; Crane and Randall, 2017; Paetzel, 2014). In some cases, proteins that are translocated across the IM continue their journey to the OM or the extracellular space.

### 2.3 Biogenesis of lipoproteins at the IM

Lipoproteins are characterized by the presence of a conserved N-terminal Cysteine that becomes triacylated, thus anchoring them to the membrane (Fig. 2). Biogenesis of lipoproteins starts in the cytoplasm, where proteins are synthesized. Lipoproteins contain a signal peptide at their N-termini that is recognized by the Sec translocon, however, some proteins can be translocated via the TAT pathway (Shruthi et al., 2010). The C-terminal region of the signal

peptide contains a particular consensus amino acid sequence, called the lipobox, consisting on [LVI][ASTVI][GAS]C residues. The Cys is strictly conserved in all lipoproteins and it permits further maturation to be anchored in the membrane (Konovalova et al., 2014). Once lipoprotein precursors are recognized by the Sec or the TAT pathway, they are translocated to the periplasmic face of the IM, where they follow a process of maturation (Fig. 2). First, after the protein is translocated, the signal peptide remains in the IM. The Lgt enzyme transfer a diacylglyceryl group from a phospholipid to the sulfhydryl group of the conserved Cys residue at the lipobox. Commonly, lipids used in this process are PhG and PhE (Konovalova et al., 2014; Olatunji et al., 2020). Then, signal peptidase II (or LspA) cleaves of the signal peptide. The structure of LspA shows a main core helix domain with a  $\beta$ -cradle and a periplasmic helix subdomains (Olatunji et al., 2020; Vogeley et al., 2016). It has been shown that LspA can only cleave the signal peptide after acylation of the conserved Cys (Inouye et al., 1983). This process is essential in bacteria and currently, the development of some antibiotics such as globomycin and myxovirescin rely on the inhibition of the activity of LspA to prevent maturation steps (Olatunji et al., 2020; Vogeley et al., 2016). After LspA cleaves the signal peptide, the protein is triacylated by the activity of the apolipoprotein N-acyltransferase Lnt. This process is the last step for lipoprotein maturation of lipoproteins at the IM (Konovalova et al., 2014). These proteins can be further exported to the OM (Fig. 2), as discussed later in this manuscript.

#### 2.4 Integral outer membrane proteins (OMPs)

Another main component of the OM consists of integral outer membrane proteins (OMPs) (Fig. 2). The OMPs polypeptides form a series of  $\beta$ -strands arranged in an antiparallel fashion in the form of a closed cylinder (or barrel) by the interactions of the first and the last  $\beta$ -strand. Notably, the last strand of this type of proteins has a conserved consensus sequence in bacteria, mitochondria and chloroplasts called the  $\beta$ -signal that has been linked to folding in the membrane (Kutik et al., 2008; Robert et al., 2006; Tommassen, 2010). The number of strands (which in bacteria is generally even) may vary and the interaction between all  $\beta$ -strands including the most N- and C-terminal ones of the barrel are stabilized by hydrogen bonds. After their folding, OMPs acquire a very stable architecture, embedded in the OM and exposing hydrophobic residues towards the exterior of the barrel. OMPs display different architectures, as they can have few  $\beta$ -strands such as OmpA (8  $\beta$ -strands) to a conspicuously higher number, such as LptD (26  $\beta$ -strands). In addition, they can possess different accessory water-soluble domains. Some examples include the Polypeptide Transport Associated (POTRA) domains of TamA and BamA, the  $\beta$ -jellyroll domain of LptD or plug domains of TonB-dependent receptors. Whereas the former water-soluble domains are N-terminal, in the case of OmpA the  $\beta$ -barrel

domain is followed by a C-terminal PG-interacting domain (Horne et al., 2020; Schiffrin et al., 2017a).

The mechanisms by which OMPs are targeted to and assembled into the OM, after transport by the Sec complex into the periplasm, will be discussed in section 3.2 of this Introduction.

## 2.5 Biogenesis and transport of membrane phospholipids

Another main component of the bacterial envelope are phospholipids. Mainly, three types of lipids can be found in *E. coli*: phosphatidylglycerol (PhG), phosphatidylethanolamine (PhE) and cardiolipin (CL) (Fig. 3A, left panel). Most  $\gamma$ -proteobacteria accumulate these three phospholipids, however some can present a different composition of phospholipids with diverse properties and structures (Duong et al., 1997; Kakimoto and Tero, 2018; Sohlenkamp and Geiger, 2016). The most abundant phospholipid of *E. coli* is PhE, a zwitterionic lipid that represents around 75% of membrane lipids. Then, the negatively charged phospholipid PhG is the second most abundant, representing around 20% of membrane lipids. Finally, the negatively charged CL is the least abundant of these three (Kakimoto and Tero, 2018; Sohlenkamp and Geiger, 2016).

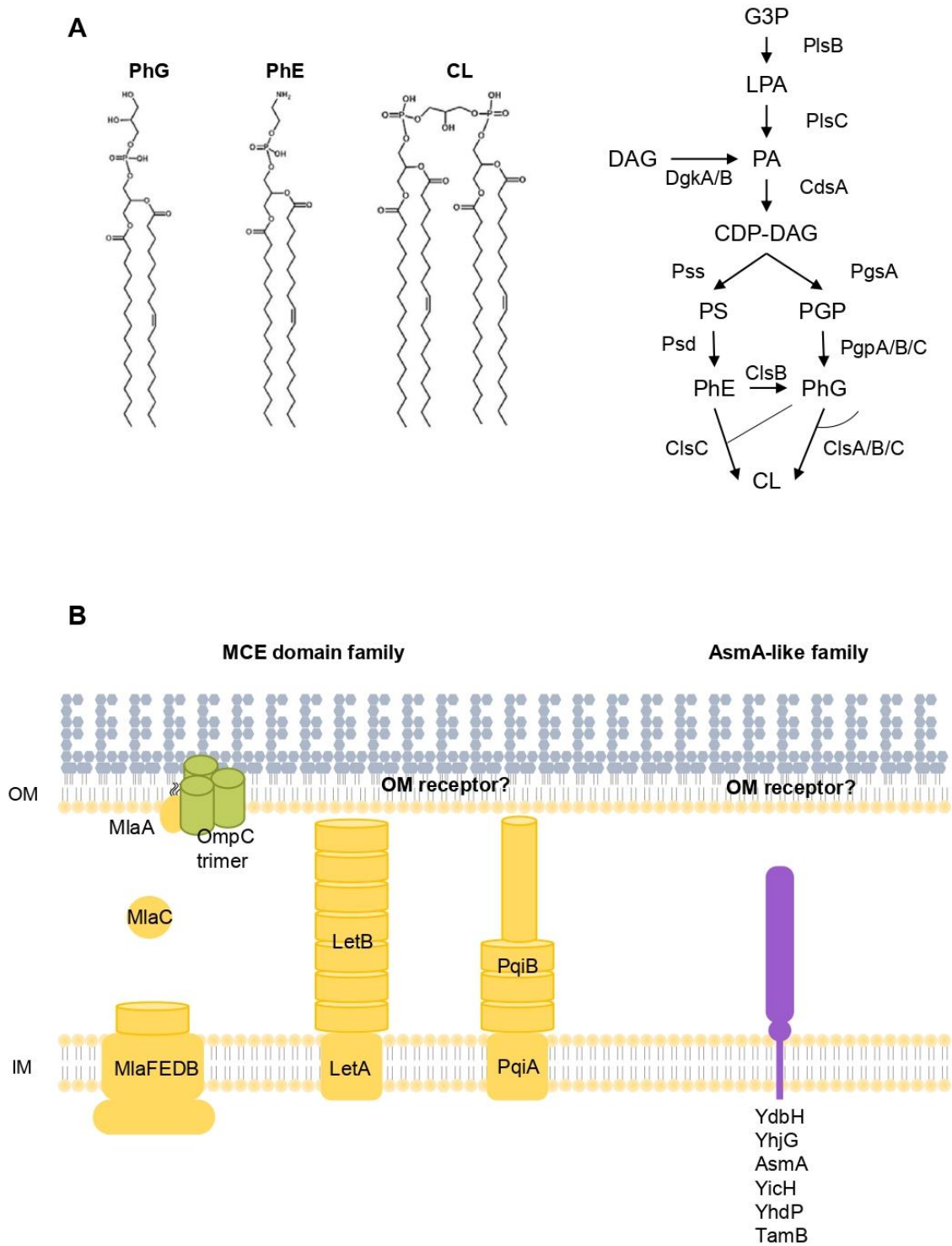


**Figure 3. Membrane phospholipid biogenesis and transport through the Gram-negative bacterial envelope.** **A.** PhG, PhE and CL and their biosynthetic pathway in *E. coli*. **B.** The transport and maintenance pathways of phospholipids to the OM. PhG: phosphatidylglycerol; PhE: phosphatidylethanolamine; CL: cardiolipin; G3P: Glycerol 3-Phosphate; LPA: lysophosphatidic acid; PA: phosphatidic acid; DAG: diacylglycerol; CDP-DAG: cytidine diphosphate-diacylglycerol; PS: phosphatidylserine; PGP: phosphatidylglycerol phosphate; MCE: Mammalian Cell Export.



### 2.5.1 Biogenesis of phospholipids

Fig. 3A (right panel) illustrates a schematics of phospholipid synthesis. This process begins with the molecule Glycerol 3-Phosphate (G3P) that is acylated by the G3P-acyltransferase PlsB to create lysophosphatidic acid (LPA). Then, LPA is transformed into phosphatidic acid (PA) by PlsC. The formation of PA can be also achieved by the transformation of diacylglycerol (DAG) by DgkA. Then, PA is transformed to cytidine diphosphate-diacylglycerol (CDP-DAG) by CdsA from the addition of Cytidine 5'-triphosphate (Parsons and Rock, 2013; Sohlenkamp and Geiger, 2016). The latter CDP-DAG precursor leads to the synthesis of phospholipids PhE, PhG and CL. To synthesize PhE, the phosphatidyl serine synthase (Pss) condenses L-serine with CDP-DAG to synthesize phosphatidylserine (PS). Then the phosphatidyl serine decarboxylase (Psd) transforms PS to phosphatidylethanolamine (PhE). In the case of the negatively charged phospholipids PhG and CL, they are synthesized by phosphatidylglycerophosphate synthase A (PsgA) by the condensation of G3P from CDP-DAG to create phosphatidylglycerol phosphate (PGP). Then, PGP is dephosphorilated by PgpA/B/C (phosphatidylglycerophosphatase A/B/C) to create phosphatidylglycerol (PhG). The cardiolipin synthase A (ClsA) can synthesize CL with two molecules of PhG. In *E. coli*, CL can be also synthesized from PhE and PhG by ClsC. Moreover, in a recent study it was shown that ClsB is able to convert PhE to PhG (Li et al., 2016; Sohlenkamp and Geiger, 2016; Tan et al., 2012). These lipids can integrate the IM by diffusion, however to arrive to the OM they must pass through different machineries that will be discussed in the section of lipid transport. Another component of the OM is the LPS, discussed in the next paragraph.

After synthesis in the cytoplasm, phospholipids have to be incorporated in the bacterial envelope membranes. The process of transport to the OM is particularly challenging, as phospholipids must cross the IM and the aqueous periplasm. Moreover, the OM must remain asymmetric, so phospholipids must remain at the internal leaflet of the OM, while molecules of LPS must remain at the outer leaflet of the OM. The process of transport of phospholipids and maintenance of the OM asymmetry involves machineries that span the bacterial envelope or involve a multi-step complex that mediate anterograde and retrograde transport of lipids. In Gram-negative bacteria, at least two systems that transport phospholipids exist: the MCE systems and the AsmA-like superfamily.

### 2.5.2 The Mammalian Cell Export (MCE) domain-containing systems to transport phospholipids

MCE systems are ubiquitously conserved in double-membrane bacteria. In *E. coli* there are three genes that code for a MCE protein family: *mld* (maintenance of OM lipid asymmetry

D), *pqiB* (paraquat inducible B) and *letB* (lipophilic envelope tunnel B) (Fig. 3B). These proteins have been implicated in several mechanisms, such as transport of lipids and other hydrophobic molecules. The architecture of the three MCE members was recently revealed in *E. coli*, which is linked to their functional role to transport substrates (Ekiert et al., 2017; Isom et al., 2020).

The MLA complex is a six subunits complex, MlaA-F, composed by the central subunit MlaD, an IM protein arranged as a hexamer. This MlaD hexamer interacts with a dimer of MlaF that spans the IM. The dimer MlaF interacts with two molecules of MlaB at the cytoplasm and provides energy to the complex, as it contains signature motifs found in ABC proteins that permit ATP hydrolysis for energizing the complex. The periplasmic protein MlaC was observed to contain a hydrophobic pocket and it has hypothesized to act as a chaperone of phospholipids (Huang et al., 2016; Thong et al., 2016). It has been shown that MlaA is possibly related to its function to preserve OM asymmetry (Yeow et al., 2018). MlaA resides as a lipoprotein embedded in the OM and interacts with the trimeric porin OmpC. Recent studies have shown MlaA interacts extensively with the OmpC trimer and MlaA forms a hydrophilic channel that could permit the transport of phospholipids (Yeow et al., 2018). MlaA interacts with MlaC by protein affinity and could transport lipids to the IM via the interaction with the MlaBDEF subcomplex (Yeow and Chng, 2022). The sense of the translocation has not yet been defined and it has been proposed that MlaC could act as a ferry by carrying phospholipids in both directions to preserve OM asymmetry or to promote their translocation to the OM (Ekiert et al., 2017).

The second structure corresponds to LetB, a tunnel-like protein complex that spans the bacterial envelope for transport of lipids. LetB arranges as a hexamer and it presents seven MCE domains. This creates an elongated seven ring-like multimer of LetB spanning the envelope. Particularly, this conformation creates a cavity where lipids could fit. The gene *letB* arranged in operon together with *letA*, suggested to be an IM protein partner (Isom et al., 2020). Each MCE domains of LetB enlarges the distance of the complex by approx. 30 Å each (approx. 220 Å for the full complex). The length of LetB is important for its function in *E. coli*, as when a  $\Delta$ *letB* was complemented with MCE proteins with different amount of rings, it failed to complement growth in the presence of lauryl sulfobetaine (LSB) when the structure became too short (Isom et al., 2020). Moreover, analysis of multibody refinement of cryoEM density maps showed the tunnel can be open or closed. This suggests the tunnel may pivot substrates for transport. Analysis by site-directed photocrosslinking suggests that the cavity of LetB is in contact with phospholipids and it could act as a tunnel to transport lipids to the OM, possibly via an OM-protein partner (Isom et al., 2020). Indeed, a recent cryoEM structure was reported in a substrate-bound state, fitting PhG (Liu et al., 2020).

Finally, the structure for PqiB was solved too. PqiB contains three MCE domains and it forms a hexamer, like the other two MCE-containing proteins. It shows PqiB organizes with an elongated C-terminal domain that arranges as a needle and the three MCE domains forming three rings, very similar to LetB. The hollow lumen of the C-terminal extension would have a size of 15 - 20 Å. These are amphipathic along their length, so phospholipids could fit inward-facing the hydrophobic cavity or outward-facing the hydrophilic exterior (Ekiert et al., 2017). The structures of PqiA and PqiC are not yet solved, however it has been proposed that PqiB could interact with PqiA and PqiC. PqiA could be an IM protein partner and PqiC an OM lipoprotein forming oligomers (Nakayama and Zhang-Akiyama, 2016; Yeow and Chng, 2022). It is still not clear how this protein promotes transport of phospholipids, but it has been hypothesized that it could act as a bridge (Ekiert et al., 2017).

### 2.5.3 *The AmsA-like superfamily*

In addition to this members of MCE domain family, there is another group that has been proposed to have a role for the transport of phospholipids: the AsmA-like superfamily. In *E. coli*, there are six members of this family and they include AmsA, TamB, YdbH, YhdP, YhjG and YicH (Fig. 3B). They are IM proteins, characterized to contain large periplasmic domains that may adopt a particular folding with hydrophobic cavities, as shown for a portion of TamB (Yeow and Chng, 2022).

Phospholipid transport in these cavities could be very similar to members of MCE domain proteins or the b-jelly roll bridge of the Lpt system, as lipids could travel from the IM to the OM using an OM protein partner. Energization from PMF or ATP hydrolysis could be possible with a cytoplasmic partner that may harness energy at the IM, as observed with the MCE proteins. Protein partners at the OM could be able to monitor quality control of phospholipids and/or receive the phospholipids for insertion, like the case of the MlaA-OmpC pair. Interestingly, TamB is known to interact with TamA, a  $\beta$ -barrel protein involved in biogenesis of OMPs (Selkrig et al., 2012), but the precise role it may have for lipid transport has never been described in the literature. Recent studies have shown the absence of YhdP, TamB, and YdbH lead to defects in transport of phospholipids (Douglass et al., 2022). Moreover, a semiredundant role has been proposed for members of this family to promote lipid homeostasis (Ruiz et al., 2021).

Overall, there are still many gaps in the understanding of the regulation processes that rule transport of lipids. However, new structural data and functional analyses permit to understand the mechanisms to promote translocation of these machineries that permit translocation of lipids through the aqueous periplasm. Here we discussed about one mechanism Gram-

negative bacteria possess to cope for defects in the bacterial envelope to maintain OM asymmetry. In the next chapter, we will focus on some of the processes bacteria have to cope for stress and maintain homeostasis when biogenesis machineries encounter some problems.

## 2.6 Lipopolysaccharide (LPS)

The OM contains LPS in the external leaflet, which is a glucosamine-based saccharolipid (Sperandeo et al., 2017). The structure of LPS may vary from bacteria to bacteria and in some bacteria it plays a role in pathogenicity (Wilkinson, 1996). LPS also creates a tightly packed layer that protects bacteria against hydrophobic compounds, such as some antibiotics (Sperandeo et al., 2017). This confers bacteria a first permeability barrier (Guest et al., 2021).

The LPS molecule is composed of three parts: Lipid A, the core oligosaccharide and the O-antigen repeats (exposed in the cell surface). Lipid A is the most conserved part of LPS. The core oligosaccharide can be further divided into two parts: the inner and outer core. The inner core is formed by at least a residue of 3-deoxy-manno-oct-2-ulosonic acid (Kdo) and of L-glycero-D-manno-heptose (heptose). The outer core is more variable in composition (Holst, 2007). The acyl chains of lipid A are saturated, whereas the polar head of lipid A contains phosphates groups that, being negatively charged, mediate interaction with divalent cations, such as  $Mg^{2+}$  and  $Ca^{2+}$  giving rigidity to the LPS layer (Guest et al., 2021; Sperandeo et al., 2017). Some non-pathogenic bacteria do not contain O-antigen repeats, as for *E. coli* K12 derivatives (Sperandeo et al., 2017). Metal-chelating agents, such as ethylenediaminetetraacetic acid (EDTA) are able to disrupt the interactions via these cations and thus interfere with LPS organization.

The cell possesses protein machineries that permit to keep the asymmetry of the OM lipid bilayer, such as the Mla lipid trafficking system (Ekiert et al., 2017), the palmitoyltransferase PagP or the phospholipase PldA (Sperandeo et al., 2017).

Biogenesis of LPS takes place in the cytoplasm, the IM and the periplasm. The biosynthetic pathway of LPS requires the convergence of Lipid A-core biosynthesis (that is the synthesis of lipid A plus the oligosaccharide core) and eventually the O-antigen synthesis pathway. The synthesis of Lipid A-core occurs at cytoplasmic leaflet of the inner membrane starting from UDP-GlcNAc (uridine diphosphate-N-acetylglucosamine). After a series of enzymatic reactions, the two Kdo residues of lipid A are covalently linked to the sugars of the core oligosaccharide. After this step, the ATP-Binding Cassette (ABC) transporter MsbA can flip this protein through the IM. There, the O-antigen can be ligated to the chain (Guest et al., 2021; Sperandeo et al., 2017; Wang and Quinn, 2010).

## 2.7 Remodeling of the bacterial envelope during cell division

In Gram-negative bacteria, cell division is a critical process that requires coordination of multiple machineries and regulatory factors. During cell division, cells need to form a division septum, duplicate and segregate genetic material, enlarge and remodel the bacterial envelope preserving the integrity of the OM, PG and IM (Egan and Vollmer, 2013). Here we will briefly illustrate how the PG is remodeled during cell division and the processes of coordination between this process and the remodeling of the IM and the OM.

### *2.7.1 PG remodeling and penicillin-binding proteins (PBP)*

The sacculus is a bag-like macromolecule made of PG chains that encases the IM of Gram-negative bacteria. This sacculus helps to maintain cell shape and provides mechanical resistance against osmotic stress (Typas et al., 2012). Renewal of PG is achieved by enzymatic removal old PG material and insertion of new strands. Removed strands of PG can be recycled for *de novo* synthesis (Park and Uehara, 2008).

Biogenesis of PG starts at the cytoplasm and it requires three main steps. First, the activated nucleotide-based precursors UDP-N-Acetylglucosamine and UDP-N-acetylmuramyl pentapeptide are synthesized in the cytoplasm (Barreteau et al., 2008). Second, precursors are assembled with undecaprenyl phosphate at the cytoplasmic side of the IM to form the monomer subunit Lipid II. This molecule is then flipped from the cytoplasmic side to the periplasmic leaflet of the IM. Finally, Lipid II is used by glycosyl transferases (GTases) to synthesize a polymer of glycans that will then be crosslinked by peptidyl transferases (TPases) (Typas et al., 2012).

During cell division, the cell must coordinate processes of biogenesis of the bacterial envelope. The sacculus must remain with approximately the same thickness and grow simultaneously. Given the structure of the PG, it would not be sufficient to attach new material to the sacculus, because it would grow in thickness and not in length. Instead, it requires the enzymatic activity to cleave and insert new PG strands and this is possible by the activity of hydrolases.

In *E. coli*, there are at least 13 hydrolases, with partially redundant activities, as none of these individual genes is essential. There are mainly three types of hydrolases: amidases, transglycosilases and endopeptidases and they all contribute to cell separation (Typas et al., 2012; Vermassen et al., 2019). Amidases cleave between N-acetylmuramic acid and a residue of the stem of the pentapeptide. Transglycosilases cleave glycosidic linkages and endopeptidases cleave between peptide residues (Vermassen et al., 2019).

In addition to these, GTases polymerize glycan chains and TPases crosslink peptides between glycan strands (Vigouroux et al., 2020). The GTase MgtA is a monofunctional synthase that has a role as a glycotransferase during cell elongation and it has been described that it may interact with other proteins to assemble PG during cell division (Derouaux et al., 2008). PG biosynthetic enzymes are also called penicillin-binding proteins (PBP) and there are two main classes: class A (aPBP) and class B (bPBP). The aPBP are bifunctional synthases that can catalyze transglycosilation and transpeptidation *in vitro* (Matsushashi, 1994). In *E. coli* PBP1A, PBP1B and PBP1C are required for mechanical stability of the PG (Vigouroux et al., 2020). PBP1A and PBP1B are partially redundant and only one is necessary for cell viability. The role of PBP1C is not yet clear, but it has the ability to interact with other PBPs, suggesting the formation of a complex containing hydrolases and polymerases (Schiffer and Höltje, 1999). PBP1B has an activity in *de novo* regeneration of the cell rod shape by repairing defects (Ranjit et al., 2017; Vigouroux et al., 2020). The bPBP are monofunctional TPases and there are two proteins: PBP2 and PBP3 (also known as FtsI). PBP2 is a transpeptidase, necessary for cell elongation and the maintenance of the correct diameter of the cell pole (Den Blaauwen et al., 2003; Özbaykal et al., 2020). PBP3 is a TPases enzyme, key element in cell separation that has a role in the recruitment of proteins at the division septum (Addinall et al., 1997; Ishino and Matsushashi, 1981; Nguyen-Distèche et al., 1998).

Other PBPs are present in *E. coli*, classified as low molecular weight or class C (cPBP). In *E. coli* there exist PBP4, PBP5, PBP6, PBP6b, PBP7, PBP4b, and AmpH. The precise role of these PBPs is not well characterized to the date, but the function of some of them is related to cell elongation and division (Kocaoglu and Carlson, 2015).

### 2.7.2 Remodeling of the bacterial envelope during cell division

From a temporal point of view, cell division can be divided in early and late steps (Aarsman et al., 2005; Egan and Vollmer, 2013). During the early steps, FtsZ, a tubulin-like protein, masters the regulation of the bacterial cell division. FtsZ associates with FtsA, ZipA, ZapA, ZapB, ZapC, ZapD and FtsEX at the future division site, where they form filaments and arches in a ring shape at the IM in a structure called the Z-ring (Aarsman et al., 2005; Margolin, 2005). Functional Z-ring is essential for the cell division and more than 10 essential proteins form it. ZipA and FtsA stabilize the Z-ring. Enzymes required for lipid II and presumably PG synthesis are recruited to the Z-ring to perform preseptal elongation (Aaron et al., 2007; Typas et al., 2012; Vollmer and Bertsche, 2008). The precise mid-cell localization of the Z-ring is controlled by MinC/MinD/MinE that inhibit the formation of this complex near the poles. SlmA has a similar

function, avoiding the formation of the Z ring near the nucleoid, that would squeeze DNA during septation (Egan and Vollmer, 2013).

To promote cell division, cells require the assembly of a series of essential proteins at the Z-ring. This process is the late step and it involves the recruitment of PBP3 by FtsW that interacts with FtsQLB, PBP1B and FtsN. Septation only occurs after the arrival of FtsW and FtsB at the mid-cell (Goley et al., 2011). *E. coli* contains at least six DD-carboxypeptidases and PBP5 is the most active (Typas et al., 2012). In addition, there are seven lytic TG: the periplasmic Slr70 and the OM lipoproteins MltA, MltB, MltC, MltD, MltE and MltF.

Amidases are critical for cell constriction, in *E. coli* the periplasmic proteins AmiA, AmiB and AmiC are responsible for this activity and they are localized at the division septum. Two different pathways of activation of amidases exist: the one activated from the IM and other activated from the OM (Fig. 4A and B). AmiA and AmiB are activated via EnvC and AmiC is activated by the OM lipoprotein NlpD (Tsang et al., 2017; Typas et al., 2012; Uehara et al., 2010). The activation of AmiA/B is dependent to the binding of EnvC to the ABC-like transporter complex FtsXE, driven by ATP hydrolysis (Cook et al., 2020).

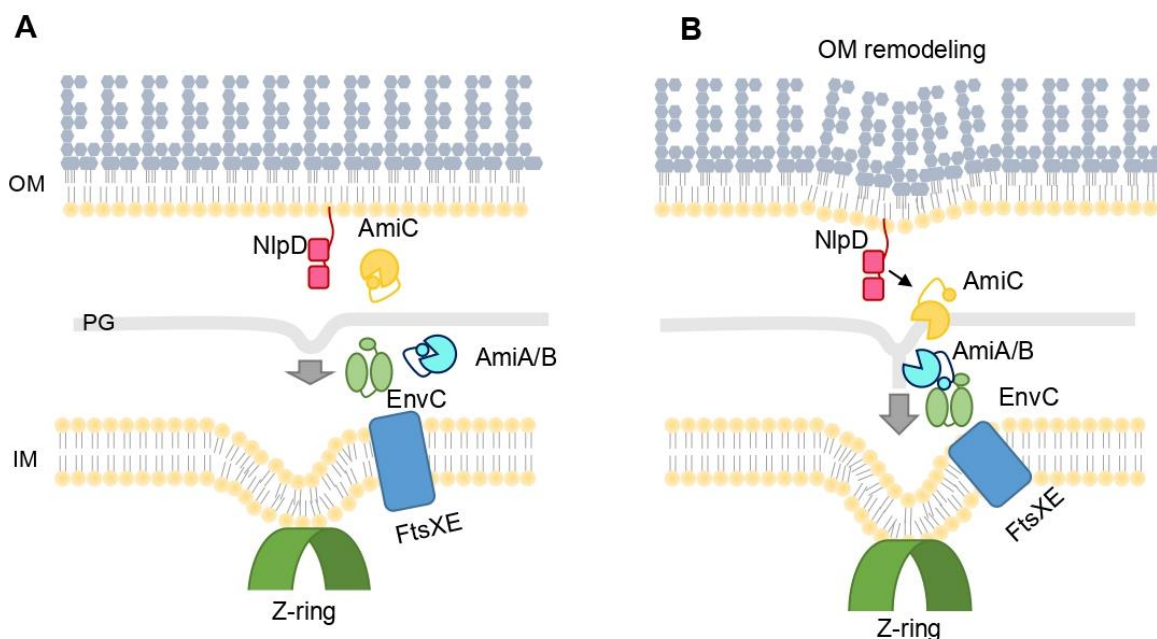


**Figure 4. Peptidoglycan remodelling during cell division.** **A.** During a late step of cell division, septal peptidoglycan is assembled at the cell division site. **B.** The activity of septal peptidoglycan amidases is necessary to allow cell separation by completing the formation of the new poles of daughter cells. Activation of amidases is necessary and can be achieved via a NlpD-regulated (at the OM) or an FtsXE/EnvC-regulated (at the IM) pathway. NlpD activates AmiC, whereas FtsXE/EnvC activates AmiA/B, respectively.

The Tol-Pal system is a multioligomeric transenvelope complex composed by the IM proteins TolA, TolQ, TolR, the soluble periplasmic TolB and the OM lipoprotein Pal. It has been suggested that this complex could play a regulatory role in activation of amidases and provide energy to process late steps of cell division (Egan and Vollmer, 2013), however this step and the precise requirement of this complex is not yet fully understood.

In conclusion, cell division involves the coordination of several factors at the different steps of cell division. It is proposed that the activity of hydrolases is triggered by the activity of IM and OM proteins, to promote PG remodeling and cell separation. This coordination should be involving several factors that are not yet known. The difficulty for their detection lies in the fact that such putative factors should form transient complexes (Typas et al., 2012).



### 3 Biogenesis of the OM

In Gram-negative bacteria, the OM is the first line of interaction between the cell and its extracellular environment. Proteins in the OM are capable of performing several functions from the import of nutrients, the export of virulence factors, the attachment to surfaces or the efflux of noxious molecules. Moreover, OM protein machineries can promote essential processes, such as the assembly of LPS and proteins in the OM. Two main topological classes of proteins can be found at the OM: OM-associated lipoproteins and OMPs (Ranava et al., 2018).

#### 3.1 Export of lipoproteins to the OM

##### 3.1.1 *The Localization of lipoproteins (LOL) pathway*

After maturation, some lipoproteins remain at the IM while many are transported to the OM by the localization of lipoprotein (LOL) pathway. The system is composed by LolCDE at the IM (an ABC transporter), LolA at the periplasm (a molecular chaperone) and LolB at the OM (a lipoprotein) (Fig. 2A). LolCDE is essential for the cell and the structure of the subcomplex, recently solved by Cryogenic electron microscopy (cryoEM), provides insights into how it functions. LolC and LolE have transmembrane segments with periplasmic domains, while LolD forms dimer at the cytoplasmic side of the IM, interacting with transmembrane segments of LolCE. From this LolCDE subcomplex, LolD is the ATPase of the ABC system. It is proposed that the substrate enters in the interface between LolC and LolE and, by hydrophobic interactions with the subcomplex, the substrate is taken from the IM. Finally, by the energization by ATP hydrolysis by LolD dimer, the subcomplex hands the substrate over to its periplasmic partner LolA via the periplasmic domains of LolCE (Sharma et al., 2021).

The periplasmic protein LolA contains a large hydrophobic cavity where the hydrophobic moiety of the lipoprotein is able to fit being shielded from the aqueous periplasm. LolA hands the substrate over to the OM lipoprotein LolB. Despite the different primary sequence, the structures of LolA and LolB are very similar, with a big hydrophobic cavity (Konovalova et al., 2014; Takeda et al., 2003). It is proposed that an opening/closing mechanism of LolA permits the release of the substrate to LolB. These hydrophobic cavities have been previously reported as incomplete or unclosed  $\beta$ -barrels and it has been proposed a “mouth-to-mouth” mechanism of transport (Oguchi et al., 2008; Okuda and Tokuda, 2009). This environment permits the transport to LolB and OM incorporation involves a protruding loop, important for protein anchoring by a still ill-defined mechanism (Grabowicz, 2019; Hayashi et al., 2014).

The LOL subunits are essential. However, it was shown that under some conditions, translocation of OM lipoproteins can occur even in the absence of *lolA* or *lolB*. It has been speculated that the main reason why LolA and LolB are essential is to prevent aberrant

localization of OM lipoproteins at the IM, which would be toxic for the cell (Grabowicz and Silhavy, 2017a).

Some lipoproteins do not follow the LOL transport pathway and remain at the IM. This process is called “the LOL avoidance” and is determined by the amino acid sequence that follows the lipobox. First, the +2 rule, where lipoproteins can avoid the pathway depending on the identity of the amino acid in position +2 after the conserved and acylated lipobox Cys (that becomes residue +1 after cleave by LspA). An Asp residue at position 2 causes retention at the IM (Terada et al., 2001; Yamaguchi et al., 1988). Moreover, it has been shown that the presence of Asp, Asn, Gln or Glu at position +3 also has a strong impact for this avoidance. It has been speculated that the interaction with LOL subunits may be affected by the presence of acidic residues (Terada et al., 2001).

Another criterion is the nature of the linker in lipoproteins. After maturation, lipoproteins contain a linker at their N-termini. It has been recently proposed that the linker has an impact for OM localization, as deletion of linker of some OM lipoproteins cause retention to the IM. It is further suggested that the length and intrinsic disorder of the linker are important parameters for optimal processing by the LOL pathway (El Rayes et al., 2021).

### 3.1.2 Lipoprotein topology in the OM

In the  $\gamma$ -proteobacterium *E. coli*, lipoproteins acquire different topologies in the OM. In their typical topology, the lipid moieties of lipoproteins are embedded in the inner leaflet of the OM and the globular protein domain is facing the periplasm. Other lipoproteins have different topologies, such as exposed at the cell surface (via the anchoring at inner leaflet of the OM) or in complex with other protein partners (Konovalova et al., 2014). Interestingly, in other bacteria, e.g. in the genus *Neisseria*, lipoproteins can be surface exposed via their anchoring at the external leaflet of the OM. This process relies on OMPs proteins called surface lipoprotein assembly modulator (Slam) (Cole et al., 2021).

Two of the two most studied lipoproteins are Lpp and Pal. As previously described, Pal participates in a late step of cell division and can interact non-covalently with the PG. Lpp (or Braun’s lipoprotein) is the most abundant lipoprotein of *E. coli* and it consists of a small protein of 6 kDa (58 residues). It has been shown that Lpp can covalently crosslink with the PG. It was also suggested that the length of Lpp plays a role in regulating the distance between the OM and the PG. Indeed, some studies have used mutant versions of Lpp that are different in size, to modify the space between the PG and the OM (Alvira et al. 2020; Asmar et al. 2017). A portion of Lpp is covalently bond, while another is not. It has been suggested that the free-form

of Lpp is cell surface-exposed, however the precise role is not yet defined (Cowles et al., 2011). This dynamic localization has been reported for other lipoproteins, such as RcsF and BamC. In the case of RcsF this dynamic localization has been linked with the activity of this lipoprotein, while in the case of BamC is not yet fully understood (Cho et al., 2014; Konovalova et al., 2014; Webb et al., 2012). The role of those proteins will be discussed in detail in the section 3.2 and 5.1 of this Introduction.

Finally, other lipoproteins can form large transmembrane multimeric channels in the OM, such as CsgG and Wza. CsgG is involved in the formation of curli for T8SS and it forms a channel in the OM composed of a nonamer of molecules that create a structure of 36  $\beta$ -strands arranged in the form of a pore. The precise mechanism of formation of this large complex is not yet known (Costa et al., 2015; Konovalova et al., 2014). The protein Wza is also involved in secretion and it can form homooligomers of eight subunits. This protein is involved in the export of capsule polysaccharides. Interestingly, the oligomerization of Wza forms a lumen by  $\alpha$ -helices, creating an  $\alpha$ -helical barrel. This represents a different folding class of integral membrane proteins in the OM (Konovalova et al., 2014; Nickerson et al., 2014).

### 3.2 Biogenesis of OMPs from the IM to the OM

One of the major questions in OM biogenesis is how OMPs are assembled into the OM. Their biogenesis requires the coordinated function of several factors in the bacterial envelope: proteins that promote translocation through the IM, chaperone molecules that recognize and escort the unfolded OMPs to the OM preventing their misfolding in the aqueous periplasm, and folding and insertion into the OM. The source of energy required for promoting assembly is not yet fully understood because the periplasmic space lacks of conventional energy-storing molecules, such as ATP, and there is no PMF across the OM (Fleming, 2015; Plummer and Fleming, 2016).

#### *3.2.1 The periplasmic journey of OMPs to the OM*

To cross the aqueous periplasm, client OMPs interact with molecular chaperones, such as the survival protein A (SurA), the seventeen kilodalton protein (Skp) and the periplasmic serine endoprotease DegP (Wang et al., 2021). These chaperones allow unfolded OMPs (uOMPs) to remain folding competent and reach the OM complex that folds and inserts them into the OM (Fig. 2B). This complex is known as  $\beta$ -barrel assembly machinery (or BAM complex).

Skp is classified as an ATP-independent holdase (Mas et al., 2019). The structure of Skp shows a stable trimer in the form of a crane claw. This is possible by the interaction of their N-

termini  $\beta$ -domains to form a small  $\beta$  structure, while their C-termini form large parallel  $\alpha$ -helices. Skp is able to interact with several uOMPs of different sizes with great affinity by hydrophobic and electrostatic interactions via its C-terminal region (Jarchow et al., 2008; Mas et al., 2019; Qu et al., 2007; Schlapschy et al., 2004). This OMP-Skp interaction is possible because the claws can be expanded to adapt to the size of the substrate (Holdbrook et al., 2017). Moreover, it has been proposed that Skp could interact with big proteins via a multivalent binding of several molecules of Skp (Schiffrin et al., 2017b, 2016).

SurA is composed by 4 domains: a large N-terminal domain, two parvulin-like peptidyl-prolyl isomerase (PPIase) domains and a short C-terminal helix (Bitto and McKay, 2002). The N- and C-terminal domains of SurA are suspected to mediate the interaction with the uOMP and they are proposed to be the core of the protein that may form a clamp to hold the client protein. PPIase domain 2 is proposed to “close” to maintain the client protein in the core domain (Bitto and McKay, 2002; Calabrese et al., 2020). SurA could recognize a motif  $\Omega X \Omega$  (aromatic, any other residue, aromatic) that is present in OMPs, suggesting specificity for this type of protein substrates (Mas et al., 2019; Xu et al., 2007).

Some authors have suggested a model where two parallel pathways exist to target uOMPs to the BAM complex: the Skp- and SurA-dependent pathways and this last is considered the main (Mas et al., 2019). Many questions are arisen from the coordination of these two chaperone pathways for delivery to the BAM complex. It is not clear what determines the requirements of the uOMP for one or the other chaperone pathway or by which mechanisms both pathways can be regulated. It is important to highlight that the affinity of SurA for an uOMP is relatively lower compared to the affinity between Skp and OMPs so it is difficult to conceive how the two chaperones regulate their biogenesis pathways and for which substrates (Mas et al., 2019).

Another model has been recently proposed in which SurA and Skp could play non-redundant roles in the control and homeostasis of biogenesis of OMP (Fig. 2B) (Combs and Silhavy, 2022). As previously stated,  $\beta$ -signals permit the correct assembly of OMPs in the OM. It has been proposed that Skp is able to interact with uOMP at the Sec translocon in an early step of transport. In this step, Skp acts as quality controller of uOMP by the recognition of defective  $\beta$ -signals and can eventually hand them over to DegP for degradation. Proteins that pass the quality check by Skp are handed over to SurA for delivery to the BAM complex (Wang et al., 2021). Interaction between the BAM complex and SurA has been identified in the past (Bennion et al., 2010; Schiffrin et al., 2022). If there is a problem in the assembly of OMPs at the BAM complex, Skp is able to remove stalled proteins at the complex to hand them over to the protease DegP (Combs and Silhavy, 2022). This opens a new perspective on how Skp and SurA would work in two non-redundant pathways and may act as quality control chaperones.

### 3.2.2 The BAM-Sec holotranslocon supercomplex

Recent studies have investigated the formation of a supercomplex between the Sec translocase and the BAM complex. It was demonstrated by site-directed photocrosslinking that SurA could be interacting with the main subunit BamA via its POTRA domains, but also with PpiD. PpiD is a protein associated to facilitate transport and biogenesis of OMPs at the Sec translocon (Fürst et al., 2018). It was previously reported that double mutant  $\Delta surA \Delta ppiD$  was synthetically lethal (Dartigalongue and Raina, 1998). This interaction hub (Sec-PpiD-SurA-BamA) may take place to promote biogenesis of OMPs and form a pathway from the IM to the OM (Wang et al., 2016).

Evidence for the formation of a BAM-Sec supercomplex was recently captured by cell fractionation of *E. coli* and cryoEM analysis. It shows an envelope spanning complex created with the BAM complex and the Sec translocon (Alvira et al., 2020). This analysis shows the formation of the supercomplex is dependent on CL. Importantly, two conformations of the Sec holotranslocon are observed as described in previous studies, an open and a compact conformation (Botte et al., 2016). The open conformation has been reported as an active form of the translocon and it was observed this form was enhanced by adding CL. Finally, the interaction between Sec and BAM seems to be an important mechanism to promote OMP biogenesis. It has been suggested that proton transport is required for OMP maturation (Alvira et al., 2020).

Altogether, this new evidence leads to hypothesize that upon OMP biogenesis, the Sec holotranslocon could interact with the BAM complex. This supercomplex must cross the PG and some chaperone molecules may be involved in mediating the interaction. This supercomplex could help resolving some unanswered question such as those relative to the energy source that drives OMP biogenesis.

### 3.2.3 The BAM complex

The central component of the BAM complex, the Omp85-family protein BamA, was discovered in the model organism *Neisseria meningitidis* (Voulhoux et al., 2003) and then identified also in *E. coli* (Werner and Misra, 2005). Thanks to genetic and structural analyses, subunits of the BAM complex were identified (Malinverni et al., 2006; Sklar et al., 2007; Wu et al., 2005). The subunit BamA is embedded in the OM and is a  $\beta$ -barrel protein itself. It belongs to the evolutionary conserved Omp85 protein family. Homologues in mitochondria include Sam50/Tob55, and in chloroplast Toc75-III and Toc75-V/Oep80. They are responsible for

folding and insertion (*i.e.* assembly) of  $\beta$ -barrel in the OM of these organelles proteins (Höhr et al., 2018; Plummer and Fleming, 2016; Sommer et al., 2011).

In *E. coli* the BAM complex is composed by BamA that interacts with other four lipoproteins BamBCDE. Structural analyses of the complex revealed that BAM is 120 Å in length, 100 Å in width and 140 Å in height. BamA is the central subunit that contains a membrane embedded domain and a periplasmic domain that mediates the interaction with other lipoproteins, forming a hat-shaped complex at the OM (Han et al., 2016).

BamA is an essential subunit, composed of two domains: a periplasmic soluble N-terminal domain and a membrane C-terminal  $\beta$ -barrel domain. The soluble domain is composed of five POTRA motifs. The  $\beta$ -barrel of BamA is an essential domain. POTRA 1 (P1) or P2 can be deleted, because they are not essential for the cell. In *E. coli*, POTRA domains 3, 4 and 5 are essential, however deletion of P3 and P4 can be generated in a lab strain that expresses an additional copy of wild-type BamA. Instead a copy of BamA lacking P5 is toxic for the cell probably as it impairs a vital function in the biogenesis of OMPs, even when full-BamA is present (Kim et al., 2007). Interestingly, in *Neisseria meningitidis* only P5 is essential for cell viability and protein function (Bos et al., 2007). This could be explained by the fact that, P3 is required for assembly of LptD and this protein is not essential in *N. meningitidis* (Bos et al., 2004) differently from *E. coli* where it is (Ruiz et al., 2006).

The POTRA motifs of BamA scaffold the interaction with BAM lipoproteins. BamB interacts directly with the POTRA domains 1-3 of BamA (Dong et al., 2012). BamB is not essential, however the deletion of its gene induces activation of the  $\sigma^E$ -mediated envelope stress response (Charlson et al., 2006; Wu et al., 2005) and results in increased sensitivity to detergents and antibiotics producing lower levels of OMPs. Moreover, this deletion leads to a synthetic phenotype with deletion of chaperones *degP* or *fkpA* (Onufryk et al., 2005). The structure of BamB shows an eight blade  $\beta$ -propeller and it has been suggested it could participate in substrate binding and delivery (Kim and Paetzel, 2011) as well as in controlling the orientation of the POTRA domains with respect to the  $\beta$ -barrel of BamA (Gu et al., 2016).

BamC is a non-essential lipoprotein. It contains two globular domains and it has been described as the most dynamic BAM subunit, because its domains are not tightly coupled to the complex (Gu et al., 2016). It has been described it interacts mainly with BamD via its N-terminal globular domain and with P1 and P2 of BamA via its C-terminal globular domain. BamC stabilizes the interaction between BamD and BamA and enhances a periplasmic ring formed by these two subunits (Gu et al., 2016). It has been suggested that BamC could be exposed at the cell surface (Webb et al., 2012), however structures of the BAM complex have shown BamC to be facing the periplasmic side (Gu et al., 2016; Iadanza et al., 2016). We could

speculate that this could correspond to a dynamic behavior of the protein related to its still unknown function.

BamD is the other essential subunit (Onufryk et al., 2005) and together with BamA, it forms the core of the complex. BamD structure reveals 10  $\alpha$ -helices containing five tetratricopeptide repeat (TPR) motifs. It interacts with P1, P2 and P5 of BamA to form a ring and it interacts with BamC and BamE. It has been suggested that it stabilizes the dynamics of POTRA domains of BamA. A slow folding OMP mutant was observed to bind BamD (Lee et al., 2018). In addition, the study of the autotransporter EspP has suggested that BamD could be implicated in a late step of the release of the folded  $\beta$ -barrel domain from the BAM complex (Ieva et al., 2011). This suggests that BamA and BamD could work in a sequential process to promote folding of OMP substrates in the OM.

BamE is the smallest component of the BAM complex, yet pull down assays have shown it is sufficient to co-purify all BAM subunits (Roman-Hernandez et al., 2014). It has been associated with correct activity of the BAM complex by stabilizing the interaction between BamA and BamD (Sklar et al., 2007) and also by modulating activity of BamA (Konovalova et al., 2016). Its deletion causes mild OM defects as these cells become sensitive to SDS and levels of OMPs are slightly reduced (Sklar et al., 2007).

#### 3.2.4 Mechanism of biogenesis

Although the precise mechanism via which BAM assists the assembly of OMPs in the membrane remains somewhat unclear, evidence for several key mechanistic details has been acquired in the last decade. It is widely accepted that BamA acts as a central catalytic subunit of the BAM complex. *In vitro* assays have shown that all subunits of the complex are necessary to assure a maximum catalytic effect to assemble OMP in membranes (Hagan et al., 2010; Roman-Hernandez et al., 2014).

OMPs can spontaneously fold *in vitro* and insert into lipid bilayers. *In vivo*, however, BamA catalyzes this process rendering it much more efficient (Gessmann et al., 2014). OMP folding by the BAM complex is improved by the presence of the molecular chaperone SurA (Bennion et al., 2010; Hagan et al., 2010; Roman-Hernandez et al., 2014). A single-residue deletion on P1 of BamA ( $\Delta$ R64) affects the interaction with SurA leading to a dramatic effect on the mechanism of biogenesis of several OMPs (Bennion et al., 2010).

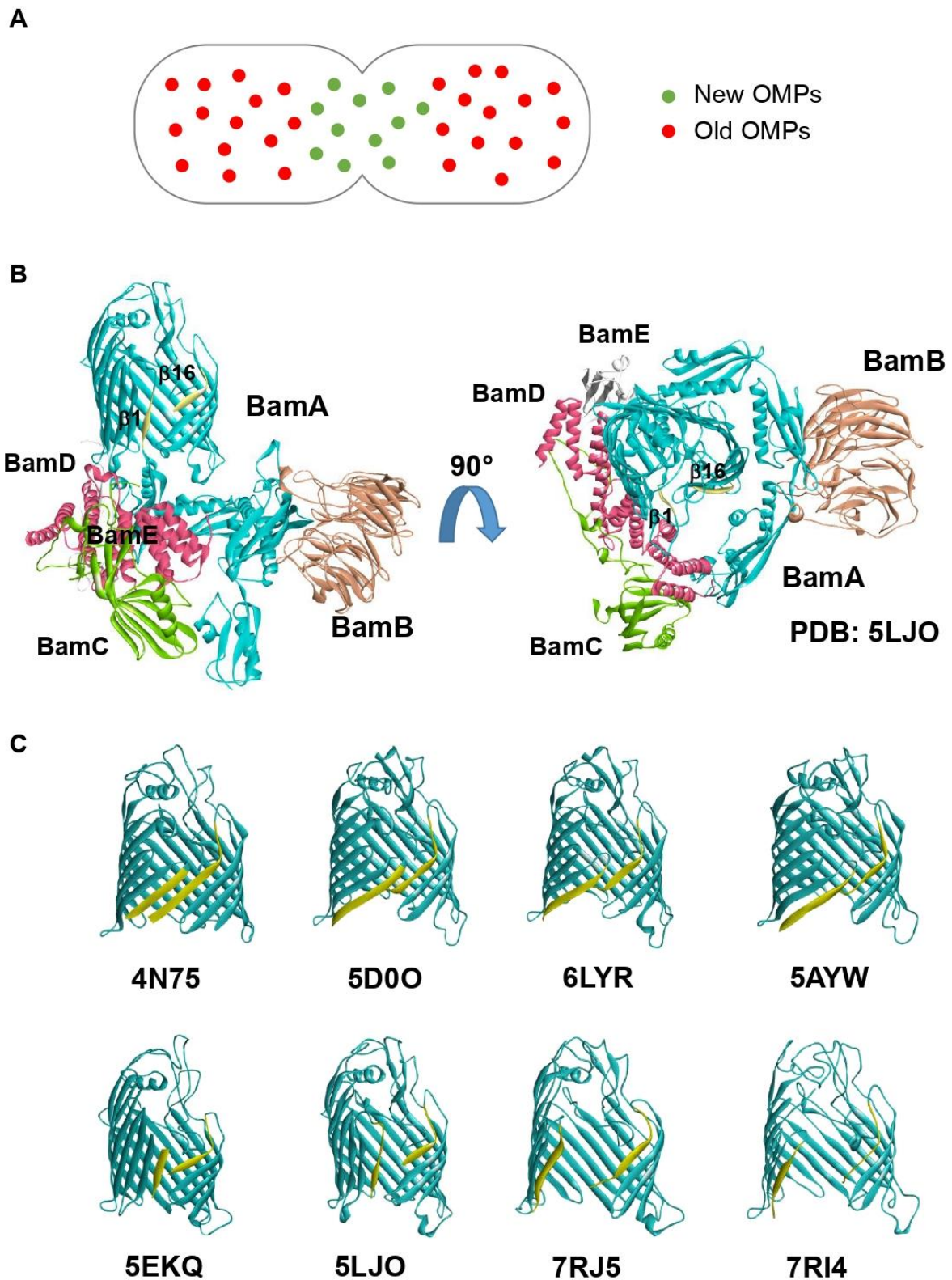


**Figure 5. The BAM complex is a dynamic machinery that promotes biogenesis of OMPs. A.** Biogenesis of OMPs occurs preferentially at the mid-cell localization. **B.** The structure of the BAM complex in an open-conformation. Blue: BamA, orange: BamB, green: BamC, pink: BamD, grey: BamE. In yellow, the lateral gate of BamA formed by  $\beta 1$  and  $\beta 16$ . **C.** The  $\beta$ -barrel domain of BamA can laterally open. Structures of BamA were



observed highlighting a dynamic arrangement of  $\beta$ 1 and  $\beta$ 16 strands during biogenesis of OMPs. Indicated PDB files were used to create structures.

It has been previously shown that the BAM complex has a homogenous localization in the OM (Gunasinghe et al., 2018; Ursell et al., 2012). However, some studies have suggested that OMP biogenesis could be enriched at mid-cell localization, suggesting that the process of OMP biogenesis is spatially organized and that turnover of OMPs may occur by segregation of older OMPs at the cell poles (Fig. 5A) (Rassam et al., 2015). Furthermore, it was reported that the BAM complex is able to span the PG with all its subunits and this could help to promote correct distance between the PG and the OM (Consoli et al., 2021a). Immunolabelling experiments revealed that the BAM complex is enriched at cell division sites. This enrichment depends on the assembly of the Z-ring but it does not require an active divisome. It was hypothesized that the BAM complex is assembled at preseptal sites supposedly in conjunction with preseptal biogenesis of PG (Consoli et al., 2021a, 2021b). This observation is in line with a model where OMP biogenesis occurs preferentially at the mid-cell (Rassam et al., 2015).

The  $\beta$ -barrel domain of BamA forms a 16 stranded  $\beta$ -barrel protein and several structures have been obtained during the past years (Fig. 5B). These structures have highlighted the dynamic interaction between the  $\beta$ -1 and  $\beta$ -16 (Fig. 5C):

- A “closed” conformation (PDB: 4N75, Ni et al. 2014)
- An “inward open” (with  $\beta$ -strands partially closing the barrel in a parallel fashion, PDB: 5D0O, 6LYR, 5AYW, Gu et al. 2016; Xiao et al. 2021; Han et al. 2016)
- An “outward open” (or “laterally open”, PDB: 5EKQ, 5LJO, Iadanza et al. 2016; Bakelar, Buchanan, and Noinaj 2016)
- An open and engaged with a substrate (PDB: 7RJ5, 7RI4, R. Wu et al. 2021).

Molecular dynamics of the C-terminal domain of BamA showed a distortion of phospholipids surrounding the protein in the  $\beta$ -barrel seam (Danoff and Fleming, 2015; Gu et al., 2016; Horne et al., 2020; Horne and Radford, 2022; Iadanza et al., 2016; Schiffrin et al., 2017b). This could be caused by the highly dynamic  $\beta$ -barrel domain that could catalyze insertion of OMPs into membranes by shrinking the thickness of the membrane region in which precursors will be assembled (Fleming, 2015).

In addition to these structures, others have highlighted mechanisms of the BAM complex (Doyle et al., 2022; Noinaj et al., 2013; Wu et al., 2020). Moreover, structural and functional assays revealed the presence of an exit pore above the lateral gate, both essential for BAM activity and required for cell viability. These analyses have shown that the lateral gate is located between the first and last  $\beta$ -strand of the  $\beta$ -barrel domain of BamA (Noinaj et al., 2014). Also,

that the complex presents a large surface hole that may function as substrate-exit pore delimited by P5, BamD, P2 and P3, as well as the first and last  $\beta$ -strands of the  $\beta$ -barrel domain of BamA at the periplasmic side of the complex (Han et al., 2016). These structures have given an unprecedented view of how the BAM complex could accommodate and handle hydrophobic substrates and make conformational changes to promote OMP biogenesis.

Recent work has demonstrated the interaction between BamA and a substrate using the model proteins EspP, LptD and BamA-substrate (BamA<sup>s</sup>). It reveals how the dynamic BamA is able to interact with its substrates to promote folding by the recognition of the  $\beta$ -signal of a client protein (Doyle et al., 2022; Doyle and Bernstein, 2019; Lee et al., 2019; Tomasek et al., 2020). In its homologous protein Sam50, the similar principle was also demonstrated (Höhr et al., 2018). This leads to three models on how the complex is working (Fig. 6).

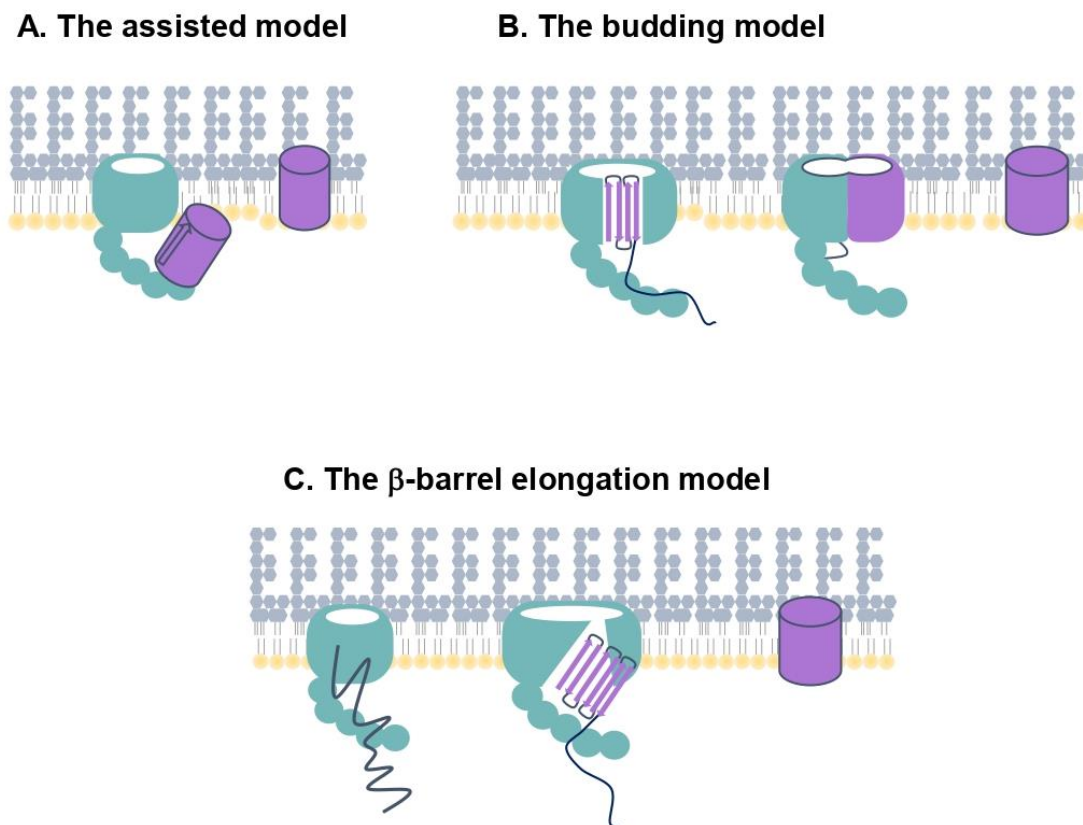


**Figure 6. Proposed models of biogenesis of OMPs mediated by BAM.** **A.** The assisted mode. The client OMP is prefolded in the periplasm, recognition of the substrate is facilitated via the  $\beta$ -signal and the BAM complex acts as an insertase to promote biogenesis. **B.** The budding model. The BAM complex recognizes the  $\beta$ -signal of client OMPs and after sequential formation of  $\beta$ -hairpins, BamA would create a hybrid barrel with the client OMP during assembly. **C.** The  $\beta$ -barrel elongation model. The client protein would be recognized via its  $\beta$ -signal and then the protein would follow steps of folding in the vicinity of the membrane. After client protein is partially prefolded forming a  $\beta$ -sheet, it would be inserted in the membrane by BamA and the barrel would close itself with its insertion.

a) The assisted model

In this model, it is proposed that the client protein undergoes a series of prefolding steps in the periplasmic space. The BAM complex would insert into the OM proteins that have already acquired to some extent a  $\beta$ -sheet structure in the periplasm, thus functioning as an insertase. The partially folded OMP would be recognized via its  $\beta$ -signal. This assembly could be facilitated by the thinning of the lipid bilayer that BAM complex causes (Fig. 6A) (Konovalova et al., 2017; Noinaj et al., 2013; Ranava et al., 2018; Schiffrin et al., 2017a). The shortcomings of this model are that  $\beta$ -barrel proteins would present a large hydrophobic surface exposed to the aqueous periplasm before insertion into the OM and that the energy required to insert a folded protein into the membrane would be very high.

b) The budding model

In this model, it is proposed that the  $\beta$ -barrel domain of BamA opens upon interaction with the client unfolded OMP (Fig. 6B). The  $\beta$ -strand 1 of BamA interacts with the  $\beta$ -signal of the client protein. Then, the client protein undergoes folding by incorporating  $\beta$ -hairpins of the substrates consecutively. The distortion of the membrane created by BamA could facilitate the adding of  $\beta$ -hairpins, one at a time.

Analysis by crosslink between the *E. coli* EspP autotransporter OMP and BamA or between a mitochondrial porin and the mitochondrial BamA-homolog Sam50 showed that these  $\beta$ -barrel proteins were folded following a step-by-step mechanism which is compatible with this budding mechanism (Doyle and Bernstein, 2019; Höhr et al., 2018; Noinaj et al., 2014; Ranava et al., 2018).

c) The  $\beta$ -barrel-elongation model

More recently, the budding model has been refined with the proposal of a mechanism where OMPs first form a  $\beta$ -sheet in continuity with BamA  $\beta$ -strand 1 creating a hybrid surface. The prefolded  $\beta$ -sheet of assembling OMPs undergoes a swing-type movement (Fig. 6C). According to this model, the client OMP could fold partially either at the periplasm or in the vicinity of the membrane, interacting with the open structure of BamA. The barrel would close its seam, because the interaction of the client protein with itself would be energetically more favorable than that of the hybrid barrel. A recent evolution of this model suggests that the forming  $\beta$ -sheet of the client OMP sheet can lead to a deflection of the plane of the membrane layer. By a “spring” effect, the elasticity of the membrane would contribute to promote a late step of OMP folding, probably inducing the formation of a new seam in the barrel of the nascent OMP (Doyle et al., 2022; Horne and Radford, 2022; Lee et al., 2019).

### 3.2.5 Assembly of some OMPs not only depends on BAM

The translocation and assembly module (TAM) is a two-subunit complex, composed by TamA and TamB (Selkrig et al., 2012). This complex participates in the assembly of a subset of OMPs, including some autotransporters and the fimbrial usher protein FimD. It has been shown that biogenesis of autotransporter OMPs such as p1121 of *Citrobacter rodentium* (heterologously expressed in *E. coli*) or EhaA and Ag43 of *E. coli* benefit from the expression of TAM. Neither TamA nor TamB are essential; however, it has been shown that the deletion of their encoding genes causes the accumulation of autotransporters in the periplasm and that capacity of virulence or colonization is reduced in several bacteria (Heinz et al., 2015; Selkrig et al., 2014, 2012; Stubenrauch et al., 2016).

Like BamA, TamA is a member of the Omp85 superfamily (Bamert et al., 2017; Heinz et al., 2015; Selkrig et al., 2015) with only three POTRA domains in the periplasmic space. TamB is an IM protein with a N-terminal transmembrane domain and a large C-terminal periplasmic soluble domain and possesses a conserved C-terminal DUF490 (TamB<sup>925-1259</sup>) suspected to mediate the interaction with the POTRA domains of TamA. A portion of the DUF490 domain of TamB has been resolved by crystallography revealing a characteristic  $\beta$ -taco fold that suggests this portion may act as an hydrophobic cavity that could bind substrates, such as hydrophobic proteins or lipids (Josts et al., 2017). Indeed, the seven C-terminal amino acids of TamB are reported to be critical for the interaction with TamA (Bamert et al., 2017; Heinz et al., 2015; Selkrig et al., 2012). The mechanism for the function of the TAM is not yet clear. Nevertheless, it has been suggested that POTRA domains of TamA may act as a lever arm via the interaction of TamB, that may cause a destabilization of the OM or a movement of TamA-bound client proteins, thus promoting somehow OMP assembly (Albenne and Ieva, 2017; Selkrig et al., 2014).

It was shown in *E. coli* that biogenesis of the chaperone-usher protein FimD requires both the BAM complex and the TAM for its efficient assembly in the OM (Costa et al., 2015; Selkrig et al., 2012; Stubenrauch et al., 2016). Regarding the conservation of this protein, most proteobacteria contain the TAM, almost all diderm bacteria encode TamB-like proteins with a DUF490 domain, but many other bacterial phyla do not contain TamA (Heinz et al., 2015). The evolutionary conservation of TamB has attracted a great deal of interest and some studies suggest that TamB plays an important but yet-to-be-identified function other than its role in association with TamA. For instance, studies on *Borrelia burgdorferi* (which does not encode *tamA*) show a functional complex between BamA and the protein encoded by a *tamB* orthologue (Iqbal et al., 2016). This study raises the question whether TamB (or TamB-like

proteins) may also interact with BamA in organisms that express both complexes, such as *E. coli*. Furthermore, a global interactome analysis conducted on the envelope of *E. coli* provided some evidence for an interaction between the BAM complex and the module TAM (Babu et al., 2017).

In general, it is clear that an interplay between BAM and TAM exists and that this may lead to a functional role in biogenesis of OMPs or some related function. Questions remain to be elucidated, such as if these proteins interact in some specific conditions (such as stress) or to accomplish the biogenesis of a particular class of OMPs or of most OMPs. Moreover, the interaction between the BAM complex and the transenvelope organized module TAM could help solving some questions concerning how the OM insertases harness energy to promote OMP folding, given that TamB spans the IM, where several forms of energy sources are available, including ATP, the PMF as well as an energy potential stored in the form of turgor pressure.

### 3.3 LPS biogenesis and transport to the OM

Another main component of the envelope is LPS in the external leaflet of the OM. The Lipopolysaccharide Transport (LPT) complex transports molecules of LPS from the IM to the external leaflet of the OM (Fig. 2C). The LPT complex is a multiprotein envelope-spanning complex composed by two subcomplexes: one at the IM and the other at the OM connected by the periplasmic component LptA.

The first subcomplex is at the IM and it is composed by a dimer of the ABC transporter protein LptB that associates with the transenvelope domains of one copy of LptFG. A molecule of LptC permits to create the interphase between the IM subcomplex and LptA (Narita and Tokuda, 2009). It has been proposed that upon energization of the IM subcomplex, a molecule of LPS can detach from the IM, similarly to the mechanisms of lipoprotein transport by the LOL machinery. The protein LptC folds into a  $\beta$ -jellyroll that could accommodate the hydrophobic moiety of LPS molecules (Sperandeo et al., 2017).

The OM LPS translocon is composed by the  $\beta$ -barrel protein LptD and the OM lipoprotein LptE. LptD is the largest monomeric OMP, composed by 26  $\beta$ -strands and a  $\beta$ -jellyroll domain. Biogenesis of LptD depends on the activity of the BAM complex that folds LptD around the lipoprotein LptE. Folding of LptD has been previously described as a step-wise and relatively slow process, as it requires many factors that promote its correct biogenesis. Mature LptD contains two non-consecutive disulfide bonds that are formed by the activity of the periplasmic oxidative folding machinery DsbA and DsbC (Chng et al., 2012; Ruiz et al., 2010).

The periplasmic component LptA creates a bridge that carries LPS from the IM to the OM. LptC and LptD folds into a  $\beta$ -jellyroll structure extending the protein-LPS contact interface across the periplasm (Sperandeo et al., 2017). After the translocation of LPS through the periplasm, LptD receives this molecule via its  $\beta$ -jellyroll domain. This  $\beta$ -jellyroll bridge of LptCAD is only able to form after assembly of LptDE subcomplex (Sperandeo et al., 2017). The precise copy number of the periplasmic component LptA is still unclear, as it forms homooligomers (Merten et al., 2012). However it has been speculated that a dimer of LptA could be enough to permit the transport of LPS to the OM, as in its homologue in *P. aeruginosa* (Shapiro et al., 2014).

It has been suggested that activity of this OM-subcomplex is dependent on the activity of a lateral gate on LptD, that would probably form between the first and the last  $\beta$ -strands of its  $\beta$ -barrel domain. Recently, a structural study performed by using nanobodies derivative molecules bound to the LptDE complex and cryoEM analysis provided evidence for partial opening of the LptD lateral gate (Botte et al., 2022). It is speculated that LPS can pass through the lateral gate of LptD and it can be positioned at the outer leaflet of the OM (Sperandeo et al., 2017).

## 4 Transport of substrates across the bacterial envelope

Substrates of the OM are synthesized at the cytoplasm, however they can only reach their final destination via envelope machineries that can promote their translocation. In this chapter, we will focus on the transport of proteins and lipids through the bacterial envelope, with an overview of secretion systems.

### 4.1 An overview of secretion systems in *E. coli*

Gram-negative bacteria have developed machineries to secrete proteins to their cell surface or across the OM into the extracellular milieu. These secreted proteins play a variety of functions, including exchange of metabolites, nutrients and noxious molecules like antibiotics, transport of DNA, and the envelope building blocks including lipids and proteins. The protein components of these machineries can be transported to the cell surface in one or two distinct steps. One-step mechanisms are mediated via the type I secretion system (T1SS), T3SS, T4SS and T6SS and they require transenvelope machineries that span both the IM and OM. In contrast to the one-step mechanism, a two-step translocation mechanism implies that proteins are first translocated into the periplasm via the Sec or TAT pathways and from there they are further exported via OM machineries, via the T2SS, T5SS, T7SS and T8SS. T7SS, initially discovered in *Mycobacteria*, is also present in other Gram-positive bacteria, whereas its presence in Gram-negative bacteria is debated (Kengmo Tchoupa et al., 2020; Unnikrishnan et al., 2017). Generally, these systems are not constitutively active and they are activated by the presence of toxic molecules in the cytoplasm, the export of virulence factors, in the response to invade a host, etc. (Costa et al., 2015). In this manuscript we will not discuss the more recently discovered T10SS nor T11SS (Filloux, 2022; Gómez-Santos et al., 2019; Palmer et al., 2021).

#### 4.1.1 *One-step secretion systems*

##### *Type I Secretion System (T1SS) and resistance-nodulation-division (RND) efflux pumps*

The T1SS is involved in the secretion of substrates from the cytoplasm to the extracellular environment. Some bacteria can secrete virulence factors and this system is closely related to the RND efflux pumps, used to eliminate secondary metabolites and antibiotics that contributes to antibacterial resistance. In this system, there are three main elements to take into account: an IM component (IMC), a membrane fusion protein (MFP) in the periplasmic space and TolC, an OMP that serves as a channel of secretion. The IMC is responsible for the first steps of recognition of the particles to secrete. Recent crystal structures have revealed different topologies this domain may adopt to engage a substrate at the cytoplasm. Energy is harnessed

from ATP hydrolysis by the ATPase of the ABC transporter (for T1SS) or by protein gradient (for RND efflux pumps) (Costa et al., 2015; Du et al., 2014; Morgan et al., 2017).

The MFP domain is pre-associated with the IMC domain and usually these two can only recognize one set of substrate, while TolC can associate with several IMC-MFP subcomplexes (Costa et al., 2015). Trimers of TolC (and its orthologues) form of a single  $\beta$ -barrel structure where each monomer contributes 4  $\beta$ -strands to the barrel. The stoichiometry of the IMC/MFP/TolC complex can vary from complex to complex, for example in the case of the efflux pump AcrB/AcrA/TolC, there is a 3/6/3 ratio, respectively (Du et al., 2014; Wang et al., 2017). When the substrates bind an IMC-MFP complex, it enables association with the periplasmic domain of TolC to enable the release of the substrate thanks to an energization at the IM (Costa et al., 2015).

#### *Type III Secretion System (T3SS)*

Bacteria can transport effector proteins to a host environment thanks to the T3SS. It consists in a machinery that spans the two membranes of Gram-negative bacteria with forming a syringe-like mechanism. The injected effectors may facilitate host invasion and colonization, like in *Salmonella enteritica* (discussed in this paragraph). The T3SS is composed of approx. 25 proteins in two main substructures. It is formed by two concentric rings (composed by PrgH, K) that are arranged at the IM in interaction with additional components (such as SpaP-S and InvA). The formation of a multimer of the protein InvG (15 copies) permits the formation of an OM ring. This multimer interacts with the PrgH-PrgK pair to create a lumen for the formation of the needle.

The protein PgrI is arranged in a polymer of more than 100 copies in the shape of a needle of approx. 30-70 nm and 10-13 nm in width. It has been shown that the lumen of the OM ring may have a diameter of 25 Å. Because the diameter is rather small, it is suggested that the substrate is unfolded upon translocation. Substrates may be carried by cytoplasmic components to their target and recruitment to the machinery. The translocation is ATP-dependent by the action of a cytosolic component, such as the ATPase InvC.

#### *Type IV Secretion System (T4SS)*

One of the function of the T4SS is to translocate DNA (in addition of proteins) to promote cell transformation (Jin et al., 1990). The best characterized systems are from the Vir family (VirB1-VirB11 and VirD4) from *Agrobacterium tumefaciens* and the T4SS produced by the pKM101 and R388 conjugative plasmids from *E. coli* (Costa et al., 2015).



The structure of a T4SS of *E. coli* expressed from R388 conjugative plasmid was obtained by electron microscopy (Low et al., 2014). It shows a core complex at the OM that spans the periplasmic space by a stem that connects to a bifurcate IM complex. The OM complex is composed by VirB7, VirB9 and VirB10 (14 copies each) and they arrange in the shape of a pore. The composition of the stem domain is not yet known. The bifurcate IM complex is composed by VirB3, VirB4, VirB6, VirB8, and VirB10 N-terminus. The copy number of these subunits varies, the 2 barrels of six copies each of VirB3-VirB4 are observed facing the cytoplasm. VirB6 and VirB8 contain 12 and 24 copies, respectively and interact with the N-terminal moiety of the 14 copies of VirB10 (Costa et al., 2015).

It was suggested this system may have a role in cell-to-cell adhesion via a pili formed in the lumen of the pore by the polymerization of VirB2 containing VirB5 at the tip of the pilus (Aly and Baron, 2007). It has been proposed that T4SS may switch between pilus biogenesis and substrate translocation mode (Ripoll-Rozada et al., 2013).

#### *Type VI Secretion System (T6SS)*

Some bacteria use the T6SS to translocate toxic effector proteins playing a role in pathogenesis and bacterial competition. The T6SS consists in a contractile machinery that injects toxins directly in a prey cell. It comprises 13 conserved core components and some accessory components that form a membrane, a baseplate and a tail complex (Gallique et al., 2017). The membrane complex serves as a docking station and platform and it is composed by the proteins TssJ, TssL and TssM that are able to create a pore-like architecture through the envelope. TssM mediates the interaction between TssJ (at the OM) and TssL (at the IM). The membrane complex is in contact with the baseplate complex at the cytoplasm, composed by the proteins TssK, TssFG and TssE. The baseplate complex is the interphase with the tail complex. The VgrG trimer forms a spike-like structure at the lumen of the baseplate and the tail complex. The tail complex is a polymer of Haemolysin co-regulated protein (Hcp) that forms hexameric rings (inner tube) and TssB-TssC that form a protective structure to the Hcp polymer, creating an external tube of the tail (Costa et al., 2015). The mechanism of secretion is proposed to take into account a contraction mechanism of the tail complex to promote translocation of an effector protein (sometimes multiple effectors), as a syringe through the lumen of the core complex (formed by the Hcp polymer). For this mechanism, ClpV has a role in the energization of the complex by hydrolysis of ATP (Bönemann et al., 2009).

#### 4.1.2 Two-step secretion systems

##### *Type II Secretion System (T2SS)*

T2SS has been previously linked to export of virulence factors and exoproteins in *P. aeruginosa*, *K. pneumoniae* and *V. cholerae* (Nivaskumar and Francetic, 2014). The overall architecture of the machinery responsible of secretion involves between 12 and 15 members of the general secretory (Gsp) pathway, assembled in the envelope. We can divide it in 4 main parts: an OM complex, an IM platform, a cytoplasmic ATPase and a periplasmic pseudopilus (Costa et al., 2015).

The OM complex is composed by GspD that forms dodecamers spanning the OM (also called T2SS secretin). Protomers of GspD contain a C-terminal domain that forms a pore through the IM, and four periplasmic N-terminal domains. When GspD is in complex it can permit the forming of a pore of approx. 155 Å in diameter, as observed in a *V. cholerae* structure (Reichow et al., 2010). The IM platform is composed by the proteins GspC, GspF, GspL and GspM. Of those, GspC interacts with GspD in the periplasm, while GspF, GspL and GspM preserve the interaction with the IM or other cellular partners (Nivaskumar and Francetic, 2014). The cytoplasmic ATPase is GspE, which is a ring shaped hexamer that interacts with GspL and GspF. Finally, the periplasmic pseudopilus is composed of GspG, which is a major component, and GspH, GspI, GspJ, GspK, which are minor components (Costa et al., 2015).

Translocation of substrates can be done via the Sec (Pugsley et al., 1991) or the TAT pathway if the substrate has to be previously folded before export (Voulhoux et al., 2001). Then, by some mechanism still unknown, the secretin can open to allow the entry of the substrate. In a movement piston-like, the substrate is propelled into the extracellular space (Costa et al., 2015; Nivaskumar and Francetic, 2014).

##### *Type V Secretion System (T5SS)*

Autotransporters are a family of OMPs classified in the type V secretion system (T5SS), which is subdivided in five different categories (a, b, c, d and e) They contain a signal peptide and two domains, an N-terminal passenger domain and a C-terminal  $\beta$ -barrel domain (Albenne and Ieva, 2017; Ieva et al., 2011; Wells et al., 2007). After transport into the periplasm by the Sec translocon, the C-terminal domain is inserted in the OM as a  $\beta$ -barrel protein (OMP with 12  $\beta$ -strands) and this process permits the translocation of the N-terminal passenger domain. The passenger domain is involved in virulence and they are found in a wide range of Gram-negative bacteria (Costa et al., 2015; Leo et al., 2012). Initially, the transport of these proteins across the bacterial envelope was thought to be autonomous (from there, the name), but studies have

shown that this transport is assisted by two translocase machineries: the BAM and TAM complexes (Costa et al. 2015; Selkrig 2014; Albenne and Ieva 2017).

Biogenesis of classical T5SSa autotransporters, such as EspP (a Serine Protease autotransporter of Enterobacteriaceae or SPATE from Enterohemorrhagic *E. coli*) depends on the activity of the BAM complex (Doyle and Bernstein, 2019; Ieva et al., 2011; Sauri et al., 2009). EspP forms part of the T5SSa and it is a protease in pathogenic *E. coli*. After folding of the  $\beta$ -barrel domain, the passenger domain is translocated to cell surface where it can be proteolytically cleaved, with the exception of some autotransporters. The cleavage between the passenger and the  $\beta$ -barrel domains can be autoproteolytic (such as for SPATE autotransporters, including EspP) or can involve other proteases. The passenger domain of autotransporters often play roles associated to virulence, as well as adhesion and motility (Grijpstra et al., 2013).

T5SSb is also named “two-partner secretion system” and it is characterized for the presence of two polypeptide chains encoded in one operon, TpsB (the translocator) and TpsA (the secreted passenger domain). TpsB is a 16 stranded  $\beta$ -barrel protein member of the Omp85 family, containing two POTRA domains (Meuskens et al., 2019).

T5SSc is also called “trimeric autotransporter adhesins” and it is characterized for the interaction of three molecules to complete a  $\beta$ -barrel (each one with 4  $\beta$ -strands). The passenger domain forms a trimeric structure with a lollipop shape. Proteins of the T5SSc are generally adhesins (Meuskens et al., 2019).

T5SSd resembles a hybrid between T5SSa and T5SSb, because it consists in a  $\beta$ -barrel domain of 16  $\beta$ -strands and only one POTRA domain, similar to T5SSb. The passenger domain remains attached and their functionality seems limited to a lipase/esterase (da Mata Madeira et al., 2016; Meuskens et al., 2019).

T5SSe is called “inverted autotransporter” and it presents a domain organization inverted with respect to the T5SSa or classical autotransporter. In the T5SSe the passenger domain is at the C-terminus and the  $\beta$ -barrel domain is at its N-terminus. The passenger domain remains attached after export (Meuskens et al., 2019).

Finally, the T5SSf was proposed as an additional group. It is still under debate whether it belongs to this secretion system, as there are some differences with classical T5SS. The first difference is that the  $\beta$ -barrel domain is only eight  $\beta$ -strands, making a smaller  $\beta$ -barrel than the rest of the others. Second, the fact the passenger domain is not situated at any extremity could mean that it could be an extended loop of the  $\beta$ -barrel domain and not a passenger domain (Coppens et al., 2018; Meuskens et al., 2019).

### *Type VIII Secretion System (T8SS) or curli biogenesis*

This secretion system is involved in the formation of curli that is a type of amyloid that promote the formation of protective biofilm. This system includes the activity of CsgABCDEF. Curli is composed by a polymer of CsgA and CsgB in the extracellular space. Transport of these proteins across the IM is mediated by the Sec translocon and after this first step of translocation, they are secreted by a multimeric complex formed by the OM lipoprotein CsgG that generates a 36  $\beta$ -strands pore in the OM. In addition, CsgG interacts with two accessory factors CsgE and CsgF (Goyal et al., 2014). CsgE forms a nonamer at the periplasmic side of the OM and acts as an adaptor to plug in CsgG and thus creating a cage for protein secretion. It is thought that the protein CsgF stimulates the formation of CsgA-CsgB polymer at the extracellular space. The role of CsgC is not yet well characterized. It is speculated that CsgB nucleates the polymerization of CgsA into curli fibers after translocation (Costa et al., 2015).

### *Chaperone-usher pathway*

The chaperone-usher pathway is involved in the biogenesis of pili or fimbriae that has a role for cell recognition and attachment. It is composed by proteins encoded by the *fim* (for type I pilus) and *pap* (for P pili proteins) operons.

The main subunits involved in this system are FimD (type I) and PapC (P pili) and they are  $\beta$ -barrel proteins with an architecture of 24  $\beta$ -strands, one of the largest OMPs described in the literature (Horne et al., 2020). It has been proposed that biogenesis of this type of OMPs benefits from the activity of the TAM (Bamert et al., 2017; Stubenrauch et al., 2016). Biogenesis of FimD/PapC is required and then, these proteins catalyze the formation of a polymer of FimA/PapA to create the extracellular extension. The mechanism of polymerization is thought to be via a donor strand exchange, in which the pilus assembles by stabilizing  $\beta$ -strands from one molecule to another. A flexible tip comprises the proteins FimH, FimG and FimF or PapE, PapF, PapK and PapG. After the export of those subunits by the Sec translocase, FimC or PapD are molecular chaperones that prevent their misfolding in the periplasm during their transport to the OM components (Costa et al., 2015).

### *Type IX Secretion System (T9SS)*

T9SS is a recently discovered secretion system, present in Bacteroidetes phylum (Lauber et al., 2018). It has been related to virulence in some bacteria (Lasica et al., 2017) and proteins transported via this secretion system are generally large. At least 15 proteins are involved in

translocation. A transperiplasmic motor is made by proteins GldK, GldL, GldM and GldM, energized from the IM by PMF. Then, proteins PorQ, PorU, PorV and PorZ create a cell surface-exposed complex in the OM. The main component in the OM is the recently discovered SprA, containing 36  $\beta$ -strands forming a barrel with a diameter of 70 Å. (Lauber et al., 2018).

The structural data obtained for SprA suggests it can form a water-filled conduct to promote the transport of large folded proteins. The protein PorV at the OM may serve as a sealing protein of the pore of SprA and act in regulating transport of substrates, possibly by their recognition inside the cavity and then by promoting their translocation. The presence of PorV may help in the monodirectional sense of translocation in the cavity of SprA (Lauber et al., 2018). Protein substrates are translocated to the periplasm via the Sec translocase and then they are targeted to the OM components via a C-terminal domain (CTD) signal composed of approx. 80 amino acids (Gorasia et al., 2020).

## 5 Homeostasis of the Gram-negative bacterial envelope

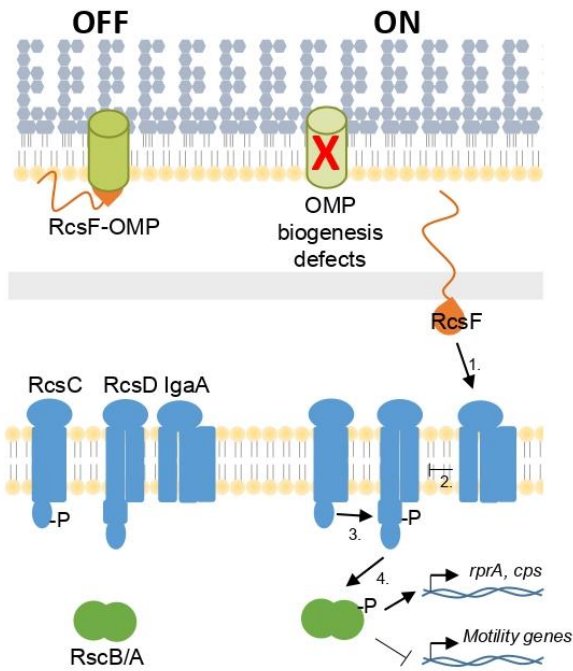
Biogenesis of the bacterial envelope is a crossroads of processes involving several machineries at the IM, PG and OM with periplasmic partners. As previously discussed, biogenesis of OM proteins depends on mainly two machineries: the BAM complex and the LOL machinery. Dysfunction of these machineries leads to the activation of extracytoplasmic stress responses (ESR). There are several ESR and we will discuss about Rcs, Cpx and  $\sigma^E$ , all linked to the activity of the transport of substrates across the envelope. There exists however other ESR, such as the Bae, Psp and Dpi not discussed in this manuscript (Delhaye et al., 2019a).

### 5.1 The Rcs response for PG homeostasis, LPS damages and BAM function

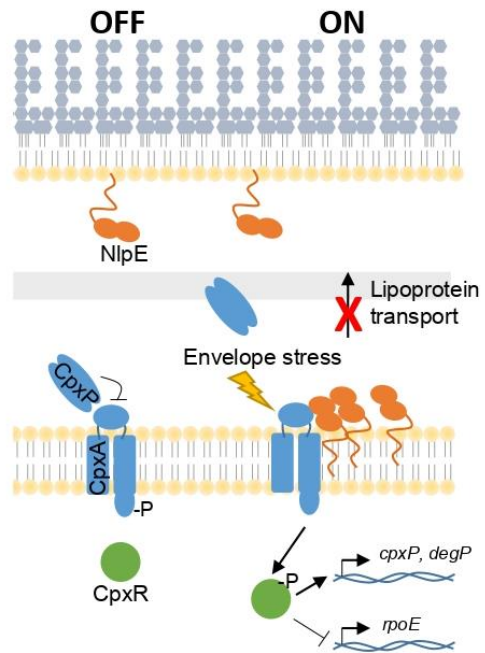
The Rcs stress response is one the most complex signaling systems and it is in charge of promoting homeostasis in response to problems in the PG and the OM (Fig. 7A) (Cho et al., 2014; Evans et al., 2013; Konovalova et al., 2014; Meng et al., 2021). It is composed by at least six components: the core proteins RcsB, RcsC and RcsD, the IM IgaA, the cytosolic partner RcsA and the protein regulators RcsF and YrfF (Cho et al., 2014; Meng et al., 2021).

Activation of this ESR consists in the autophosphorylation of RcsC at its histidine kinase domain, at the cytoplasm. Phosphorylation of RcsC is induced via stress stimuli. It has been demonstrated that RcsF is able to interact with IgaA to trigger the Rcs response (Cho et al., 2014). In a recent study it was demonstrated that the protein IgaA negatively regulates RcsD (Wall et al., 2020). This leads to the model where the RcsF-IgaA interaction leads to the activation of the IM proteins RcsC/D. RcsC autophosphorylates and then it phosphorylates RcsD to trigger stress response via the activation of RcsB/A dimer at the cytosol (Mitchell and Silhavy, 2019). This activation consists in the transfer of a phosphoryl group to RcsB. RcsB is a DNA-binding transcriptional activator and it can form homo or heterodimers to promote expression of genes involved in restoring homeostasis (Meng et al., 2021). When RcsB forms a homodimer, it promotes the upregulation of RprA, controlling the expression of factors involved in the formation of biofilm, and negatively regulates *gadA* that is involved in the formation of glutamate decarboxylase synthesis. RcsB can form heterodimers with RcsA to promote the expression of *cps* involved in the production of colanic acid and the downregulation of *flhDC*, involved in motility. The expression of these genes can be used to monitor the activation of the Cpx response (Castanié-Cornet et al., 2014; Cho et al., 2014). Finally, RcsB can form a heteroligomer with BglJ, MatA and GadE to promote the expression of *bgl*, *mat* and *gad*, involved in the production of D-glucoside, Mat fimbria and acid resistance, respectively (Meng et al., 2021).

### A. The Rcs response



### B. The Cpx response



### C. The $\sigma^E$ response

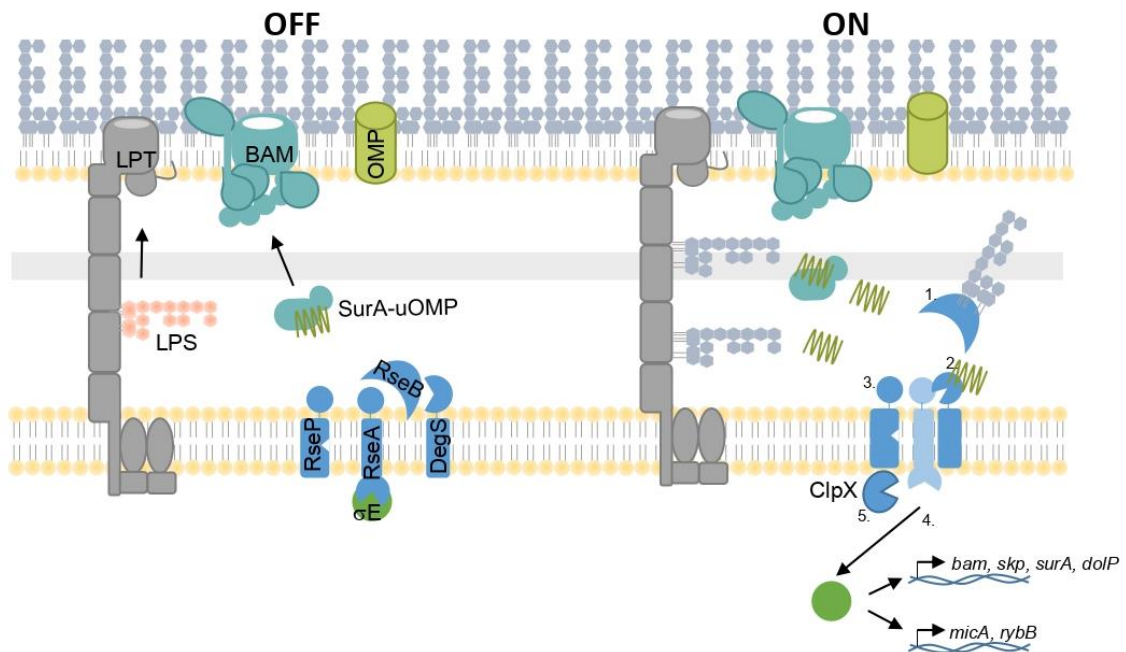


**Figure 7. Stress responses in the Gram-negative bacterial envelope. A. The Rcs stress response.** In non-stressed conditions, a complex between RcsF and an OMP is formed. When there are some problems in the formation of the OMP-RcsF complex, RcsF may interact with IgaA at the IM to and leads the activation of the IM proteins RcsC/D. RcsC autophosphorylates and then it phosphorylates RcsD to trigger stress response via

the activation of RcsB homodimer or RcsB/A heterodimer at the cytosol. This promotes the upregulation of *rprA* or *cps* and the downregulation of motility genes. **B.** The Cpx stress response. In non-stressed conditions, the lipoprotein NlpE is localized at the OM and CpxP protects the IM protein CpxA. When there are some problems in lipoprotein transport or other type of stress in the envelope, CpxP is presumably degraded by DegP and leaves CpxA exposed to autophosphorylation. Then, CpxA phosphorylates CpxR that upregulates genes such as *cpxP* or *degP* and downregulates *rpoE*. **C.** The  $\sigma^E$  stress response. In non-stressed conditions, BAM promotes the biogenesis of OMPs at the OM after they are delivered by chaperone proteins (such as SurA). In parallel, LPS is able to be transported via the LPT pathway. The  $\sigma^E$  factor is sequestered by the IM protein RseA and its periplasmic domain is protected from degradation by DegS at the periplasm by RseB. The transmembrane domain of RseA cannot be degraded by RseP if RseA has its periplasmic domain. When uOMPs and LPS accumulate in the periplasm, the  $\sigma^E$  stress response is triggered. First, a molecule of LPS binds RseB and frees the periplasmic domain of RseA. DegS is activated by the binding of an uOMP and is then able to degrade the periplasmic domain of RseA and this permits RseP to degrade the transmembrane domain of RseA. The degradation of RseA permits that frees the  $\sigma^E$  factor. A cytoplasmic protease (such as ClpX) degrades the cytosolic domain of RseA. The  $\sigma^E$  factor upregulates genes, such as *bam* subunits, *skp*, *degP* and *doiP*, and posttranslationally downregulates OMPs by the production of the sRNAs MicA and RybB.

Recently, the Rcs response has been linked to the activity of the BAM complex. The lipoprotein RcsF is an OM lipoprotein that interacts with OMPs, such as OmpA or OmpC to create a complex. This complex is formed by the activity of BamA to assemble OmpA/C and funnel the lipoprotein RcsF (Cho et al., 2014; Konovalova et al., 2017). It has been debated whether RcsF is exposed to the cell surface by its lipid moiety at its N-terminus (Cho et al., 2014; Konovalova et al., 2014). Recent structural data has revealed the protein RcsF resides in the seam of the  $\beta$ -barrel domain of BamA via the periplasmic side of the OM. It is proposed that BamA may create an inward-to-outward movement that would funnel RcsF to an OMP during its biogenesis, creating an RcsF-OMP complex. The topology of the RcsF-BamA complex suggests RcsF may not be exposed to the cell surface (Rodríguez-Alonso et al., 2020). This leads to the model that the Rcs response system can sense correct functioning of the BAM complex for OMP biogenesis.

## 5.2 The Cpx response for lipoprotein homeostasis

The Cpx stress response is a major actor in promoting homeostasis in *E. coli* and other  $\gamma$ -proteobacteria (Fig. 7B) (Raivio, 2014). It is composed by CpxA at the IM, CpxR at the cytoplasm, CpxP at the periplasm and the lipoprotein NlpE (Delhaye et al., 2019b).

CpxA is an IM protein that can autophosphorylate its histidine kinase domain to promote activation of the transcriptional regulatory protein CpxR at the cytoplasm. CpxA is composed of two transmembrane domains and a periplasmic loop that acts as stress sensor. It has been



suggested that CpxA is able to sense stress by itself (Raivio and Silhavy, 1997). Phosphorylation of CpxA may occur by different stimuli, such as damages in the PG, elevated pH, high salt concentrations, alteration in the IM composition and missfolding of periplasmic and IM proteins (Grabowicz and Silhavy, 2017b; Raivio, 2014). It has been recently proposed that problems in the trafficking of lipoproteins trigger the Cpx response by the activation via the lipoprotein NlpE (Delhaye et al., 2019b). CpxR is a cytoplasmic protein that binds a specific DNA binding site to regulate gene expression (Grabowicz and Silhavy, 2017b; Raivio and Silhavy, 1997), possibly by increasing the activity of the RNA polymerase (Guharajan et al., 2021).

The Cpx response involves the OM lipoprotein NlpE, the stress response sensor. It is composed by two domains: an N- and a C-terminal domain. It has been demonstrated that NlpE acts as a protein sensor that upon damage in the envelope interacts with CpxA to promote signaling cascades and restore homeostasis. It has been demonstrated that the N-terminal domain of NlpE is responsible of activation of Cpx response. It is intriguing how the OM lipoprotein NlpE activates CpxA at the IM, considering the N-terminal domain would be very close to the OM. It has been proposed that during problems in trafficking of lipoproteins, NlpE can induce Cpx response by its accumulation at the IM to promote activation of CpxA (Delhaye et al., 2019b).

The periplasmic protein CpxP acts as a negative regulator of the response. It protects the periplasmic loop of CpxA to prevent the activation of the Cpx response. It has been demonstrated that DegP is able to degrade CpxP (Buelow and Raivio, 2005). CpxR activation leads to the upregulation of both *degP* and *cpxP* (Yamamoto and Ishihama, 2006), this suggests that Cpx stress response can be autoregulated after homeostasis is restored.

Some of the upregulated genes include the chaperone protease DegP, the periplasmic chaperones CpxP and Spy, the bond-forming oxidoreductase DsbA, etc. This upregulation suggest that Cpx stress response is implicated in processes of degradation and folding of envelope proteins (Hews et al., 2019).

NlpE has disulfide bonds at its N- and C-terminal domains. The formation of NlpE disulfide bonds has been related to its activity to induce stress response via the activation of the Cpx response. This maturation of NlpE is accomplished via the oxidoreductase DsbA, as a *dsbA* mutant strain triggers Cpx response dependent on NlpE. Interestingly, when Cpx response is active, *dsbA* is upregulated that suggests the stress response has a mechanism to autoregulate its protein sensor (Delhaye et al., 2019b).

### 5.3 The $\sigma^E$ response for OMPs and LPS homeostasis

The  $\sigma^E$  stress response is one of the best-characterized envelope stress responses (Fig. 7C). The name of this stress response comes from the name of the alternative  $\sigma$  factor, RpoE or  $\sigma^E$ . This factor permits the RNA polymerase to transcribe genes that are involved in the homeostasis of the bacterial envelope (Rhodius et al., 2005).

In non-stressed conditions, the  $\sigma^E$  factor is sequestered by the anti- $\sigma^E$  factor RseA (Missiakas et al., 1997). RseA is an IM protein that contains a periplasmic, a transmembrane and a cytoplasmic domain. RseA sequesters  $\sigma^E$  by its cytoplasmic domain, but it can be released by a series of proteolytic processes that enable its association to the RNA polymerase and promote gene transcription. RseB protects RseA to prevent its degradation from the proteases DegS and RseP (Lima et al., 2013).

It has been previously reported that deletion of *surA* triggers  $\sigma^E$  response, resulting in lower levels of OMPs and susceptibility to antibiotics and SDS (Onufryk et al., 2005; Rouvière and Gross, 1996), leading to the observation that malfunctions in the OMP biogenesis pathway leads to trigger  $\sigma^E$  stress response. In *E. coli*, it has been proposed that activation of the  $\sigma^E$  stress response involves two factors: the accumulation in the periplasm of uOMPs and LPS. LPS assembly intermediates that accumulate in the periplasm are recognized by RseB. The recognition of LPS is mediated probably via its hydrophobic moiety (Lima et al., 2013). It has been debated how it is possible that LPS, a highly hydrophobic molecule can be free at the periplasm. For this, some authors propose that another protein partner could be mediating the transport from the LPT complex to interact with RseB under stressed conditions (Grabowicz and Silhavy, 2017b).

After RseB interacts with LPS, RseA becomes more accessible to proteases. DegS recognizes uOMPs via its PDZ periplasmic domain and this activates DegS to degrade the periplasmic domain of RseA (Walsh et al., 2003). The IM protein RseP is able to degrade RseA only after partial degradation by DegS, otherwise it cannot be active (Akiyama et al., 2015). This degradation frees the cytoplasmic domain of RseA and then cytoplasmic proteases as ClpXP can release the  $\sigma^E$  factor (Grabowicz and Silhavy, 2017b). Gene transcription involves mainly two mechanisms: the upregulation of biogenesis factors, and the posttranslational downregulation of OMPs via sRNA (Grabowicz and Silhavy, 2017b).

One of the consequences of  $\sigma^E$  stress response is the decrease in OMP levels. This is possible thanks to the posttranslational downregulation of small non-coding RNAs *micA* and *rybB*. Both genes have strong promoters and produce sRNA. MicA is able to regulate OmpA and LamB

production, while RybB is able to control OmpC and OmpX (Coornaert et al., 2010; Johansen et al., 2006). This process is essential to alleviate the workload for biogenesis machineries.

Upregulation of biogenesis factors include several proteins, such as subunits of the BAM complex, molecular chaperones such as SurA and Skp, DsbC (involved in proper maturation of LptD), DegP and proteins of still unknown function (Dartigalongue et al., 2001). Interestingly, *degP* is one of the genes that are upregulated during both  $\sigma^E$  and Cpx stress response.

Altogether, the activity of the BAM complex to promote OMP biogenesis seems to be a process that involves the regulation of several molecular actors in an interconnected network (Fig. 8):

- i) Upregulation of OMP or malfunctions in their process of biogenesis can cause their accumulation at the periplasm triggering  $\sigma^E$  that promotes upregulation of biogenesis factors and posttranslational downregulation of OMP synthesis (Lima et al., 2013). The Cpx response also triggers this posttranslational downregulation of OMPs, however it seems that Cpx may act as a second step stress response by modulating the activity of  $\sigma^E$ . Indeed, CpxR posttranslationally downregulates *rpoE* (that codes for  $\sigma^E$ ) (Grabowicz and Silhavy, 2017b).
- ii) During activation of  $\sigma^E$  and Cpx responses, *degP* is upregulated, which facilitates alleviating stress response by degradation of unfolded/aberrant OMPs (Combs and Silhavy, 2022). Malfunctions in the OMP biogenesis pathway can cause aberrant localization of OMPs by Skp. Skp is a  $\sigma^E$  upregulated gene, but posttranslationally downregulated in the Cpx by the sRNA CpxQ. At an early stage of envelope stress, Skp would be needed to hand OMPs over to DegP for their degradation. Subsequently, *skp* would be downregulated by CpxQ to reduce its activity afterwards and prevent their misslocalization in the IM supposedly by a poorly understood mechanism of spontaneous insertion (Gerken et al., 2010; Grabowicz et al., 2016). In this context, Cpx would help to control a possible detrimental effect of  $\sigma^E$  activation.
- iii) Malfunctions of BAM causes Rcs response by failing to form the OMP-RcsF complex (Cho et al., 2014; Rodríguez-Alonso et al., 2020). Moreover, when RcsF is stalled at the BAM complex by deletion of *bamB* and *bamE*, cells are not viable. Conditional deletion *bamB* and *bamE* triggers  $\sigma^E$  response to restore homeostasis of non-functional BAM and this effect is corrected by the deletion of RcsF (Hart et al., 2019a).

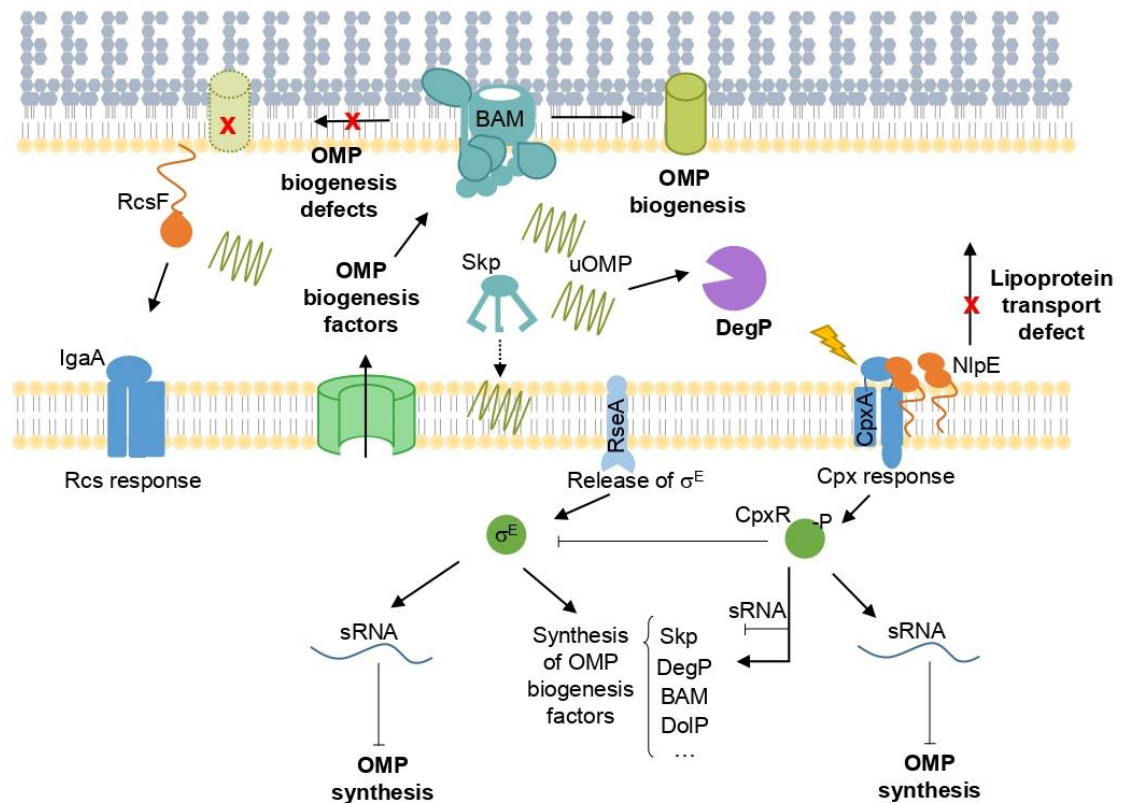


**Figure 8. An interconnected network of stress responses regulates the activity of the BAM complex.** The BAM complex promotes biogenesis of OMPs and malfunctions in its activity may trigger stress responses. Malfunctions of BAM may lead to activation of Rcs response by failing to form OMP-RcsF complex. When uOMPs accumulate at the periplasm triggers  $\sigma^E$  stress response, upregulating biogenesis factors such as BAM, Skp, DegP and DoIP and posttranslational downregulation of OMPs. The Cpx response triggers posttranslational downregulation of genes that code for OMPs, Skp and  $\sigma^E$ . Skp activity involves the handling of uOMPs to DegP, but also to the misslocalization of OMPs at the IM.

#### 5.4 DoIP is a poorly characterized factor upregulated by the $\sigma^E$ response.

The *doIP* gene (formerly known as *yraP*) is a constitutively expressed gene that can be upregulated in a  $\sigma^E$ -dependent manner, but whose function remains ill-defined. It encodes a lipoprotein that has been linked to maintenance of OM homeostasis. In fact the deletion of *doIP* is synthetically lethal with the deletion of *surA* (Onufryk et al., 2005), suggesting a link with OMP biogenesis involving the BAM pathway. The deletion of *doIP* also leads to sensitivity to SDS, suggesting a problem in preserving the permeability barrier of the OM (Onufryk et al., 2005). More recently DoIP has also been linked to activation of septal PG hydrolysis by the amidase AmiC (Goyal et al., 2014), however the mechanisms that mediates such regulation remains unexplored (Fig. 9A). The structure of a non-native form of DoIP expressed as a water-soluble protein in the periplasm of *E. coli* was solved by NMR in 2020 (Fig. 9B). The structure

shows two BON domains downstream of a flexible N-terminal region (Bryant et al., 2020). This form of DoIP was shown to be monomeric. In contrast, it was suggested recently that the homologue of DoIP in *Acinetobacter baumannii*, BonA, forms dimers that supposedly associate in a larger decameric complex (Fig. 9C) (Grinter et al., 2021). It has been proposed that BON domains are domains of approximately 60 residues each that can interact with hydrophobic ligands (Yeats and Bateman, 2003). Very recently, in the case of DoIP, it was shown that only BON 2 contains a lipid binding site at its position W127, where it binds to negatively charged phospholipids (Bryant et al., 2020).

Similar to what was observed for DoIP, its orthologue in *Neisseria meningitidis* (GNA2091) was shown to be important for OM homeostasis (Bos et al., 2014; Seib et al., 2019). Notably, GNA2091 is also a component of a recently developed and marketed recombinant vaccine against serogroup B meningococcus (Seib et al., 2019). In addition, a different study conducted on another dual-BON domain protein OsmY of *E. coli* revealed that this protein promotes biogenesis of a major family of OMPs, the autotransporters (Yan et al., 2019). Notably, *osmY* is regulated by RpoS (or  $\sigma^S$ ), the general stress response transcription initiation factor. Taken together, these findings highlight that dual-BON domain proteins could play roles important to overcome stress conditions, although especially in the case of DoIP and GNA2091 their molecular functions remain unknown.

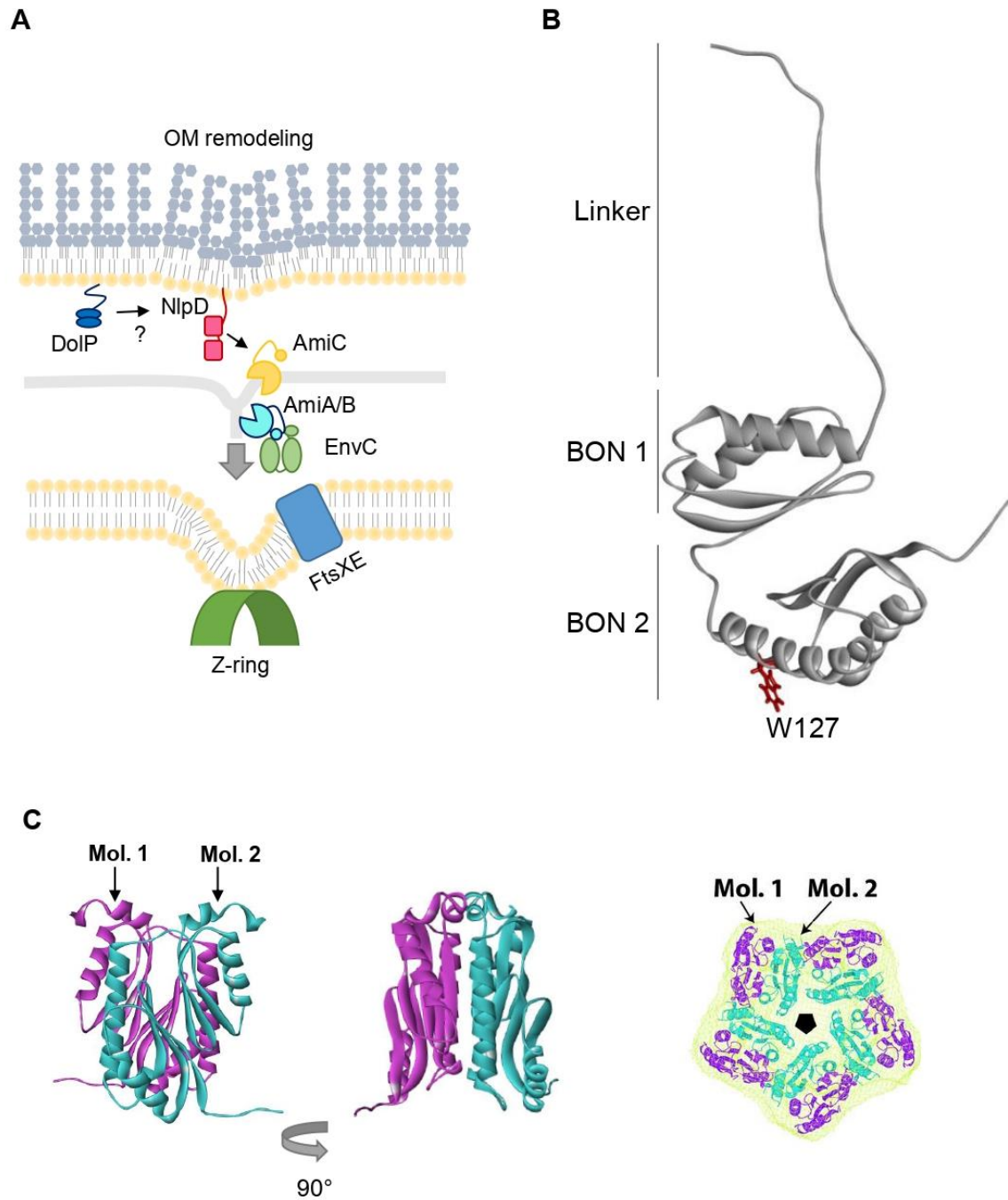


**Figure 9. DolP is a  $\sigma^E$ -induced factor.** **A.** DolP may have a role in the activation of AmiC during late steps of cell division. **B.** Structure of DolP reveals two BON domains and it contains a lipid-binding motif in BON 2, at position W127 (PDB: 7A2D). **C.** The homolog of DolP, BonA from *Acinetobacter baumannii*, can form large homooligomers formed by a pentamer of dimers (adapted from Grinter et al., 2021).

## **Work objective**

Multiple processes of lipid and protein transport contribute to form the Gram-negative bacterial envelope. Mechanisms of biogenesis of OMPs by the BAM complex have been studied from a structural and functional point of view. Sophisticated models have been proposed concerning how the BAM complex promotes the assembly of OMPs in the bacterial envelope. The activity of other envelope machineries can be beneficial for some of the functions of BAM, including the SEC translocon in the IM and the transenvelope TAM module. Finally, envelope stress surveillance mechanisms monitor the activity of the BAM complex.

Together, these observations highlight that the BAM complex plays a central role during envelope formation, and point to the possibility that other envelope biogenesis and remodelling processes are intimately coordinated with OMP assembly by the BAM complex.

In this work, we aimed to gain insights into mechanisms of regulation of OMP biogenesis by identifying protein partners of the BAM complex. For this, we explored whether the BAM complex interacts with other machineries in the membrane. We designed an experimental strategy to identify possible BAM interactors and characterize their physiological role in supporting or regulating envelope biogenesis.

## Results

### 1 Affinity-purification of the BAM complex for quantitative proteomics analyses

#### 1.1 SILAC-based strategy used for the BAM interactomic analysis

The BAM complex is an essential machinery required for the biogenesis of the bacterial envelope, and more specifically for the assembly of OMPs in the OM. As explained in the introduction, a number of machineries contribute to the assembly of other distinct components of the envelope. To gain insights into how the BAM complex functions and cooperates with other envelope machineries, we aimed to describe the interactome of BAM. This global analysis will enable us to get an unprecedented view on the regulation and coordination of the BAM activity during the biogenesis of the envelope of the Gram-negative bacterial model organism *E. coli*.

One of the main difficulties for such global interactomic analyses is to discriminate specific interactors from non-specific ones. To address this problem, we employed a methodology based on Stable Isotope Labeling by Amino Acids in Cell culture (SILAC) labeling prior to affinity-purification of the BAM complex and further identification of proteins co-eluted together with BAM by mass spectrometry. The technique relies on the use of stable isotopes  $^{13}\text{C}$  and  $^{15}\text{N}$  contained in arginine (Arg) and lysine (Lys) residues. Because trypsin cleaves the protein polypeptide backbone after Lys and Arg, these amino acids are chosen to ensure the incorporation of at least one heavy amino acid in each tryptic peptide, leading to an increase in mass of 8 and 10 Da for each peptide cleaved after Lys or Arg, respectively.

The experimental strategy is summarized in Figure 10. *E. coli* cells overproducing the full BAM complex are grown on M9 minimal medium supplemented with either light or heavy Arg and Lys. A recombinant version of the BAM complex in which BamE is fused to a tag is produced using light amino acids whereas the BAM complex without tag is overproduced in the presence of heavy Arg and Lys. After isolation of the cell envelope fraction, membrane proteins are solubilized using a mild non-ionic detergent that preserves the overall integrity of membrane complexes.



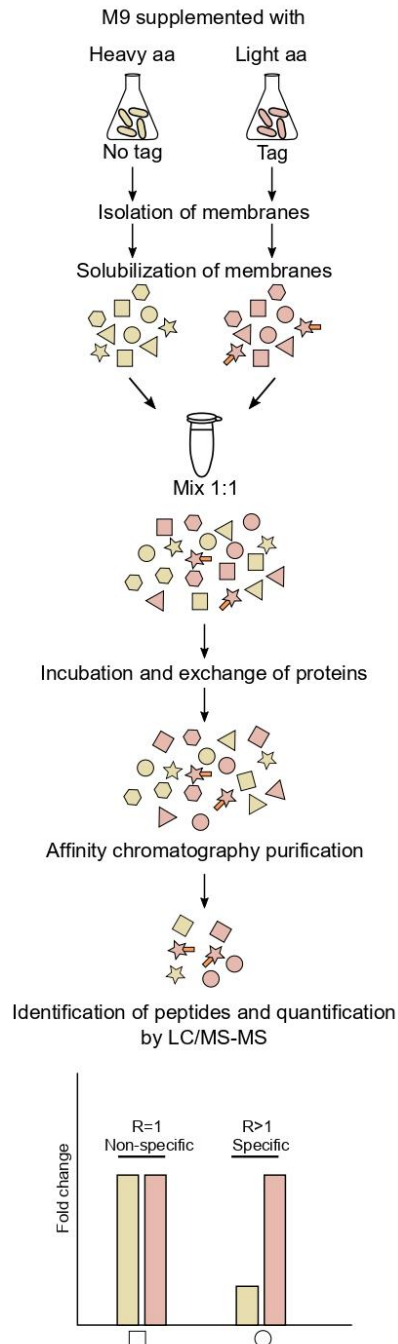


**Figure 10. Strategy used to define the interactome of the BAM complex.** Two strains were cultured using M9 minimal medium: one expressing a non-tagged version of the BAM complex was grown in the presence of heavy amino acids and the other expressing a tagged version of the BAM complex was grown in the presence of light amino acids. After cell fractionation, membranes were isolated and solubilized using a mild detergent. Membrane proteins were mixed in equal amounts prior purification using Ni-affinity chromatography. After trypsin digestion, proteins were analyzed by mass spectrometry to identify and quantify peptides. Proteins identified with a light/heavy ratio of their tryptic peptides (fold change) higher than 2 were considered as specific interactors.

Membrane protein extracts from the two different cultures are then mixed 1:1 in the presence

of affinity-chromatography resin to promote binding of the affinity-tagged BAM complex. During this step, that lasts 1h, protein partners of the tagged BAM complex produced with light residues can potentially exchange with their identical counterparts from the sample labeled with heavy isotopes. Proteins that interact specifically with BAM will have a stronger tendency to remain bound to the bait compared to low affinity partners or non-specific interactors. Upon washes of the resin and elution of the affinity-tagged BAM complex, the eluate is subjected to LC-MS/MS analysis to identify all proteins present and determine the light/heavy ratio of their tryptic peptides. An enriched light/heavy peptide ratio is indicative of a stable or specific interactor, whereas a ratio close to one indicates interactor with fast binding and dissociation kinetics or non-specific interactors.

As a first step of our BAM interactomic strategy, it was crucial to set up a purification method permitting to obtain highly purified BAM complex. For this purpose, we performed several assays to define the optimal parameters for the affinity chromatography used to isolate BAM and its specific interactors, including the type of tag, the nature of the detergent used for membrane solubilization and the composition of the growth medium.

## 1.2 Choice of the purification method of the BAM complex

Two strategies of affinity purification were considered to purify the BAM complex: one based on an octahistidine polypeptide as an affinity tag, and another one based on a *Staphylococcus aureus* protein A-derivative tag. To this purpose, two constructs were used: both contain a  $P_{lac}$  promoter followed by all *bam* encoding open reading frames (ORFs) with *bamE* fused either to an octahistidine tag (pBAM<sup>His</sup>) or to a protein A-heptahistidine tag (pBAM<sup>ProtA</sup>) at its C-terminal end (Fig. 11A, right panel). The construct pBAM<sup>His</sup> (or pJH114) was available in the lab at my arrival and has been already described in the literature (Roman-Hernandez et al., 2014). To create pBAM<sup>ProtA</sup>, we performed a restriction-free cloning after amplification of a construct encoding the protein A fused to a heptahistidine tag from the plasmid pYM10 (Knop et al., 1999) to replace the octahistidine tag of BamE in pBAM<sup>His</sup>. A Tobacco Etch Virus (TEV) cleavage site was present upstream of the protein A tag to permit elution of the protein by TEV protease digestion (Fig. 11A, right panel). After controlling the expression of BamE<sup>ProtA</sup>, we used these two constructs to optimize the purification conditions of the BAM complex.

First, we used the procedure already described for the Ni-affinity purification of the BAM complex (Roman-Hernandez et al., 2014) using both pBAM<sup>His</sup> and pBAM<sup>ProtA</sup> as both constructs contain a poly-histidine tag. An *E. coli* MC4100 derivative strain transformed with pBAM<sup>His</sup> or pBAM<sup>ProtA</sup> were grown in rich medium until mid-exponential phase. Then, the expression of recombinant BAM was induced by supplementing Isopropyl  $\beta$ -D-1-

thiogalactopyranoside (IPTG) to cell cultures. Cells were collected and subjected to mechanical disruption. After clarification spin, the supernatant was used to isolate the envelope fraction by ultracentrifugation. The non-ionic detergent n-dodecyl  $\beta$  D-maltoside (DDM) was used to solubilize membrane fractions and, after an additional clarifying spin step, the supernatants containing membrane proteins were added to nickel-nitrilotriacetic acid (Ni-NTA) coupled to agarose beads. After binding and extensive washing, the bound proteins were eluted using an excess of imidazole.

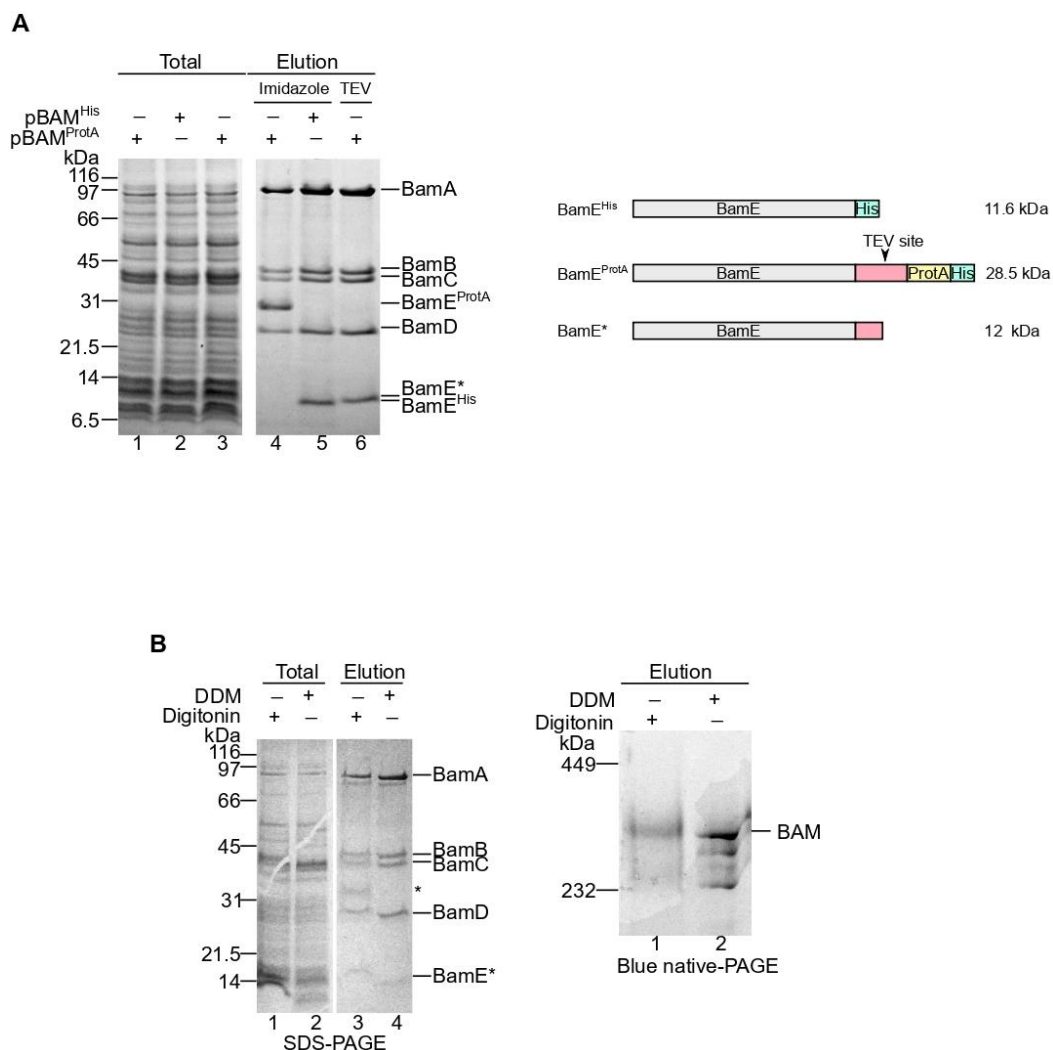


**Figure 11. The purification of the BAM complex can be efficiently optimized for further LC-MS/MS analysis.** **A.** Comparison between the methods of purification of the BAM complex. **Left.** *E. coli* MC4100 derivative strains ectopically expressed BAM complex fused to a Protein A tag (pBAM<sup>ProtA</sup>) or to a poly-histidine tag (pBAM<sup>His</sup>). BAM<sup>His</sup> was purified using Ni-affinity chromatography after solubilization using 1% DDM. After extensive washes, proteins were eluted using an excess of imidazole. In parallel, BAM<sup>ProtA</sup> was purified using IgG coupled to sepharose beads. A cleavage site was included in the tag between BamE and the Protein A, allowing to elute protein using a TEV protease. Four proteins corresponding to the BAM subunits (BamA to BamD) were clearly detected by Coomassie Brilliant Blue staining SDS-PAGE. BamE migrates at different

sizes according to its C-terminal tag, with BamE\* corresponding to the form of BamE obtained after TEV digestion slightly higher than BamE<sup>His</sup>. **Right.** Schematic representations of the bait protein BamE fused to a poly-histidine tag (BamE<sup>His</sup>, 11.6 kDa), to a Protein A tag (BamE<sup>ProtA</sup>, 28.5 kDa) and the form after TEV protease digestion (BamE\*, 12 kDa). **B.** Comparison of the detergents used for solubilization of proteins prior to purification of the BAM complex. **Left.** *E. coli* MC4100 derivative strains ectopically expressed BAM complex fused to a Protein A tag. The complex was solubilized using 1% DDM or 1% digitonin. Then the BAM complex was purified using IgG coupled to sepharose beads and proteins were eluted using the TEV protease. Proteins were separated by SDS-PAGE and subjected to Coomassie Brilliant Blue staining. **Right.** Analysis by BN-PAGE of the elution fractions using the two conditions revealed a band migrating at 250 kDa approx., the size of the BAM complex, with putative incomplete versions of the BAM complex using DDM.

Second, we developed a purification technique by using human serum Immunoglobulin G (IgG) conjugated to sepharose beads to bind the BAM<sup>ProtA</sup> complex, and TEV protease digesting to cleave off the complex from the IgG-bound tag and promote its elution. Proteins produced in a MC4100 *E. coli* derivative strain carrying pBAM<sup>ProtA</sup> were solubilized from the envelope fraction and incubated with human IgG coupled to sepharose beads. After extensive washes of the beads, the TEV protease was added to cleave between BamE and Protein A to elute BamE\*, corresponding to a version of BamE slightly modified with 15 additional amino acids before the TEV protease cleavage site (Fig. 11A, right panel, BamE\*). Finally, Ni-NTA agarose beads were added to the elution fraction to retain the TEV protease that is tagged with a poly-histidine tag. After incubation, the flow-through constituted the BAM purified fraction.

Total membrane and elution fractions obtained using the two constructs and the two purification approaches were analyzed by SDS-PAGE. Coomassie Brilliant Blue staining of the gel revealed a similar amount of proteins in the total membrane fractions (Fig. 11A, lanes 1-3), suggesting that the solubilization of the membrane fractions for the three samples was similarly efficient. Then, we observed in the elution fractions four bands with apparent molecular weights of approximately 97, 40, 37 and 25 kDa (lanes 4-6). These correspond to the expected molecular weights of BamA, BamB, BamC and BamD, respectively. For the purification of the sample BAM<sup>ProtA</sup> by Ni-NTA, we observed also a protein band running with an apparent molecular weight of 28 kDa, which is the expected molecular weight of BamE<sup>ProtA</sup> (Fig. 11A, lane 4). Instead, the elution samples containing either BamE<sup>His</sup> or BamE<sup>ProtA</sup> presented an additional protein band running with an apparent molecular weight of approximately 12 kDa, corresponding to the size of BamE<sup>His</sup> (lane 5) or BamE\* (lane 6). It should be noted that BamE\* is slightly bigger than BamE<sup>His</sup>.

Altogether, these results suggest that the BAM complex can be efficiently purified using both IgG- and Ni-affinity chromatography of tagged BamE.

Both purification strategies show that the quaternary organization of the BAM complex was preserved during the purification procedure and no major contaminants were co-purified. For our interactomic analysis, we chose to purify the BAM complex via the IgG-protein A affinity procedure, as an enzymatic elution is likely to yield less contaminants compared to imidazole elution of nickel bound proteins. In fact, nickel may also interact with metal-binding proteins that are endogenously produced by the bacterial cells.

### 1.3 The detergent used for solubilization of membranes has an impact on the stability of the BAM complex

Another criterion to take into account for sample preparation prior MS analysis is the preservation of the integrity of the BAM complex and its partners during purification. Membrane solubilization is a critical step and optimal conditions should be set up to preserve the native conformation of proteins and their quaternary organization. We tested two non-ionic detergents for the solubilization of total membrane fraction prior to purification of the BAM complex: digitonin and DDM. Previous studies have used DDM as non-ionic detergent (Roman-Hernandez et al., 2014). Digitonin is another detergent that has been used in the past for the solubilization of BamA from *Neisseria meningitidis* prior to functional analyses *in vitro* (Kozjak-Pavlovic et al., 2011), however no study has been reported for purification of the full BAM complex in *E. coli* using this detergent. Although we expected digitonin to be less efficient than DDM in extracting protein complexes from the *E. coli* envelope fraction (Stenberg et al., 2005), we hypothesized that the milder solubilizing behavior of digitonin could help preserving BAM interactions, as previously shown for other complexes including the respiratory chain supercomplexes obtained from the inner membrane of both bacteria and mitochondria (Schägger, 2002). We thus aimed to analyze the yield of purified BAM complex using these two detergents prior to affinity purification.

We used IgG-affinity purification of BAM<sup>ProtA</sup> from the *E. coli* envelope fraction solubilized with either 1% w/v DDM (as used in the optimization assays) or 1% w/v digitonin. Total membrane and elution fractions were analyzed by SDS-PAGE. Coloration of the gel using Coomassie Brilliant Blue revealed that the patterns of total membranes solubilized with DDM or digitonin were similar (Fig. 11B, left panel, lanes 1 and 2). Elution fractions (lanes 3 and 4) showed the five subunits of the BAM complex, as previously observed. The purification yield of BAM seems to be higher using DDM, suggesting that digitonin could be less efficient in extracting membrane-embedded protein complexes. We could also observe a band running with an apparent molecular weight of 32 kDa when proteins were solubilized with digitonin (Fig. 11B, lane 3). This band was identified by MALDI-TOF MS as the TEV protease (data not shown),

suggesting that removal of TEV by Ni-NTA affinity chromatography in the last step of our procedure was not efficient in this specific experimental replicate. We can assume that the amount of Ni-NTA resin added was not sufficient to completely retain the protease from this sample.

To gain insights into the integrity of the complex using both detergents, we subjected the elution fractions to Blue Native-PAGE (BN-PAGE). As this analysis is performed under native conditions protein complexes are preserved during electrophoresis, allowing the separation of large protein complexes based on their mass. After coloration using Coomassie Brilliant Blue, a band of 250 kDa was observed in both samples (Fig. 11B, right panel). This band is likely to correspond to the full BAM complex, as previously described in the literature (Roman-Hernandez et al., 2014). Remarkably, sample solubilized with DDM displays additional fast-migrating bands, which may be indicative of a less stable BAM complex under these conditions (Fig. 11B, right panel, lane 2).

It has been previously reported that the lipoprotein BamB can dissociate from the BAM complex during purification using DDM (Gu et al., 2016). Moreover, the lipoproteins BamC, BamE and BamD form a subcomplex that interacts with BamA (Hagan et al., 2010; Iadanza et al., 2016). We can thus assume that the DDM may partially affect the stability of the BAM complex during purification steps, leading to the formation of subcomplexes of BAM subunits. Even though DDM is more efficient for the solubilization of proteins compared to digitonin, digitonin seems to be a milder detergent and helps preserving the integrity of the full BAM complex. Regarding our objective to analyze the BAM interactome, preserving protein-protein interactions during the sample preparation is crucial. For these reasons, we will then use digitonin as non-ionic detergent for solubilization of membranes prior to BAM purification and further MS analyses.

#### 1.4 Yield of the BAM complex from cells grown on minimal medium

After obtaining a highly purified and stable BAM complex under standard culture conditions (rich LB medium, 37°C), we aimed to set up a protocol for further SILAC labeling prior to BAM purification and LC-MS/MS analyses. Because the method relies on the incorporation of heavy amino acids in culture, we needed to perform culture on minimal medium supplemented with or without heavy-isotope Arg and Lys amino acids. For an initial set-up, we used two minimal media: one medium that we routinely use in the lab for pulse-chase radiolabeling of cells, which contains all amino acids except Met and Cys; the second medium lacks amino acids except Arg, Lys and Pro. In the latter case, Arg and Lys were specifically selected because the SILAC relies on their incorporation in cell culture in their light or heavy forms. An excess of light proline

was added to prevent that Arg could be converted to Pro and bias the quantification of tryptic peptides in the mass spectrometry analysis (Bendall et al., 2008; Chen et al., 2015).

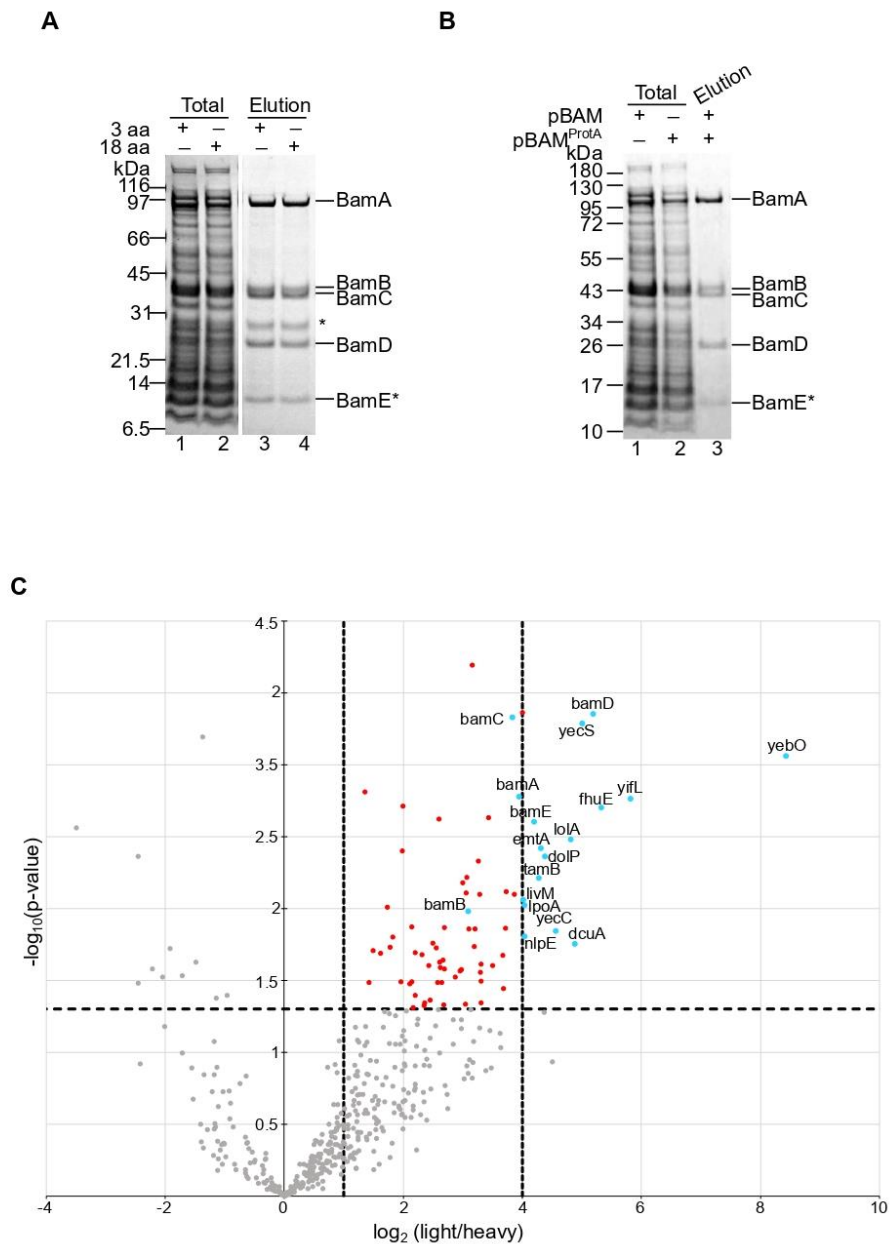


**Figure 12. The BAM complex can be efficiently purified from cells grown on minimal medium to obtain a high confidence interactome.**

**A.** Comparison of the composition of the minimal medium used for cell culture. *E. coli* MC4100 derivative strains carrying pBAM<sup>ProtA</sup> were grown in minimal medium supplemented with Lys, Arg and Pro (3 aa) or with all amino acids, except Met and Cys (18 aa). The BAM complex fused to a Protein A tag was ectopically expressed and after solubilization using 1% digitonin, membrane protein extracts were used to purify the BAM<sup>ProtA</sup> complex using IgG coupled to sepharose beads. Proteins were eluted using the TEV protease. Proteins were analyzed by SDS-PAGE and subjected to Coomassie Brilliant Blue staining.

**B.** SILAC of *E. coli* MC4100 derivative strain carrying pBAM or pBAM<sup>ProtA</sup>. Cells were cultured in minimal medium supplemented with light or heavy Arg and Lys and an excess of light Pro, as indicated in Fig. 10.

Samples were solubilized using 1% digitonin and proteins were bound to IgG sepharose beads. Proteins were eluted using the TEV protease, as indicated previously. Proteins were loaded to a SDS-PAGE and subjected to coloration by Coomassie Brilliant Blue staining. **C.** Representation of proteins identified by SILAC LC-MS/MS analyses. Proteins identified by the four biological replicates (one replicate using MC4100 derivative strain and three using strain BW25113) are represented in the volcano plot, according to the  $\log_2$  of their enrichment light/heavy and the  $-\log_{10}$  of the p-value by the T-test. In total, 75 proteins are highlighted (red and blue), as they were selected as specific BAM interactors, based on a light/heavy ratio of tryptic peptides  $> 2$  and a p-value  $< 0.05$  (corresponding to  $x=1$  and  $y=1.3$  on the plot). Proteins in blue represent the top 18 interactors with a  $\log_2$  of their enrichment light/heavy  $>4$ , except for BamA ( $x=3.94$ ), BamB ( $x=3.09$ ) and BamC ( $x=3.83$ ).

Cells were grown in these two different minimal media and membranes were isolated as described previously. After solubilization using digitonin, total membrane protein extracts were subjected to IgG chromatography to purify the BAM complex. SDS-PAGE analyses of the total extracts and the elution fractions revealed that the BAM complex could be efficiently purified in minimal media (Fig. 12A). Also in these cases, the TEV protease was not efficiently removed from our elution fraction.

Since the BAM complex is efficiently produced from cells cultured on minimal media supplemented with only Arg, Lys and Pro, we decided to choose this medium for further SILAC-based MS experiments. Overall, the whole production and purification process, starting from 200 ml of culture, led to a final elution fractions of 150  $\mu$ l containing approximately 0.5 to 1 mg/ml of purified BAM complex, which is sufficient for MS analyses.

### 1.5 SILAC-based analysis of the BAM interactome

As previously described in the introduction of this result section (paragraph 1.1), the SILAC-based proteomics approach chosen to analyze the BAM interactome relies on the quantification of proteins co-eluted with BAM and the measurements of the light/heavy ratio for each protein peptide, representative of the specificity of the interaction with BAM.

MC4100 cells transformed with pBAM<sup>ProA</sup> or pBAM (expressing untagged version of BAM) were grown using minimal media supplemented with light or heavy Arg and Lys, respectively. Total membrane protein extracts were obtained after solubilization of isolated membranes using digitonin. Proteins from both extracts were quantified by measuring tryptophan UV-absorbance using a Nanodrop spectrophotometer, and equivalent amounts of membrane proteins were mixed prior to purification using IgG chromatography.

After IgG-protein A binding, extensive washes were performed and the TEV protease was added to cleave between BamE and protein A tag eluting the BAM complex. After depleting



the TEV protease using Ni-NTA agarose beads, elution fractions were collected and further analyzed by SDS-PAGE and Coomassie Brilliant Blue staining.

We can observe a difference in the concentration of proteins between both total membrane extracts (Fig. 12B, lanes 1 and 2). This difference, quantified by tryptophan UV-absorbance, was taken into account to mix equivalent amounts of total protein extracts during the binding step. This is particularly critical to accurately evaluate the light/heavy ratio of protein peptides observed after purification in the elution fractions, which reflect the propensity of proteins to exchange during the binding step. The analysis of the elution fraction shows five bands corresponding to all subunits of BAM (Fig. 12B, lane 3). This fraction was directly analyzed by LC-MS/MS analysis.

Our first optimization SILAC-based MS analysis was performed using an MC4100 derivative strain. However, in the perspective of using *E. coli* mutants of the putative interactors of the BAM complex, we decided to repeat the experiment using the BW25113 strain, which was used to generate the Keio collection of *E. coli* strains, a library of single-gene deletion mutant strains each lacking one of the non-essential gene in *E. coli* (Baba et al. 2006).

To this purpose, the BW25113 strain was transformed with pBAM or pBAM<sup>ProtA</sup> and the same experiment was carried out in three independent biological replicates. Altogether, the elution fractions from the four independent biological replicates (one with MC4100 and three with BW25113) were analyzed by LC-MS/MS at the Infrastructure de Protéomique de Toulouse at the IPBS of Toulouse (<https://proteotoul.ipbs.fr>).

To validate the labeling method, a quality control experiment was performed to assess the incorporation of heavy amino acids in proteins. For this, the total membrane fraction of the protein extracts from the heavy amino acids culture (expressing BAM without tag) was analyzed. After quantification, 65% of unique peptides were found to be entirely labelled, 27% were labelled between 80-100%, 6% were labelled between 60-80% and only 2% were not labelled, meaning that 98% of unique peptides were found to be labeled with heavy Lys and Arg. This preliminary analysis validates the method of labeling that is important for the quantification of the light/heavy ratio values obtained for each peptide.

Elution samples were concentrated to approximately 1 mg/ml and loaded onto a C18 HPLC precolumn. Peptides were then analyzed using a nanoLC/ESI Orbitrap (Q-exactive Plus). This analysis permitted the identification of proteins by bottom-up proteomics and their quantification by comparing the signal of non-labelled proteins vs labelled (*i.e.* light vs heavy). A p-value (based on the T-test) was calculated based on the results obtained with the four biological replicates and the MaxQuant software. Identified proteins were represented using a volcano plot with the log<sub>2</sub> of average light/heavy peptide ratio obtained for each protein (*i.e.*

$\log_2 \left( \frac{\text{mean intensity light}}{\text{mean intensity heavy}} \right)$  on the x-axis and the inverse of  $\log_{10}$  of the p-value (i.e.  $-\log_{10}(p - \text{value})$ ) on the y-axis. It should be noted that only proteins with a gene ontology (GO) terms related to envelope protein localization were considered to build the volcano plot (Fig. 12C).

| Gene name   | $\log_2$ (L/H) | $-\log_{10}$ (p-value) | Annotated function   |
|-------------|----------------|------------------------|--|
| <i>yebO</i> | 8.42           | 3.06419269             | Integral component of membrane [GO:0016021]; plasma membrane [GO:0005886]  |
| <i>yifL</i> | 5.81           | 2.76518831             | Plasma membrane [GO:0005886]   |
| <i>fhuE</i> | 5.33           | 2.7012652              | Cell outer membrane [GO:0009279]; integral component of membrane [GO:0016021]; iron ion binding [GO:0005506]; receptor activity [GO:0004872]; ion transport [GO:0006811]; iron ion homeostasis [GO:0055072]; siderophore transport [GO:0015891]  |
| <i>bamD</i> | 5.19           | 3.35713706             | Cell outer membrane [GO:0009279]   |
| <i>yecS</i> | 5.00           | 3.29055169             | Integral component of membrane [GO:0016021]; plasma membrane [GO:0005886]; transporter activity [GO:0005215]; amino acid transport [GO:0006865]  |
| <i>dcuA</i> | 4.88           | 1.75611475             | Integral component of membrane [GO:0016021]; plasma membrane [GO:0005886]; C4-dicarboxylate transmembrane transporter activity [GO:0015556]  |
| <i>lolA</i> | 4.80           | 2.48124512             | Periplasmic space [GO:0042597]; lipoprotein transporter activity [GO:0042954]  |
| <i>yecC</i> | 4.55           | 1.84423288             | Plasma membrane [GO:0005886]; amino acid-transporting ATPase activity [GO:0015424]; ATP binding [GO:0005524]; L-cystine transmembrane transporter activity [GO:0015184]; ATP hydrolysis coupled cation transmembrane transport [GO:0099132]; cysteine transmembrane transport [GO:1903712]; L-cystine transport [GO:0015811]   |
| <i>dolP</i> | 4.37           | 2.36542409             | Periplasmic space [GO:0042597]   |
| <i>emtA</i> | 4.31           | 2.42144703             | Cell outer membrane [GO:0009279]; carbon-oxygen lyase activity, acting on polysaccharides [GO:0016837]; lytic endotransglycosylase activity [GO:0008932]; lytic transglycosylase activity [GO:0008933]; cell wall macromolecule catabolic process [GO:0016998]; cell wall organization [GO:0071555]; peptidoglycan metabolic process [GO:0000270]  |
| <i>tamB</i> | 4.28           | 2.21181568             | Integral component of plasma membrane [GO:0005887]; TAM protein secretion complex [GO:0097347]; protein secretion [GO:0009306]   |
| <i>bamE</i> | 4.19           | 2.60250905             | Cell outer membrane [GO:0009279]   |
| <i>nlpE</i> | 4.04           | 1.80507315             | Cell outer membrane [GO:0009279]; cell adhesion [GO:0007155]; regulation of cell-substrate adhesion [GO:0010810]   |
| <i>lpoA</i> | 4.04           | 2.02438559             | Cell outer membrane [GO:0009279]; periplasmic side of cell outer membrane [GO:0031241]; periplasmic space [GO:0042597]; enzyme regulator activity [GO:0030234]; hydrolase activity, hydrolyzing O-glycosyl compounds [GO:0004553]; peptidoglycan biosynthetic process [GO:0009252]; regulation of cell shape [GO:0008360]  |
| <i>livM</i> | 4.01           | 2.05967286             | Integral component of plasma membrane [GO:0005887]; plasma membrane [GO:0005886]; branched-chain amino acid transmembrane transporter activity [GO:0015658]; L-isoleucine transmembrane transporter activity [GO:0015188]; L-phenylalanine transmembrane transporter activity [GO:0015192]; L-valine transmembrane transporter activity [GO:0005304]; branched-chain amino acid transport [GO:0015803]; isoleucine transmembrane transport [GO:1903714]; L-valine transmembrane transport [GO:1903785]; phenylalanine transport [GO:0015823] |

**Table 1. List of top score interactors according to their enrichment light/heavy.** *E. coli* cells were cultured using the SILAC procedure described in Fig. 10 to purify the BAM complex by affinity chromatography. List of the top 15 interactors identified using the SILAC-based BAM interactomic approach described on Figure 10. The selection criteria (i.e.  $\log_2$  (light/heavy) > 4 and  $-\log_{10}$  of the p-value > 2). The  $\log_2$  of their light/heavy fraction is reported. Values of the  $-\log_{10}$  of the p-value by the T-test are presented, together with the annotated

function according to gene ontology (GO), proposing a cellular localization or a cellular function. In bold, we present subunits of the BAM complex, DolP and TamB.

## 1.6 Interactome of the BAM complex

The volcano plot presented on Fig. 12C highlights in red the proteins identified with a  $\log_2$  light/heavy fractions  $> 1$  and a p-value  $< 0.05$  (in the volcano plot, this represents values  $x=1$ ,  $y=1.3$ , respectively). In total, 75 putative interactors were identified using these criteria. A group of top 15 interactors, selected for presenting a  $\log_2$  light/heavy fraction  $> 4$  are labeled in blue and are listed in Table 1.

Among the 75 putative interactors (light/heavy fraction  $>2$ ), we identified 17 proteins (22.6%) related to transport of substrates across the membrane, 29 proteins (38.6%) related to synthesis/transporter pathways (ATP, amino acid, etc.), 8 proteins (10.6%) related to PG remodeling, 3 proteins (4%) related in envelope stress-response, 3 proteins (4%) of miscellaneous functions and 14 proteins (18.6%) with an unknown function. As expected, the BAM subunits were all identified in this interactome, in agreement with our SDS-PAGE analysis of the sample. It should be noted that BamB appears with a relative low score (ratio light/heavy) compared to other BAM subunits. This is in accordance with the literature, as BamB is described as a less stably-bound component of the complex (Gu et al., 2016).

Interestingly, RcsF, a component of the Rcs stress response system, is part of the BAM interactome ( $\log_2$  light/heavy labeled peptide fraction=3), validating our experimental approach as RcsF is a known BamA interactor. Indeed, recent studies have shown that BamA is able to interact with RcsF via the lumen of its  $\beta$ -barrel domain (Rodríguez-Alonso et al., 2020). Of note, OmpA, which is one of the most abundant OMP in *E. coli* envelope, was not identified among the putative BAM interactors. It was identified with a  $\log_2$  light/heavy labeled peptide fraction  $< 1$ , indicating that the interaction between BAM and its client OMPs are transient.

Interestingly, TamB, which is part of the Translocation and Assembly Module (TAM), an ancillary module composed by TamA and TamB proposed to promote the assembly of some type of OMPs (Selkrig et al., 2012) was identified in the top list of interactors (Table 1). As previously stated, TAM shares common tasks with BAM in the assembly of OMPs yet the molecular basis of this putative coordinative job has remained unknown. It should be noted that, differently from TamB, the light/heavy peptide fraction observed for TamA, which is an homologous of BamA, was close to 1, suggesting that BAM is less likely to interact with TamA.

Several pieces of evidence have suggested an interplay between BAM and TamB in *Borrelia burgdorferi* (Babu et al., 2017; Iqbal et al., 2016), a bacterium that lacks TamA. However, in *E. coli* no formal experimental proof of an interaction between BAM and any of the two TAM subunits had been described yet in the literature. In this context, the identification of TamB in our BAM interactome attracted our attention and we decided to dedicate a part of this PhD work to initiate the characterization of the interaction between the BAM complex and TamB. This work is presented in the final chapter of this manuscript.

The main objective of my PhD work was the characterization of the BAM-DolP interaction given that DolP is critical to preserve OM homeostasis but its molecular function remains unknown. Elucidating the mechanism by which DolP promotes OM homeostasis is particularly relevant in the fight against bacterial drug resistance as the inactivation of DolP could hinder the envelope permeability barrier to antibiotics.

At the beginning of my PhD, multiple pieces of evidence had suggested that this protein is critical in the maintenance of OM homeostasis. The *dolP* gene is upregulated during  $\sigma^E$  stress response (Onufryk et al., 2005) and the deletion of this gene makes cells hypersensitive to detergents, suggesting that DolP is important to preserve outer membrane homeostasis (Onufryk et al. 2005; Tsang, Yakhnina, and Bernhardt 2017; Morris et al., 2018). Moreover, it has been suggested that DolP in *Neisseria meningitidis* was required for proper biogenesis of a set of OMPs (Bos et al., 2014; Seib et al., 2019). However, the molecular bases underlying the function of DolP were unknown and the interaction with BAM was never reported before. Furthermore, it was unclear why DolP is upregulated during activation of the  $\sigma^E$  response. Considering the physiological importance of DolP in promoting OM biogenesis and its unprecedented link with BAM, my work aimed to gain new insights into the function of DolP and to understand why it interacts with the BAM complex. Through the exploration of the role of the BAM-DolP interaction, we expect to better understand the molecular basis underlying the ability of DolP to promote OM homeostasis.

## 2 DoIP is a putative interactor of the BAM complex

### 2.1 DoIP is an OM lipoprotein

DoIP is a lipoprotein conserved among  $\gamma$ -proteobacteria. It contains a predicted signal peptide that permits its trafficking via the Sec translocon through the IM. The signal peptide includes a lipobox, the consensus sequence for N-terminal modification of lipoproteins (Konovalova and Silhavy, 2015; Onufryk et al., 2005). Following the lipobox, DoIP contains a linker region and two BON domains (Fig. 13A and B). As described in the introduction, the precise function of BON domains is not yet fully understood, however it has been speculated that they could play a role in the binding to hydrophobic ligands (Yeats and Bateman, 2003).

In *E. coli*, the lipobox of DoIP corresponds to the sequence  $_{16}\text{LQGC}_{19}$ . The conserved lipid-modified Cys at position 19 is triacylated to be anchored to the membrane. Bioinformatics analyses of DoIP sequences from  $\gamma$ -proteobacteria reveals this Cys is strictly conserved (Fig. 13C). Moreover, the residue after the conserved Cys defines the localization of the lipoprotein at either the IM or OM (Konovalova and Silhavy, 2015). In the case of DoIP, a residue different than Asp is found at this key position, suggesting DoIP is an OM lipoprotein (Fig. 13C).

To obtain a more direct evidence that DoIP resides in the OM, we performed cell fractionation to separate the IM and the OM by differential centrifugation using sucrose gradients. This is based on differential density of each membrane, given that the presence of LPS confers a higher density to the OM.

*E. coli* BW25113 cells were grown to mid-exponential phase, collected and subjected to plasmolysis using EDTA and lysozyme to permeabilize the envelope. Then, cells were collected and mechanically disrupted. After a clarifying spin to remove cell debris, the supernatant was subjected to analytical ultracentrifugation to isolate the total membrane fraction. These membranes were then resuspended and subjected to a new step of ultracentrifugation through a sucrose gradient. The samples were separated in two fractions, corresponding to both membranes. Both fractions were carefully collected prior analysis by SDS-PAGE and Western blot. Heat-modifiability and immunoblotting assays were performed to reveal components of each membrane fraction and assess the quality of the separation of the OM from the IM. This heat-modifiability helps to identify OMPs as these proteins adopt a characteristic  $\beta$ -barrel fold, which is refractory to denaturation by SDS, unless a sufficient amount of energy is provided by heating. When analyzing proteins by SDS-PAGE without boiling of the samples prior to gel loading, OMPs remain partially folded, and they migrate faster (Noinaj et al., 2015).

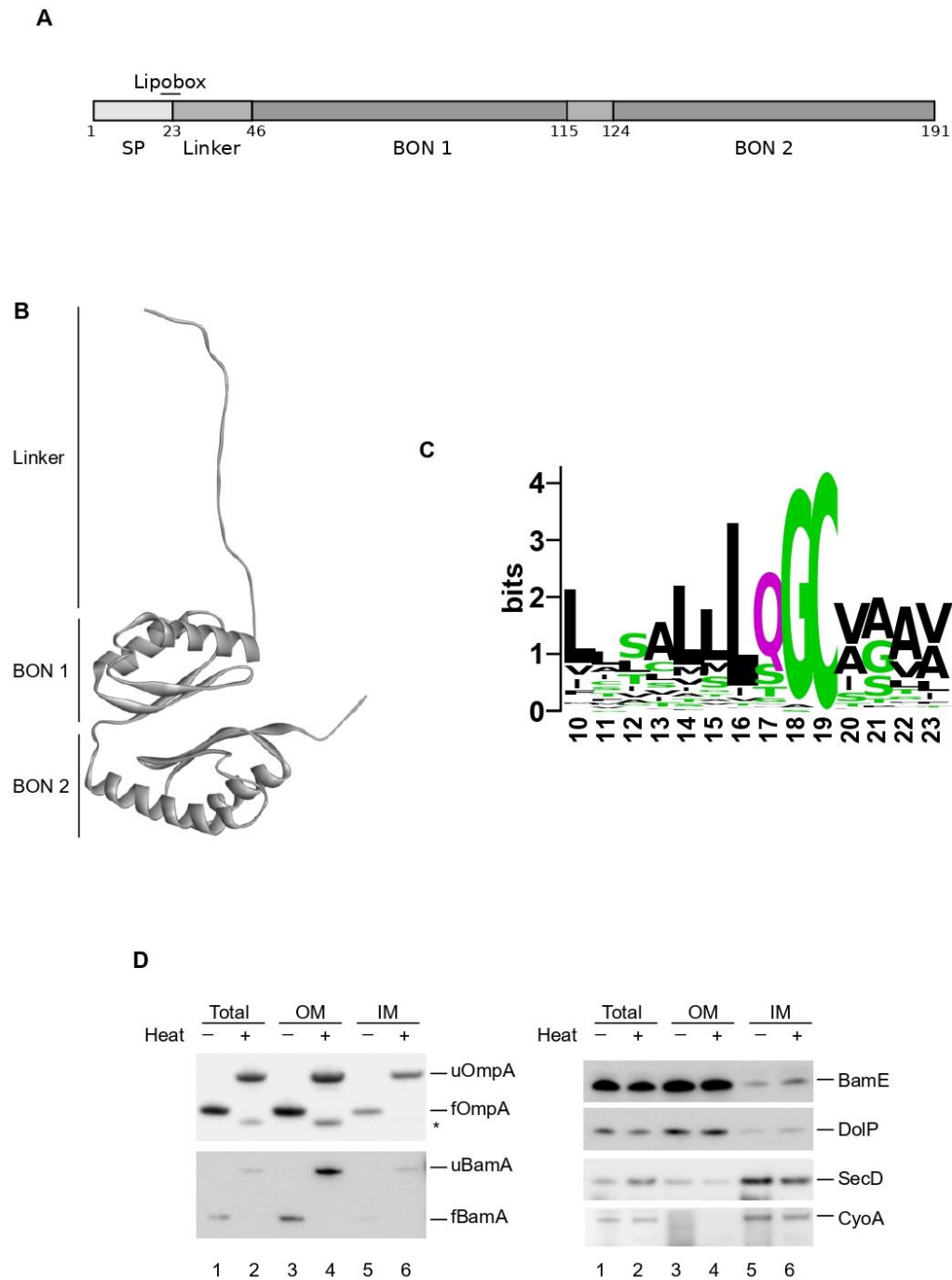


**Figure 13. DoIP is an OM lipoprotein. A.** Representation of the primary structure of DoIP. DoIP is composed by a signal peptide from residues 1-23 that contains a lipobox with Cys19 being acylated. Then, from residues 23-46 there is a flexible linker, followed by two BON domains from residues 47-115 and 125-191, respectively. BON domains are separated by a small linker from residues 116-124. **B.** NMR structure of DoIP (PDB: 7A2D, Bryant et al. 2020) **C.** Logo plot of the lipobox of DoIP in  $\gamma$ -proteobacteria. A conserved Cys at position 19 permits the acylation of the protein. Residues 20 and 21 are not predicted to allow the LOL avoidance, suggesting DoIP is localized at the OM. **D.** DoIP accumulates in the OM fraction. *E. coli* BW25113 strain was grown and cells were subjected to differential centrifugations to allow the isolation of the envelope fraction (total), the OM fraction (OM) and the IM fraction (IM). Proteins were subjected to a heat-modifiability assay to

observe patterns of migration of OMPs. DoIP remains mostly enriched in the OM fraction, demonstrating its localization is at the OM.

Samples mixed with Laemmli buffer were split in two, one half was subjected to boiling at 98°C and the other kept on ice. After separation by SDS-PAGE at 4°C, proteins were transferred onto a Polyvinylidene fluoride (PDVF) membrane and subjected to immunodetection using available antisera against several membrane proteins. We observed that BamA and OmpA, two OMPs are indeed enriched in the OM fraction (Fig. 13D, lanes 3 and 4), compared to their signals in the total membrane fractions (lanes 1 and 2) and in the IM fraction (lanes 5 and 6). We can also distinguish their migration patterns by heat-modifiability as these proteins migrate faster when the samples were not boiled. The OM lipoprotein BamE was also enriched in the OM fraction compared to the total membrane and IM fractions. In addition, proteins such as SecD and CyoA were enriched in the IM fraction, where they normally reside (lanes 5 and 6).

Even though we can observe a weak contamination of both membranes, we can conclude that our fractionation method permits to get proteins enriched in either OM or IM and to investigate their cellular localization.

The detection of DoIP using proper antiserum reveals a clear signal at the expected molecular weight in the total membrane fraction, which is much more intense in the OM fraction, whereas it is very low in the IM fraction (Fig. 13D). This result clearly demonstrates that DoIP localizes at the OM and we can conclude that DoIP is an OM lipoprotein.

## 2.2 DoIP is required for OM integrity

It was previously reported that deletion of *dolP* causes sensitivity to SDS (Onufryk et al., 2005). However, at the beginning of my PhD, no data was available to know whether deletion of *dolP* could cause a growth defect, or more specifically, sensitivity to large hydrophilic antibiotics, such as vancomycin (1449 Da), that cannot pass the OM by diffusion. In fact, the molecular weight diffusion cut-off of porins is approximately of 600 Da (Welte et al., 1995), and therefore too small to allow the entry of vancomycin.

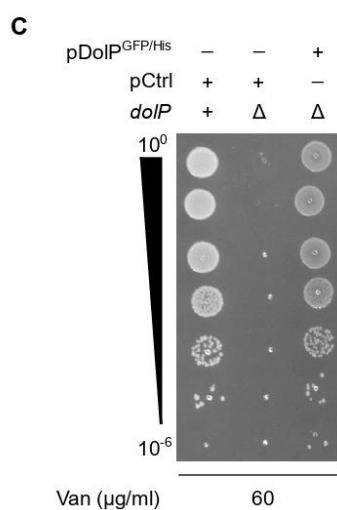
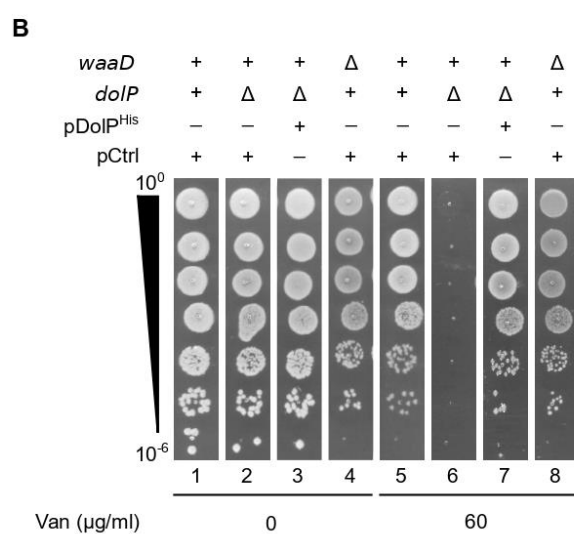
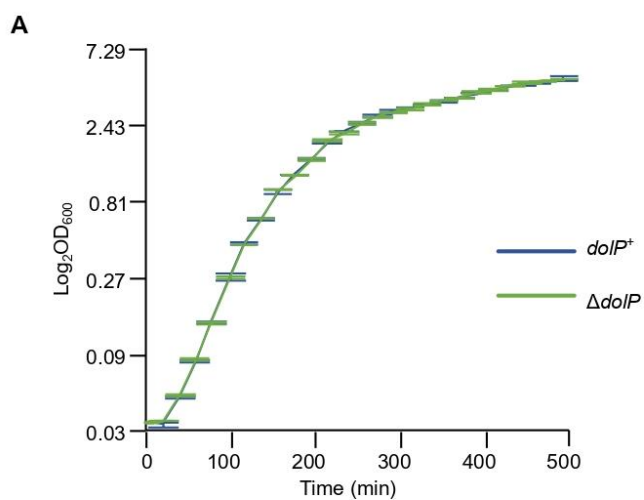


**Figure 14. DoIP is a critical component for envelope integrity.** **A.** BW25113 and  $\Delta$ *dolP* cells were cultured in LB medium. Cell densities of both cultures were monitored by measuring the OD<sub>600</sub> at regular time intervals. The graph reports mean values of independent cultures  $\pm$  standard deviation (SD, N = 3). **B. and C.** BW25113,  $\Delta$ *dolP* and  $\Delta$ *waaD* cells carrying the indicated plasmids were serially diluted and spotted on LB lacking or



containing 60 µg/ml vancomycin. Ectopic expression was driven by the leaky transcriptional activity of  $P_{trc}$  or  $P_{tac}$  in the absence of IPTG.

First a new  $\Delta dolP$  strain was generated by P1 transduction of the *dolP::kan* construct present in the corresponding *dolP* Keio deletion strain (Baba et al., 2006). This strain was used for further experiments in this manuscript. We grew  $\Delta dolP$  cells in rich liquid medium and monitored the growth at regular time intervals by the measure of OD<sub>600</sub>. Strains carrying or not *dolP* were inoculated to the same initial OD<sub>600</sub> and then their density was monitored over time. Values of OD<sub>600</sub> were blotted on a logarithmic scale over time on a linear scale (Fig. 14A). The growth curve indicates that there is no difference in cell growth between WT and  $\Delta dolP$  strains, suggesting that *dolP* does not alter bacteria fitness under normal growth conditions (rich medium, 37°C, no treatment).

To check if the deletion of *dolP* also leads to vancomycin sensitivity, growth assays were performed in agar media using WT and  $\Delta dolP$  strains, as well as with complementation  $\Delta dolP$  strains that had been transformed with either pDoIP<sup>His</sup> or pDoIP<sup>GFP/His</sup>, encoding DoIP C-terminally fused to either an His tag or to superfolder Green Fluorescent Protein (GFP) followed by a His tag. Then, we performed some serial dilutions and we spotted these dilutions on LB agar plates supplemented or not with 60 µg/ml of vancomycin. We can observe that the deletion of *dolP* makes cells hypersensitive to vancomycin, whereas normal resistance to this antibiotic was restored in the complementation strain containing pDoIP<sup>His</sup> (Fig. 14B) or pDoIP<sup>GFP/His</sup> (Fig. 14C). This result suggests that DoIP is crucial to maintain the OM permeability barrier to large molecules.

To go further into the characterization of the  $\Delta dolP$  strain, we wondered if its sensitivity to vancomycin might be linked to membrane fluidity or maturation of LPS, as  $\Delta dolP$  was shown to have a marginal increment on membrane fluidity (Bryant et al., 2020). To address this point, we decided to test whether the deletion of *waaD*, that causes a much more prominent increment in membrane fluidity (Bryant et al., 2020; Storek et al., 2019), induces sensitivity to vancomycin. WaaD is an ADP-L-glycero-D-mannoheptose-6-epimerase involved in the biogenesis of a precursor of the LPS molecule. As a consequence, the *waaD* deletion strain presents a truncated LPS structure and is hypersensitive to novobiocin and other hydrophobic drugs (Coleman, 1983). Moreover, it was reported that the deletion strain triggers formation of colanic acid independently of Rcs response and dependent to the upregulation of the RpoS operon (Joloba et al., 2004). Serial growth assay of  $\Delta waaD$  strain in rich medium in the presence of vancomycin reveals that this strain is not sensitive to this antibiotic (Fig. 14B), suggesting that the OM integrity defect caused by the deletion of *dolP* is not related to the

marginal increment of membrane fluidity observed for the latter strain. This result suggests that the enhanced permeability of the  $\Delta doIP$  has a different cause.

### 3 Characterization of the interaction between DoIP and the BAM complex

As DoIP was identified as a putative interactor of BAM in our interactomic approach, we wanted to confirm the interaction between DoIP and the BAM complex. To this purpose, we used native pull down assays to check that DoIP and the BAM complex interact with each other in the envelope of *E. coli*. Moreover, we aimed to reconstitute the interaction *in vitro*.

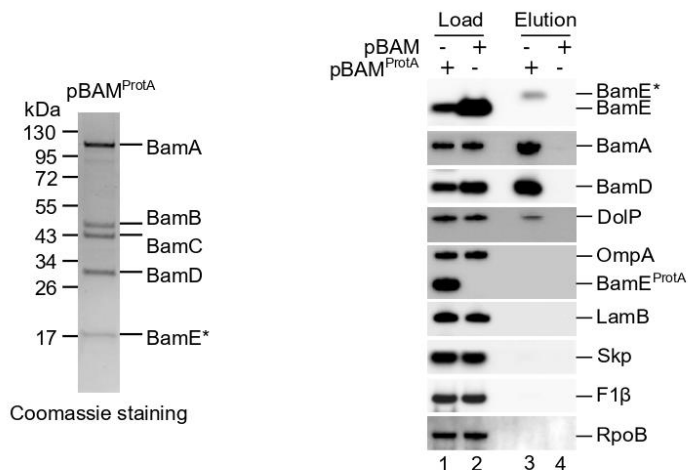
#### 3.1 DoIP and the BAM complex interact *in vivo*

The BAM interactome identified DoIP as a putative interactor of the BAM complex. Indeed, light DoIP at the BAM complex exchanged inefficiently with its heavy counterparts from the sample labeled with heavy-isotope amino acids, which is indicative of a stable interaction. To confirm such interaction, we performed the purification of BAM<sup>ProtA</sup> under native conditions to assess the co-isolation of DoIP using immunoblotting. Cells harboring pBAM<sup>ProtA</sup> or pBAM (encoding the full BAM complex, with BamE tagged with protein A or non-tagged, respectively) were cultured to mid-exponential phase prior to induction of plasmid-borne BAM expression for 1h. After collecting cells, the total membrane fraction was isolated. Membranes were solubilized with 1% (w/v) digitonin supplemented with 0.1 % (w/v) DDM to favor efficient solubilization. Membrane extracts were mixed with IgG-sepharose beads and proteins were eluted using proteolytic digestion by TEV. We confirmed the integrity of the BAM complex by SDS-PAGE and Coomassie Brilliant Blue staining that colors bands corresponding to the five subunits of the BAM complex (Fig. 15A, left panel). The total membrane fraction (loads) and elutions were also run on another gel and proteins were transferred to a PVDF membrane to perform Western blot.

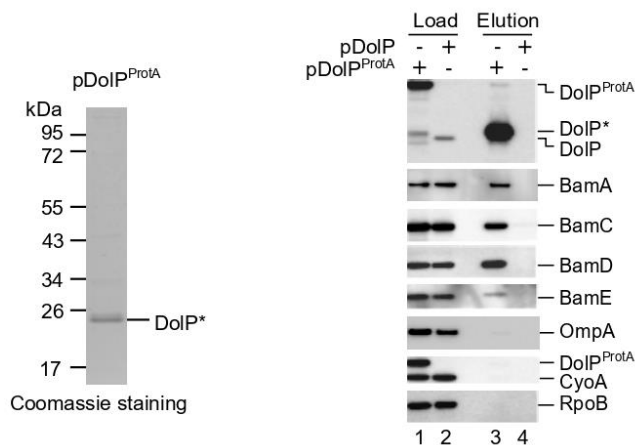
When membranes were immunodecorated with antibodies directed against subunits of the BAM complex ( $\alpha$ -BamA,  $\alpha$ -BamD,  $\alpha$ -BamE), we obtained clear signals at their expected sizes, validating our pull down (Fig. 15A, right pane, lane 3). In addition, we observed a signal using DoIP antiserum in the elution of the sample pBAM<sup>ProtA</sup> confirming that DoIP is co-purified with BAM<sup>ProtA</sup>. No signal was detected in the sample pBAM, our negative control. The OMPs OmpA and LamB were not detected in the elution fraction, demonstrating the specificity of our pull-down procedure. OmpA and LamB are assembled by the BAM complex into the OM. This reaction however involves transient BAM-client protein interactions (Doyle et al., 2022; Schiffrin et al., 2017a; Xiao et al., 2021), therefore these proteins are not detected in our BAM<sup>ProtA</sup> pull-down. In addition, the subunit F1 $\beta$  from the ATP synthase complex in the inner membrane and the cytosolic protein RpoB, used as negative controls, were not detected. Finally, the periplasmic chaperone Skp was also not detected.

To have another proof of this interaction, we aimed to perform the reverse experiment by purifying DolP. In this purpose, we constructed pDolP<sup>ProtA</sup> by replacing the poly-histidine tag of pDolP<sup>His</sup> by protein A tag. We created also another plasmid by introducing a stop codon between the sequence of DolP and Protein A (pDolP), which will be used for a mock control of the purification procedure.

**A**



**B**



**C**

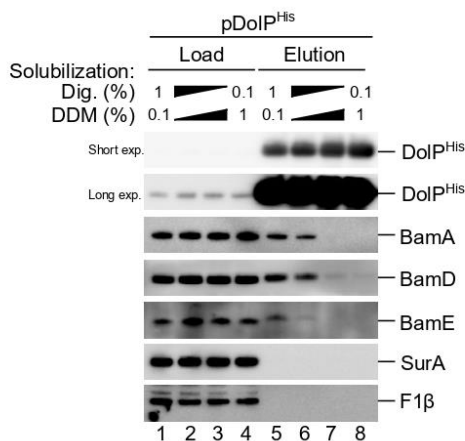


**Figure 15. DoIP and the BAM complex interact *in vivo*.** **A. Left.** Envelope fractions of BW25113 cells carrying pBAM<sup>ProtA</sup> were solubilized with 1% (w/v) digitonin and 0.1% (w/v) DDM and subjected to IgG-affinity purification of protein A-tagged BamE (pBAM<sup>ProtA</sup>). Elution fraction was loaded onto a SDS-PAGE and Coomassie Brilliant Blue stained, revealing 5 bands corresponding to the 5 BAM subunits. **Right.** The load and elution fractions were analyzed by SDS-PAGE and then transferred onto a PVDF membrane and proteins were detected by immunolabeling using the indicated antisera. Loads were set to 1% and elution to 100%. **B. Left.** The envelope fractions of BW25113 cells carrying the indicated plasmids were solubilized with 1% (w/v) digitonin and 0.1% (w/v) DDM and subjected to IgG-affinity purification of protein A-tagged DoIP. The load and elution fractions were analyzed by SDS-PAGE and Coomassie Brilliant Blue stained. **Right.** Proteins were transferred onto a PVDF membrane and blotted protein from load and elution fractions were detected by immunolabeling using the indicated antisera. Loads were set to 0.5% and elution to 100%. **C.** Equal aliquots of the envelope fraction of BW25113 cells expressing His-tagged DoIP were solubilized with the indicated concentrations (w/v) of digitonin and DDM, respectively: 1%, 0.1% (lane 1), 0.8%, 0.3% (lane 2), 0.3%, 0.8% (lane 3), 0.1%, 1% (lane 4). His-tagged DoIP was purified by Ni-affinity chromatography. In all cases, proteins were eluted in the presence of 0.3% (w/v) digitonin and 0.03% (w/v) DDM. Loads were set to 0.2% and elution to 100%.

Cells were cultured as described previously for the purification of BAM<sup>ProtA</sup>. Membrane protein extracts obtained upon solubilization of the envelope fraction with a mixture of 1% (w/v) digitonin and 0.1% (w/v) DDM were bound to IgG-conjugated beads. TEV digestion eluted DoIP\*, a slightly modified version of DoIP that harbors 15 additional residues at the C-terminal end. Total membrane proteins (loads) and elution fractions were analyzed by SDS-PAGE.

Coloration of the gel by Coomassie Brilliant Blue staining shows a single band running with an apparent molecular weight of 20 kDa, the expected size of DoIP\*, in the elution fraction (Fig. 15B, left panel). To further confirm this is DoIP, analysis by Western blot was conducted. The  $\alpha$ -DoIP antiserum decorated a band corresponding to DoIP\* in the TEV elution fraction (Fig. 15B, right panel, lane 3), validating our purification procedure. In addition, when membranes were incubated with antisera directed against BAM subunits, signals were detected with antisera specific for BamA, BamC, BamD and BamE in the elution sample of DoIP<sup>ProtA</sup>. Besides, decoration with  $\alpha$ -OmpA,  $\alpha$ -CyoA and  $\alpha$ -RpoB antisera showed no signal in the elution samples, demonstrating the specificity of the binding between DoIP and BAM. Taken together, these results confirm that DoIP is a *bona fide* BAM interactor.

### 3.2 DoIP – BAM interaction is detergent-sensitive

In an attempt to purify native BAM and DoIP as separated components for further *in vitro* complex reconstitution experiments, we looked for conditions in which the interaction between DoIP and BAM could be reduced. To this purpose, we tested mixtures of detergents, containing different concentrations of DDM and digitonin. Total membrane extracts of *E. coli* producing

recombinant DoIP<sup>His</sup> were obtained using different ratios of digitonin/DDM: 1%/0.1%, 0.8%/0.3%, 0.3%/0.8% and 0.1%/1% (w/v), respectively. After binding on Ni-NTA agarose beads and extensive washes, proteins were eluted using an excess of imidazole. Proteins of the total membrane and elution fractions were separated by SDS-PAGE and then transferred onto a PVDF membrane, prior to immunodetection. Whereas similar amounts of DoIP<sup>His</sup> were purified from all samples, we observed a reduction in the amounts of BAM subunits co-eluted along with DoIP<sup>His</sup> at concentrations of DDM between 0.3% and 1% (Fig. 15C, lanes 6 to 8). This suggests that a concentration of DDM above 0.3% (w/v) interferes with the interaction between DoIP and the BAM complex. Instead, digitonin preserves the interaction between BAM and DoIP. Based on these results, we used a concentration of 1% of DDM to purify BAM and DoIP as separate components for further *in vitro* assays. Conversely, a combination of 1% digitonin and 0.1% DDM seems to work best to extract efficiently membrane proteins while preserving the BAM-DoIP interactions.

### 3.3 DoIP and the BAM complex can be purified separately

To better understand whether the DoIP-BAM interaction requires other protein partners, we aimed to set up a protocol to test the interaction *in vitro*, after purifying separately both components.

To obtain a large amount of protein required for the *in vitro* assays, a scaled-up procedure was conducted using larger cultures of cells. As described before, plasmid-borne gene expression was induced by supplementing IPTG. After membrane isolation and solubilization using DDM, clarified total membrane protein extracts were loaded onto a HisTrap column for metal ion affinity chromatography using an automated ÄKTA machine. Proteins bound to the column were eluted using a gradient of imidazole and monitored during the chromatography process by measuring OD<sub>280</sub>. The fraction containing the protein of interest were pooled and loaded on a gel filtration column to fractionate the proteins according to their size.

In the case of the BAM complex, the gel filtration elution profile shows a single-peak at 114 min (Fig. 16A, right panel). Based on the peaks obtained with a high molecular weight calibration kit (data not shown), the BAM sample peaks corresponds to a complex of approximately 250 kDa, in accordance with previous reports (Roman-Hernandez et al., 2014). Analysis by SDS-PAGE and Coomassie Brilliant Blue staining of the elution fraction shows that all five BAM subunits are present in the elution fraction (Fig. 16A, left panel).

Interestingly, in the case of DoIP, several peaks were visible in this GF elution profile, suggesting DoIP could form multiple protein complexes by homooligomerization (Fig. 16B, right panel). Elution fractions were pooled and samples were concentrated prior SDS-PAGE

analysis and Coomassie Brilliant Blue staining, revealing a single band running with an apparent molecular weight corresponding to that of DoIP<sup>His</sup> (Fig. 16B, left panel).

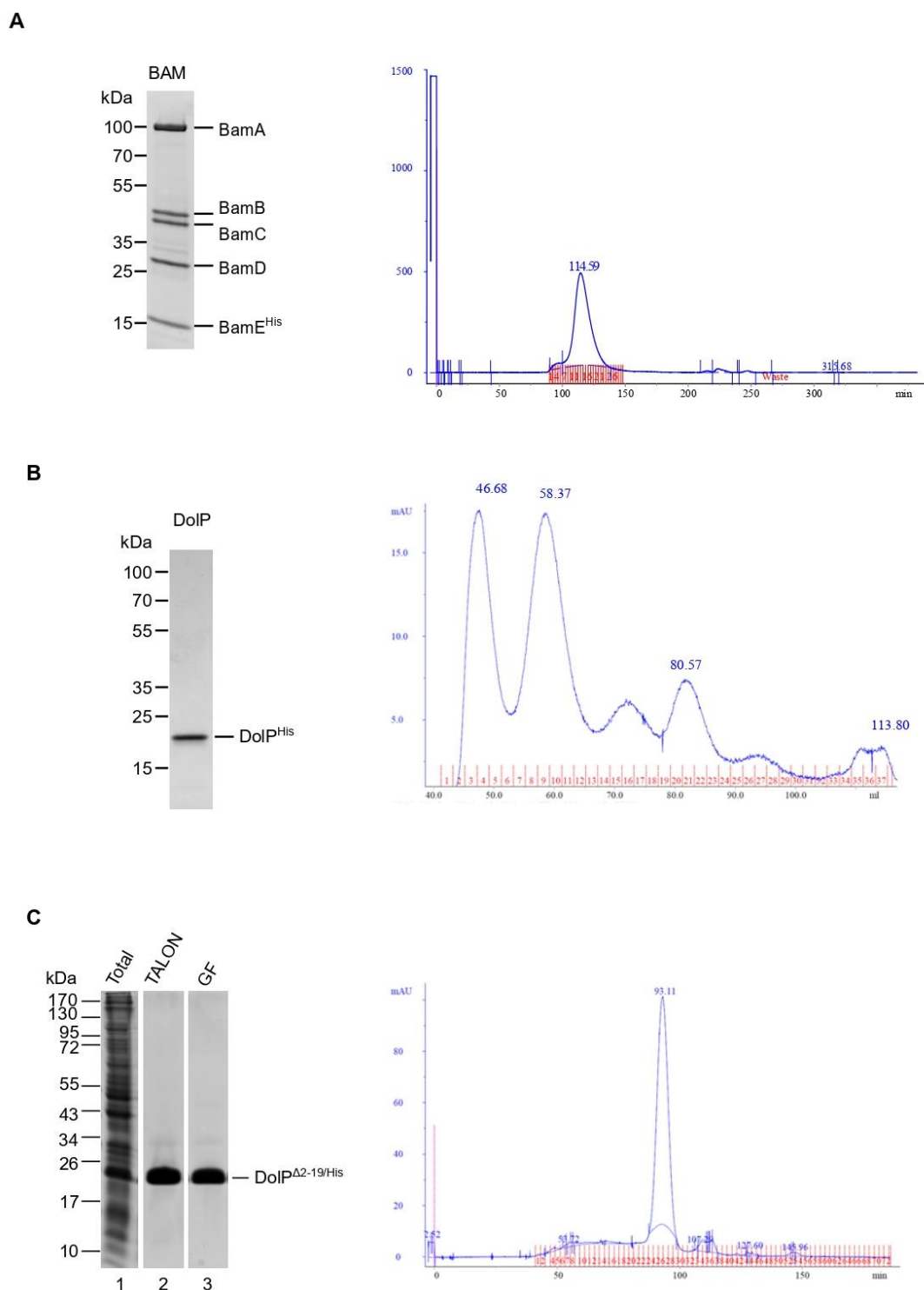


**Figure 16. DoIP and the BAM complex can be efficiently purified as separate components.** **A.** The envelope fraction of BW25113 cells overproducing BAM<sup>His</sup> was subjected to protein solubilization with 1% (w/v) DDM, Ni-affinity purification, and gel filtration chromatography. **Left.** The elution fractions were analyzed by SDS-PAGE and Coomassie Brilliant Blue staining. **Right.** GF chromatogram shows a single peak at the

expected size for the BAM complex (around 250 kDa). **B.** The envelope fraction of  $\Delta dolP$  cells overproducing DolP<sup>His</sup> was subjected to protein solubilization with 1% (w/v) DDM, Ni-affinity purification, and gel filtration chromatography. **Left.** The elution fractions corresponding to the size of DolP were pooled, concentrated and analyzed by SDS-PAGE and Coomassie Brilliant Blue staining. **Right.** GF chromatogram reveals several peaks at different sizes, indicating an heterogeneous oligomeric pattern for DolP. **C.** Total soluble fraction of  $\Delta dolP$  cells overproducing DolP <sup>$\Delta$ 2-19/His</sup> was subjected to protein solubilization with 1% (w/v) DDM, Cobalt-affinity purification, and gel filtration chromatography. **Left.** The elution fractions were analyzed by SDS-PAGE and Coomassie Brilliant Blue staining. **Right.** GF chromatogram reveals a single peak corresponding to the size of monomeric DolP.

### 3.4 Soluble DolP can be expressed in the cytosol and purified

We engineered a recombinant water-soluble form of DolP by deleting residues 2-19 (corresponding to its signal peptide including the conserved lipobox Cys residue) and fusing its C-terminus to a poly-histidine tag (DolP <sup>$\Delta$ 2-19/His</sup>). This form of DolP was expressed as a cytosolic protein, as it lacks the lipoprotein signal peptide. Cells transformed with the corresponding vector pDolP <sup>$\Delta$ 2-19/His</sup> (encoding this water-soluble form of DolP under the control of an IPTG-inducible promoter) were cultured, supplemented with IPTG at mid-exponential phase and collected to purify DolP <sup>$\Delta$ 2-19/His</sup> after cell disruption and removal of the membrane fraction. The supernatant was loaded onto a TALON column for affinity purification using an automated ÄKTA machine. TALON, a metal-affinity chromatography resin charged with cobalt, was used to increase the specificity of protein binding and improve the purity of the eluted proteins of interest. Proteins bound to the column were eluted using a gradient of imidazole. SDS-PAGE analysis and Coomassie Brilliant Blue staining of the elution fraction showed a prominent unique band, revealing efficient purification of DolP <sup>$\Delta$ 2-19/His</sup> (Fig. 16C, left panel, lane 2). Purified DolP <sup>$\Delta$ 2-19/His</sup> was then loaded onto a gel filtration column, revealing a single peak corresponding to a monodisperse species (Fig. 16C, right panel) of around 20 kDa by comparison with a small molecular weight calibration kit (data not shown). SDS-PAGE analysis of pure DolP <sup>$\Delta$ 2-19/His</sup> showed a unique band at the expected size for DolP (Fig. 16C, left panel, lane 3). This results confirms that a water-soluble form of DolP is monomeric, as previously shown for a non-native water-soluble form of DolP targeted to the bacterial periplasm (Bryant et al., 2020).

To confirm that native DolP can form homooligomers in the OM, we analyzed purified DolP <sup>$\Delta$ 2-19/His</sup> and DolP<sup>His</sup> by BN-PAGE. Then, the gel was blotted onto a PVDF membrane and incubated with  $\alpha$ -DolP antibodies. Western blot analysis of the sample containing DolP <sup>$\Delta$ 2-19/His</sup> showed a smear signal migrating with an apparent molecular weight ranging from 140 to 280 kDa approximately (Fig. 17A, lane 1). However, DolP<sup>His</sup> (purified from the OM) showed a diffuse signal between 250 and 600 kDa (Fig. 17A, lane 2). Interestingly, we observed soluble



DoIP migrated at a high molecular weight considering it is monomeric, however this sample seems very different to the OM-produced DoIP that seems to make very large multimers. This observation could be due to migration in BN-PAGE that could favor the formation of complexes after purification. These results suggest that native DoIP presents a dynamic multimeric organization.

Altogether, our results reveal that, upon native purification, DoIP can form at least in part large oligomers. This behavior is reminiscent of the multimeric organization of BonA from *A. baumannii*, which displays a dynamic multimeric organization consisting of pentamers of dimers (Grinter et al., 2021). BonA is an OM lipoprotein that contains an N-terminal extension, two BON domains and a C-terminal extension. However, the functional role of BonA homooligomerization process remains unknown. Similarly, further experiments should be conducted to determine how DoIP of *E. coli* oligomerizes and how such quaternary organization promotes function.

### 3.5 DoIP and the BAM complex interact *in vitro*

In order to assess if DoIP and the BAM complex could interact *in vitro*, we decided to reconstitute the BAM complex in proteoliposomes in presence of either native DoIP or its water-soluble variant. The reconstitution of the BAM complex in proteoliposomes has been already described (Roman-Hernandez et al., 2014). Following a similar procedure, purified *E. coli* phospholipids were resuspended in water and mixed with purified protein solutions containing DDM-solubilized BAM<sup>His</sup> alone, or equivalent amounts of purified BAM<sup>His</sup> with either DoIP<sup>Δ2-19/His</sup> or with DoIP<sup>His</sup> (Fig. 17B, lanes 1-3). After incubation, these reactions were diluted to promote formation of proteoliposomes and subjected to ultracentrifugation. The pellets were then resuspended and loaded on a SDS-PAGE to assess reconstitution of proteins. After migration, the gel was submitted to coloration by Coomassie Brilliant Blue. For the sample containing only the BAM complex, we observed five bands corresponding to subunits of the BAM complex (Fig. 17B, lane 4), demonstrating proteins were reconstituted in proteoliposomes. For the sample where the BAM complex was mixed with DoIP<sup>His</sup>, we observed the presence of a band migrating at the expected size of DoIP, suggesting this protein was reconstituted with the complex (lane 5). This was not the case for the sample where the BAM complex was mixed with the cytosolic DoIP (DoIP<sup>Δ2-19/His</sup>, lane 6), suggesting this reconstitution is dependent on the purified form of DoIP.

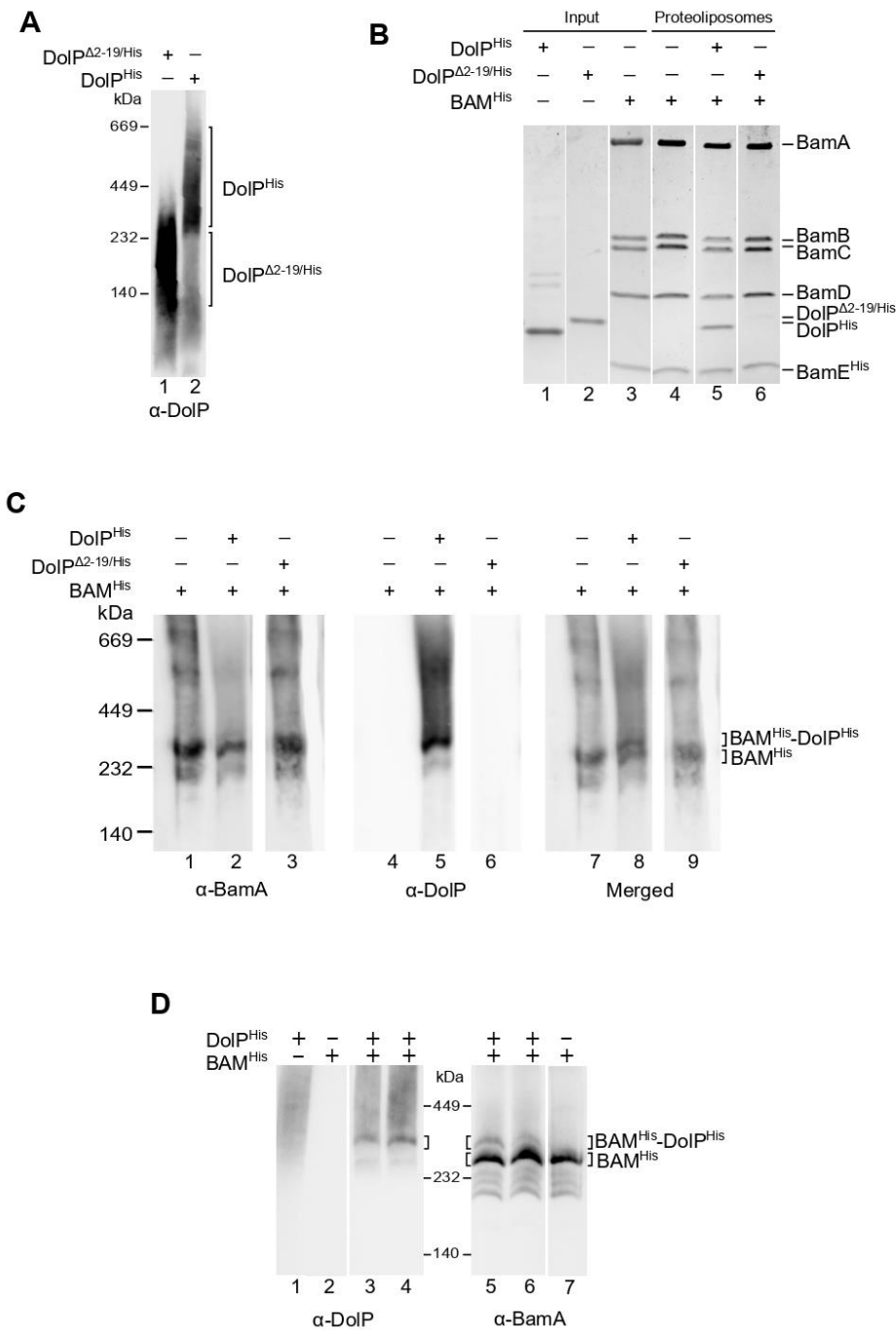


**Figure 17. The BAM complex and DolP can interact *in vitro*.** **A.** Purified proteins (DolP<sup>His</sup> and DolP<sup>Δ2-19/His</sup>) were analyzed by BN-PAGE and Western blot using DolP antibodies. **B.** Equimolar amounts of proteins were mixed and reconstituted into proteoliposomes. Analysis by SDS-PAGE and Coomassie Brilliant Blue staining of the input reveals the amount of protein used (lanes 1-3) and the amount retrieved after proteoliposome reconstitution (lanes 4-6). **C.** Proteins after proteoliposome reconstitution were then subjected to BN-PAGE and transferred onto a PVDF membrane. Membranes were analyzed using indicated antisera. **D.** Roughly equimolar quantities of purified His-tagged BAM complex and DolP were incubated alone for 1 hr at 4°C (lanes 1, 2, and 7), or together for 1 hr at 4°C (lanes 3 and 6) or for 30 min at 25°C (lanes 4 and 5), prior to BN-PAGE and immunoblotting using the indicated antisera.

To further verify this reconstitution, samples were loaded in a BN-PAGE to observe formation of protein complexes. Proteins were then transferred onto PVDF membranes and subsequently immunodetected using BamA or DoIP antibodies. For the sample containing only BAM in proteoliposomes, we observed a signal using BamA antibodies at 250 kDa approximately, the size of the BAM complex (Fig. 17C, lane 1). Interestingly, for the sample BAM<sup>His</sup> mixed with DoIP<sup>His</sup>, we observed a faint signal just above the main band of the BAM complex (lane 2). When membranes were incubated with DoIP antibodies, a signal in the upper part of the gel was observed for the sample in which BAM is mixed with DoIP<sup>His</sup> corresponding to the signal previously observed for DoIP<sup>His</sup> (lane 5). This signal however was not visible for the soluble version of DoIP (lane 6), corroborating the fact that this soluble version was not reconstituted in proteoliposomes. When we merged both signals, we can observe the two bands in the presence of BAM and DoIP<sup>His</sup>, suggesting the formation of a supercomplex only with the OM-version of DoIP (lane 8).

Considering the fact that the yield of protein incorporation into proteoliposomes was low, we decided to work in the presence of only detergents, assuming they could be sufficient to maintain DoIP-BAM interaction. In this experiment, we used low concentrations of DDM (0.03% w/v) to maintain protein soluble after purification. Purified proteins were mixed in roughly equimolar amounts and then incubated with low amounts of DDM and subsequently diluted with buffer containing digitonin. Then, samples were analyzed by BN-PAGE. As negative control, purified proteins alone were also analyzed.

After BN-PAGE, proteins were transferred onto a PVDF membrane and then decorated using  $\alpha$ -DoIP or  $\alpha$ -BamA antisera. When decorated with DoIP antibodies, a diffuse signal of DoIP was observed in the upper part of the gel, as in previous analyses (Fig. 17D, lane 1). When BAM and multimeric DoIP<sup>His</sup> were mixed, we obtained a diffuse signal at the top of the gel, but also a clear band migrating around 280 kDa (lanes 3 and 4). As expected, no signal was obtained for BAM, using DoIP antibodies (lane 2).

When using BamA antibodies, a signal at 250 kDa was observed for the sample containing only BAM<sup>His</sup>, confirming the full complex was reconstituted (lane 7). Some less abundant bands were observed below the expected weight of the BAM complex, which suggest the presence of incomplete forms of the BAM complex, as seen in previous experiments when BAM is purified with DDM (Fig. 11B, right panel, lane 2) or in the literature (Rodríguez-Alonso et al., 2020). When DoIP<sup>His</sup> and BAM<sup>His</sup> were incubated, we obtained an additional band above that of the BAM complex around 280 kDa (lanes 5 and 6). This band displays the same Rf as the one observed using  $\alpha$ -DoIP, suggesting it corresponds to the same complex. Altogether, our data suggest that DoIP and the BAM complex may form, in the presence of detergents, a

supercomplex migrating around 280 kDa in BN-PAGE. It is to note that this supercomplex is non-stoichiometric, as we can observe a significant amount of BAM and DoIP that are still migrating independently. We can observe also that DoIP is migrating mostly as a multimer and only a small proportion of DoIP forms a supercomplex with BAM, suggesting the interaction is labile.

We demonstrated that only the OM-associated DoIP is able to interact with the BAM complex. Besides, as OM-associated DoIP is oligomeric, we assume DoIP oligomerization could be critical for BAM-DoIP interaction. However, the apparent molecular weight observed for the supercomplex (around 280 kDa) suggests that DoIP may interact with the BAM complex as a monomer or dimer.

Previous studies have suggested the interaction between DoIP and BAM (Babu et al., 2017; Bryant et al., 2020), but to date, no formal proof of this interaction was available in the literature. Here we show that DoIP can interact with the BAM complex both *in vivo* and *in vitro* and our data demonstrate that the native form of DoIP is required to promote the interaction. Moreover, our data suggest that DoIP is able to form homooligomers *in vivo* only when it is produced as a membrane-anchored lipoprotein. However, when DoIP interacts with BAM, it is most likely under a monomeric or dimeric form, suggesting it may display a dynamic behavior, shifting from a multimeric form when anchored in the OM to a monomeric/dimeric version when it interacts with BAM. The interaction between DoIP and BAM is however not stoichiometric and a large portion of BAM and DoIP do not interact. More studies should be conducted to investigate the biological relevance of these different populations of DoIP.

We now wanted to further characterize the DoIP-BAM interaction by identifying the subunit of the BAM complex that interacts with DoIP, using pull down experiments and crosslinking assays.

### 3.6 BamA is efficiently co-purified with DoIP when both proteins are overproduced

We first hypothesized that DoIP could interact with BamA as this subunit makes contact to other lipoproteins including the BamBCDE subunits and the Rcs sensor protein RcsF (Cho et al., 2014; Konovalova et al., 2014; Rodríguez-Alonso et al., 2020)

To test this hypothesis, we co-overproduced DoIP<sup>His</sup> together with BamA using the plasmid pBamA-DoIP<sup>His</sup>. Upon purification, proteins in the elution fraction were separated by SDS-PAGE. The Coomassie stained gel shows two bands, one migrating at around 20 kDa, which corresponds to the bait DoIP<sup>His</sup> and one at 90 kDa, which is the size of BamA (Fig. 18A). This result suggests that BamA, the core component of the BAM complex, can directly interact with

DoIP. It should be noted that the amount of co-purified BamA is still submolar compared to DoIP<sup>His</sup>, even though the concomitant overproduction of BamA together with DoIP<sup>His</sup> improves the co-purification efficiency compared to the condition where only DoIP is overproduced (Fig. 15B).

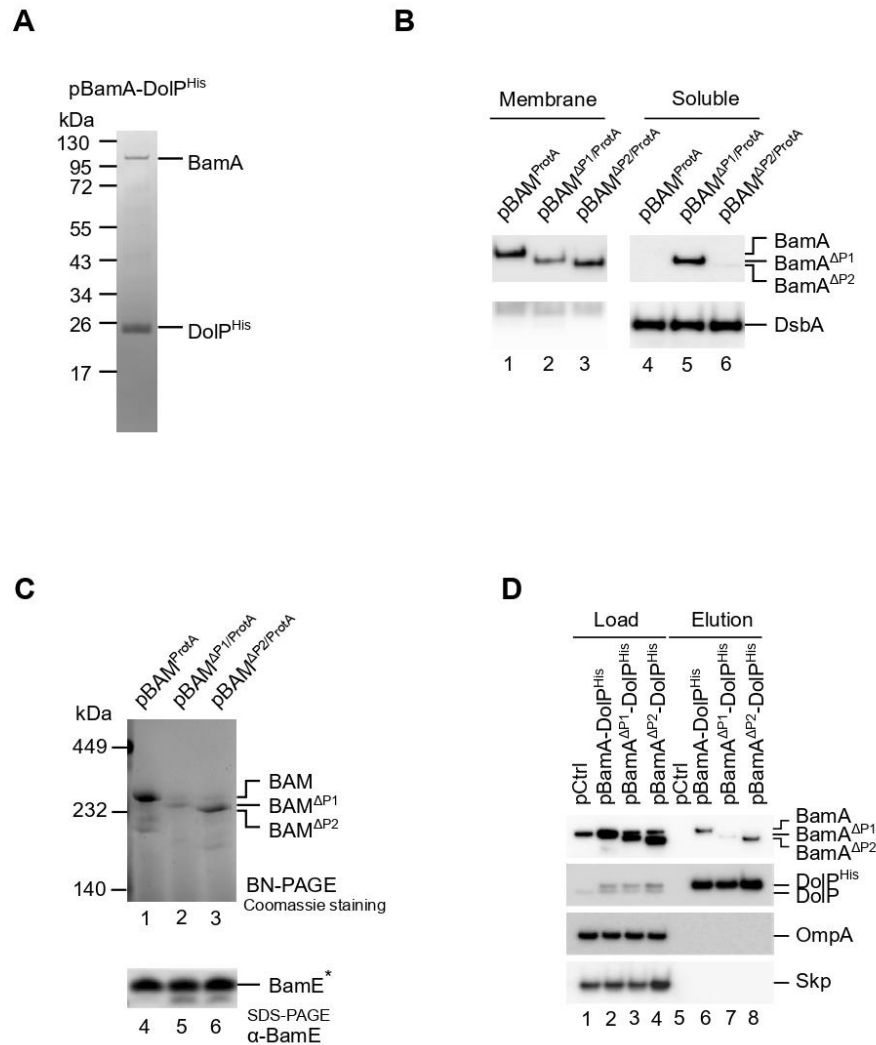


**Figure 18. BamA in the OM is a critical determinant for the interaction with DoIP.** **A.** Envelope fractions of BW25113 cells carrying the plasmids overproducing His-tagged DoIP and BamA were used for Ni-affinity purification after solubilization using 1% (w/v) digitonin and 0.1% (w/v) DDM. Eluted proteins were analyzed by SDS-PAGE and Coomassie Brilliant Blue staining. **B.** Envelope fractions of BW25113 cells carrying the plasmids overproducing the BAM complex with variants of BamA (deleted of POTRA1 or of POTRA2) were used for cell fractionation upon treatment with lysozyme and EDTA. Samples were analyzed by SDS-PAGE and Western blot for the total membrane fraction (lanes 1–3) and soluble fraction containing the periplasmic protein DsbA (lanes 4–6). **C.** Envelope fractions of cells overproducing BAM<sup>ProtA</sup>, BAM<sup>ΔP1/ProtA</sup>, or BAM<sup>ΔP2/ProtA</sup> were solubilized with 1% (w/v) digitonin and 0.1% (w/v) DDM. Fractions were subjected to native IgG-affinity purification and samples were eluted using TEV protease. These samples were analyzed by BN-PAGE and Coomassie Brilliant Blue staining (lanes 1-3) and SDS-PAGE and Western blot using BamE antibodies (lanes 4-6). **D.** Envelope fractions of BW25113 cells carrying the plasmids overproducing His-tagged DoIP and the

indicated BamA protein variants (deleted of POTRA1 or of POTRA2) were solubilized with 1% (w/v) digitonin and 0.1% (w/v) DDM and subjected to Ni-affinity purification. Proteins were eluted with an excess of imidazole and subjected to SDS-PAGE and Western blot analysis. Loadings were set to 2% and elutions to 100%.

### 3.7 DolP interacts with OM-assembled BamA

We wondered whether DolP would interact with BamA prior to or after its assembly into the BAM complex at the OM. To address this question, we monitored the interaction of DolP with wild-type BamA or a mutant form of BamA that is inefficiently assembled in the OM.

BamA contains a  $\beta$ -barrel domain and five POTRA domains. It was previously reported that the deletion of POTRA 1 (P1, residues 24-91) affects efficient assembly of BamA in the OM and for the formation of the complex (Bennion et al., 2010), providing a useful tool to monitor the interaction of DolP with BamA at different assembly states of the latter protein. We engineered the assembly defective BamA mutant form that lacks P1, as well as a version deleted from the P2 (residues 91-172) known to be functional and properly assembled in the OM (Bennion et al., 2010). The plasmid pBAM<sup>ProtA</sup> was used as template to create pBAM <sup>$\Delta$ P1/ProtA</sup> and pBAM <sup>$\Delta$ P2/ProtA</sup> (that harbor deletion of P1 or P2, respectively). To confirm the cellular localization of these BamA mutant forms, we performed cell fractionation by treating cells with EDTA and lysozyme to weaken the cell envelope in the absence of any osmoprotectant. Under these conditions, the cytoplasmic turgor pressure causes cell lysis. This allowed us to collect the cell soluble fraction (which includes the cytosol and the periplasm) and the total membrane fraction. SDS-PAGE and Western blot analysis revealed that BamA <sup>$\Delta$ P1</sup> (80.6 kDa) accumulated in the soluble fraction, while full-length BamA (88.1 kDa) or BamA <sup>$\Delta$ P2</sup> (79.2 kDa) were enriched in the membrane fraction (Fig. 18B).

Upon purification of BamE<sup>ProtA</sup> via IgG-affinity chromatography followed by SDS-PAGE (to detect the bait protein by Western blot) and BN-PAGE (to detect the BAM complex by Coomassie Brilliant Blue staining), we observed that the amount of BAM complex for the sample harboring deletion of P1 was much lower compared to the full BamA or to the sample containing the deletion of P2 (Fig. 18C, lanes 1-3). This result demonstrates that the deletion of P1 of BamA alters significantly the formation and/or the stability of the full BAM complex. As expected the BAM complex migrated with an apparent molecular weight of 250 kDa (full BamA, lane 1), and faster with the deletions of P1 or P2, respectively 240 kDa (BamA <sup>$\Delta$ P1</sup>, lane 2) and 230 kDa (for BamA <sup>$\Delta$ P2</sup>, lane 3). Taken together, these results confirmed that BamA <sup>$\Delta$ P1</sup> assembles inefficiently in the OM whereas the deletion of P2 has no effect on membrane assembly of BamA, as previously described in the literature (Bennion et al., 2010).

To further investigate whether DoIP preferentially interacts with OM-assembled BamA or with a form of BamA that accumulates in the periplasm, we co-overexpressed DoIP together with BamA or its two variant forms and performed purification of DoIP<sup>His</sup> using the same conditions as described previously. After pull down, proteins were transferred onto a PDVF membrane and then incubated with appropriate antibodies. Decoration using DoIP antiserum shows a similar amount of bait protein DoIP<sup>His</sup> for the three elutions (Fig. 18D, lanes 6-8). For BamA antiserum, we observed signals for BamA corresponding to the three versions of the protein (full version or deleted of one POTRA domain), in similar amounts in the total extracts (lanes 2-4). However, whereas the amount of co-purified BamA<sup>ΔP2</sup> was similar to that obtained with BamA (lanes 6 and 8), BamA<sup>ΔP1</sup> was much less abundant in the elution fraction (lane 7), suggesting that the OM localization of BamA is crucial for the interaction with DoIP.

To conclude, our data revealed that DoIP interacts directly with OM-assembled BamA.

## 4 Characterization of DoIP interactors by crosslinking approaches

In an attempt to provide more insights into the interacting landscape of DoIP, *i.e.* to characterize the interaction with BamA and to identify other protein partners involved, we carried out crosslink experiments, using either chemical or site-directed photoactivable crosslinker.

### 4.1 Chemical crosslinking of DoIP did not permit to detect BAM subunits

To confirm the fact that DoIP and BamA interact directly, we set up chemical crosslinking experiments. Four different crosslinkers were used, based on their chemical properties:

- i) DSP (Dithiobis(succinimidyl propionate)), containing a spacer arm of 12 Å
- ii) EGS (ethylene glycol bis(succinimidyl succinate)), containing a spacer arm of 16.1 Å
- iii) DSG (disuccinimidyl glutarate), containing a spacer arm of 7.7 Å
- iv) BS3 (bis(sulfosuccinimidyl)suberate), containing a spacer arm of 11.4 Å

Upon overproduction of BamA together with DoIP<sup>His</sup> and membrane isolation, proteins were crosslinked and DoIP<sup>His</sup> was purified under denaturing conditions. Total membranes and elution samples were loaded on a SDS-PAGE and proteins were transferred onto a PVDF membrane for Western blot analysis. Membranes were immunodecorated using  $\alpha$ -BamA and  $\alpha$ -DoIP antibodies (Fig. 19, A: low exposure, B: high exposure). For DoIP decoration, we can observe in the total membrane extract a clear signal at an apparent molecular weight of 20 kDa, the size of DoIP. For the crosslinked samples, additional smeared signals were observed at higher molecular weights in the total membrane extracts (lanes 2, 6 and 14), suggesting the presence of DoIP crosslink products. Notably, we can observe a major smear signal at around 180 kDa in the case of DSP (Fig. 19B, lane 2) and BS3 (lane 14), suggesting the formation of high molecular weight complexes.

In the case of BamA decoration of the total membranes, we observe a signal at an apparent molecular weight of 90 kDa, the size of BamA. Besides, additional signals at higher molecular weights were detected with total membrane samples supplemented with crosslinkers (lanes 2, 6 and 14), suggesting the presence of BamA crosslink products. In the case of EGS (lane 6), we can observe a smear at around 250 kDa, that could correspond to the BAM complex.

In the case of BamA decoration of the total membranes, we observe a signal at an apparent molecular weight of 90 kDa, the size of BamA. Besides, additional signals at higher molecular weights were detected with total membrane samples supplemented with crosslinkers (lanes 2,



6 and 14), suggesting the presence of BamA crosslink products. In the case of EGS (lane 6), we can observe a smear at around 250 kDa, that could correspond to the BAM complex.

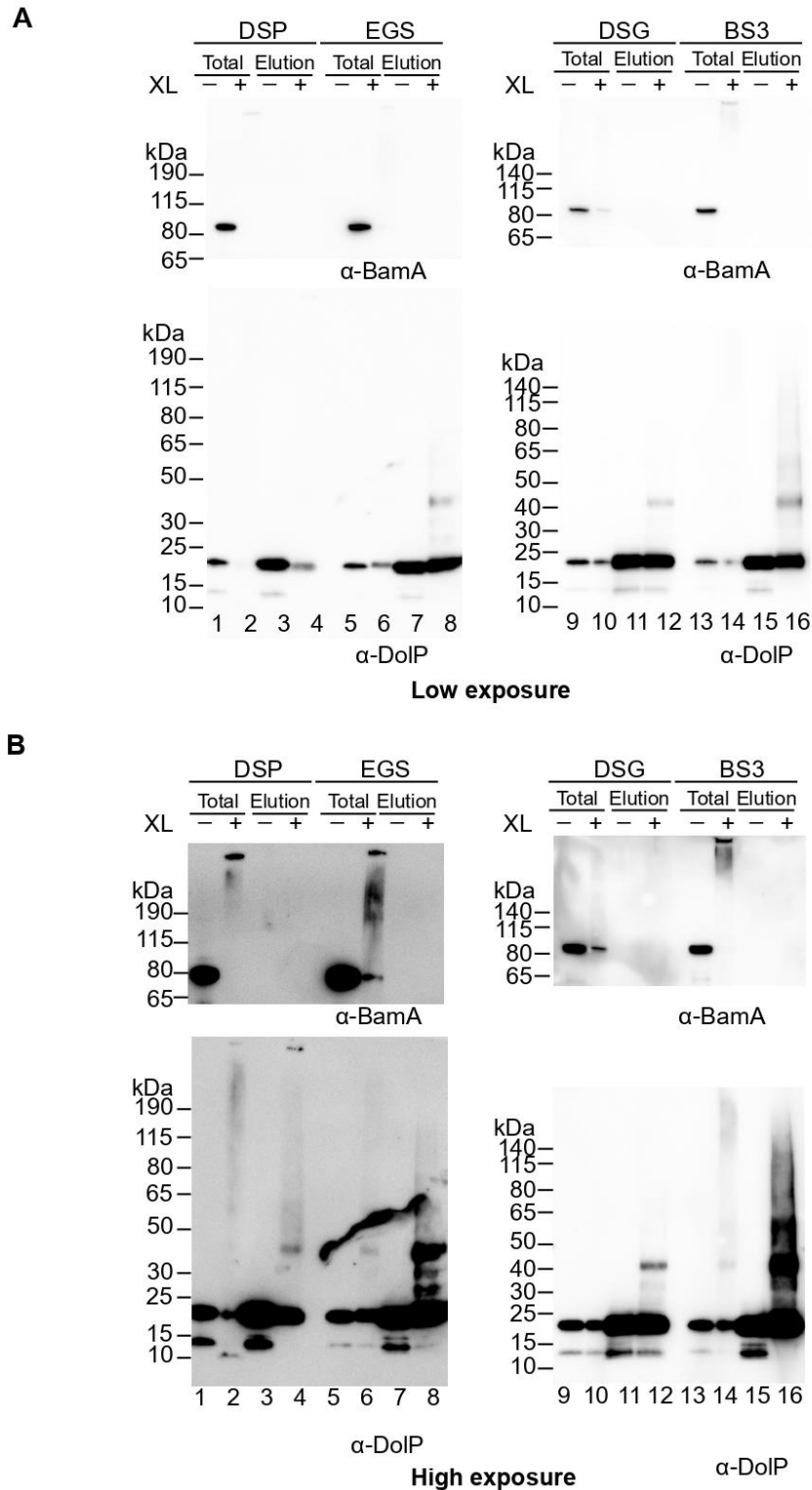


**Figure 19. DolP can be chemically crosslinked *in vivo*.** A. Envelope fractions of BW25113  $\Delta dolP$  cells carrying the plasmid overproducing His-tagged DolP and BamA were isolated and resuspended in PBS buffer.

Envelope resuspension was mixed with indicated crosslinkers and incubated for 30 min. After quenching, proteins were TCA precipitated and pellets were used to perform denaturing Ni-affinity chromatography purification. Proteins were eluted with an excess of imidazole and subjected to SDS-PAGE and Western blot analysis. Antibodies against DoIP and BamA were used for immunodetection. **A.** Low exposure and **B.** High exposure.

In the case of BamA decoration of the total membranes, we observe a signal at an apparent molecular weight of 90 kDa, the size of BamA. Besides, additional signals at higher molecular weights were detected with total membrane samples supplemented with crosslinkers (lanes 2, 6 and 14), suggesting the presence of BamA crosslink products. In the case of EGS (lane 6), we can observe a smear at around 250 kDa, that could correspond to the BAM complex.

In the case of the elution samples, we can observe using  $\alpha$ -DoIP decoration that DoIP is enriched, showing the purification worked. For the crosslinked samples, we can observe signals migrating at 40 kDa for all crosslinking conditions (lanes 4, 8, 12 and 16), suggesting possible dimerization of DoIP. Interestingly, crosslinker BS3 (lane 16) shows crosslink products at 40, 60, 80 and 100 kDa that could correspond to a pattern of homooligomerization of DoIP, in line with our previous gel filtration and BN-PAGE data.

Concerning BamA decoration, we cannot see any signal in the elution samples, suggesting BamA is not crosslinked to DoIP in these experimental conditions.

In conclusion, our chemical *in vivo* crosslinking assays confirm that DoIP can form homooligomers as previously shown using other approaches. However, we could not show the DoIP-BAM association with this approach. We thus decided to test an alternative strategy based on site-directed crosslinking to further characterize the DoIP- BAM interaction.

#### 4.2 Site-directed photocrosslinking of DoIP

We used a different approach, site-directed photocrosslinking, to obtain further evidence that DoIP makes direct contact to the BAM complex and identify the sites of interaction in DoIP. This approach relies on the incorporation of a synthetic photoactivable amino acid analog (such as para-benzoyl-phenylalanine, Bpa), along the amino acid sequence of DoIP. This incorporation is achieved directly in cells using an amber suppression method, where an engineered orthogonal tRNA synthetase and an amber-suppressor tRNA introduced the amino acid analog in correspondence of an amber codon introduced in a gene of interest (Chin et al., 2002). Thus, we designed oligonucleotide pairs to perform site-directed mutagenesis to introduce amber codons (TAG) at unique positions along the sequence of *doIP*, generating a series of pDoIP<sup>Bpa/His</sup> derivative plasmids.

Since Bpa is a rather hydrophobic residue, we selected non-polar/hydrophobic amino acids along the sequence of DoIP (*i.e.* Phe, Val, Tyr, Trp, Leu and Ile) for substitution with Bpa. Then, upon irradiation with a UV source of light (350-360 nm), Bpa forms a radical that reacts with carbon-hydrogen bonds in forming a covalent crosslink (Chin et al., 2002; Young et al., 2010). Because the size of Bpa is similar to that of natural amino acids, crosslink products indicate that the covalently bound protein is in close proximity of the engineered protein of interest.

We created a collection of 24 pDoIP<sup>Bpa/His</sup> derivative plasmids containing amber codons along the sequence of *doIP* (Fig. 20A). One position (V9) was on the signal peptide (as a negative control since Bpa will not be present in the mature protein cleaved at position 19), five positions on the linker region between the lipid-modified N-terminal cysteine and BON1 (V20, V25, V30, V41, V45), eight positions in BON 1 (V52, L58, I64, V72, Y75, L90, V101, Y108) and nine positions in BON 2 (W127, V132, V142, V149, F157, V162, V177, F189). Cells were co-transformed with plasmids harboring amber codons (pDoIP<sup>Bpa/His</sup>) and pEVOL, a plasmid harboring the genes encoding for the tRNA/RNA synthase pair required for Bpa incorporation in the sequence of DoIP by amber suppression (Chin et al., 2002). After induction with IPTG and addition of Bpa, cell cultures were split in two halves: one half was UV-irradiated on ice to promote activation of Bpa and the other half was kept in the dark on ice. Membranes were then isolated and proteins were purified in denaturing conditions, as in previous experiments. Elution samples were then analyzed by SDS-PAGE.

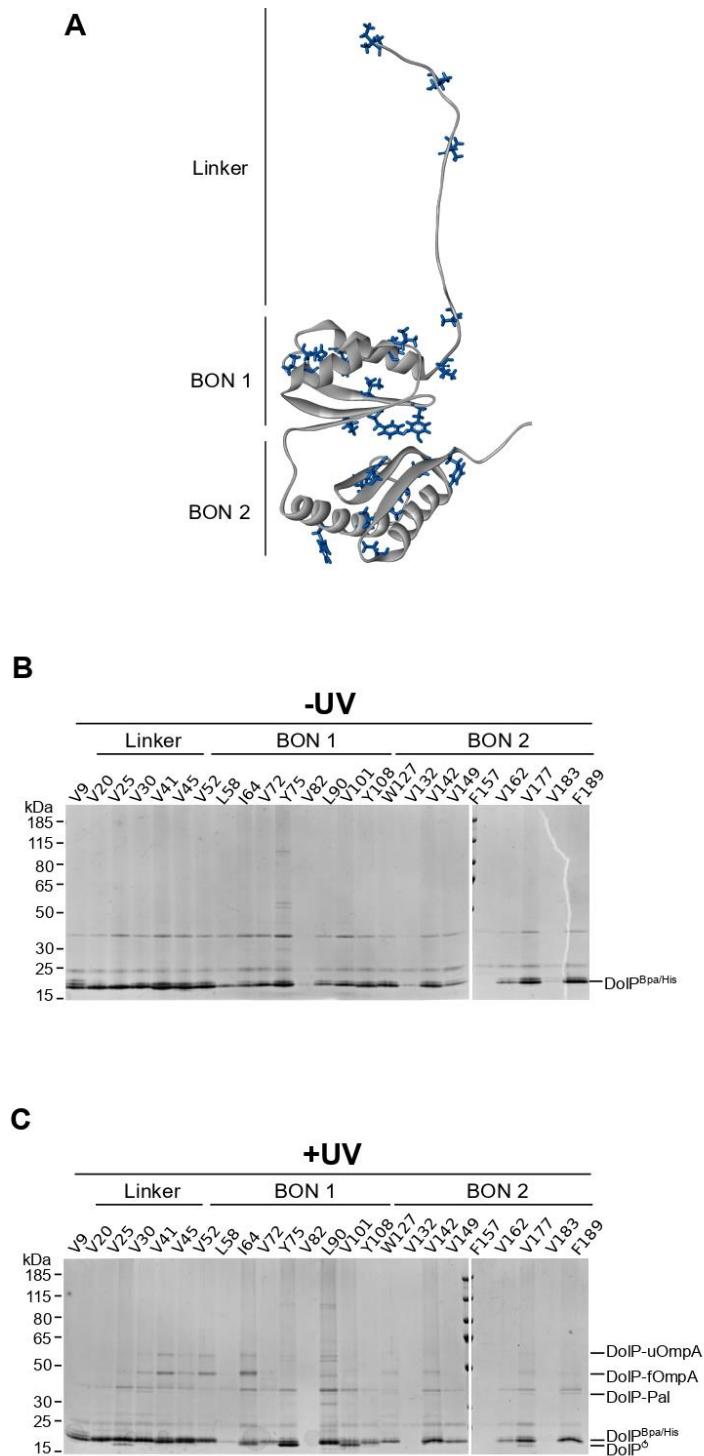


**Figure 20. DoIP can be efficiently purified after site-directed photocrosslinking.** **A.** Cartoon representation of DoIP structure (PDB: 7A2D), highlighting residues where Bpa was introduced by amber codon suppression. **B and C.** BW25113  $\Delta dolP$  cells carrying pEVOL-pBpF and a pDoIP<sup>His</sup> with amber codons engineered at different positions of the *dolP* ORF were grown in M9 minimal medium supplemented with glucose, in the presence of Bpa. After inducing gene expression by supplementation with IPTG, fractions were split in two: one was UV-irradiated (+UV, **C**) and the other was kept on ice without irradiation (-UV, **B**). Envelope fractions corresponding to these cultures were subjected to denaturing Ni-affinity chromatography purification. Proteins

were eluted using an excess of imidazole after extensive washes. Elution fractions were analyzed by SDS-PAGE and Coomassie Brilliant Blue staining.

For the non-irradiated samples, analysis by Coomassie Brilliant Blue staining of the gel revealed a band migrating at approx. 20 kDa that corresponds to DoIP<sup>His</sup> (Fig. 20B). A similar yield of purification of DoIP<sup>Bpa/His</sup> for all samples was observed, except for positions V82, V132, F157 and V183, for which we obtained less bait protein. This suggests Bpa might have not been properly incorporated at these positions, or that these mutations may affect the stability of the protein and consequently its purification.

For the UV-irradiated samples, we observed some additional bands that were not present in the gel containing –UV samples. These bands are likely to represent crosslink products (Fig. 20C). Two bands migrating at 50 and 60 kDa were visible for almost every position where Bpa is inserted in the linker region of DoIP as well as in BON 1. These bands were also visible for some positions of BON 2. Interestingly, position V25, Y75, V101 and V177 revealed faster migrating bands, just below the band that corresponds to DoIP<sup>Bpa/His</sup>. Finally, in some cases, in particular for V30, V142 and F189, a band running with an apparent molecular weight of 38 kDa approx. was visible.

To identify proteins crosslinked with DoIP, two approaches were carried out: MALDI-TOF MS, and Western blot analysis using different antisera.

#### 4.3 Identification of Bpa-crosslink proteins by MALDI-TOF MS

In a first attempt to identify crosslink products, we carried out MALDI-TOF MS to identify proteins. This technique relies on the excision of gel bands corresponding to crosslink products stained by Coomassie Brilliant Blue. After tryptic digestion, peptides were analyzed by MALDI-TOF MS and proteins were identified by peptide mass fingerprinting. We were able to confirm the incorporation of Bpa in the sequence of DoIP by identifying the peptide with the expected molecular mass after Bpa substitution. This identification was possible for almost all DoIP<sup>Bpa/His</sup> variants, in their non-crosslinked form (band excised at 20 kDa). Notably, the identified Bpa-containing peptides were not detected in the samples corresponding to crosslink products (bands at higher molecular weights), confirming DoIP formed crosslink products after UV irradiation. MS analyses allowed the identification of several envelope proteins crosslinked with DoIP listed below (Table 2).

| Position | Proteins identified | Bpa peptide (m/z) | Notes                          |
|----------|---------------------|-------------------|--------------------------------|
| V9       | DoIP                | ND                | Peptide Bpa cleaved            |
| V20      | DoIP                | ND                |                                |
| V25      | DoIP, OmpA          | ND                |                                |
| V30      | DoIP, Pal, OmpA     | ND                |                                |
| V41      | DoIP, OmpA          | ND                |                                |
| V45      | DoIP, OmpA          | ND                | Analysis by MALDI TOF TOF      |
| V52      | DoIP, OmpA          | 1627              | Analysis by MALDI TOF TOF      |
| L58      | N/A                 |                   |                                |
| I64      | DoIP, OmpA          | ND                |                                |
| V72      | DoIP                | 1145              |                                |
| Y75      | DoIP                | 1081              | Intramolecular crosslink       |
| V82      | N/A                 |                   |                                |
| L90      | DoIP                | 1691              | Possibly contaminants detected |
| V101     | DoIP                | 2031              |                                |
| Y108     | DoIP                | 1967              |                                |
| W127     | DoIP, OmpA          | 2081              |                                |
| V132     | N/A                 |                   |                                |
| V142     | DoIP, Pal           | 1255              |                                |
| V149     | DoIP                | 2047              |                                |
| F157     | N/A                 |                   |                                |
| V162     | DoIP                | LD                |                                |
| V177     | DoIP                | LD                |                                |
| V183     | N/A                 |                   |                                |
| F189     | DoIP, Pal           | 1131              |                                |

**Table 2. Proteins identified crosslinked to DoIP by MALDI-TOF MS analysis.** List of the proteins crosslinked to DoIP identified by MALDI-TOF MS analysis. After SDS-PAGE and Coomassie Brilliant Blue staining, proteins were excised and washed prior tryptic digestion. Identification of proteins was made using Protein Prospector software. This table includes the position where Bpa was introduced along the sequence of DoIP (N/A: not analyzed), the proteins identified in each sample (including the bait protein), the m/z value of the Bpa-containing peptide (ND: not detected; LD: limit of detection) and additional notes, such as a further fragmentation by MALDI-TOF/TOF MS analyses at positions V41 and V52 for analysis for OmpA crosslink and Y75 for analysis of the intramolecular crosslink.

## *OmpA*

The Outer Membrane Protein A (OmpA) was identified together with DolP in the band clearly visible around 60 kDa, when Bpa was incorporated at various positions of DolP, especially in the linker and the domain BON 1 (Fig. 20C). The apparent molecular weight observed for this crosslink product is in accordance with the expected size of DolP-OmpA (20 and 37 kDa for DolP and OmpA, respectively). OmpA is one of the most abundant proteins in the Gram-negative bacterial envelope and it is composed of two domains: a  $\beta$ -barrel (N-terminal) domain, which is embedded in the OM, and a periplasmic (C-terminal) domain. We identified OmpA also in the crosslink product migrating at 50 kDa (Fig. 20C). This lower OmpA band can be a degradation product of DolP-OmpA or it may represent a faster migrating isoform of the crosslink product. We asked if DolP interacts with the  $\beta$ -barrel or the periplasmic domains of OmpA. To this end, we predicted all putative crosslinked dipeptides containing the tryptic peptide of DolP with Bpa at position V41 or V52 and any possible tryptic peptide of OmpA. By comparing all these theoretical masses with the experimental ones, we identified a very intense peak at  $m/z=2227.09$  in the MALDI-TOF spectra (Fig. 21B and C). Because V41 or V52 are part of the same tryptic peptide of DolP, the mass of the crosslinked dipeptide is the same for both samples. The mass of the tryptic peptide of OmpA fitting with the  $m/z$  signal at 2227.09 is 599.33 Da, corresponding to the sequence  $_{289}\text{GIPADK}_{294}$  in the periplasmic domain of OmpA.

We carried out the fragmentation of the peptide at  $m/z=2227.09$  ( $_{289}\text{GIPADK}_{294}$ ) using MALDI-TOF/TOF and of the corresponding miscleaved peptide at  $m/z=2653.36$  ( $_{289}\text{GIPADKISAR}_{298}$ ) by LC-MS/MS. This fragmentation confirmed the primary sequence of both peptides (from DolP and from OmpA) (Fig. 21D and E). Besides, y ions from the OmpA peptide were clearly identified until y7, suggesting the covalent bound is more probably positioned between G288 and P290. This is in agreement with the detection of b ions of OmpA peptide whose masses included the mass of the DolP crosslinked peptide (Figure 21F). These data suggest a close proximity between the BON1 domain of DolP and the identified region of the periplasmic domain of OmpA.

Our data suggests that, *in vivo*, the BON 1 domain of DolP (Fig. 21G) is proximal to the periplasmic domain of OmpA (Fig. 21G). In the structure of the periplasmic domain of OmpA, crosslinked residues are part of the  $\alpha$ -5 of this domain. Interestingly, this particular region of OmpA has been proposed to create a bulge that denatures at low temperature and may be a putative interface for dimerization of OmpA. Dimerization of OmpA has been suggested to promote the formation of a larger pore (Ishida et al., 2014). Our data raise the question of the role of DolP in the regulation of the function of OmpA. It should be noted that, in our previous pull downs assays, we did not observe OmpA to be co-purified with DolP, suggesting that the

interaction between DoIP and OmpA may be very transient or non-specific and the crosslink reaction is probably favored by the fact that OmpA is highly abundant in the OM.

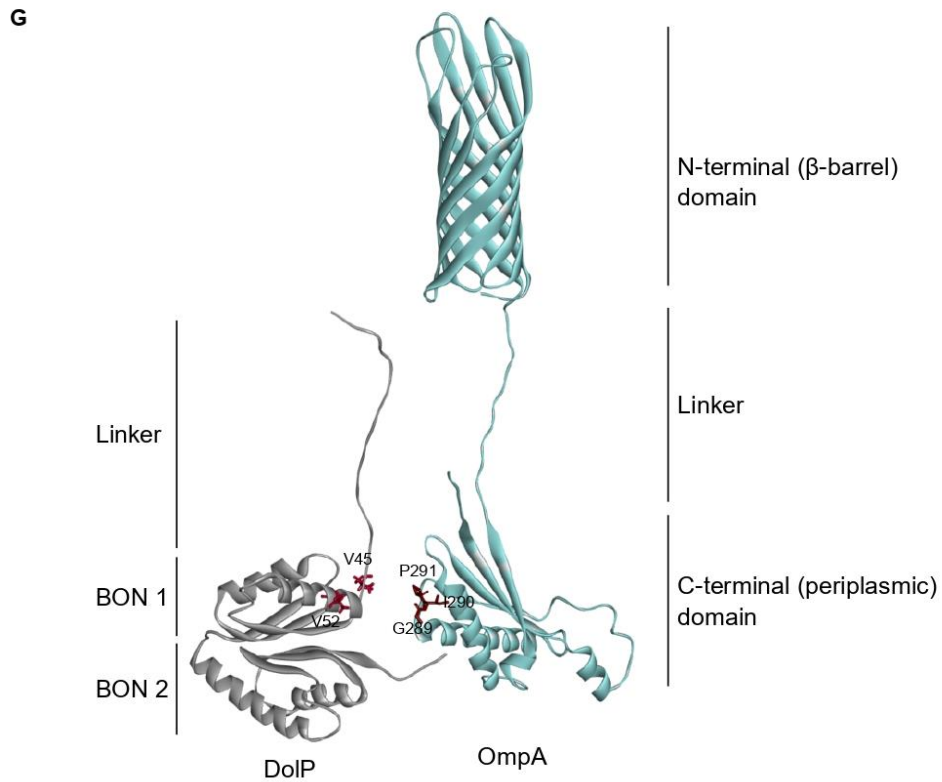
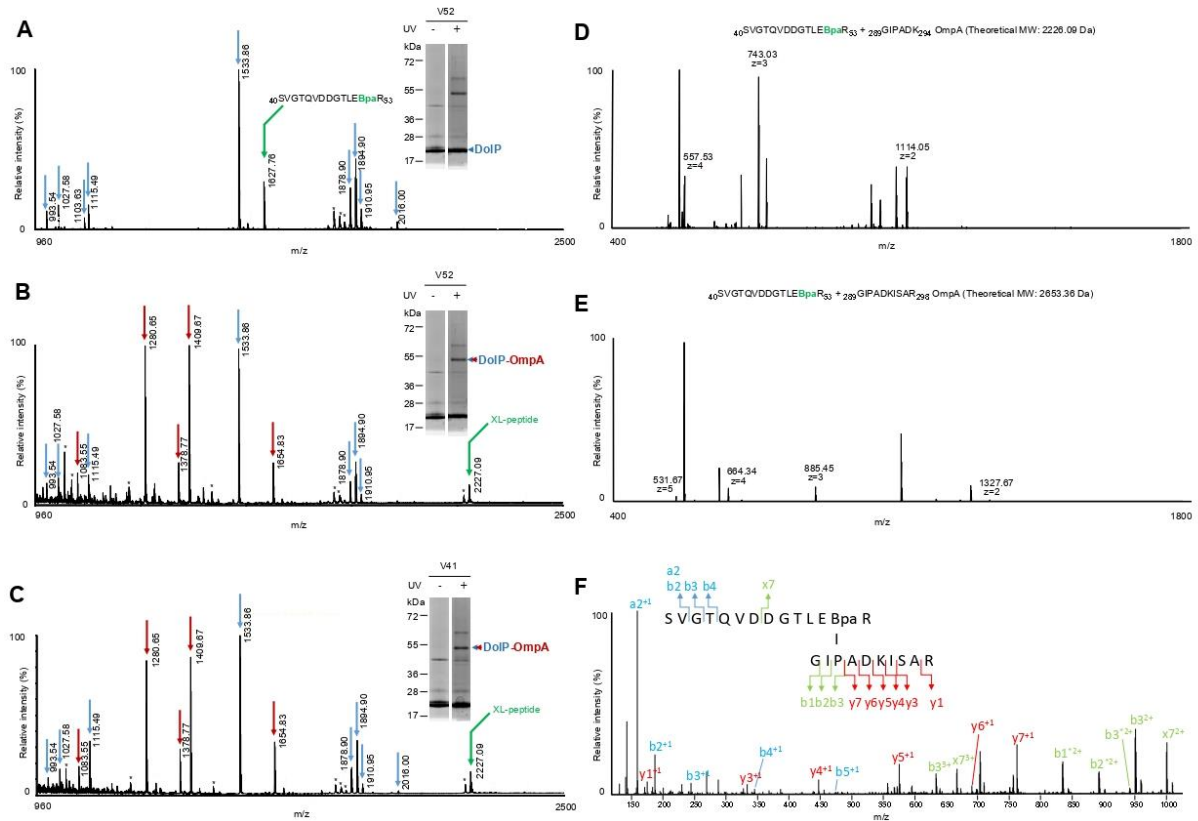




**Figure 21. DoIP interacts with the periplasmic C-terminal domain of OmpA.** Bands corresponding to DoIP<sup>Bpa/His</sup> at position V41 and V52 and its major UV-specific crosslink products (respectively, single and double arrowheads) were trypsin digested and subjected to MALDI-TOF MS and LC-ESI-MS/MS analyses. DoIP<sup>Bpa/His</sup> (blue arrows), OmpA (red arrows) and DoIP<sup>Bpa/His</sup>-OmpA (green arrows) were identified by peptide mass fingerprinting using tryptic peptide predicted patterns for each protein. **A.** Analysis of DoIP<sup>Bpa/His</sup> at position V52 revealed the presence of a peptide containing Bpa at position V52 ( $m/z = 1627.76$ ). Analysis of DoIP<sup>Bpa/His</sup> at position V41 did not revealed the expected Bpa peptide (data not shown). **B and C.** Analysis of the major crosslink product revealed a new mass ( $m/z = 2227.09$ ) predicted to correspond to a crosslinked peptide (XL-peptide) between DoIP (<sub>40</sub>SVGTQVDDGTLE[Bpa]R<sub>53</sub>) or DoIP (<sub>40</sub>S[Bpa]GTQVDDGTLEVR<sub>53</sub>) and OmpA (<sub>288</sub>GIPADK<sub>294</sub>), respectively. Bpa peptide at  $m/z = 1627.76$  was not detected in these analyses. Tryptic peptides from keratins or autodigestion of trypsin are labelled with asterisks. Indicated masses correspond to  $[M+H]^+$  ions. **D and E.** BW25113 cells carrying pEVOL-pBpF and pBamA-DolPHis with amber codons engineered at positions V52 of the *dolP* ORF were subjected to UV crosslinking. After Ni-affinity purifications, eluates were trypsin digested and subjected to LC-ESI-MS/MS analyses. **D.** MS spectrum at 69.0 min showed a peptide at 2226.08 Da predicted to correspond to the crosslinked peptide identified by MALDI-TOF MS (see B and C). **E.** MS spectrum at 71.4 min showed a species at 2653.32 Da predicted to include the OmpA crosslinked peptide identified by MALDI-TOF with a C-terminal miscleavage (<sub>288</sub>GIPADKISAR<sub>298</sub>). **F.** MS/MS (HCD 30 NCE) of the ion at  $m/z=664.34$  ( $z=4$ ) confirmed the crosslink between peptide <sub>40</sub>SVGTQVDDGTLE[Bpa]R<sub>53</sub> of DoIP and peptide <sub>288</sub>GIPADKISAR<sub>298</sub> of OmpA. **G.** Right. Cartoon representation of DoIP (PDB: 72AD), positions V45 and V52 are highlighted. Left. Cartoon representation of AlphaFold prediction of OmpA, positions <sub>289</sub>GIP<sub>291</sub> are highlighted.

### *Pal*

The peptidoglycan associated lipoprotein (Pal) was identified crosslinked to DoIP in the 38 kDa crosslink products of the gel shown in Fig. 20C. This crosslink product was obtained with Bpa at three different position of DoIP (V30, V142 and F189). The size of the band is in accordance with the expected molecular weight of the DoIP-Pal crosslink product (20 and 18 kDa for DoIP and Pal, respectively). The crosslink identified between DoIP and Pal seems relevant since Pal localizes at the septum during cell division, like DoIP. This finding suggests that both proteins may cooperate to promote proper cell division.

It has been previously reported that the lack of Pal or DoIP makes cells sensitive to detergents (Tsang et al., 2017). Together with TolA, TolQ, TolR and the periplasmic protein TolB, Pal is part of the transenvelope Tol-Pal complex (Gerding et al., 2007). Furthermore, Pal also tethers PG, as OmpA, and it has been reported that TolB can chemically crosslink Pal and OmpA (Clavel et al., 1998). Our result suggests that DoIP and Pal could be in relatively close proximity and may create an interaction hub important during the late step of cell division, for instance regulating AmiC. Indeed inactivation of both Pal and DoIP causes concatenation of cells lacking EnvC, which revealed that both Pal and DoIP are involved in the regulation of AmiC activity (Tsang et al., 2017). The newly identified interaction between DoIP and Pal should be

furthered explored and may provide new insights into the coordination steps during cell division.

#### *DolP-DolP intramolecular crosslink*

We excised one of the faster-migrating bands obtained upon UV crosslinking, in particular that obtained when Bpa was introduced at position Y75 for further MALDI-TOF MS analyses. Of note, these bands were not observed in the non UV-irradiated samples, suggesting that they could correspond to putative intramolecular crosslinks of DolP. Only DolP peptides were identified by MS in these samples, confirming they correspond to a fast-migrating form of DolP (Fig. 22A, right panel).

To further characterize these crosslink products, we predicted all possible combinations of the Bpa-containing peptide (at position Y75) with any other peptide of DolP. By comparing the theoretical intramolecular dipeptides for DolP with the experimental data, we identified the peptide at  $m/z=2976.14$  as a putative intramolecular crosslink product of DolP (Fig. 22A). Analysis of the fragmentation pattern of this peptide confirmed that the Bpa-containing tryptic peptide (with a theoretical  $m/z=1081.75$ ) was covalently linked to the DolP tryptic peptide at  $m/z=1894.89$ . These peptides are located in the first  $\beta$ -strand ( $\beta 1$ ) of BON1 that contains Y75 and in  $\beta 2$  of BON2, respectively, suggesting the two BON domains are interacting face to face. We could identify b and y peaks until position M159/G160 of the tryptic peptide in BON2, suggesting one these amino acids was crosslinked with position Y75 (Fig. 22B). The intramolecular crosslink of DolP is in accordance with the structure of DolP solved by NMR recently published (Fig. 22C), showing the residue Y75 is in front of G160 and provides a structural support between the two BON domains (Bryant et al., 2020). This suggests that the 3D structure of native DolP is very similar to that of the soluble DolP used for NMR experiments (Bryant et al., 2020).

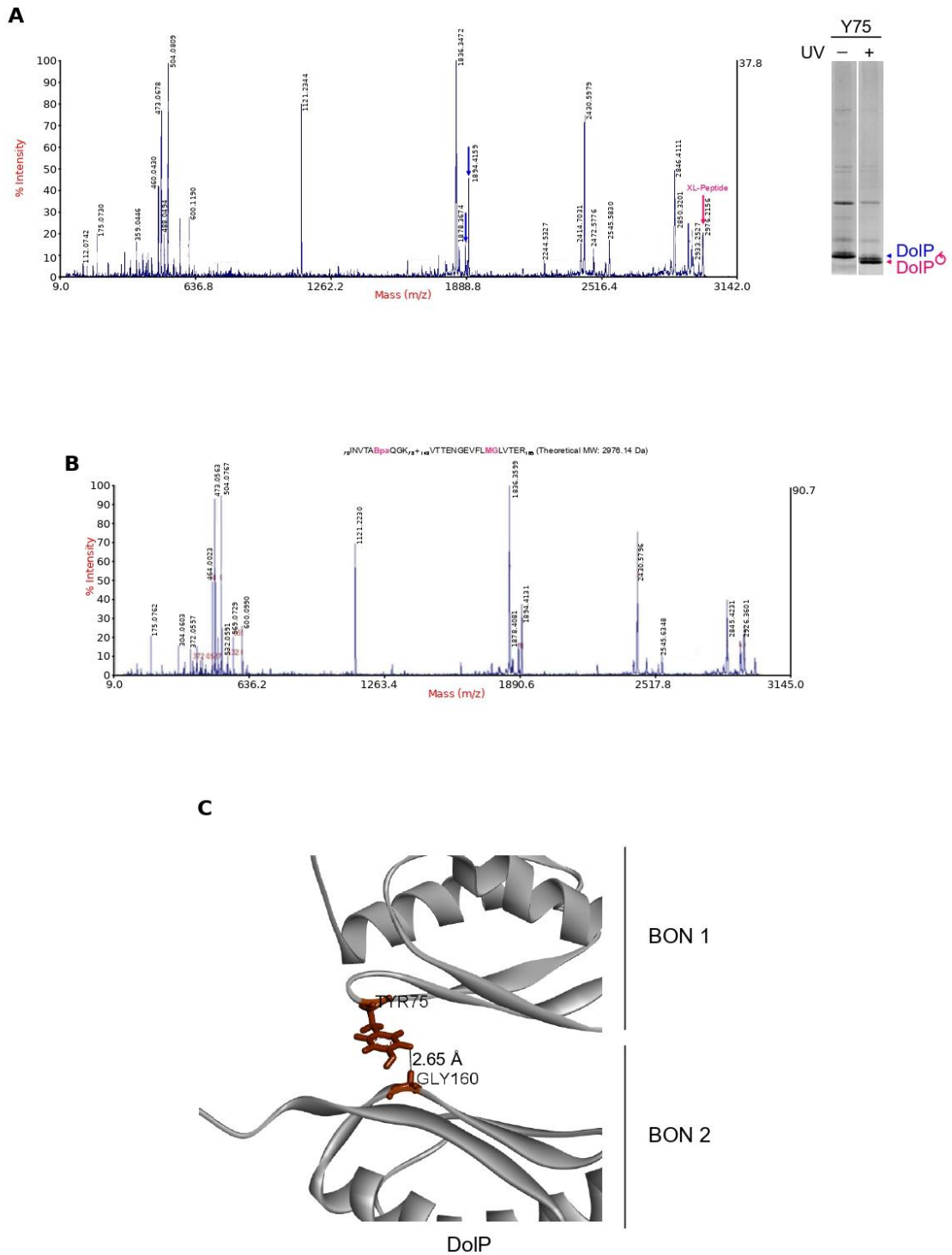


**Figure 22. DoIP can crosslink to itself. A and B.** Fast-migrating band (pink arrow) corresponding to DoIP<sup>Bpa/His</sup> with Bpa introduced at position Y75 were trypsin digested and subjected to MALDI-TOF MS (A) and MALDI-TOF/TOF MS/MS (B) analyses. Fragmentation analysis of the peptide at  $m/z=2976.14$  revealed that the Bpa-containing tryptic peptide (with a  $m/z=1081.75$ ) was covalently linked to the DoIP tryptic peptide at  $m/z=1894.89$ . **C.** Cartoon representation of the interface BON1-BON2 of DoIP (PDB: 72AD). Positions Y75 and G160 are highlighted and distance was measured at its nearest point.

#### 4.4 Identification of Bpa-crosslink products by immunodetection

In an attempt to identify other proteins crosslinked to DoIP that were not Coomassie Brilliant Blue stainable, we performed immunodetection of the elution fractions using available antisera.

The DoIP specific antiserum detected the bait protein and no major signal above this band was observed for the non-irradiated samples (Fig. 23A). On the contrary, a number of signals above the expected size of DoIP were detected for the irradiated samples, suggesting the detection of DoIP crosslink products (Fig. 23B). Interestingly, we can observe signals at around 38 kDa, 50 kDa and 60 kDa corresponding to the Coomassie Brilliant Blue stained bands where Pal and OmpA were identified, respectively. In addition, at positions L58 and V72, we can observe a remarkable “ladder” pattern of crosslinks products with a regular increment of mass of about 20 kDa between each band. This pattern suggests the protein is forming homooligomers, as previously observed using chemical crosslinking.

Immunodetection using  $\alpha$ -OmpA revealed the bands at 50 and 60 kDa indeed contained OmpA (Fig. 23C), as previously shown by MALDI-TOF MS analyses. Remarkably, crosslink products with OmpA gave more intense signals when Bpa was introduced in the linker region and in BON 1, especially when Bpa is substituted at positions V41 to I64.

In addition, we used a BamA antiserum in an attempt to detect any possible crosslink with BamA. We can observe some faint signals at around 115 kDa for positions localized mainly in BON 1 (I64, Y75 and L90) (Fig. 23D) which may correspond to DoIP-BamA crosslink product. These weak signals, in particular at position L90, are encouraging and may suggest DoIP and BamA interact directly via the BON1 domain of DoIP. However, only faint signals were detected, suggesting the crosslink between DoIP and BamA is not favorable under our experimental conditions.

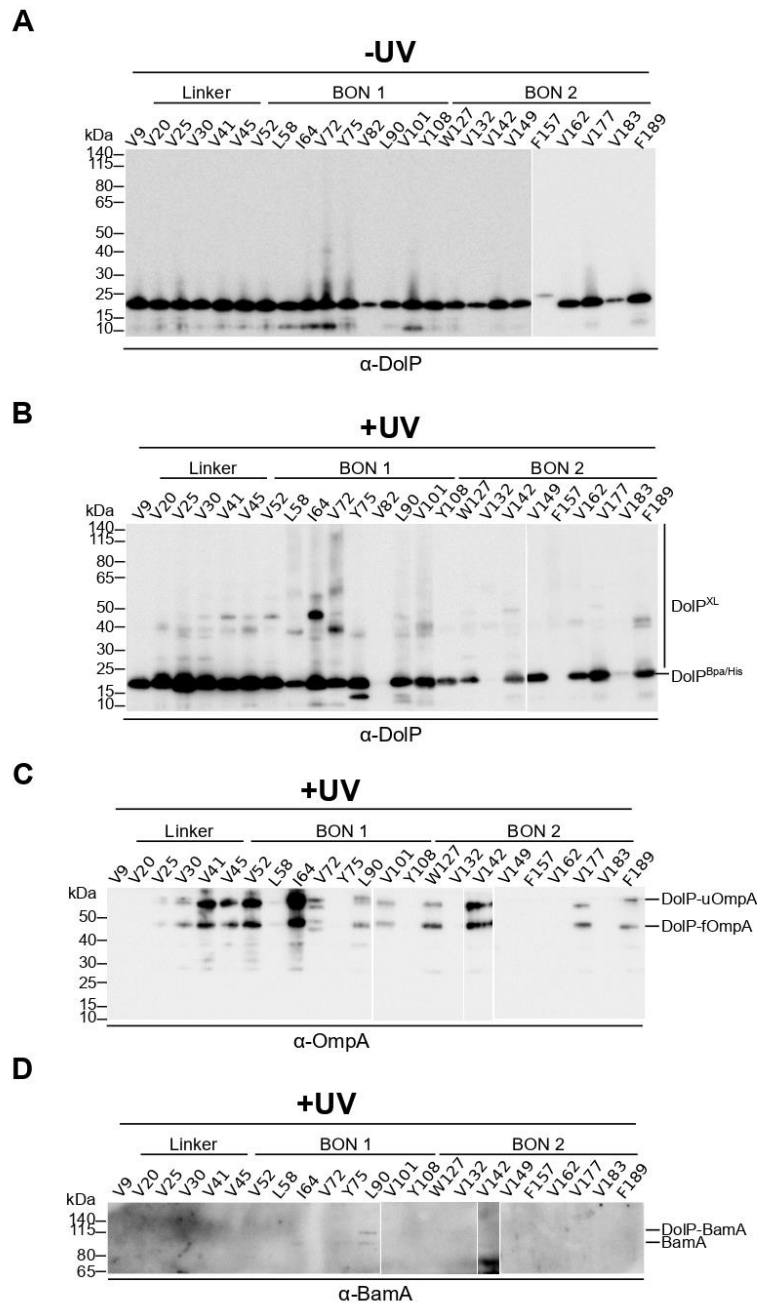


**Figure 23. DolP crosslinks to OMPs.** BW25113  $\Delta dolP$  cells carrying pEVOL-pBpF and a pDolP<sup>His</sup> with amber codons engineered at different positions of the *dolP* ORF were cultured in minimal medium supplemented with glucose in the presence of Bpa. These fractions were split in two: one half was UV-irradiated and the other was kept on ice without irradiation. Envelope fractions corresponding to these cultures were subjected to denaturing Ni-affinity chromatography purification and eluted using an excess of imidazole after extensive washes. Proteins of the total envelope and elution fractions both – and + UV treated were subjected to immunodetection after SDS-PAGE and membrane blotting. **A.** Analysis of elution fractions of the – UV samples using DolP antiserum. **B to E.** Analysis of elution of the + UV samples using DolP antiserum (**B**), OmpA antiserum (**C**), BamA antiserum (**D**)

Altogether, we successfully established a site-directed photocrosslinking approach that permitted to describe the interactions of DoIP. We observe DoIP forms homooligomers and can be proximal to Pal as well as to the very abundant OM protein OmpA. Moreover, we could observe that DoIP is crosslinking to itself, confirming previous structural analyses.

#### 4.5 BON 1 interacts directly with BamA

As endogenous DoIP and BamA are produced with similar copy numbers per wild-type cell (Li et al., 2014), we reasoned that a better strategy to detect the interaction of DoIP with BamA would be to overproduce both proteins. To this end, we conducted the site-specific photocrosslinking experiment with cells transformed with 17 variants of the plasmid pBamA-DoIP<sup>Bpa/His</sup> harboring amber codons at 17 distinct position of the open reading frame of DoIP: three in the linker region, eight in BON 1 and six in BON 2. The procedures of membrane preparation and solubilization as well as Ni-affinity chromatography were the same as previously described. Elution fractions were loaded on an SDS-PAGE and proteins were analyzed by Western blot using DoIP and BamA antisera. Decoration of the –UV samples did not reveal any major band in addition to DoIP or to BamA detected in the total membrane fraction of a representative culture (Fig. 24A). Instead, the analysis of +UV elution samples using DoIP antiserum revealed DoIP in all samples and a number of slower migrating crosslink products (Fig. 24B). Notably, we can observe a ladder of signals at 40, 60, 80 and 100 kDa for positions I64, V72 and F157, corroborating the pattern of homooligomerization previously observed. We also observed the intramolecular crosslink of DoIP at position Y75, as previously. This was also observed for V82. Both positions are situated at very close proximity, at the interface between BON 1 and BON2. This suggests that the conformation of DoIP is not altered by the overproduction of BamA.

Previously, we observed two signals for the crosslink of OmpA at 50 and 60 kDa which may correspond to the crosslinked folded OmpA (50 kDa) and unfolded OmpA (60 kDa). For this new experiment, denaturing temperature was increased to fully denature OmpA. Under these conditions and using DoIP antisera, we observed clear signals at 60 kDa for several positions but not at 50 kDa. This result confirms that DoIP can be crosslinked to OmpA *in vivo* through residues from its linker region (V41 and V45) and its BON 1 domain (V52, I64, V72, V101). In BON 2, these signals were only visible weakly for position W127 and possibly F157 (as decoration using  $\alpha$ -OmpA in previous experiments did not give any signal at this position, Fig. 23C).

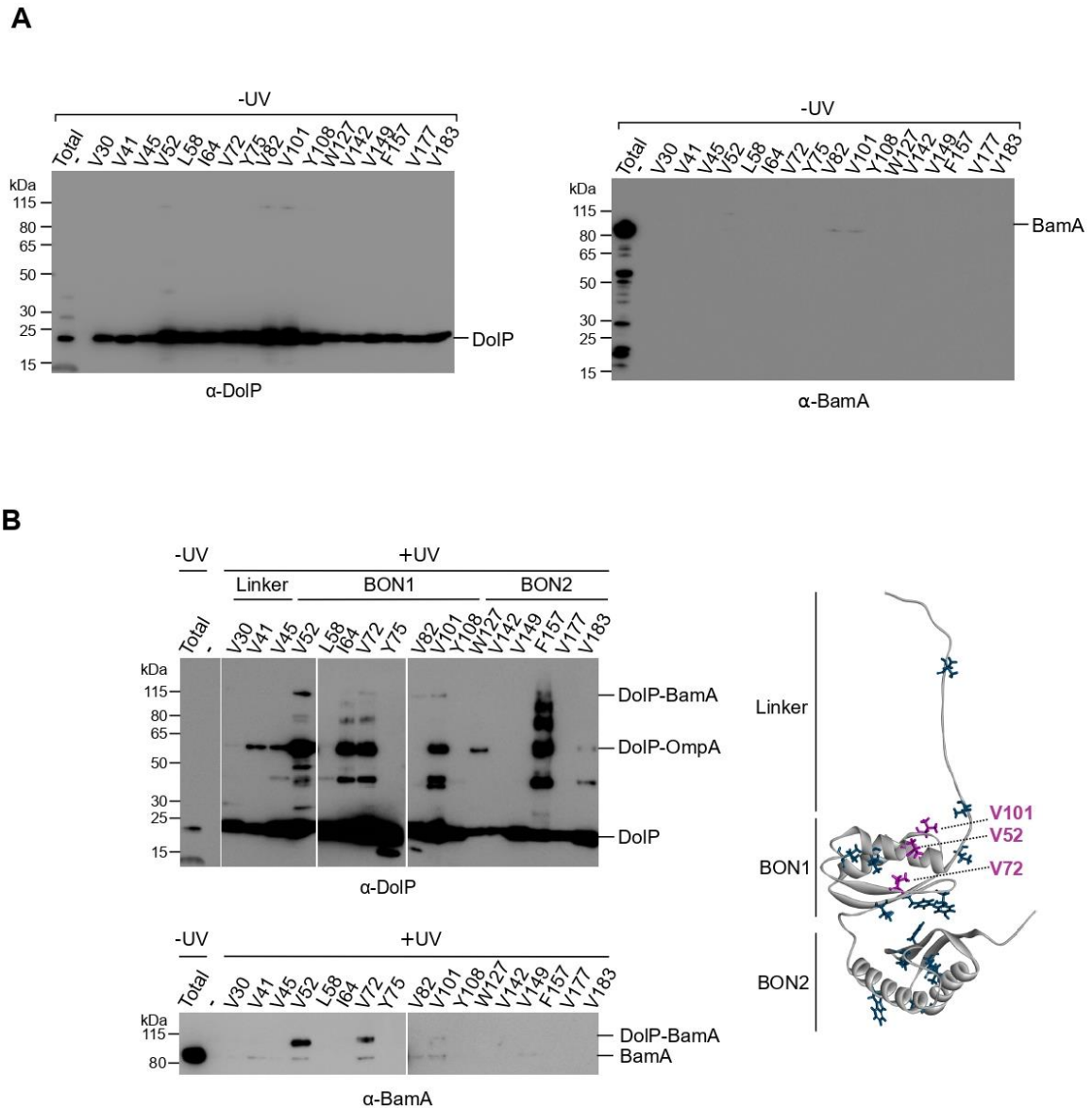


**Figure 24. DolP interacts with BamA via its BON 1.** BW25113  $\Delta dolP$  cells carrying pEVOL-pBpF and a pBamA-DolP<sup>His</sup> with amber codons engineered at different positions of the dolP ORF. Strains were cultured in minimal medium supplemented with glycerol in the presence of Bpa. These fractions were split in two: one half was UV-irradiated and the other was kept on ice without irradiation. Envelope fractions corresponding to these cultures were subjected to denaturing Ni-affinity chromatography purification and eluted using an excess of imidazole after extensive washes. Proteins of the total envelope and elution fractions both – and + UV treated were subjected to immunodetection after SDS-PAGE and blotting. **A.** Analysis of –UV fraction of the total envelope fraction with elutions using DolP (left) and BamA (right) antisera. **B.** Left. Analysis of the +UV elution fractions decorated with DolP and BamA antisera. **Right.** Cartoon representation of DolP structure (PDB: 7A2D) highlighting Bpa positions (in blue) and Bpa-crosslink positions to BamA (in pink).

We also noticed that the sample containing Bpa at V52 presented an intense crosslink product of 110 kDa (Fig. 24B, lower panel). Considering the apparent molecular weight of this band, we hypothesized it could correspond to the crosslink product between DolP (20 kDa) and

BamA (90 kDa). Moreover, this additional signal at 110 kDa was also visible with a lower intensity in the samples containing Bpa at positions V72 and V101.

Interestingly, Western blot using  $\alpha$ -BamA antiserum also revealed a signal at 110 kDa for the samples V52, V72 and V101, confirming it corresponds to DoIP-BamA crosslink product (Fig 24B, lower panel). Of these, the sample V52 displays the strongest relative signal, suggesting this position of DoIP is the most favorable to establish a crosslink with BamA when substituted with Bpa. This result provides clear evidence that DoIP makes direct contact to BamA. The three positions 52, V72 and V101 belong to the BON 1 domain of DoIP, revealing a site of BamA-interaction on DoIP (Fig. 24B, right panel).

Altogether, our data suggest that DoIP is interacting directly with BamA via its BON 1 domain. Importantly, the interaction with OmpA seems to be mediated by the same BON 1 domain.



## 5 DolP is necessary for proper folding and activity of BamA

### 5.1 OmpA is not required for DolP function

Both our native purification approach and our crosslink strategy revealed that DolP interacts with BamA. We also identified crosslinks of DolP to OmpA, although this interaction was not observed with our native protein isolation protocol. To investigate if OmpA is critical for DolP function we tested whether a strain deleted of *ompA* is sensitive to vancomycin similar to the  $\Delta dolP$  strain. We thus deleted *ompA* and we observed using serial dilution assays that  $\Delta ompA$  cells were not sensitive to vancomycin (Fig. 25A). Therefore, OmpA is not required for the role of DolP in preserving the outer membrane permeability barrier to antibiotics. We also showed that lack or overproduction of OmpA does not interfere with the distribution of DolP<sup>GFP</sup> in the bacterial envelope (Ranova et al., 2021).

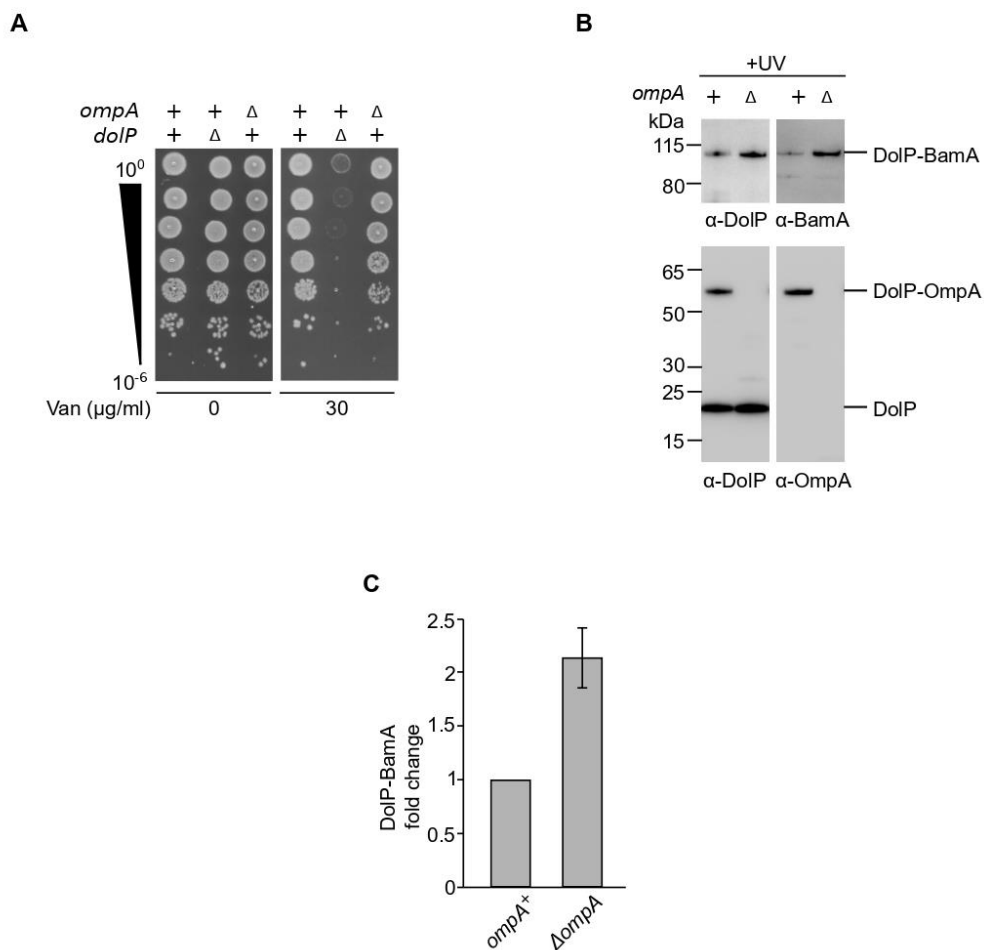


**Figure 25. OmpA may compete with BamA for the interaction with DolP.** **A.** BW25113,  $\Delta dolP$  and  $\Delta ompA$  cells were serially diluted and spotted on LB containing 30 μg/ml vancomycin. **B.** BW25113  $\Delta dolP$  or  $\Delta dolP\Delta ompA$  cells carrying pEVOL-pBpF and a pBamA-DolP<sup>His</sup> with amber codons engineered at position V52 of the *dolP* ORF. Strains were cultured in minimal medium supplemented with glycerol in the presence of Bpa. Envelope fractions corresponding to these cultures were subjected to denaturing Ni-affinity chromatography

purification and eluted using an excess of imidazole after extensive washes. Elution of the + UV fractions were subjected to immunodetection after SDS-PAGE using BamA, OmpA and DoIP antisera. **C.** The amount of DoIP-BamA crosslink product obtained with samples lacking OmpA was expressed as fold change of the amount of the same product obtained in samples expressing OmpA. Data are reported as mean  $\pm$  SEM (N = 3).

Next, because upon activation of the  $\sigma^E$  stress response, both *bamA* and *doIP* are upregulated, whereas the levels of OmpA are post-transcriptionally reduced, we aimed to monitor the interaction of DoIP with BamA upon deleting OmpA, a condition that mimics in part the OMP depletion that may occur during envelope stress response. To this end, we performed site-directed photocrosslinking on position V52 of DoIP that crosslinks efficiently with BamA.  $\Delta doIP$  or  $\Delta ompA \Delta doIP$  strains were transformed with pBamA-DoIP<sup>V52Bpa/His</sup>. Upon UV-crosslinking and isolation of DoIP under denaturing conditions, Western blot analysis showed that the amount of the DoIP-BamA crosslink product was increased in cells harboring *ompA* deletion (Fig. 25B). To confirm this result, three biological replicates of this experiment were conducted and signals of the DoIP-BamA crosslink were quantified from each experiment. The quantifications indicated that the amount of DoIP-BamA crosslink in the strain where *ompA* is deleted is twice as intense compared to the signal obtained with the strain where *ompA* is present. (Fig 25C). Altogether, our results suggest that OmpA and BamA compete for the interaction with DoIP.

We speculate that under normal conditions, OmpA could interact with low affinity with DoIP. During  $\sigma^E$  stress response, *doIP* and *bamA* upregulation, together with OmpA depletion, may result in the release of DoIP from OmpA and favor DoIP-BamA interaction, promoting OM biogenesis. This hypothesis could be supported by the fact that the sites of interaction between DoIP and OmpA or DoIP and BamA mainly map in BON 1, suggesting BamA and OmpA could compete for the same DoIP sites.

## 5.2 Overproduction of BamA causes a detrimental effect that is opposed by DoIP

To further test the role of DoIP at the BAM complex, we wanted to assess the effect of the overproduction of BamA (its direct interactor) in the absence of DoIP by serial dilution assay. WT or  $\Delta doIP$  strains were transformed with pCtrl, pBAM<sup>His</sup>, pBamA or pOmpA<sup>His</sup>. After growth in liquid medium and serial dilutions, cells were spotted on LA plates supplemented with IPTG to induce gene expression. We observed that overproduction of the full BAM complex or of BamA caused a detrimental effect on cell growth (Fig. 26A). It should be noted that, when 400  $\mu$ M of IPTG is used to induce gene expression, our culture yields levels of BAM subunits that are roughly similar to the levels of the major OMPs in the OM, such as OmpA and OmpC/OmpF

(Fig. 26B). Remarkably, we observed that the detrimental effect caused by BamA overproduction was exacerbated by the deletion of *doIP*. Furthermore, we observed that overproduction of OmpA did not cause any growth defect, highlighting this detrimental effect is specifically linked to BAM or BamA overproduction (Fig. 26A).

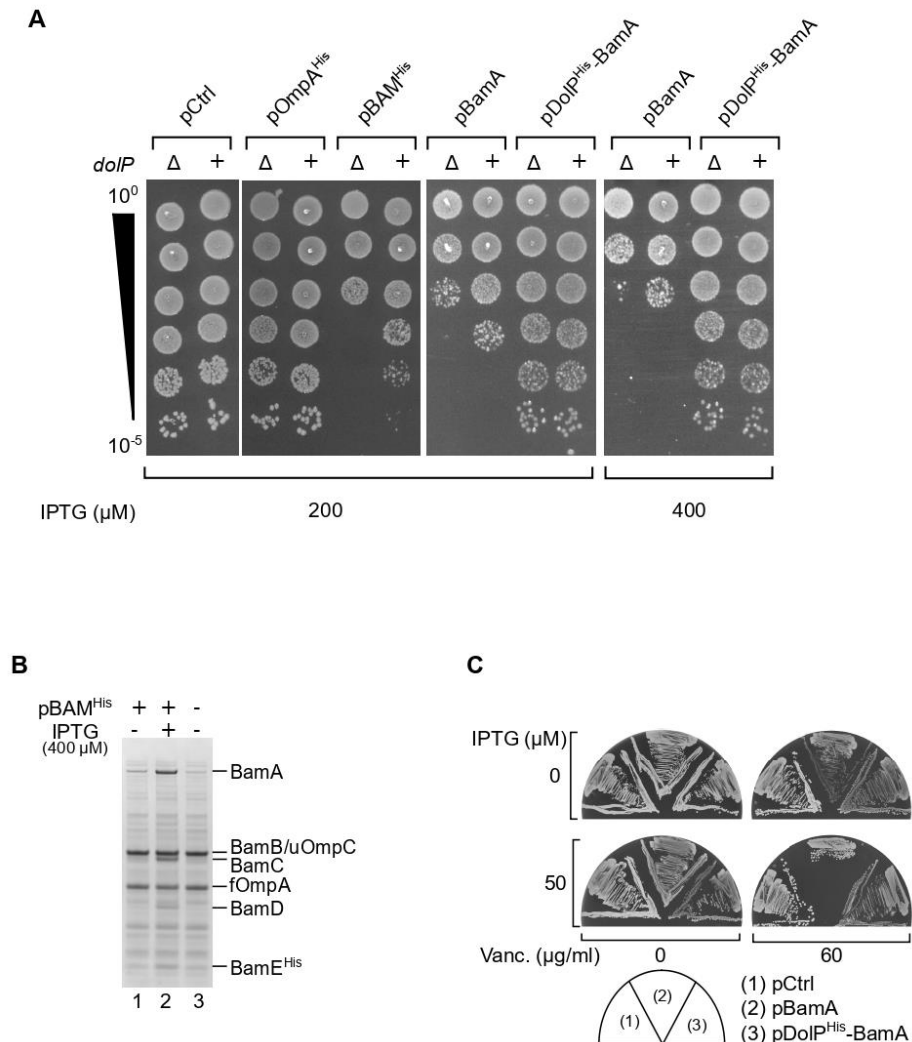


**Figure 26. Overproduction of BamA is detrimental for the cell.** **A.** BW25113 and  $\Delta doIP$  cells carrying indicated plasmids were serially diluted and spotted on LB containing 200 or 400  $\mu\text{M}$  of IPTG. **B.** BW25113 cells harbouring pBAM<sup>His</sup> where indicated were cultured and supplemented with no IPTG or 400  $\mu\text{M}$  IPTG for 1 hr prior to collecting cells. The protein contents of the envelope fractions were analyzed by SDS-PAGE and Coomassie Brilliant Blue staining. Prior to loading, samples were heated for 5 min at 90°C, a temperature that is not sufficient to fully denature OmpA (folded OmpA, fOmpA). The band of BamB overlaps with the band of the major porin unfolded OmpC (uOmpC). **C.** BW25113 cells carrying the indicated plasmids were cultured overnight and streaked onto LB agar containing IPTG and vancomycin, as indicated.

In light of these observations, we wondered whether the concomitant overproduction of DoIP together with BamA could restore the detrimental defect caused by BamA overproduction. To this end, we transformed cells with pDoIP<sup>His</sup>-BamA. We observed that concomitant

overexpression of DoIP<sup>His</sup> restored the growth defect caused by the overproduction of BamA (Fig. 26A).

Next, we asked if overproduction of BamA impairs OM integrity. To do so we induced a low degree of BAM overproduction that did not impair growth of cells on LB agar. We tested BW25113 strains harboring pCtrl, pBamA or pDoIP-BamA on LB agar media alone or supplemented with vancomycin (60 µg/ml) or IPTG (50 µM) or both. We observed that BamA mild overproduction in the absence of IPTG or in the presence of 50 µM IPTG interfered with the OM permeability barrier to vancomycin (Fig. 26C), suggesting that higher levels of BamA enhance OM permeability. Vancomycin-resistance was restored to a large extent by the concomitant production of DoIP, suggesting a specific role of DoIP to prevent the OM permeabilization effect caused by BamA. These results suggest that, already upon mild overproduction, BamA influence the OM by enhancing its permeability and that this effect is opposed by DoIP.

These results clearly show a functional link between DoIP and BamA and suggest that DoIP may function as an assembly or folding factor of BamA at the OM.

### 5.3 DoIP promotes proper folding of BamA

Because BamA overproduction is detrimental and this effect is opposed by DoIP, we decided to investigate the folding of overproduced BamA. To this end, we analyzed the heat modifiability behavior of BamA. WT or  $\Delta dolP$  strains transformed with pBamA or pDoIP<sup>His</sup>-BamA were cultured until mid-exponential phase prior to inducing protein expression by IPTG. Upon cell lysis, protein separation by SDS-PAGE and Western blot using BamA-specific antibodies, we observed in not boiled samples signals at an apparent molecular weight of 90 kDa and 70 kDa corresponding to uBamA and fBamA, respectively (Fig. 27A). The band of 90 kDa was more intense than the band at 70 kDa, indicating that the majority of BamA was unfolded. Instead, when DoIP was co-overproduced, all BamA migrated as folded form at 70 kDa in non-boiled samples (lanes 5-8). This suggests the detrimental effect of BamA overproduction could be related to a defect in its folding, compromising its ability to properly assemble OMPs.

To verify this effect was specific to BamA, we tested the overproduction of another OMP: OmpA. For this, WT and  $\Delta dolP$  strains were transformed with pOmpA<sup>His</sup>. Upon overproduction of OmpA, the membrane fractions were analyzed by heat-modifiability as previously. Two bands, were observed at 30 and 35kDa, (Fig. 27B), corresponding to fOmpA and uOmpA, respectively. When samples were not boiled, we observed that the totality of OmpA remained

folded, even if the protein was overproduced. This suggests that overexpression of OMPs leads to the accumulation of unfolded forms only in the case of BamA and that this defect is linked to the detrimental effect of BamA overproduction. Of note, we observed that BamA migrated completely folded when OmpA<sup>His</sup> was overproduced, providing a control for the previous experiment suggesting that the folding defect of BamA was not caused by saturation of the OMP secretory apparatus.

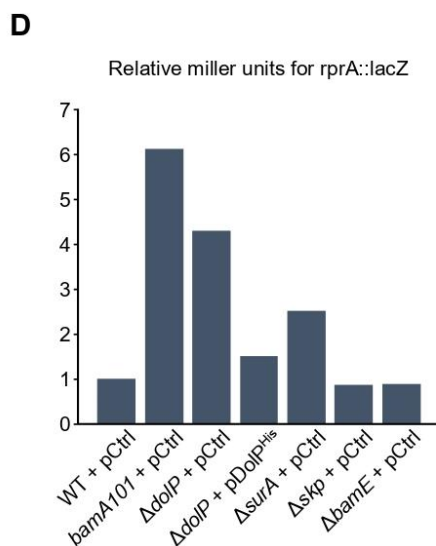
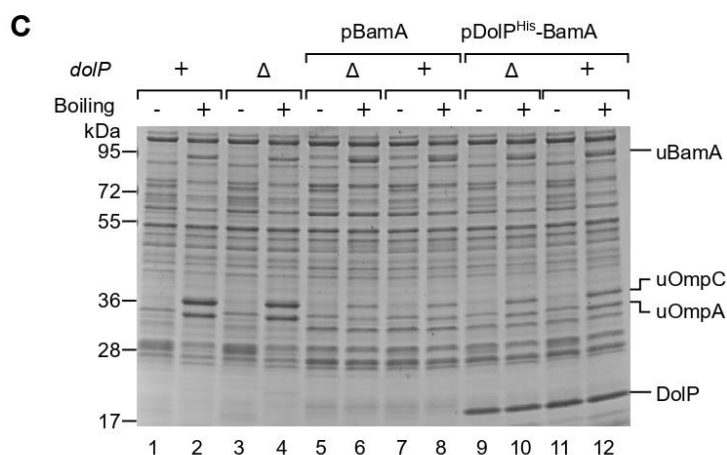
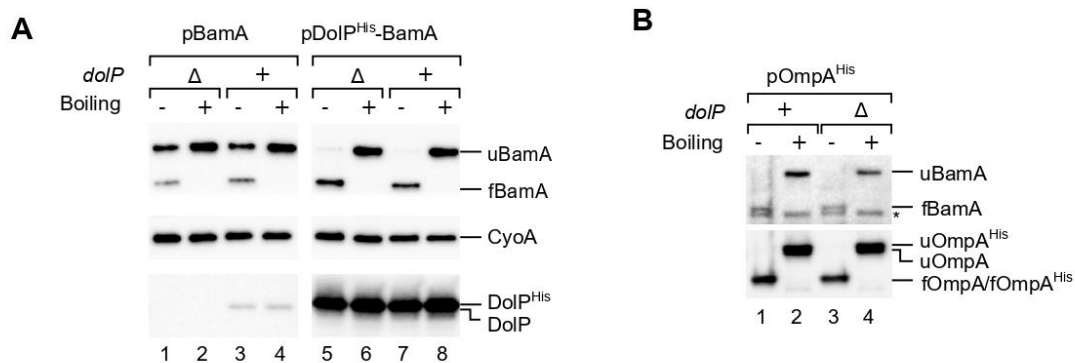


**Figure 27. DoIP promotes proper folding of BamA.** **A and B.** BW25113 and  $\Delta dolP$  carrying indicated plasmids were induced for 2h with 200  $\mu$ M IPTG when they reached exponential phase. Total cell extracts were normalized and mixed with Laemmli buffer and subjected to heat-modifiability assay. Sample proteins were incubated at 25°C (Boiling –) or at 99°C (Boiling +), separated by SDS-PAGE and analyzed by immunoblotting using the indicated antisera. u, unfolded; f, folded. \* indicates a non-specific cross-reaction. **C.** Total envelope fractions of BW25113 and  $\Delta dolP$  carrying indicated plasmids were subjected to a heat-modifiability assay. Plasmid-borne genes were induced with 200  $\mu$ M IPTG for 2 h prior to collecting cells. The envelope fractions were mixed with SDS-PAGE loading buffer, incubated at 25°C (Boiling –) or 99°C (Boiling +) for 10 min, and analyzed by SDS-PAGE and Coomassie Brilliant Blue staining. u: unfolded. **D.** Strains MC4100,  $\Delta dolP$ ,  $\Delta surA$ ,  $\Delta skp$ ,  $\Delta bamE$  or mutant *bamA101* harboring a transcriptional fusion of *rprA* to *lacZ* (*rprA::lacZ*) and carrying indicated plasmids were subjected to a  $\beta$ -galactosidase assay using ONPG. When sample reactions reached a yellow color, reactions were stopped and Miller units were obtained. Miller units are expressed as relative using as reference the WT strain transformed with pCtrl

#### 5.4 DoIP contributes to promote BamA activity

To test whether the accumulation of unfolded BamA has an effect on OMP biogenesis, we isolated membranes from  $\Delta dolP$  and WT strains, as previously described and patterns of OMPs were monitored by heat-modifiability assay, comparing denatured or not denatured samples (Fig. 27C). Two bands migrating at 36 and 34 kDa were visible in wild-type boiled samples, corresponding to uOmpC and uOmpA, respectively (lanes 2 and 4). The levels of OmpC and OmpA were strongly reduced when BamA was overproduced, indicating a major defect in OMP biogenesis. With the concomitant overproduction of DoIP, the levels of OmpA and OmpC were partially restored. We suspect that full OMP levels restoration was not achieved as BamA was overproduced in the absence of the other BAM lipoproteins. This may lead to relatively inefficient OMP biogenesis as a portion of BamA lacks its partner subunits.

Given that DoIP is critical for BamA folding, we asked whether the deletion of DoIP would mimic to some extent a partial depletion of BamA. To test this hypothesis, we exploited the knowledge that a strain harboring a transposon insertion in the promoter of *bamA*, namely *bamA101*, produced levels of BamA that are reduced by more than 90% compared to wild-type cells (Aoki et al., 2008; Cho et al., 2014). The strain *bamA101* has been previously reported to have an activated Rcs response because the RcsF is not efficiently funneled through OmpA (Cho et al., 2014).

First, we wondered whether deletion of *dolP* could trigger the Rcs response. For this,  $\Delta dolP$  cells harboring a transcriptional fusion of the gene *rprA* to *lacZ* were prepared to assess Rcs response, as previously described (Castanié-Cornet et al., 2006). To complete our

investigation on the Rcs response, the same approach was used to measure this stress response in the *bamA101*,  $\Delta$ *surA*,  $\Delta$ *skp*,  $\Delta$ *bamE* strains.

Deletion of *surA* has been previously identified as a mutant that has several damages especially defects in OMP biogenesis (Rouvière and Gross, 1996) and triggering stress responses at the envelope, such as activation of  $\sigma^E$  (Vertommen et al., 2009) and Rcs responses (Castanié-Cornet et al., 2006). Activation of Rcs by deletion of other chaperones, such as *skp*, or *bam* subunits, such as *bamE* has not been reported in the literature.

As expected, we observed that deletion of *surA* and depletion of *bamA* trigger Rcs response as these samples presented a high degree of  $\beta$ -galactosidase activity (Fig. 27D). Interestingly, deletion of *dolP* also triggers Rcs response, almost at the level as *bamA101*, with a relative  $\beta$ -galactosidase activity increased 4-fold compared to the WT. The basal WT Rcs response level was almost completely restored in the complementation strain ( $\Delta$ *dolP* transformed with pDolP<sup>His</sup>). On the contrary, deletion of *skp* or *bamE* did not have any effect on the Rcs stress response. Altogether, our results show that the deletion of *dolP* phenocopies the depletion of BamA. Although we cannot exclude the possibility that lack of DolP induces activation of the Rcs response independently of BamA, our results support a model where DolP is critical for efficient BamA assembly and function in the OM.

## 6 Molecular characterization of DoIP to promote OM homeostasis

DoIP contributes to maintain OM integrity, conferring resistance to large antibiotics, such as vancomycin. Besides, it was established that DoIP is localized at the division septum and promotes proper activation of amidase activity upon cell division (Tsang et al., 2017). Additionally, we demonstrated that DoIP and the BAM complex are able to interact via the domain BON 1 of DoIP and that DoIP promotes proper folding of BamA at the OM. Interestingly, a recent study revealed that OsmY, which also possesses two BON domains, facilitates biogenesis of an OMP (Yan et al., 2019), suggesting BON domains may have a role in promoting OMP folding. However, the molecular bases underlying BON domain function still have to be elucidated. In an attempt to gain further insights into the structure/function relationships of DoIP, we created a collection of mutants of DoIP and performed functional assays.

### 6.1 Both BON domains of DoIP are necessary for the proper function of the protein

As previously described, DoIP possesses two BON domains. To date, the molecular bases underlying the function of DoIP and the role of each BON domain are unknown. As other BON domains described in the literature (Yeats and Bateman, 2003), the two BON domains of DoIP share some similarities. Indeed, they display a characteristic  $\alpha\beta\beta\alpha\beta$  folding, with two  $\alpha$ -helices and three  $\beta$ -strands. So far, besides DoIP, only three 3D-structures of BON domains have been solved, such as that of the potassium binding protein (Kbp containing 2 BON domains; PDB: 5FIM) from *E. coli* (Ashraf et al., 2016), BonA (containing 2 BON domains) (PDB: 6V4V) from *Acinetobacter baumannii* (Grinter et al., 2021) and CdsD (containing 3 BON domains, PDB: 4QQ0) from *Chlamydia trachomatis* (Meriläinen et al., 2016). BON domains arrange as a three-stranded mixed parallel/antiparallel  $\beta$ -sheets packed against two  $\alpha$ -helices (Bryant et al., 2020) (Fig 28A).

We performed an alignment of the amino acid sequence of these BON-containing proteins by using an alignment software (Corpet, 1988) (<http://multalin.toulouse.inra.fr/multalin/>), and we observed some conserved features of BON domains (Fig. 28B), as previously described in the literature (Yeats and Bateman, 2003). In particular, there is a Gly conserved in all the sequences considered (highlighted with a \* in Fig. 28). This feature has been previously described in the literature as one of the main characteristics of BON domains. In the case of DoIP, they correspond to G83 and G160 in the  $\alpha$ -helix 2 of each BON domain. A conserved Leu/Ile is also strictly conserved in the  $\alpha$ -helix 1 of each BON domain (*i.e.* L58 in BON 1 and L136 in BON 2 for DoIP). Besides, two hydrophobic residues in the first  $\beta$ -strand of each BON domain (I70 and V72 in BON 1 and V147 and V149 in BON 2 of DoIP) are also conserved.



Finally, a hydrophobic motif in the  $\beta$ -strand 2 (VLL79-81 in BON 1 and VFL156-158 in BON 2 of DoIP) was also identified as a remarkable feature conserved in all BON domains. This suggests the BON domains may contain some characteristic features, probably related to their function.

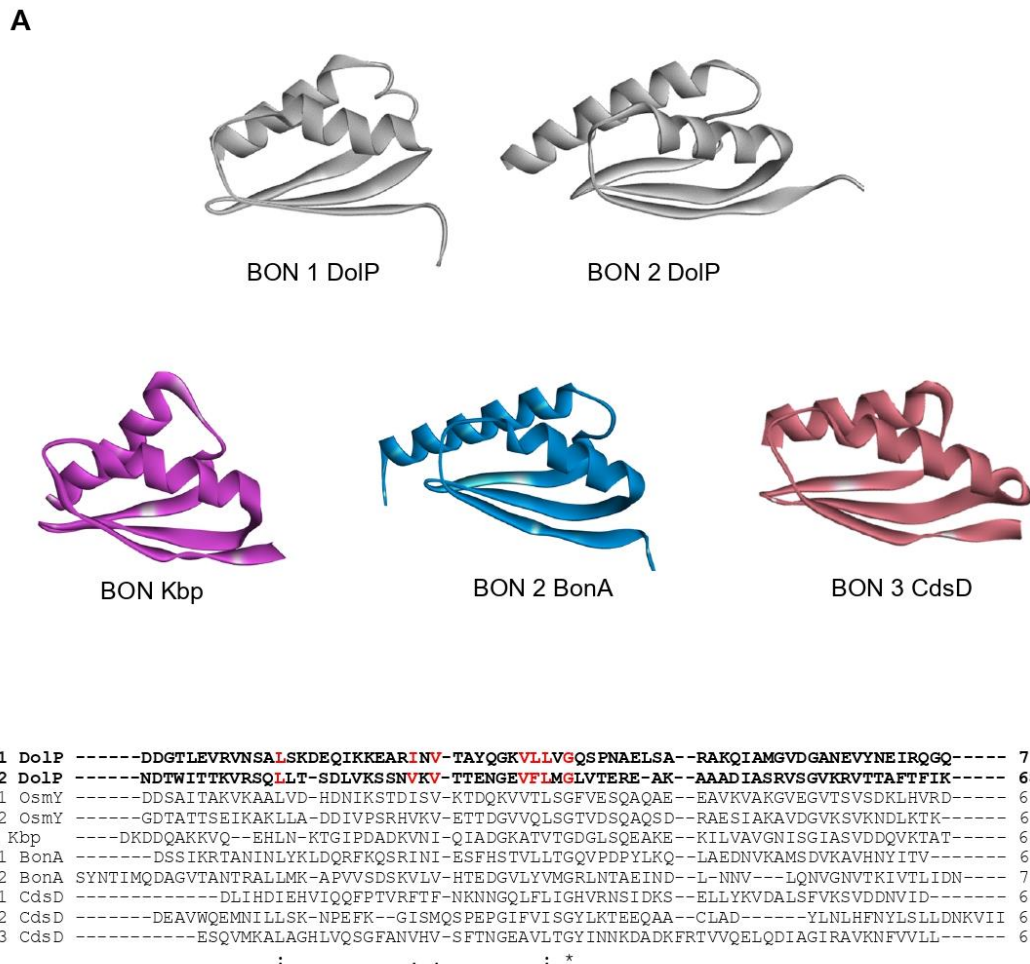


**Figure 28. BON domains have conserved features.** **A.** Cartoon representations of BON domains of DoIP (*E. coli*, PDB: 7A2D), Kbp (*E. coli*, PDB: 7PVC), BonA (*Acinetobacter baumannii*, PDB: 6V4V) and CdsD (*Chlamydia trachomatis*, PDB: 4QO6). **B.** Alignment of BON domains of OsmY, DoIP, Kbp, BonA and CdsD. “.” represent conserved residues, “.” represent semiconservative residues and “\*” the same residue.

To further test this hypothesis and better understand the role of each BON domain, we created truncated versions of DoIP by deleting either BON 1 or BON 2 and monitored its ability to fold BamA, as previously described. It was previously reported that DoIP binds to negatively charged phospholipids in its domain BON 2 by the residue W127. Mutation W127E abolishes this function of DoIP to bind to phospholipids (Bryant et al., 2020). We used this additional mutant to assess whether lipid binding by DoIP is critical for BamA folding.

Total cell extracts were collected and were used to perform heat-modifiability assay. Then, proteins were transferred and Western blot analysis was performed. Signal was quantified and expressed in ratio according to the fBamA/uBamA. We observed that when BamA was overproduced, only 20.8% of the protein is folded, which is in accordance with previous analyses (Fig. 29A). On the contrary, when DoIP is concomitantly produced with BamA, the ratio of folded BamA increases to 79.6%, confirming our previous experiments.

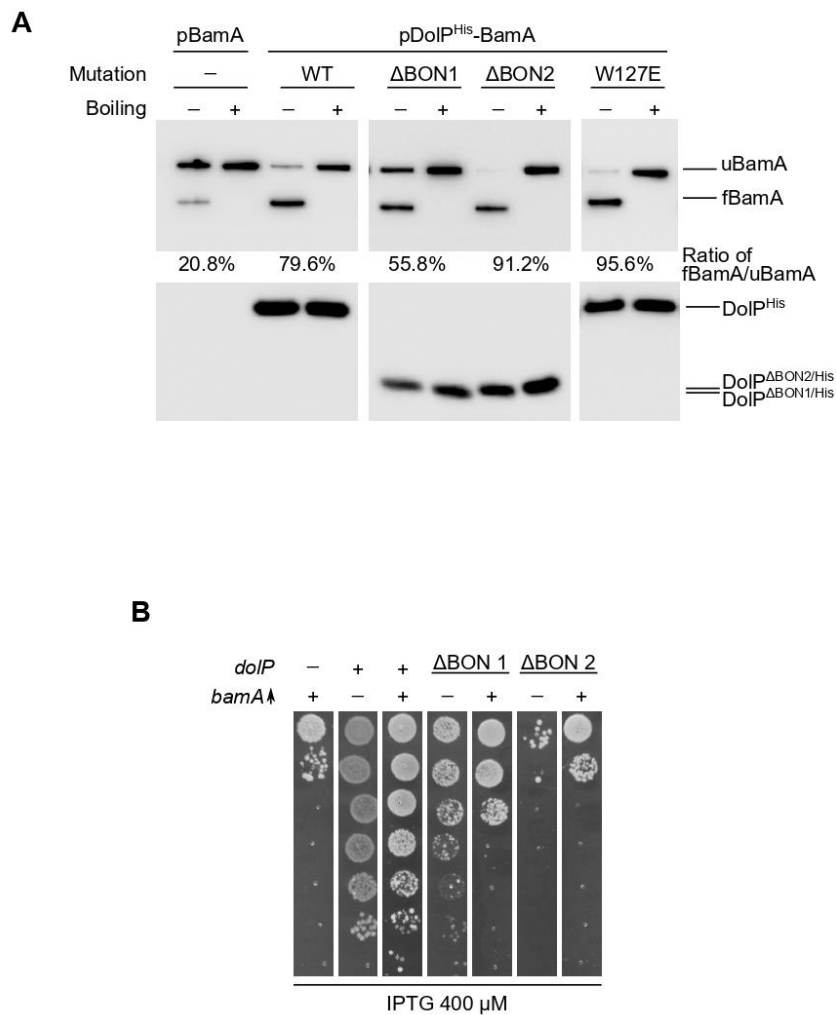


**Figure 29. Deletion of BON domains affect its function. A.** Total cell extracts were obtained from BW25113  $\Delta$ dolP strains transformed with indicated plasmid after induction with IPTG for 1.5 h. Total cell extracts were normalized and mixed with Laemmli buffer and subjected to heat-modifiability assay. Sample proteins were incubated at 25°C (Boiling -) or at 99°C (Boiling +), separated by SDS-PAGE and analyzed by immunoblotting using the indicated antisera. u: unfolded; f: folded. **B.** BW25113  $\Delta$ dolP strains transformed with indicated plasmids (where BamA or DoIP were overproduced alone or co-overproduced) were serially diluted and spotted on LB containing 400  $\mu$ M of IPTG.

Interestingly, the deletion of BON 1 had an effect to promote folding of BamA, as we can see that only 55.8% of the protein is folded (Fig. 29A). On the other hand, deletion of BON 2 did

not impair the ability of DoIP to promote folding of BamA (91.2%). The mutant W127E was able to fold BamA in a similar fashion as the deletion of BON 2 (95.6%). This result suggests that the catalytic domain of DoIP could reside in BON 1, and BON 2 may have a regulatory function. Phospholipid binding at the W127 site is not required to promote BamA folding.

These results are encouraging to continue the characterization of the function of BON domains to promote folding of BamA. As this phenotype was linked to its ability to counteract BamA detrimental effect, we aimed to observe if the expression of BON 1 or BON 2 alone were sufficient to restore the BamA-overproduction detrimental effect. However, we observe that expression of DoIP (pDoIP<sup>His\*</sup>) containing only one BON domain was toxic even in the absence of BamA overproduction (Fig. 29B). These results suggest that both BON domains are required for proper function of DoIP to promote BamA folding.

## 6.2 Strategy for mutagenesis of DoIP

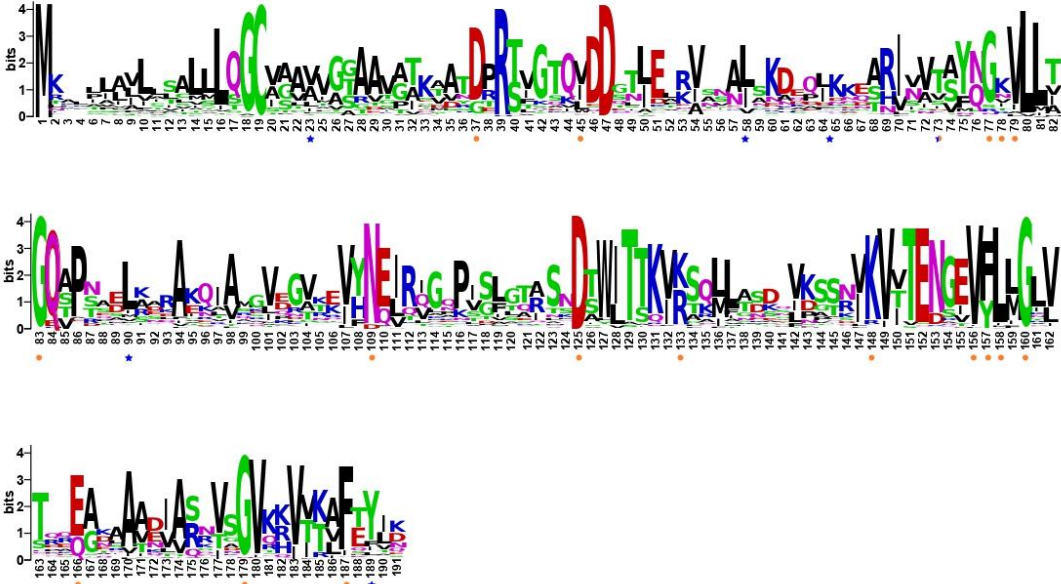
To assess the function of DoIP, we decided to use Alanine scanning to investigate the role of conserved residues. In order to identify the residues to target for this mutagenesis approach, we performed an analysis of conserved residues of DoIP among  $\gamma$ -proteobacteria. This work was done on collaboration with the team Fichant of the CBI of Toulouse and we obtained a conservation map represented as a logo plot for DoIP homologs in  $\gamma$ -proteobacteria (Fig. 30A).

DoIP has been identified in 196 out of the 266 genomes available, representing about 74% of the  $\gamma$ -proteobacteria. We observed that residue C19 responsible for acylation is strictly conserved (Fig. 30A), corroborating DoIP is a conserved lipoprotein. Besides, this analysis revealed other strictly conserved residues, such as R39 in the linker region or D47, G83, Q84, P86, N109 and the motif VLL79-81 in BON 1, as well as D125, W127, T129, K148, V149, G160, G179, F187 and the motifs TEN151-153 and VFL156-158 in BON2.

We selected some of these conserved residues to perform site-directed mutagenesis. In addition to the conserved residues, we also considered some of the residues previously identified by our crosslinking approach as relevant targets for site-directed mutagenesis. Mutations to Alanine were chosen to assess the impact of these residues while the global folding is preserved (Morrison and Weiss, 2001). Altogether, 20 point mutations were introduced across the sequence of DoIP in the linker (V30A, R39A), in BON 1 (D47A, L58A, I64A, V72A, Y75A, L80A, G83A, L90A, N109A) and in BON 2 (D125A, R133A, K148A, F157A, G160A, E166A, G179A, F187A, F189A) (Fig. 30A and B). In addition, triple mutations VLL79-81AAA and VFL156-158AAA were also generated. Finally, we included deletions of BON 1

and BON 2 to complete this characterization. Plasmids derivative from pDoIP<sup>GFP/His</sup> were used as template for site-directed mutagenesis and mutants were produced in  $\Delta doIP$  strain.

**A**



**B**

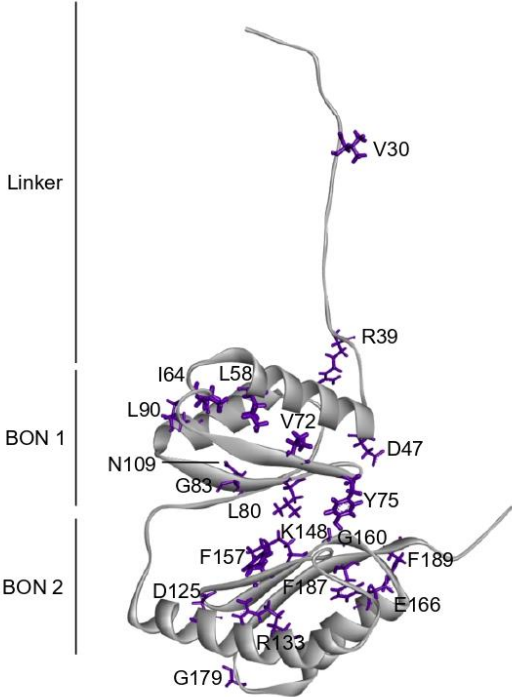


**Figure 30. DoIP has conserved residues among  $\gamma$ -proteobacteria. A.** Logo plot analysis of conserved residues of DoIP in  $\gamma$ -proteobacteria. Blue star: residues selected from crosslink experiments, orange dot: conserved residues identified by sequence analysis. Numbering of DoIP from *E. coli* is indicated. **B.** Cartoon representation of DoIP (PDB: 7A2D), highlighting residues mutated in Alanine.

To perform a first screening for our collection of mutants, we selected two key properties of DoIP previously described: (i) its ability to promote OM integrity and (ii) its localization at the division septum.

### 6.3 Mutations on DoIP affect its ability to promote OM integrity

First, we performed a screening according to the function of DoIP to promote OM integrity by serial dilution assays using rich medium supplemented with vancomycin and SDS, as known to cause a growing defect phenotype on  $\Delta doIP$  strain. These assays were conducted in the absence of IPTG, as we had estimated that the transcriptional leaky activity of the  $P_{tac}$  promoter generates an amount of DoIP similar to its endogenous level.

As expected, we could observe that WT strain grows properly in the presence of vancomycin or SDS, while deletion of *doIP* impairs cell growth (Fig. 31B and C). Complementation strain is able to grow in both conditions, confirming the leaky expression is sufficient to produce DoIP at a level similar to physiological conditions. Interestingly, some mutations did not complement the ability to promote OM integrity. For example, mutation R39A in the linker region compromises OM integrity and in BON 1, mutations D47A and Y75A have a similar effect. On the opposite, none of the mutations done in BON 2 led to a major growth defect. However, we could observe smaller colonies for mutants G83A, N109A, F157A, G160A and F187A, only in the presence of SDS (Fig. 31C).

Interestingly, residues R39 and D47 are expected to be in proximity to the OM, suggesting they could control the anchorage of DoIP in the OM. Moreover, these residues are conserved in nearly 100% of the sequences of DoIP homologs (Fig. 30A), suggesting these residues are critical for the proper function of DoIP. Even though residue Y75 is not strictly conserved, this position can be occupied by an aromatic residue. Of note, Y75 is located at the interphase between BON 1 and BON 2 domains, and this position was shown to be critical for the folding of DoIP as it could mediate the interaction between BON 1 and BON 2, previously analyzed by site-directed photocrosslinking assays. This result suggests that this position could provide hydrophobic platform between the BON domains of DoIP. Also, it could be speculated that correct conformation of BON domains is critical for the function of DoIP to promote OM integrity.

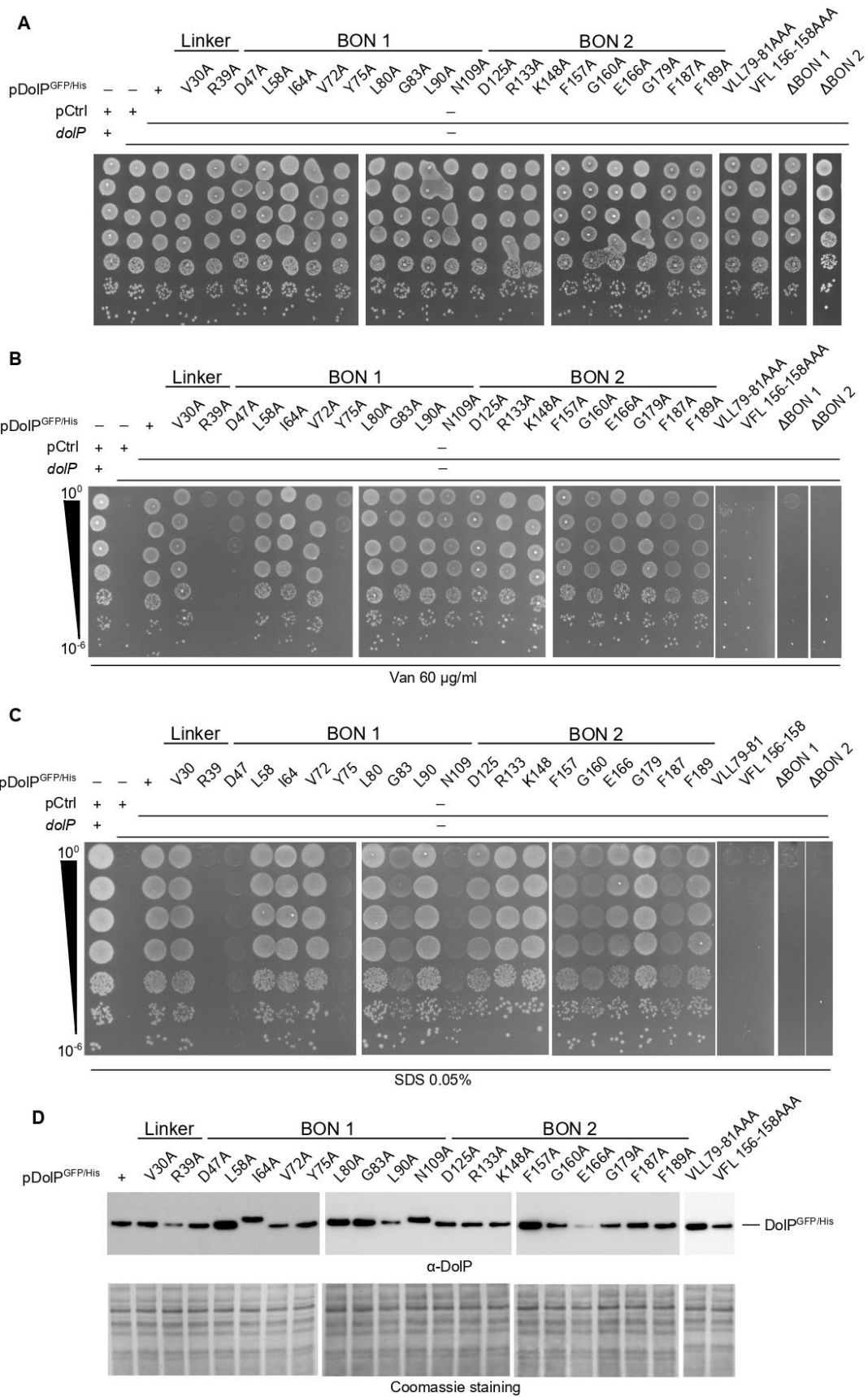


**Figure 31. Mutations on DolP affect its ability to promote OM integrity. A and B. BW25113 and  $\Delta dolP$**

cells carrying pCtrl or pDoIP<sup>GFP/His</sup> engineered with Ala codons at indicated positions of the *doIP* ORF were serially diluted and spotted on LB **(A)**, supplemented with 60 µg/ml of vancomycin **(B)** or SDS 0.05% **(C)**. Ectopic expression was driven by the leaky transcriptional activity of P<sub>tac</sub> in the absence of IPTG. **D**. Total cell extracts of BW25113 and  $\Delta doIP$  cells carrying pDoIP<sup>GFP/His</sup> engineered with Ala codons at different positions of the *doIP* ORF were normalized and mixed with Laemmli buffer. After denaturation of samples, they were separated by SDS-PAGE and analyzed by immunoblotting using DoIP antiserum. Coomassie Brilliant Blue staining of membrane was included as a loading control.

Besides, we can observe that the triple mutations VLL79-81AAA and VFL156-158AAA had a major growth defect in the presence of vancomycin and SDS, suggesting these hydrophobic residues are critical for the function of the protein. Interestingly, these two motifs correspond to similar hydrophobic patches found in each BON domain, previously discussed. These conserved features of the protein could play a role in the function or the structure of DoIP but further analyses should be carried out to investigate further the role of these residues and how they contribute to maintain OM integrity.

Finally, deletions of BON 1 or BON 2 lead to a growth defect in the presence of vancomycin or SDS, suggesting both BON domains are required for the function of DoIP to maintain OM integrity.

To validate our growth assays, we wanted to verify DoIP<sup>GFP</sup> protein expression in each strain. Normalized total cell extracts were loaded on SDS-PAGE prior protein transfer onto a PVDF membrane and immunodetection using DoIP antibodies (Fig. 31D). A signal at 37 kDa, corresponding to the size of DoIP<sup>GFP/His</sup> is visible for each mutant, indicating DoIP is expressed correctly, except for few mutants, suggesting expression or stability issues (such as mutations R39A, V72A, L90A and E166A). Interestingly, for some mutants (notably E166A), the phenotype of DoIP to promote OM integrity was maintained even if protein production was reduced compared to the non-mutated DoIP. Considering this, we speculate that mutation R39A abolished the function of the protein, even if protein levels were reduced.

Protein was not detected for the mutants where BON 1 or BON 2 was deleted (data not shown). To address this limitation, in a later experiment we use fluorescence microscopy to visualize DoIP<sup>GFP</sup> fusion proteins lacking either BON 1 or BON 2 and obtained evidence that both are expressed (Fig. 32).

Overall, this screening permitted to identify key residues of DoIP which are critical to promote OM integrity. Some mutations in the linker and in BON 1 have a major effect, compared to mutations in BON 2. Of note, it seems the conservation of residues does not necessary imply these positions are critical to promote function of DoIP, however it is possible that replacing these residues with an amino acid different than alanine may cause a different phenotype.

Mutations in conserved G83 and G160 (Yeats and Bateman, 2003) did not abolish function, as previously reported in the literature. Only when mutations on both BON domains were made simultaneously had an impact on the function of DoIP (Bryant et al., 2020). However, our data revealed that the phenotype observed when DoIP was mutated at conserved position D47 (in BON 1) was different from that of its counterpart D125 (in BON 2). Altogether, we speculate that the two BON domains may have distinct roles and BON 1 could be critical in promoting OM integrity.

#### 6.4 Mutations on DoIP may affect its recruitment to the division septum

DoIP, during a late step of cell division, localizes at the mid-cell. This localization pattern can be observed when cells harboring the chromosomal *doIP* with a construct encoding superfolder GFP. Plotting the fluorescence of a collective number of dividing cells over the cell axis reveals a characteristic fluorescence profile with a signal peak for the mid-cell constriction site (Ranova et al., 2021). Here, we aimed to determine if mutations on DoIP could affect such localization pattern. To this end, we analyzed the localization of our 24 DoIP<sup>GFP</sup> variants *in vivo* by fluorescence microscopy, using cells harboring plasmids derivative from pDoIP<sup>GFP/His</sup>.



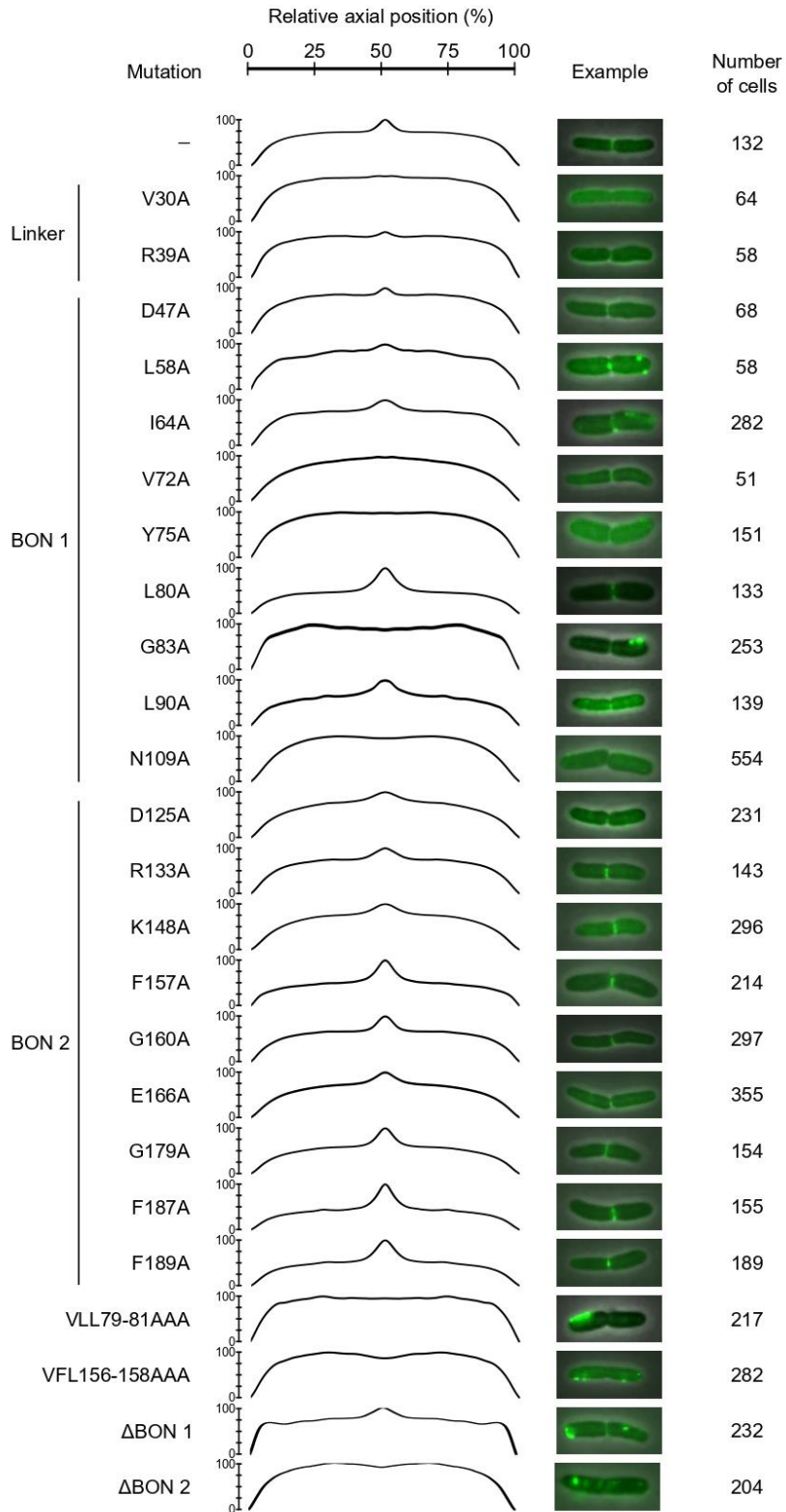


**Figure 32. Mutations on DoIP affect its recruitment to the division septum.** Overnight cultures of BW25113 cells carrying pDoIP<sup>GFP/His</sup> engineered with Ala codons at different positions of the *doIP* ORF were freshly diluted in LB medium, incubated at 37°C until early exponential phase. Cell samples were spotted and visualized on

1% (w/v) agarose pads by phase contrast and fluorescence microscopy. Collective profiles of fluorescence distribution versus the relative position along the cell axis were plotted (N = 51 - 554). Fluorescence intensities were normalized to the maximum value obtained for each sample.

A summary of this screening is presented in Figure 32. Collective plot profiles of fluorescence distribution versus the relative position along the cell axis were generated using the Coli-Inspector software (Vischer et al., 2015). The expression of plasmid borne DoIP<sup>GFP</sup> showed the characteristic signal peak of the cell division site that was previously described ((Bryant et al., 2020; Ranava et al., 2021; Tsang et al., 2017). Mutations in the linker at positions V30 and R39 impaired the localization of DoIP as we can observe a reduced amount of fluorescence at division sites and an increased peripheral distribution of the signal. We can observe that some mutations in domain BON 1 impaired localization of DoIP at division sites and in some cases, protein formed clusters of fluorescence at different sites especially near the poles (mutants L58A, I64A, G83A and L90A). Moreover, we can observe an increase in the peripheral localization of DoIP for Y75A and N109A mutants. Mutation V72A gave a collective plot that is not too dissimilar from wild-type DoIP. However very few cells were analyzed in this case and a more extensive analysis of this mutant will be required. Finally, mutations at positions D47 and L80 have no effect compared to the non-mutated DoIP, as we can observe a fluorescence signal at the division septum.

Mutations in BON 2 had a marginal effect, as we can observe fluorescence signal predominant at the division septum for all mutants, suggesting that the localization of DoIP is not affected. Finally, we can observe a signal in foci outside the division septum for the triple mutations at positions VLL79-81 and VFL156-158. These results suggest that the hydrophobic patch is required to promote septal localization of the protein.

Then, we investigated if the localization of DoIP was affected by BON domain deletions. We could observe that deletion of BON 1 marginally affected the ability of DoIP to localize to the septum, as we can still detect the protein at mid-cell (Fig. 32). The levels of fluorescence are comparable to the WT and cell morphology does not seem affected by the production of the recombinant protein. On the contrary, deletion of BON 2 totally abolished the septal localization of the protein. In addition, very low levels of fluorescence were observed. Analysis by contrast microscopy of cells expressing DoIP deleted of BON 2 showed larger cells compared to the WT and in some cases, the formation of vesicles and round objects with high fluorescent signals (data not shown). For this, we speculate that deletion of BON 2 provokes toxic effects, probably leading to shedding of the cell envelope by vesiculation.

Altogether, we can conclude that both BON domains are required to assure DoIP function. Deletion of BON 2 is particularly toxic (Fig. 29B) and we speculate this could be related at least in part to a deregulated ability of BON 1 to interact with BamA. BON 2 could act as a regulatory domain of DoIP, and its deletion could lead to non-controlled activity of DoIP, which could be toxic.

## 7 TamB is a putative interactor of the BAM complex

Another putative interactor of the BAM complex was TamB, the inner membrane subunit of the TAM module. TAM is a two-subunit complex, composed by TamA and TamB (Selkrig et al., 2012). This complex participates in the assembly of autotransporters, such as p1121 of *Citrobacter rodentium* or EhaA and Ag43 of *E. coli*. Experimental evidence has suggested that TAM can be beneficial to promote efficient biogenesis of OMPs, including some autotransporters and FimD of the chaperone-usher pathway (Babu et al., 2017; Bamert et al., 2017; Selkrig et al., 2012).

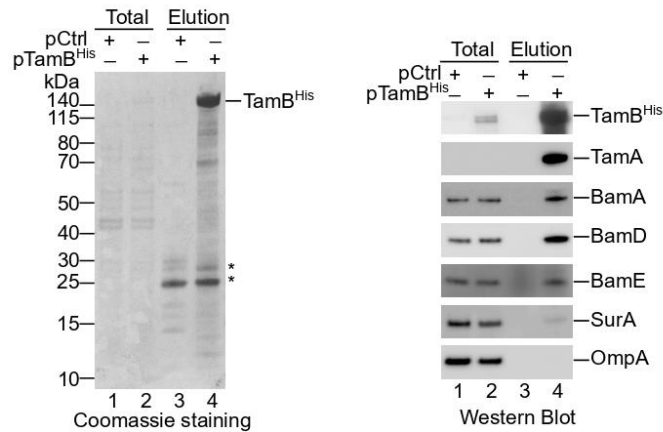
TamA is a member of the Omp85 superfamily, evolutionary related to BamA (Bamert et al., 2017; Heinz et al., 2015; Selkrig et al., 2015) with three POTRA domains in the periplasmic space and a 16 stranded  $\beta$ -barrel. TamA interact with TamB via their periplasmic domains. TamB is anchored to the IM via an N-terminal transmembrane segment (Josts et al., 2017; Selkrig et al., 2012). Downstream of this sequence, TamB presents a large periplasmic domain of unknown function, DUF 490 (Selkrig et al., 2012). To date, only a part of its soluble domain has been solved by X-ray crystallography (residues 963 - 1138). The structure shows a particular  $\beta$ -taco folding, revealing a hydrophobic interior in which amphipathic  $\beta$ -strands could form a cavity for binding of cargo proteins. For this, it has been speculated that TamB may have a role of chaperone (Josts et al., 2017). It has been hypothesized that its periplasmic domain should be large enough to span the periplasm so it could reach TamA in the OM (Selkrig et al., 2012).

The interaction between the BAM complex and TamB has been speculated in the past by several authors. Indeed, in the model organism *Borrelia burgdorferi*, a bacterium that lacks TamA, BamC and BamE, there is a functional complex composed by TamB and BamABD (Iqbal et al., 2016). Interestingly, while several bacterial genera lack TamA, almost all diderm bacteria encode for a TamB-like protein with a DUF490 domain (Heinz et al., 2015). Moreover, a global interactome analysis on *E. coli* envelope has suggested BAM and TAM could cooperate for the biogenesis of autotransporters (Babu et al., 2017). Finally, TamB is suggested to interact with the POTRA 1 domain of TamA and given that BamA and TamA have conserved features (Bamert et al., 2017), it was proposed that TamB could interact with BamA in a similar fashion (Selkrig et al., 2015, 2012) but experimental evidence was still missing. In this context, the fact that TamB was identified in our BAM interactome is very interesting and may constitute the first piece of evidence for a possible interaction between BAM and TAM. We thus decided to further investigate this interaction in order to unravel the possible interplay between BAM and TAM.

### 7.1 TamB interacts with the BAM complex *in vivo*

We first aimed to confirm the interaction between TamB and BAM. To this end, we cloned the gene encoding TamB fused to a poly-histidine tag to perform nickel-affinity chromatography and check if BAM subunits are co-purified with TamB<sup>His</sup>.

**A**



**B**

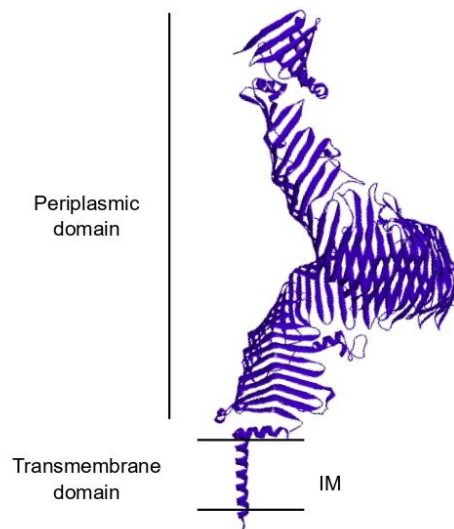


**Figure 33. TamB interacts with the BAM complex *in vivo*.** **A.** Envelope fractions of BW25113 carrying pCtrl or  $\Delta tamB$  cells carrying pTamB<sup>His</sup> were solubilized with 1% (w/v) DDM and subjected to Ni-affinity purification. The load and elution fractions were analyzed by SDS-PAGE. Proteins were loaded to a SDS-PAGE and were Coomassie Brilliant Blue stained (left). Proteins were transferred to a PVDF membrane and blotted protein from load and elution fractions were detected by immunolabeling using the indicated antisera. Loads were set to 0.04% and elutions to 100%. \* indicates a contaminant. **B.** Cartoon representation of the TamB structure predicted by AlphaFold.

TamB<sup>His</sup> was produced in a  $\Delta tamB$  strain (Baba et al., 2006). The total membrane fraction was solubilized with 1% (w/v) DDM, as our preliminary analyses revealed digitonin was inefficient in solubilizing TamB (data not shown). The solubilized total membrane and elution fractions were analyzed by SDS-PAGE. A coloration by Coomassie Brilliant Blue revealed a major band in the elution fractions at the expected size of 140 kDa of TamB<sup>His</sup> (Fig. 33A, left panel), suggesting that TamB<sup>His</sup> was efficiently purified. Besides, we could observe few bands below the bait protein. Of note, a band migrating with an apparent molecular weight of 25 kDa was also present in the negative control, suggesting it is a contaminant of the purification. The bands that are not present in this control are assumed to correspond to specific interactors of TamB or some degradation products.

Western blot analyses revealed that TamA was co-purified with TamB<sup>His</sup> (Fig. 33A, right panel), showing that the TamB-TamA interaction is preserved during sample preparation. Interestingly, signals for several subunits of the BAM complex were obtained by using the corresponding antibodies (Fig. 33A, right panel), confirming that TamB interacts with the BAM complex and thus, confirming our interactome analysis. Of note, the abundant OmpA protein was not co-purified with TamB<sup>His</sup> indicating that TamB interacts specifically with TamA but also with subunits of the BAM complex *in vivo*. We did observe low levels of SurA, which is not surprising as this chaperone can interact with the BAM complex.

## 7.2 The C-terminus of TamB is critical for the interaction with the BAM complex

TamB must span the PG to reach the OM and interact with TamA or BamA. However, to date, no 3D-structure has been solved for the full protein (Josts et al., 2017). We used the predicted AlphaFold 3D-structure of TamB available on the Uniprot server. AlphaFold is a high-throughput software that enables to predict structures with high confidence (Jumper et al., 2021). The model had a predicted Local Distance Difference Test (pLDDT) >90%. The predicted structure reveals a hydrophobic N-terminal  $\alpha$ -helical domain (corresponding to the predicted IM-spanning segment of TamB) and a  $\beta$ -taco folding that may span the periplasmic space (Fig. 33B). The predicted structure suggests that the  $\beta$ -taco folding extends almost all the full TamB periplasmic domain, except for the very last residues at its C-terminus. The 70 last residues at the C-terminal domain fold in a particular conformation that resembles an open  $\beta$ -barrel protein. Moreover, after analyzing the hydrophobicity of the periplasmic domain, we observed that the last 70 residues have a hydrophobic surface and a hydrophilic interior, which is the opposite of the hydrophobic distribution found in the  $\beta$ -taco subdomain. The hydrophobic distribution of this C-terminal subdomain is similar to that observed in  $\beta$ -barrel proteins (Fig 34A). Notably, the last residues of this domain are conserved among different TamB and it

was speculated to have a function for the interaction with TamA (Heinz et al., 2015). It was suggested that this motif could promote the recognition of OM substrates targeted to TAM. Moreover, the last residues of the putative  $\beta$ -barrel domain were similar to those found in  $\beta$ -signals, the recognition signals specific for  $\beta$ -barrel proteins, suggesting they could play a role in the recognition with the BAM complex, as for other  $\beta$ -barrel proteins.

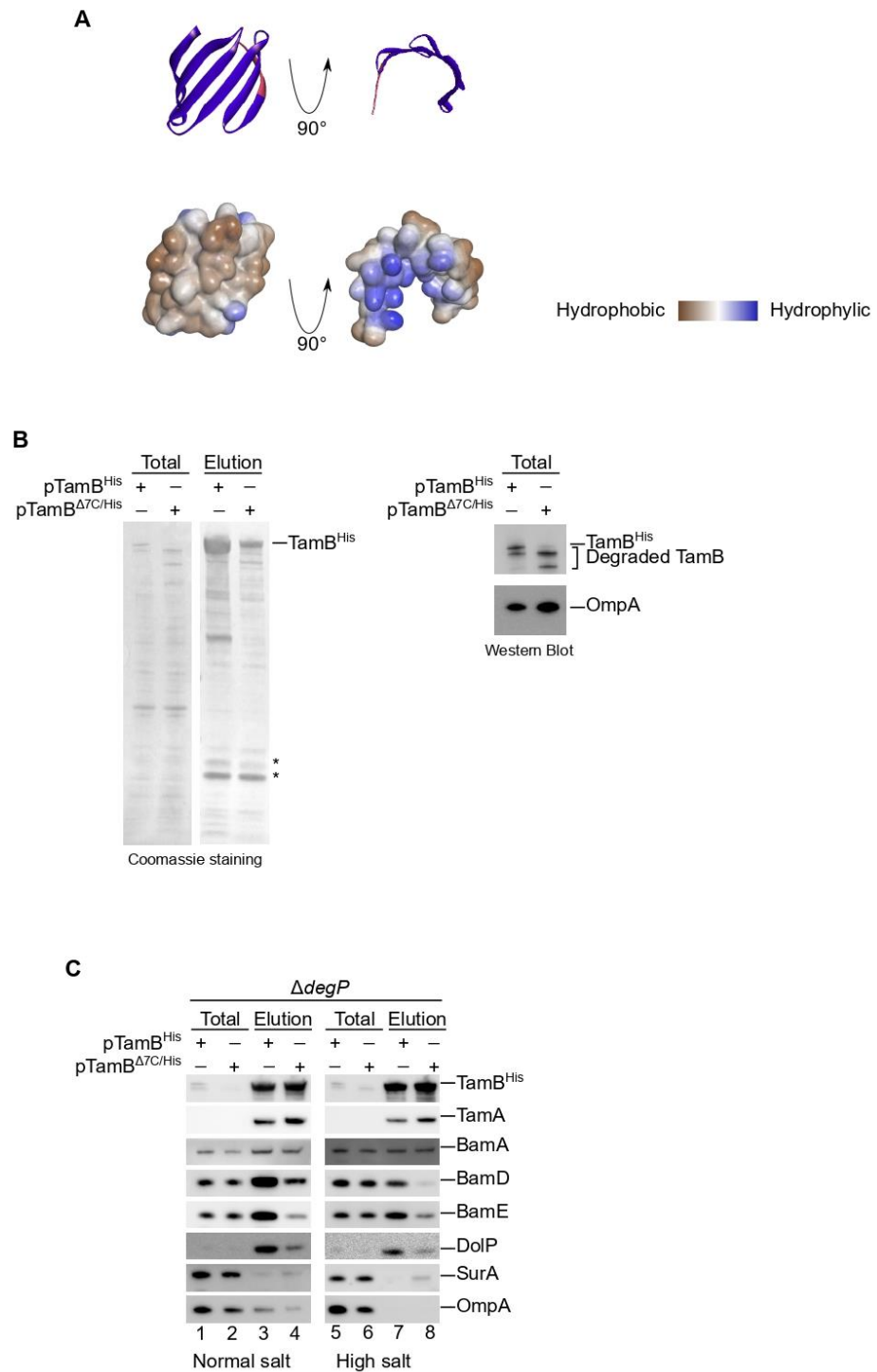


**Figure 34. The C-terminus of TamB is crucial for the interaction with the BAM complex.** **A.** . Cartoon representation of the C-terminal domain of TamB predicted by AlphaFold. Brown surface represents hydrophobic densities and blue, hydrophilic. **B.** Envelope fractions of  $\Delta tamB$  cells carrying pTamB<sup>His</sup> or pTamB <sup>$\Delta 7C/His$</sup>  were solubilized with 1% (w/v) DDM and subjected to Ni-affinity purification. The load and elution fractions were analyzed by SDS-PAGE and Coomassie Brilliant Blue stained (left). Proteins were transferred to a PVDF membrane and blotted protein from total fractions were detected by immunolabeling using the indicated antisera. **C.** Envelope fractions of  $\Delta degP$  carrying pTamB<sup>His</sup> or pTamB <sup>$\Delta 7C/His$</sup>  were solubilized with 1% (w/v) DDM and subjected to Ni-affinity purification. The load and elution fractions were analyzed by SDS-PAGE. Proteins were transferred to a PVDF membrane and blotted proteins from total and elution fractions were detected by immunolabeling using the indicated antisera. Loads were set to 0.04% and elutions to 100%.

As part of a collaborative study with the team of Trevor Lithgow, Monash University, we decided to test this hypothesis. To this end, we deleted the last seven residues, previously demonstrated to be crucial for the interaction with TamA (Selkrig et al., 2012). *E. coli*  $\Delta tamB$  cells transformed with plasmid pTamB<sup>His</sup> and pTamB <sup>$\Delta 7C/His$</sup>  were cultured and after IPTG induction, pull down assays were performed from total membrane protein fractions obtained as previously detailed. SDS-PAGE analysis showed a reduced amount of bait protein for TamB <sup>$\Delta 7C/His$</sup>  in the elution fraction (Fig. 34B, left panel). Western blot analysis of the total fraction revealed a clear band below the band that corresponds to the TamB that was a major product with the samples expressing TamB <sup>$\Delta 7C/His$</sup> . We suspected that TamB <sup>$\Delta 7C/His$</sup>  could be partially degraded at its C-terminus, and we speculated that when TamB is truncated of its seven last residues, it might become less stable and more susceptible to degradation processes.

To assess this point, we decided to use a strain harbouring the deletion of the periplasmic protease DegP. During  $\sigma^E$  stress response, *degP* is upregulated to maintain homeostasis of the bacterial envelope by promoting folding and degradation of unfolded OMPs accumulated in the periplasm (Jones et al., 1997; Krojer et al., 2008; Zhang et al., 2019). The function of this protease has been related to the degradation of some non-competent BAM-mediated assembly of OMPs in the periplasm, for example for OMPs with non-functional  $\beta$ -signals (Combs and Silhavy, 2022; Soltes et al., 2017). Based on this, we hypothesized that the deletion of *degP* could improve the stability of the truncated form of TamB, as this sequence is very similar to a  $\beta$ -signal.  $\Delta degP$  cells were transformed with pTamB<sup>His</sup> and pTamB <sup>$\Delta 7C/His$</sup>  and TamB<sup>His</sup> and TamB <sup>$\Delta 7C/His$</sup>  were purified as previously described. After SDS-PAGE and Western blot analyses, we could observe that both versions of TamB were purified in similar amounts, suggesting the purification issue observed previously was due to a degradation by DegP.



Most notably, our Western blot analysis revealed that the deletion of the seven residues of the C-terminus of TamB reduced the interaction with the subunits of the BAM complex compared to its full version. Instead, the amount of co-purified TamA appeared marginally increased using the truncated form of TamB (Fig. 34C, lanes 1-4). A similar result was obtained also using high ionic strength during the purification procedure to be more stringent. Western blot analyses showed that the deletion of the C-terminus of TamB still impairs the interaction with BAM subunits but not with TamA (Fig. 34C, lanes 5-8). These results suggest that the C-terminus of TamB is critical for the interaction with the BAM complex. When these residues are deleted, TamB seems to have a reduced affinity towards BAM, while the interaction with TamA seems to be increased. This finding suggests that TamA and the BAM complex may compete for an interaction with TamB. It is possible that the interaction TamB-BAM or TamB-TamA could be formed to respond to different needs for OM biogenesis. Interestingly, we observed that TamB<sup>His</sup> was able to co-purify DolP in the presence of DDM and the deletion of its C-terminus decreased the interaction, as other BAM subunits. At least two scenarios can explain this result: TamB may stabilize the interaction of BAM with DolP, or a subunit of the TAM complex directly interacts with DolP.

TamB<sup>Δ7C</sup> is more stable when DegP is missing, suggesting it is degraded by this protease. It is known that BamA or BamD recognize  $\beta$ -signals of unfolded OMPs (Germany et al., 2021; Lundquist et al., 2021; Ricci and Silhavy, 2019), suggesting these subunits may promote the interaction with TamB by binding its C-terminal segment. More studies will be needed to further investigate the TamB-BAM interaction and the role of the last seven residues of TamB. The importance of the function of this TamB-BAM complex still needs to be characterized and it would be interesting to study biogenesis of OMPs that benefit for both BAM and TAM, such as FimD and some autotransporters (Bamert et al., 2017).

## Conclusions and perspectives

The BAM complex is an essential machinery of cell envelope of Gram-negative bacteria. Until now, many studies have investigated its function to promote the biogenesis of OMP with the objective to decipher its structure-function relationships. However, how the BAM complex is able to coordinate its function with other machineries in the Gram-negative bacterial envelope was still ill-defined.

This work aimed at defining the BAM interactome in the envelope of *E. coli*. Few of the identified interactions were previously reported, while the majority of these had not been described in the literature. We focused on two top-score interactors: DoIP and TamB with the objective of understanding the physiological roles of their interplay with the BAM complex.

The first part of this work focused on characterizing the interaction between DoIP and BAM. We obtained data suggesting that DoIP has a dynamic organization, as we can observe the formation of homooligomers of different sizes, a feature observed in another DoIP ortholog in *Acinetobacter baumannii* (Grinter et al., 2021). Moreover, our *in vitro* data suggests that when DoIP interacts with the BAM complex, it is probably in the form of a monomer or a dimer. Whether the organization of DoIP is a critical parameter that regulates its interaction with the BAM complex is not yet fully understood, however we obtained some preliminary results that could support this hypothesis. More studies have to be conducted to obtain information on how DoIP multimerization could regulate its function and whether these oligomeric states of DoIP could be related to specific roles.

We demonstrated that DoIP is able to interact with OM-assembled BamA and the interaction is mediated via the domain BON 1 of DoIP. We showed that BamA at high levels can be potentially detrimental for the cell, and we observed that DoIP opposes this effect, restoring normal growth. From a molecular point of view, the detrimental effect of BamA overproduction on cell growth effect was linked to the accumulation of a non-properly folded conformation of BamA that associates to the membrane fraction. Concomitant overproduction of DoIP supports BamA folding. This observation may explain why DoIP expression is upregulated by  $\sigma^E$ , as incremental levels of DoIP could be beneficial to promote the folding of newly synthesized BamA that is also upregulated during envelope stress. It is also important to highlight that the deletion of *doIP* triggers the Rcs response, phenocopying the BamA depletion strain *bamA101* (Cho et al., 2014). This result is in line with a model where efficient BamA assembly requires DoIP. These results suggest that the  $\sigma^E$ -mediated upregulation of DoIP could play a role in supporting the activity of the BAM complex as, upon activation of the envelope stress response, the upregulation of BAM is needed to restore OMP biogenesis. This link between the Rcs and the  $\sigma^E$  stress responses is reminiscent of the link between the  $\sigma^E$ -mediated

upregulation of *skp* and its repression by the Cpx stress response: in fact, after  $\sigma^E$  activation, *skp* is upregulated possibly to help alleviate BAM from stalled OMPs but also to hand misfolded OMPs over to DegP for degradation. However, a prolonged activity of Skp is detrimental because of the aberrant function to localize OMPs at the IM, therefore Skp is postrationally downregulated by Cpx (Combs and Silhavy, 2022; Grabowicz et al., 2016; Grabowicz and Silhavy, 2017b).

Although, the functional link between DoIP and BAM is still ill defined and *in vitro* analysis should be conducted to gain insights into the mechanism by which DoIP supports BAM folding and activity, some mechanistic hypothesis can be raised.

It was shown that DoIP can bind to negatively charged phospholipids (Bryant et al., 2020). Lipid binding can play important regulatory roles on protein complex stability and function. For instance, it was shown that cardiolipin improves the formation of the BAM-Sec holotranslocon supercomplex (Alvira et al., 2020). We could speculate that the function of DoIP could be related to the binding/recruitment of this type of phospholipids at BAM sites and this could improve the function of the BAM complex during OMP biogenesis by formation of a functional OMP assembly machinery. However, in contrast to this hypothesis we have shown that a mutation, W127E, in DoIP that should abolish the ability of BON 2 to bind phospholipids (Bryant et al., 2020) can nevertheless promote BamA folding. Lipid binding was however proposed to be a general feature of BON domains (Yeats and Bateman, 2003) therefore it is possible that DoIP binds lipids by different mechanisms. Alternatively, DoIP may function similar to a chaperone promoting the folding of BamA during its assembly into the OM, as it was shown for the DoIP homolog OsmY that supports the folding of autotransporter proteins (Yan et al., 2019).

Finally, we have shown an interaction of DoIP with Pal. Although experiments conducted by other members of the team have revealed that Pal is not required for mid-cell localization of DoIP (data not shown) this interaction highlights the critical role of DoIP in coordinating a late step of cell division as also Pal localizes at division septa. In light of the fact that BAM is more concentrated at cell constriction sites (Consoli et al., 2021b) and that *de novo* assembly of OMPs occurs preferentially at the mid-cell (Rassam et al., 2015), it will be interesting to investigate whether DoIP locally support BAM activity when it is localized at the mid-cell.

We also begun the characterization of the link between the structure and function of DoIP. By the generation of a collection of DoIP mutant constructs, we were able to observe that the two DoIP BON domains play distinct roles. Globally, we can observe that BON 1 is sufficient to promote BamA folding. Strikingly, however, the overproduction of this truncated form of DoIP is toxic. Whether this toxicity is caused by a deregulated activity of BON 1 on BamA (for

instance by forming a stable complex that titrates BamA and prevents its assembly into a functional BAM complex) will require further investigation. It will also be interesting to decipher the ability of BON domains to promote biogenesis or proper folding of proteins and in particular OMPs.

Concerning the interaction with TamB and the BAM complex, we only started the characterization of the interaction and more experiments are needed to investigate if this interaction can lead to a function in promoting OMP biogenesis. A good candidate to analyze is FimD or some autotransporters (such as p1121, EhaA and Ag43), as biogenesis of these OMPs benefits from the expression of TAM (Babu et al., 2017; Bamert et al., 2017; Selkrig et al., 2012).

More generally, more work is yet to be conducted to further characterize the other BAM interacting proteins and eventually identify key BAM partners, providing new insights into the regulation of BAM function and its interplay with other OM biogenesis machineries. These investigations may pave the way for the identification of new targets for the development of antimicrobial strategies to fight against noxious Gram-negative bacteria.

## Materials and Methods

### 1 Plasmid construction

Plasmids encoding for ectopic BAM, BamA, OmpA, DoIP (except DoIP<sup>GFP/His</sup>), and their tagged and/or mutant versions are derivative from pTrc99A vector (Roman-Hernandez et al., 2014; Szabady et al., 2005) that includes a P<sub>trc</sub> promoter (IPTG inducible) and an ampicillin resistance gene. Plasmid encoding for DoIP<sup>GFP/His</sup> is derivative from pJF119eh (Fürste et al., 1986) that contains a P<sub>tac</sub> promoter (IPTG inducible) and an ampicillin resistance gene.

Plasmid pBAM<sup>His</sup> has been already described in the literature (pJH114) and comprises an ORF that encodes the five subunits of BAM (BamA-BamE) with a octahistidine tag fused to the sequence of BamE at its C-terminus (Roman-Hernandez et al., 2014). For construction of plasmid pBAM<sup>ProtA</sup>, the encoding genes for TEV-ProtA–His were amplified by PCR with primers harboring extremities from plasmid pYM10 (Knop et al., 1999) and introduced by restriction-free cloning into pBAM<sup>His</sup> to replace the poly-histidine tag. The construct pBAM was made by introducing two stop codons between *bamE* and the *protein A* tag by site-directed mutagenesis.

The plasmid pCtrl was created by excising the ORFs of BAM (*bamA* start codon to *bamE* stop codon) from pJH114 (Roman-Hernandez et al., 2014) by site-directed mutagenesis. Plasmid pBamA<sup>His</sup> was generated by restriction-free cloning, inserting the *bamA* ORF without its stop codon downstream of the P<sub>trc</sub> promoter and upstream of an octahistidine encoding region in pCtrl.

Plasmids encoding the BamA variant deleted of the POTRA domains 1 or 2 were obtained by site-directed mutagenesis deleting the portion of *bamA* ORFs corresponding to residues E22-K89 or P92-G172, respectively.

Plasmid pDoIP<sup>His</sup>, pTamB<sup>His</sup> and pOmpA<sup>His</sup> were created by amplifying genomic *doIP*, *tamB* and *ompA* sequence from the BW25113 strain to replace the *bamABCDE* ORFs in pJH114 by using primers harboring flanking extremities to permit restriction-free cloning.

pDoIP<sup>GFP/His</sup> was created by amplifying *doIP-gfp* sequence from chromosomal mutant described in the literature (Ranava et al., 2021). This DNA sequence was cloned in plasmid pJF119eh by restriction free cloning. Finally, an octahistidine tag was introduced at the C-terminus of GFP by restriction free cloning.

Plasmid pDoIP<sup>ProtA</sup> was created by amplifying the encoding gene of Protein A tag from pBAM<sup>ProtA</sup> and further restriction-free cloning, as previously described.

The plasmid pBamA-DolP<sup>His</sup> was generated by restriction-free cloning of the *bamA* ORF between the P<sub>trc</sub> promoter and *dolP* in pDolP<sup>His</sup>. pDolP<sup>His</sup>-BamA was built in two steps starting from pDolP<sup>His</sup>. First, the sequence of the *E. coli* K12 *bamA* ribosome-binding site was deleted, positioning the *dolP* ORF eight nucleotides downstream of the ribosome-binding site of the pTrc99a multiple cloning site. The resulting plasmid was then used to insert a segment of pJH114 containing the entire *bamA* ORF including the *E. coli bamA* ribosome-binding site.

Mutations on the sequence of *dolP* (deletion, point mutations or amber codon mutations) were introduced by site-directed mutagenesis using plasmids pDolP<sup>His</sup>, pDolP<sup>GFP/His</sup>, pBamA-DolP<sup>His</sup> and pDolP<sup>His\*</sup> harboring mutation codons. All plasmid sequences were confirmed by sequencing.

## 2 Cell cultures

### 2.1 Bacterial culture

Cells were grown in liquid cultures in Lysogenic Broth (LB) medium (1% (w/v) tryptone, 0.5% (w/v) yeast extract, 1% NaCl), supplied from Fisher® or Difco®, supplemented with antibiotics when necessary, at 30 or 37°C with an agitation of 180 rpm. Antibiotics were used at the following concentrations: Ampicillin (Amp) 100 µg/ml, Kanamycin (Kan) 50 µg/ml, Chloramphenicol (Cm) 30 µg/ml, and Vancomycin (Van) 60 µg/ml, except if otherwise indicated. For cultures on minimal medium (M9 salt 1X (33.7 mM Na<sub>2</sub>HPO<sub>4</sub>, 22 mM KH<sub>2</sub>PO<sub>4</sub>, 8.55 mM NaCl, 9.35 mM NH<sub>4</sub>Cl), 1 mM MgSO<sub>4</sub>, 100 mM CaCl<sub>2</sub>, 0.2% glucose or glycerol, as indicated), cells were grown in the same conditions.

### 2.2 Lambda red recombination

Strains used for this recombination were previously transformed with the thermosensitive plasmid pKOBEG and they were freshly made electrocompetent as previously described, with a few modifications, as follows. Cells were grown at 30°C and when they reached an early exponential phase, they were induced by 0.05% arabinose to allow gene expression. They were incubated until late mid-exponential phase and then they were heat shocked at 42°C (or 37°C) for 20 min cure for pKOBEG plasmid. They were then incubated on ice and they were made electrocompetent, as previously described. Preparation of DNA fragments to recombine was made by PCR amplification of the DNA sequence of interest with extremities of around 50 nt homologous to the sequence downstream and upstream for recombination. DNA sequence included a kanamycin cassette surrounded by FRT sites, as described for pKD4 plasmid. DNA sequence of *dolP* mutants was amplified from plasmid derivatives of pBamA-DolP<sup>His</sup> and the

two plasmid terminators were included in this construction downstream the ORF of *doiP*. PCR amplification was made using high fidelity polymerase (PrimeStar, Takara Bio). This DNA was purified by gel excision or by a purification kit. Then, at least 200 ng of DNA was used to transform electrocompetent cells using electroporator in the same condition as previously described. After phenotypic expression, cells were plated in appropriate medium supplemented with antibiotics. Clones were assessed by PCR on colony and sequencing to confirm the sequence.

### 2.3 Excision of antibiotic resistance

Cells harboring kanamycin cassette flanked by FRT sites were made chemically competent as previously described and transformed with the thermosensitive plasmid pCP20, previously described in the literature (Cherepanov and Wackernagel, 1995). After phenotypic expression, cells were spread on LB supplemented with Cm and incubated overnight at 30°C. The next day, single colonies were streaked in a fresh LB agar plate without antibiotic and grown overnight at 42°C to cure for plasmid. The day after, single colonies were streaked once more in three LB agar plates: one without antibiotic, one supplemented with Kan and the other with Cm. The next day, positive clones were selected when they could not grow in the presence of Kan nor Cm, but could grow on LB without antibiotic. For some strains, it was beneficial to grow single colonies in liquid medium for 2 hours prior to make the first streak for thermic shock to promote loss of plasmid. Positive colonies were confirmed by Western blot or PCR on colony.

### 2.4 Preparation of electro competent cells

*E. coli* strain to transform was grown in 100 ml of LB medium using proper antibiotics (when necessary) was inoculated with an overnight culture at an OD<sub>600</sub> of 0.05 approx. (dilution 1:100). When cultures reached an OD<sub>600</sub> of 0.6-0.8, cells were pelleted by centrifugation at 4°C for 15 minutes at 6000 x *g*. Pellets were washed twice with sterile cold water (100 ml and 50 ml, respectively) and once with cold sterile glycerol 10% (25 ml) following the same conditions of centrifugation. Then, pellets were resuspended in 0.5 ml of sterile glycerol 10% and they were used for transformation using proper DNA.

Transformation was carried out using electroporator (Bio-Rad Gene Pulser II). To transform, 50 µl of electrocompetent cells were mixed with 10-100 ng of DNA and transferred to an ice-cold electroporation cuvette 1 mm. Electroporation was performed using the following settings: voltage 1.75 kV, resistance 200 Ω, capacitance 25 µF. Then, cells were mixed with 1 ml of LB

medium and incubated for 1 h at 37°C to promote phenotypic expression. Then, a part of this mix was plated on LB agar medium supplemented with proper antibiotics. For thermosensitive plasmids, cells were incubated at 30°C.

## 2.5 Preparation of chemical competent cells

A culture of 100 ml of LB medium using proper antibiotics (when necessary) was inoculated with an overnight culture at an OD<sub>600</sub> of 0.05 approx. (dilution 1:100). When cultures reached an OD<sub>600</sub> of 0.6-0.8, cells were pelleted by centrifugation at 4°C for 15 minutes at 6000 x *g*. Then, pellets were washed with 5 ml of TFB1 (100 mM RbCl, 50 mM MnCl<sub>2</sub>, 30 mM potassium acetate, 10 mM CaCl<sub>2</sub>, 15% glycerol), and then resuspended in 0.5 ml of TFB2 (10 mM MOPS, 10 mM RbCl, 75 mM CaCl<sub>2</sub>, 15% glycerol) following the same conditions of centrifugation. After chilling on ice for 30 min, cells were ready for transformation using proper DNA.

Transformation was carried out via thermic shock. For this, 50 µl of cells were mixed with 10-100 ng of DNA and incubated on ice for 10 min. Then, cells were incubated at 42°C for 45 s and then on ice for 2 minutes. Then, 1 ml of LB medium was added and cells were incubated for 1h at 37°C to induce phenotypic expression. Finally, a part of this mix was plated on LB agar medium supplemented with proper antibiotics. The amount of this mix used for plating depended on the DNA used for transformation and the strain, and it ranged between 25 – 1000 µl. For thermosensitive plasmids, thermic shock was done at 37°C and overnight culture, phenotypic expression and incubation were done at 30°C.

## 2.6 P1 transduction

Two cultures were prepared: one donor and one acceptor strain. Donor strain was grown in LB medium with proper antibiotics in the presence of 5 mM of CaCl<sub>2</sub>. When cells reached an early exponential phase, WT bacteriophage P1<sub>vir</sub> solution stock was added and cells were incubated until complete lysis of bacteria. After this time, enough chloroform was added for 5 min at 37°C to create a separation phase. After a clarification spin, this cell lysate was used to transduce an acceptor strain. Acceptor strain was grown using the same conditions in the presence of 5 mM of CaCl<sub>2</sub> and when cells reached late exponential phase, cell lysate of the donor strain was added to the cell culture. Cells were incubated for 30 min at 37°C and sodium citrate pH 5.5 was added to this reaction to a final concentration of 166 mM. Then, cells were collected by centrifugation for 5 min at 6000 rpm and resuspended in LB with 100 mM of sodium citrate and incubated for 1h at 37°C. Then, cells were collected by centrifugation as previously described and spread in LB agar with proper antibiotics.



## 2.7 Spot test assay

Cells were inoculated in LB medium (Fisher®) at a dilution of 1:200 (OD<sub>600</sub>=0.03 approx.) and cultured to mid-log phase. Then, cells were collected by centrifugation and kept on ice and resuspended with M9 salts 1X to normalize at OD<sub>600</sub>=1. These samples were serially diluted in ice-cold M9 salts prior to spotting on agar plates supplemented with proper antibiotics or IPTG, as indicated.

## 2.8 SILAC labeling

*E. coli* MC4100 derivative or BW25113 strains transformed with pBAM or pBAM<sup>ProtA</sup> were grown overnight at 37°C in minimal medium supplemented with L-amino acids (1X M9 salt, 1 mM MgSO<sub>4</sub>, 100 mM CaCl<sub>2</sub>, 0.2% glucose, 10 µg/ml Thiamine, 250 mg/L L-Arg (heavy or light), 250 mg/L L-Lys (heavy or light), 500 mg/mL L-Pro (light). Heavy amino acids are provided by Eurisotop, Cambridge Isotope Laboratories, Inc® and light ones by Sigma Aldrich®). Overnight precultures were used to inoculate 200 ml to a 1:100 dilution and cells were grown until exponential phase (OD<sub>600</sub>=0.5-0.6). The cultures were then induced with IPTG at a final concentration of 400 µM and incubated for 1.5 hours.

## 2.9 β-galactosidase assay

Precultures of cells harboring chromosomal fusions of lacZ to promoter of interest were used to inoculate fresh LB medium with proper antibiotics to a dilution 1:500. Cells were incubated until mid-log phase OD<sub>600</sub> of 0.3-0.5. Then, cells were chilled out on ice for 20 min and OD<sub>600</sub> was recorded. Then, 250 µl of this sample was diluted 4 times with Z buffer (60 mM Na<sub>2</sub>HPO<sub>4</sub>·7H<sub>2</sub>O, 40 mM NaH<sub>2</sub>PO<sub>4</sub>·H<sub>2</sub>O, 10 mM KCl, 1mM MgSO<sub>4</sub>, 50 mM β-mercaptoethanol (BME)) and cells were permeabilized by adding 25 µl chloroform and 50 µl of 0.1% SDS. After mixing, samples were equilibrated 5 min at 28°C. Then, 200 µl of o-nitrophenyl-β-D-galactoside (ONPG; 4 mg/mL diluted in 100 mM PBS buffer pH 7) solution were added. When color changed to a visible yellow, reaction was stopped by adding 0.5 ml of 1M Na<sub>2</sub>CO<sub>3</sub>. After a clarifying spin, supernatant was used for record OD at 420 and 550 nm. Miller units were calculated using the formula:

$$\text{Miller units} = 1000 \times \frac{OD_{420} - 1.75 OD_{550}}{t (\text{min}) \times V (\text{ml}) \times OD_{600}}$$

## 2.10 Fluorescence microscopy and analysis

*E. coli* BW25113 harboring plasmids pDoIP<sup>DGFP/His</sup> and derivatives were grown overnight in LB medium supplemented with Amp. They were grown until an early exponential phase at 37°C and then they were kept on ice for 10 min. Meanwhile, agarose (1% (w/v)) was diluted in a phosphate-buffered saline (PBS) solution (137 mM NaCl, 2.7 mM KCl, 10 mM Na<sub>2</sub>HPO<sub>4</sub> 1.8 mM, KH<sub>2</sub>PO<sub>4</sub>) and pads were made. A volume of 0.6 µl of cell culture was then spotted in these agarose pads and they were used for visualization by contrast/fluorescence microscopy. Cells were imaged at 30°C using an Eclipse TI-E/B Nikon wide field epifluorescence inverted microscope with a phase contrast objective (Plan APO LBDA 100X oil NA1.4 Phase) and a Semrock filter mCherry (Ex: 562BP24; DM: 593; Em: 641BP75) or FITC (Ex: 482BP35; DM: 506; Em: 536BP40). Images were acquired using a CDD OrcaR2 (Hamamatsu) camera with illumination at 100% from a HG Intensilight source and with an exposure time of 1–3 s, or using a Neo 5.5 sCMOS (Andor) camera with illumination at 60% from a LED SPECTRA X source (Lumencor) with an exposure time of 2 s. Nis-Elements AR software (Nikon) was used for image capture. Image analysis was conducted using the Fiji and ImageJ software.

Collective profiles of fluorescence distribution versus the relative position along the cell axis were generated using the Coli-Inspector macro run in ImageJ within the plugin ObjectJ (Vischer et al., 2015). Fluorescence intensities were normalized to 100% for the maximum value of fluorescence.

## 3 **Cell fractionation**

### 3.1 Preparation of crude envelope fraction

After growing cultures in the conditions described previously, cells were pelleted by centrifugation at 6,000 x *g* for 15 min at 4°C. Then, pellets were resuspended in 3 mL of cold 20 mM Tris-HCl pH 8 for subsequent mechanical disruption at 0.82 kPa using Cell Disruption (Constant Systems LTD®). Then, this sample was centrifuged at 6,000 x *g* for 10 min at 4°C to get rid of cell debris. The supernatant was then subjected to ultracentrifugation at 50000 rpm for 30 min at 4°C (rotor TLA 110). Supernatant was then discarded and the pellet corresponding to the envelope fraction kept for further experiments.

### 3.2 Cell fractionation by sucrose gradients

We used a protocol previously described (Cian et al., 2020), with minor modifications. Cells were grown in LB medium supplemented with antibiotics and collected, as previously described. Then, cell pellets were resuspended in 12.5 ml of Buffer A (0.5 M sucrose, 10 mM

Tris pH 7.5) supplemented with lysozyme to a concentration of 144 µg/ml, while agitating for 2 min on ice. Then, 12.5 ml of 1.5 mM EDTA were added while agitating for another 7 min on ice. This sample was then centrifuged at 10000 × g for 10 min at 4 °C and pellet was kept. The pellet was resuspended adding 25 ml of buffer B (0.2 M sucrose, 10 mM Tris pH 7.5), 55 µl of 1M MgCl<sub>2</sub> and 1 µl of protease inhibitor cocktail (Roche). Then, this sample was subjected to mechanical disruption at 0.82 kPa, as previously described. After a clarifying spin at 5300 rpm (rotor JS-5.3) for 15 min at 4°C, the supernatant was subjected to ultracentrifugation at 184,000 × g and 4°C for 1h. The pellet was resuspended in 1 ml of the low-density isopycnic-sucrose gradient solution (20% w/v sucrose, 1 mM EDTA, 1 mM Tris pH 7.5). Sucrose gradient was prepared by dispensing isopycnic-sucrose gradient solutions (1 mM EDTA, 1 mM Tris pH 7.5 supplemented with sucrose, ranging from 20 to 73%). These sucrose solutions were introduced successively to a centrifuge tube in the following order: 2 ml of 73% sucrose solution (bottom), 4 ml of 53% sucrose solution (middle), 1 ml of resuspended pellet and 6 ml of 20% solution (top). Tubes were placed in a cold swing SW41 rotor and centrifuged at 288,000 × g for at least 16h at 4°C. After this step, two distinctive phases were visible, the IM (the upper one) and the OM (the lower one) and they were collected by pipetting.

### 3.3 Preparation of spheroplasts

Spheroplasts were prepared by collecting cells in early exponential phase by centrifugation at 6000 × g for 15 min at 4°C. Then, pellets were resuspended in 33 mM Tris-HCl, pH 8, 40% (w/v) sucrose and normalized to an OD<sub>600</sub> of 1. Then, lysozyme and EDTA were added to a final concentration of 0.1 mg/ml and 2 mM, respectively. Samples were then incubated on ice for 20 min to induce lysis. MgSO<sub>4</sub> was added to a final concentration of 10 mM and spheroplast fraction was collected by centrifugation at 16000 × g. Supernatant was then ultracentrifuged at 50000 rpm (rotor TLA110) to remove any residual membrane fraction. Soluble fraction was subjected to trichloroacetic acid (TCA) precipitation by adding 10% of ice-cold TCA. A final clarifying spin was performed to get rid of the supernatant and to recover precipitated proteins in the pellet. A similar procedure, with a cell resuspension buffer lacking sucrose, was used to lyse cells and obtain the membrane and soluble fractions.

## **4 Protein purification**

### 4.1 Ni-NTA affinity native purification

Total membrane fraction were prepared from liquid cultures of 200 ml. Pellets were resuspended for 1 hour at 4°C under agitation using 1.6 ml of imidazole solubilization buffer

containing non-ionic detergents digitonin and/or DDM as indicated in figure legends (50 mM Tris HCl pH 8, 150 mM NaCl, 2 mM PMSF, 1X cOmplete™ Protease Inhibitor Cocktail, supplemented with detergents (digitonin and/or DDM, as specified), supplemented with 20 mM of imidazole. Following a clarifying spin at 15000 x *g* for 15 min at 4°C, the supernatant was then mixed with 30-50 µl (representing 1 column volume) of Ni-NTA beads (Protino) previously equilibrated with solubilization buffer. Binding was performed in batch for 1h at 4°C under mild agitation. After this step, the mix was transferred to a microcolumn prior a low speed centrifugation (30 seconds at 800 x *g*) to get rid of the flow-through. After extensive washes using washing buffer containing 50 mM imidazole and a concentration of detergents of 0.3% (w/v) digitonin and/or 0.03% (w/v) DDM, proteins were eluted with 3 column volumes with the same buffer containing 500 mM imidazole.

#### 4.2 IgG-affinity native purification

Crude membrane fractions and total membrane fractions were obtained as previously described. Membrane protein samples were mixed with 30-50 µl (representing 1 column volume) of homemade IgG-sepharose beads (previously equilibrated with solubilization buffer) for 1 to 1.5 h at 4°C under mild agitation. After binding, the mix was transferred to a microcolumn prior a low speed centrifugation (30 seconds at 800 x *g*) to get rid of the flow-through. Then, extensive washes were done using the solubilisation buffer supplemented with 0.3% digitonin or 0.03% DDM. Proteins were eluted by incubating overnight with 100 µl of solubilisation buffer supplemented with 30 U of Invitrogen™ AcTEV™ protease, at 4 °C and under agitation at 1000 rpm. The next day 20-25 µl of previously equilibrated Ni-NTA agarose resin was added to the IgG-resin and incubated for 30 min at 4 °C at 1000 rpm. Then, elution fraction was recovered by centrifugation for 1 min at 240 x *g* at 4 °C. An additional volume of 50 µl of wash buffer was used to fully extract eluted protein from the beads.

#### 4.3 Protein purification scale-up using FPLC automate

In some cases, the proteins of interest were purified using an FPLC automate (ÄKTA Purifier 10 (GE Healthcare)) to scale-up the purification processes. After membrane solubilisation, proteins were purified by Ni-affinity and size exclusion chromatography, adapting a previously published protocol. Briefly, after membrane solubilization with 50 mM Tris-HCl pH 8.0, 150 mM NaCl, and 1% (w/v) DDM, insoluble material was removed by ultracentrifugation at 100,000 x *g*, 4°C for 1h. Solubilised proteins were loaded onto a Ni-column (HisTrap FF Crude, or TALON, GE Healthcare) pre-equilibrated with equilibration buffer (50 mM Tris-HCl pH 8.0, 150 mM NaCl, and 0.03% (w/v) DDM) at 1 ml/min at 4°C. The column containing bound proteins

was washed with equilibration buffer supplemented with 50 mM imidazole. Proteins were eluted using equilibration buffer, applying a gradient of imidazole from 50 mM to 500 mM. Proteins eluted were further separated by gel filtration using a HiLoad 16/600 Superdex 200 (GE Healthcare) in equilibration buffer using a flow rate of 1 ml/min. Eluted proteins were concentrated using an ultrafiltration membrane with a 10 kDa molecular weight cut-off (Vivaspin 6, Sartorius).

## **5 Analyses of protein-protein interaction**

### **5.1 Chemical crosslink**

Crude envelope fractions from strain transformed with pBamA-DolP<sup>His</sup> were isolated as described previously. These envelope pellets were resuspended in chemical crosslinker buffer (10 mM PBS buffer, 100 mM NaCl, pH 7.4) and proteins were quantified using NanoDrop. Crosslinker solution was freshly made by preparing a 25  $\mu$ M solution of DSP, EGS, DSG or BS3, diluted in DMSO or water following the providers recommendations (ThermoFischer). Then, crosslinking was performed by adding 80  $\mu$ l of envelope resuspension (*i.e.* 80-160  $\mu$ g of protein), to the crosslinker solution at a final concentration of 0.75 mM. Negative controls were made under similar conditions without crosslinker. Samples were incubated for 30 min at 30°C and 300 rpm and then glycine was added at 100 mM final to quench the reaction. Samples were chilled on ice and then TCA precipitation was made as previously described. After this step, pellets were resuspended with 70  $\mu$ l of SDS solubilization buffer and boiled for 5 min at 98°C and 1000 rpm. RIPA buffer with 20 mM imidazole was then added at a final concentration of 0.3% SDS and samples were agitated at 1000 rpm at room temperature for 5 min. After a clarifying spin, samples were mixed with 30-50  $\mu$ l (1 column volume) of preequilibrated Ni-NTA agarose beads and incubated for 1 h at 4°C under mild agitation. Then, samples were transferred to a microcolumn to get rid of the flow-through. After extensive washes with RIPA buffer with 50 mM imidazole, proteins were eluted using 3 volumes of RIPA buffer supplemented with 500 mM imidazole.

### **5.2 Site-specific photocrosslinking**

Strains harboring deletion of *dolP* were transformed with pEVOL-pBpF (Chin et al., 2002) and plasmids (pBamA-DolP<sup>His</sup> or pDolP<sup>His</sup>) containing amber codons in the sequence of DolP. Cells were then cultured in M9 minimal medium supplemented with glucose or glycerol, as specified, until early exponential phase. Cultures were then supplemented with 1 mM Bpa (Bachem) and 400  $\mu$ M IPTG for 1.5 hr. Cultures were divided into two equal parts, one left on ice and one

subjected to UV irradiation for 10 min on ice, using a UV-A LED light source (Tritan 365 MHB, Spectroline). Cells were pelleted and kept at -20°C until needed. Then, pellets were resuspended in 20 mM Tris pH 8 and subjected to mechanical disruption and envelope isolation as previously described. Then, envelope fractions were solubilized using 80 µl of SDS solubilization buffer (13% Glycerol, 195 mM Tris base, 15 µM EDTA, 4% SDS, 2 mM PMSF) and boiled at 98°C and 1000 rpm for 5 min to denature samples. Then RIPA buffer (150 mM NaCl, 1% NP-40 (IGePALCA-630), 0.5% Deoxycholic acid, 0.1% SDS, 50 mM Tris HCl pH 8) supplemented with 20 mM imidazole was added to dilute SDS concentration to 0.3% and samples were subjected to agitation at 1000 rpm for 5 min. Samples were then subjected to a clarifying spin and supernatant was subjected to Ni-affinity chromatography, in batch mode as previously described. After binding, extensive washes were done using RIPA buffer with 50 mM imidazole, and proteins were eluted using 500 mM imidazole in the same buffer. Equal portions of the elution fractions were separated by SDS-PAGE and subjected to immunoblotting.

### 5.3 In vitro reconstitution of protein-protein interaction

Envelope fractions were obtained from cells carrying pBAM<sup>His</sup> or pDoIP<sup>His</sup> and cultured until early exponential phase in LB medium at 37°C and subsequently supplemented with 400 µM IPTG for 1.5 h to induce the expression of the BAM complex or DoIP.

BAM-DoIP reconstitution was performed by mixing equimolar concentrations of purified proteins. This mix was incubated in equilibration buffer (50 mM Tris-HCl pH 8.0, 150 mM NaCl, and 0.03% (w/v) DDM) for 1h at 4°C or for 30 min at 25°C. This reaction was diluted four times using ice-cold blue native buffer. This mix was loaded into a 5-13 % homemade blue native polyacrylamide gradient gel and proteins migrated at 4°C at a maximum of 16 mA per gel to avoid heating of the sample. Proteins were analyzed by Coomassie Brilliant Blue staining or Western blot.

## 6 Protein analyses

### 6.1 SDS-PAGE

Samples were mixed with Laemmli buffer (Bio-Rad) and proteins were separated by SDS-PAGE using NuPAGE® Bis-Tris Mini Gel (Invitrogen®) or home-made gels. When indicated, samples were boiled at 98°C. Migration was performed using 2-(N-morpholino) ethanesulfonic acid (MES) buffer (50 mM MES, 50 mM Tris Base, 0.1% SDS, 1 mM EDTA, pH 7.3) or 3-(N-morpholino)propanesulfonic acid (MOPS) buffer 1X (50 mM MOPS, 50 mM Tris Base; 0.1%

SDS, 1 mM EDTA, pH 7.7) at 200 V for 30-50 min. For semi-native gels, the conditions of migrations were done at 4°C and 120 V for 150 min.

Staining was made using Coomassie Brilliant Blue staining solution (0.2% (w/v) Coomassie BB R-250, 10% (v/v) acetic acid, 25% (v/v) ethanol) for 20-40 , followed by several washes using the destaining solution (10% (v/v) acetic acid, 40% (v/v) ethanol), until enough contrast is obtained. Gels were washed with miliQ water and kept at 4°C.

## 6.2 Blue Native (BN)-PAGE

Protein analysis by BN-PAGE was made by using homemade gels, in polyacrylamide gradient (4-16.5%). Protein samples were mixed with blue native buffer (20 mM Tris-HCl pH 7.4, 50 mM NaCl, 0.1 mM EDTA, 1% (w/v) digitonin, 10% w/v glycerol) and incubated for 15 min on ice. After a clarifying spin, samples were mixed with blue native loading dye (5% Coomassie BB G-250, 100 mM Bis-Tris-HCl, pH 7.0, 500 mM 6-aminocaproic acid) and loaded on the gel. Migration was performed overnight at a maximal intensity of 16 mA per gel.. Staining was done using Coomassie Brilliant Blue Brilliant as previously described.

## 6.3 Western blot

After separation by SDS-PAGE, proteins were transferred to a polyvinylidene fluoride (PVDF) activated membrane (Immobilon®-P) for 150 min at 250 mA using 1X Blot Buffer (20 mM Tris, 150 mM glycine, 0.02% (w/v) SDS, 20% (v/v) ethanol) using a semidry transfer cell. To control the transfer of the proteins onto the membrane, a short staining of the membrane was done using Coomassie Brilliant Blue followed by a complete destaining using 96% ethanol. Then, washes were made using 1X TBS (150 mM NaCl, 50 mM Tris-HCl pH 7.6) and the membrane was saturated using 5% skin milk (Rota®) in TBST (TBS supplemented with 0.5% (v/v) Tween 20) for at least 30 min. After this incubation, primary antibodies diluted 1:500 in 5% skin milk/TBST were incubated with the membrane for 2-3h at room temperature, or overnight at 4°C. After washes of the membrane with TBS, a secondary antibody (dilution 1:5000, 5% skin milk/TBST) was incubated for 45-60 min. Proteins were detected by Clarity Western enhanced chemoluminescence (ECL) blotting substrate (Bio-Rad), using Fijifilm® LAAS 4000 and Image Reader software. The signal intensities of protein bands were quantified using a Multi Gauge (Fujifilm) software.

Western blots were performed using epitope-specific rabbit polyclonal antisera, with the exception of RpoB that was labelled using a mouse monoclonal antibody (NeoClone

Biotechnology). The secondary immunodetection was conducted using anti-rabbit or anti-mouse antibodies conjugated to horseradish peroxidase produced in goat (Sigma).

#### 6.4 Heat-modifiability assay

After resuspension of total cell lysates or crude envelope fractions, samples were normalized according to their OD<sub>600</sub> and equal amounts were mixed with Laemmli buffer. Two aliquots were taken from each sample, one was kept on ice and the other was denatured. For denaturation, samples were incubated at 98°C for 7 min and 1000 rpm of agitation. Then, SDS-PAGE was carried out at 4°C and 110 V for 2.5 h.

### 7 **Mass spectrometry analyses**

All mass spectrometry (MS) analyses were done at the Toulouse Proteomics Infrastructure (<https://www.ipbs.fr/toulouse-proteomics-infrastructure>).

#### 7.1 SILAC NanoLC ESI MS-MS analysis

After proteins were digested with trypsin, peptides were analyzed by nanoLC-MS/MS: Nano-Cap-System NCS-3500RS coupled to a Q-ExactivePlus mass spectrometer (Thermo Fisher Scientific, Bremen, Germany). Five µl (i.e. 5 µg) of each sample were loaded onto a C18 guard column (300 µm ID x 5 mm, Dionex) at 20 µl/min in 5% acetonitrile, 0.05% TFA. After 5 min of desalting, peptides were loaded onto a C18 analytical column (75 µm ID x 50 cm, Repronil) equilibrated in 95% solvent A (5% acetonitrile, 0.2% formic acid) and 5% solvent B (80% acetonitrile, 0.2% formic acid). The peptides are eluted following a 5 to 50% solvent B gradient for 105 min at a flow rate of 300 nl/min (total run of 160 min, gradient of 105 min). The mass spectrometer operates in "data-dependent acquisition mode" with XCalibur (software). The Survey scan MS is done in the Orbitrap with a mass range of 350-1500 m/z and a resolution of 70000. The 10 most intense ions on each survey scan are selected for the HCD fragmentation, the resulting fragments are analyzed in Orbitrap at 17500 resolution. A dynamic exclusion of 30 seconds is used to avoid repetitive selections of the same peptide.

Identification and quantitative analysis were performed with Maxquant software (v 1.5.5.1). Andromeda is used for research in a SwissProt database of *E. coli*; in which were added the sequences of the most frequently observed contaminants as well as the reverse sequences of all the peptides in the library. A maximum of 2 "missed cleavages" are allowed. The carbamidomethylcysteine was defined as a fixed modification while N-acetylation protein and



methionine oxidation were defined as variable modifications. The allowed mass deviation was set at 4.5 ppm for precursor ions and 20 ppm for MS/MS fragments. For validation, the false positive rate (FDR) at peptide and protein level was set at 1%.

## 7.2 MALDI-TOF MS

After protein separation by SDS-PAGE, gels were subjected to Coomassie Brilliant Blue staining. Bands of interest were excised and cut into pieces. Then, these pieces were washed twice with 100  $\mu$ l of 25 mM ammonium bicarbonate, 50% (v/v) acetonitrile for 10 min under agitation. Bands were dried using a Speed Vac and then rehydrated with 10  $\mu$ l of a solution of modified trypsin (Promega) at 10  $\mu$ g/ml in 25 mM ammonium bicarbonate and digested overnight at 37°C. Acetonitrile was then added to the digest to a final concentration of 10% (v/v). Samples were then sonicated for 5 min and 1  $\mu$ l of this solution was spotted on a sample plate of the mass spectrometer, mixed with 1  $\mu$ l of matrix solution (6 mg/ml of  $\alpha$ -cyano-4-hydroxycinnamic acid in 50% (v/v) acetonitrile and 0.1% (v/v) trifluoroacetic acid).

Analysis was performed using a MALDI-TOF/TOF mass spectrometer (Voyager 5800, Applied Biosystems/MDS, Sciex) in positive reflectron mode with the following parameters: accelerating voltage, 20 kV; grid voltage, 68%; extraction delay time, 200 ns; shoot number, 1000. Acquisition range was between 750 and 3000 m/z. Spectra were treated using the Data Explorer software (Applied Biosystems).

## 7.3 Fragmentation of crosslink products by NanoLC-MS/MS

To analyze crosslink products, 70  $\mu$ g of eluted proteins from each sample (+ UV or – UV) were digested with trypsin (Promega) using S-Trap Micro spin columns (Protifi) according to the manufacturer's instruction (HaileMariam et al., 2018). Digested peptide extracts were analyzed by online nanoLC using an UltiMate 3000 RSLCnano LC system (ThermoScientific) coupled with an Orbitrap Fusion Tribrid mass spectrometer (Thermo Scientific) operating in positive mode. Five microliters of each sample (5  $\mu$ g) were loaded onto a 300  $\mu$ m ID  $\times$  5 mm PepMap C18 pre-column (Thermo Scientific) at 20  $\mu$ l/min in 2% (v/v) acetonitrile, 0.05% (v/v) trifluoroacetic acid. After 3 min of desalting, peptides were on-line separated on a 75  $\mu$ m ID  $\times$  50 cm C18 column (in-house packed with Reprosil C18-AQ Pur 3  $\mu$ m resin, Dr. Maisch; Proxeon Biosystems) equilibrated in 90% buffer A (0.2% (v/v) formic acid), with a gradient of 10–30% buffer B (80% (v/v) acetonitrile, 0.2% (v/v) formic acid) for 100 min, then 30–45% for 20 min at 300 nl/min. The instrument was operated in data-dependent acquisition mode using a top-speed approach (cycle time of 3 s). Survey scans MS were acquired in the Orbitrap over

375–1800 m/z with a resolution of 120,000 (at 200 m/z), an automatic gain control (AGC) target of 4e5, and a maximum injection time (IT) of 50 ms. Most intense ions (2+ to 7+) were selected at 1.6 m/z with quadrupole and fragmented by Higher Energy Collisional Dissociation (HCD). The monoisotopic precursor selection was turned on, the intensity threshold for fragmentation was set to 25,000, and the normalized collision energy (NCE) was set to 30%. The resulting fragments were analyzed in the Orbitrap with a resolution of 30,000 (at 200 m/z), an AGC target of 1e5, and a maximum IT of 100 ms. Dynamic exclusion was used within 30 s with a 10 ppm tolerance. The ion at 445.120025 m/z was used as lock mass. The dipeptides were searched manually in Xcalibur using ms2 reporter ions of the modified peptide (m/z 159.11; 187.11; 244.13) and MSMS spectra of the crosslinked peptides were annotated manually using GPMaw (Peri et al., 2001).

## 8 Bioinformatic analysis of DolP/YraP sequences in $\gamma$ -proteobacteria

The dataset was obtained by analysing 266 non-redundant fully sequenced and annotated  $\gamma$ -proteobacteria. Non-redundant means that if the genomes of several strains of the same species were present, only one genome was considered in the analysis. DolP/YraP has been identified in 196 of the 266 genomes, representing about 74% of the  $\gamma$ -proteobacteria. To avoid gaps in this alignment, all positions conserved in at least 90% of these genomes were considered. Then, these sequences were plotted using WebLogo (<http://weblogo.berkeley.edu/logo.cgi>).

## 9 Strains

| Name              | Genotype and relevant features   | Source                  |
|-------------------|--|-------------------------|
| AD202<br>(MC4100) | F-, [araD139]B/r, $\Delta$ (argF-lac)169, ompT1000::kan, $\lambda$ -, flhD5301, $\Delta$ (fruK-yeiR)725(fruA25), relA1, rpsL150(strR), rbsR22, $\Delta$ (fimB-fimE)632(::IS1), deoC1 | (Akiyama and Ito, 1990) |
| BW25113           | $\Delta$ (araD-araB)567 $\Delta$ (rhaD-rhaB)568 lacZ4787(::rrnB-3) hsdR514 rph-1 (wild-type reference)   | (Grenier et al., 2014)  |
| Stellar           | F-, endA1, supE44, thi-1, recA1, relA1, gyrA96, phoA, _80d lacZ_M15, $\Delta$ (lacZYA - argF) U169, $\Delta$ (mrr - hsdRMS - mcrBC), $\Delta$ mcrA, $\lambda$ -                      | Clontech®               |

|   |   |                                |
|---|---|--------------------------------|
| $\Delta dolP$                                 | BW25113 $\Delta dolP$                                     | (Ranava et al., 2021)          |
| $\Delta tamB$                                 | BW25113 <i>tamB::kan</i>                                  | (Grenier et al., 2014)         |
| $\Delta degP$                                 | BW25113 <i>degP::kan</i>                                  | (Ranava et al., 2021)          |
| $\Delta ompA$                                 | BW25113 <i>ompA::kan</i>                                  | (Ranava et al., 2021)          |
| $\Delta waaD$                                 | BW25113 <i>waaD::kan</i>                                  | (Grenier et al., 2014)         |
| MC4100<br><i>rprA::lacZ</i>                   | MC4100 <i>ara<sup>+</sup> rprA142p::lacZ</i>              | (Castanié-Cornet et al., 2006) |
| MC4100<br><i>rprA::lacZ</i> $\Delta dolP$     | MC4100 <i>ara<sup>+</sup> rprA142p::lacZ dolP::kan</i>    | This study                     |
| MC4100<br><i>rprA::lacZ</i><br><i>bamA101</i> | MC4100 <i>ara<sup>+</sup> rprA142p::lacZ bamA101::kan</i> | This study                     |
| MC4100<br><i>rprA::lacZ</i> $\Delta surA$     | MC4100 <i>ara<sup>+</sup> rprA142p::lacZ surA::kan</i>    | This study                     |
| MC4100<br><i>rprA::lacZ</i> $\Delta skp$      | MC4100 <i>ara<sup>+</sup> rprA142p::lacZ skp::kan</i>     | This study                     |
| MC4100<br><i>rprA::lacZ</i><br>$\Delta bamE$  | MC4100 <i>ara<sup>+</sup> rprA142p::lacZ bamE::kan</i>    | This study                     |

## 10 Plasmids

| Name                            | Relevant features   | Source                         |
|---------------------------------|---|--------------------------------|
| pCtrl                           | Reference empty vector for ectopic protein expression   | (Ranava et al., 2021)          |
| pBAM                            | Ectopic expression of all 5 BAM subunits  | (Ranava et al., 2021)          |
| pBAM <sup>His</sup><br>(pJH114) | Ectopic expression of all 5 BAM subunits; BamE is C-terminally His-tagged                           | (Roman-Hernandez et al., 2014) |
| pBAM <sup>ProtA</sup>           | Ectopic expression of all 5 BAM subunits; BamE is C-terminally Protein A and His-tagged; a TEV site | (Ranava et al., 2021)          |

|   |  |                       |
|---|--|-----------------------|
|   | amino acid linker is positioned immediately upstream of the tag  |                       |
| pBAM <sup>ΔP1/ProtA</sup>                 | Ectopic expression of all 5 BAM subunits; BamA harbours the deletion of POTRA1 and BamE is C-terminally Protein A-tagged; a TEV site amino acid linker is positioned immediately upstream of the tag | (Ranava et al., 2021) |
| pBAM <sup>ΔP2/ProtA</sup>                 | Ectopic expression of all 5 BAM subunits; BamA harbours the deletion of POTRA2 and BamE is C-terminally Protein A-tagged; a TEV site amino acid linker is positioned immediately upstream of the tag | (Ranava et al., 2021) |
| pBamA                                     | Ectopic expression of wild-type BamA   | (Ranava et al., 2021) |
| pBamA-DolP <sup>His</sup>                 | Ectopic expression of BamA and C-terminally His-tagged DolP.   | (Ranava et al., 2021) |
| pBamA-pDolP <sup>AMB/His</sup>            | Ectopic expression of BamA and C-terminally His-tagged DolP. The sequence of the <i>dolP</i> open reading frame was mutated to introduce an amber codon in place of the residue indicated.           | (Ranava et al., 2021) |
| pBamA <sup>ΔP1</sup> -DolP <sup>His</sup> | Ectopic expression of a BamA variant lacking POTRA1 and C-terminally His-tagged DolP   | (Ranava et al., 2021) |
| pBamA <sup>ΔP2</sup> -DolP <sup>His</sup> | Ectopic expression of a BamA variant lacking POTRA2 and C-terminally His-tagged DolP   | (Ranava et al., 2021) |
| pDolP                                     | Ectopic expression of wild-type DolP (no tag)  | (Ranava et al., 2021) |
| pDolP <sup>ProtA</sup>                    | Ectopic expression of C-terminally protein A-tagged DolP, a TEV site amino acid linker is positioned immediately upstream of the tag.  | (Ranava et al., 2021) |
| pDolP <sup>His</sup>                      | Ectopic expression of C-terminally His-tagged DolP.  | (Ranava et al., 2021) |
| pDolP <sup>AMB/His</sup>                  | Ectopic expression of C-terminally His-tagged DolP. The sequence of the <i>dolP</i> open reading frame was mutated to introduce an amber codon in place of the residue indicated                     | This study            |

|                                  |   |                       |
|----------------------------------|---|-----------------------|
| pDoIP <sup>His</sup> -BamA       | Ectopic expression of C-terminally His-tagged DoIP and BamA. Compared to pBamA-DoIP <sup>His</sup> , this plasmid allows a more efficient overproduction of DoIP.     | (Ranava et al., 2021) |
| pDoIP <sup>ΔBON1/His</sup> -BamA | Ectopic expression of C-terminally His-tagged DoIP and BamA. The sequence of the <i>doIP</i> open reading frame was mutated to introduce deletion of BON 1            | This study            |
| pDoIP <sup>ΔBON2/His</sup> -BamA | Ectopic expression of C-terminally His-tagged DoIP and BamA. The sequence of the <i>doIP</i> open reading frame was mutated to introduce deletion of BON 1            | This study            |
| pOmpA <sup>His</sup>             | Ectopic expression of C-terminally His-tagged OmpA  | (Ranava et al., 2021) |
| pEVOL-pBpF                       | Expression of tRNA synthetase and tRNA for the <i>in vivo</i> incorporation of Bpa at protein positions encoded by an amber codon                                     | (Chin et al., 2002)   |
| pYM10                            | TEV site and the tandem Protein-A tagging construct   | (Knop et al., 1999)   |
| pDoIP <sup>GFP/His</sup>         | Ectopic expression of C-terminally GFP and His-tagged DoIP. The sequence of the <i>doIP</i> open reading frame was mutated to introduce mutation to Ala, as indicated | This study            |
| pDoIP <sup>ΔBON1/GFP/His</sup>   | Ectopic expression of C-terminally GFP and His-tagged DoIP and BamA. The sequence of the <i>doIP</i> open reading frame was mutated to delete BON 1                   | This study            |
| pDoIP <sup>ΔBON2GFP/His</sup>    | Ectopic expression of C-terminally GFP and His-tagged DoIP and BamA. The sequence of the <i>doIP</i> open reading frame was mutated to delete BON 2                   | This study            |
| pDoIP <sup>His*</sup>            | Ectopic expression of C-terminally His-tagged DoIP. This plasmid allows a more efficient overproduction of DoIP compared to pDoIP <sup>His</sup> .                    | This study            |
| pDoIP <sup>ΔBON1/His*</sup>      | Ectopic expression of C-terminally His-tagged DoIP. The sequence of the <i>doIP</i> open reading frame was mutated to delete BON 1                                    | This study            |

|                             |  |                           |
|-----------------------------|--|---------------------------|
| pDoIP <sup>ΔBON2/His*</sup> | Ectopic expression of C-terminally His-tagged DoIP. The sequence of the <i>doIP</i> open reading frame was mutated to delete BON 2 | This study                |
| pKOBEG                      | This plasmid encodes for the lambda red machinery to perform recombination   | (Chaveroche et al., 2000) |

## Bibliography

- Aaron, M., Charbon, G., Lam, H., Schwarz, H., Vollmer, W., Jacobs-Wagner, C., 2007. The tubulin homologue FtsZ contributes to cell elongation by guiding cell wall precursor synthesis in *Caulobacter crescentus*. *Mol. Microbiol.* 64, 938–952. <https://doi.org/10.1111/j.1365-2958.2007.05720.x>
- Aarsman, M.E.G., Piette, A., Fraipont, C., Vinkenvleugel, T.M.F., Nguyen-Distèche, M., Blaauwen, T. den, 2005. Maturation of the *Escherichia coli* divisome occurs in two steps. *Mol. Microbiol.* 55, 1631–1645. <https://doi.org/10.1111/j.1365-2958.2005.04502.x>
- Addinall, S.G., Cao, C., Lutkenhaus, J., 1997. FtsN, a late recruit to the septum in *Escherichia coli*. *Mol. Microbiol.* 25, 303–309. <https://doi.org/10.1046/j.1365-2958.1997.4641833.x>
- Akimaru, J., Matsuyama, S., Tokuda, H., Mizushima, S., 1991. Reconstitution of a protein translocation system containing purified SecY, SecE, and SecA from *Escherichia coli*. *Proc. Natl. Acad. Sci.* 88, 6545–6549. <https://doi.org/10.1073/pnas.88.15.6545>
- Akiyama, K., Mizuno, S., Hizukuri, Y., Mori, H., Nogi, T., Akiyama, Y., 2015. Roles of the membrane-reentrant  $\beta$ -hairpin-like loop of RseP protease in selective substrate cleavage. *eLife* 4, e08928. <https://doi.org/10.7554/eLife.08928>
- Akiyama, Y., Ito, K., 1990. SecY protein, a membrane-embedded secretion factor of *E. coli*, is cleaved by the ompT protease in vitro. *Biochem. Biophys. Res. Commun.* 167, 711–715. [https://doi.org/10.1016/0006-291X\(90\)92083-C](https://doi.org/10.1016/0006-291X(90)92083-C)
- Akopian, D., Shen, K., Zhang, X., Shan, S., 2013. Signal Recognition Particle: An essential protein targeting machine. *Annu. Rev. Biochem.* 82, 693–721. <https://doi.org/10.1146/annurev-biochem-072711-164732>
- Albenne, C., Ieva, R., 2017. Job contenders: roles of the  $\beta$ -barrel assembly machinery and the translocation and assembly module in autotransporter secretion. *Mol. Microbiol.* <https://doi.org/10.1111/mmi.13832>
- Alvira, S., Watkins, D.W., Troman, L., Allen, W.J., Lorrimer, J.S., Degliesposti, G., Cohen, E.J., Beeby, M., Daum, B., Gold, V.A., Skehel, J.M., Collinson, I., 2020. Inter-membrane association of the Sec and BAM translocons for bacterial outer-membrane biogenesis. *eLife* 9, e60669. <https://doi.org/10.7554/eLife.60669>
- Aly, K.A., Baron, C., 2007. The VirB5 protein localizes to the T-pilus tips in *Agrobacterium tumefaciens*. *Microbiology* 153, 3766–3775. <https://doi.org/10.1099/mic.0.2007/010462-0>
- Aoki, S.K., Malinverni, J.C., Jacoby, K., Thomas, B., Pamma, R., Trinh, B.N., Remers, S., Webb, J., Braaten, B.A., Silhavy, T.J., Low, D.A., 2008. Contact-dependent growth inhibition requires the essential outer membrane protein BamA (YaeT) as the receptor and the inner membrane transport protein AcrB. *Mol. Microbiol.* 70, 323–340. <https://doi.org/10.1111/j.1365-2958.2008.06404.x>
- Ashraf, K.U., Josts, I., Mosbahi, K., Kelly, S.M., Byron, O., Smith, B.O., Walker, D., 2016. The Potassium Binding Protein Kbp Is a Cytoplasmic Potassium Sensor. *Structure* 24, 741–749. <https://doi.org/10.1016/j.str.2016.03.017>
- Asmar, A.T., Ferreira, J.L., Cohen, E.J., Cho, S.-H., Beeby, M., Hughes, K.T., Collet, J.-F., 2017. Communication across the bacterial cell envelope depends on the size of the periplasm. *PLOS Biol.* 15, e2004303. <https://doi.org/10.1371/journal.pbio.2004303>
- Auclair, S.M., Bhanu, M.K., Kendall, D.A., 2012. Signal peptidase I: Cleaving the way to mature proteins. *Protein Sci. Publ. Protein Sci.* 21, 13–25. <https://doi.org/10.1002/pro.757>
- Baba, T., Ara, T., Hasegawa, M., Takai, Y., Okumura, Y., Baba, M., Datsenko, K.A., Tomita, M., Wanner, B.L., Mori, H., 2006. Construction of *Escherichia coli* K-12 in-frame, single-gene knockout mutants: the Keio collection. *Mol. Syst. Biol.* 2, 2006.0008. <https://doi.org/10.1038/msb4100050>
- Babu, M., Bundalovic-Torma, C., Calmettes, C., Phanse, S., Zhang, Q., Jiang, Y., Minic, Z., Kim, S., Mehla, J., Gagarianova, A., Rodionova, I., Kumar, A., Guo, H., Kagan, O., Pogoutse, O., Aoki, H., Deineko, V., Caufield, J.H., Holtzapfel, E., Zhang, Z., Vastermark, A., Pandya, Y., Lai, C.C.-L., El Bakkouri, M., Hooda, Y., Shah, M., Burnside, D., Hooshyar, M., Vlasblom, J., Rajagopala, S.V., Golshani, A., Wuchty, S., F Greenblatt, J., Saier, M., Uetz, P., F Moraes, T., Parkinson, J., Emili, A., 2017. Global landscape of cell envelope protein complexes in *Escherichia coli*. *Nat. Biotechnol.* <https://doi.org/10.1038/nbt.4024>
- Bakelar, J., Buchanan, S.K., Noinaj, N., 2016. The structure of the  $\beta$ -barrel assembly machinery complex. *Science* 351, 180–186. <https://doi.org/10.1126/science.aad3460>
- Bamert, R.S., Lundquist, K., Hwang, H., Webb, C.T., Shiota, T., Stubenrauch, C.J., Belousoff, M.J., Goode, R.J.A., Schittenhelm, R.B., Zimmerman, R., Jung, M., Gumbart, J.C., Lithgow, T., 2017. Structural basis for substrate selection by the translocation and assembly module of the  $\beta$ -barrel assembly machinery. *Mol. Microbiol.* 106, 142–156. <https://doi.org/10.1111/mmi.13757>
- Barreteau, H., Kovač, A., Boniface, A., Sova, M., Gobec, S., Blanot, D., 2008. Cytoplasmic steps of peptidoglycan biosynthesis. *FEMS Microbiol. Rev.* 32, 168–207. <https://doi.org/10.1111/j.1574-6976.2008.00104.x>
- Beena, K., Udgaonkar, J.B., Varadarajan, R., 2004. Effect of Signal Peptide on the Stability and Folding Kinetics of Maltose Binding Protein. *Biochemistry* 43, 3608–3619. <https://doi.org/10.1021/bi0360509>
- Bendall, S.C., Hughes, C., Stewart, M.H., Doble, B., Bhatia, M., Lajoie, G.A., 2008. Prevention of Amino Acid Conversion in SILAC Experiments with Embryonic Stem Cells. *Mol. Cell. Proteomics* 7, 1587–1597. <https://doi.org/10.1074/mcp.M800113-MCP200>
- Bennion, D., Charlson, E.S., Coon, E., Misra, R., 2010. Dissection of  $\beta$ -barrel Outer Membrane Protein Assembly Pathways through Characterizing BamA POTRA 1 Mutants of *Escherichia coli*. *Mol. Microbiol.* 77, 1153–1171. <https://doi.org/10.1111/j.1365-2958.2010.07280.x>
- Berg, B. van den, Clemons, W.M., Collinson, I., Modis, Y., Hartmann, E., Harrison, S.C., Rapoport, T.A., 2004. X-ray structure of a protein-conducting channel. *Nature* 427, 36–44. <https://doi.org/10.1038/nature02218>
- Bitto, E., McKay, D.B., 2002. Crystallographic Structure of SurA, a Molecular Chaperone that Facilitates Folding of Outer Membrane Porins. *Structure* 10, 1489–1498. [https://doi.org/10.1016/S0969-2126\(02\)00877-8](https://doi.org/10.1016/S0969-2126(02)00877-8)
- Blobel, G., Dobberstein, B., 1975. Transfer of proteins across membranes. I. Presence of proteolytically processed and unprocessed nascent immunoglobulin light chains on membrane-bound ribosomes of murine myeloma. *J. Cell Biol.* 67, 835–851. <https://doi.org/10.1083/jcb.67.3.835>
- Bolhuis, A., Mathers, J.E., Thomas, J.D., Barrett, C.M.L., Robinson, C., 2001. TatB and TatC Form a Functional and Structural Unit of the Twin-arginine Translocase from *Escherichia coli* \*. *J. Biol. Chem.* 276, 20213–20219. <https://doi.org/10.1074/jbc.M100682200>
- Bönemann, G., Pietrosiuk, A., Diemand, A., Zentgraf, H., Mogk, A., 2009. Remodelling of VipA/VipB tubules by ClpV-mediated threading is crucial for type VI protein secretion. *EMBO J.* 28, 315–325. <https://doi.org/10.1038/emboj.2008.269>

- Bos, M.P., Grijpstra, J., Boxtel, R.T., Tommassen, J., 2014. Involvement of Neisseria meningitidis Lipoprotein GNA2091 in the Assembly of a Subset of Outer Membrane Proteins. *J. Biol. Chem.* 289, 15602–15610. <https://doi.org/10.1074/jbc.M113.539510>
- Bos, M.P., Robert, V., Tommassen, J., 2007. Functioning of outer membrane protein assembly factor Omp85 requires a single POTRA domain. *EMBO Rep.* 8, 1149–1154. <https://doi.org/10.1038/sj.embor.7401092>
- Bos, M.P., Tefsen, B., Geurtsen, J., Tommassen, J., 2004. Identification of an outer membrane protein required for the transport of lipopolysaccharide to the bacterial cell surface. *Proc. Natl. Acad. Sci.* 101, 9417–9422. <https://doi.org/10.1073/pnas.0402340101>
- Botte, M., Ni, D., Schenck, S., Zimmermann, I., Chami, M., Bocquet, N., Egloff, P., Bucher, D., Trabuco, M., Cheng, R.K.Y., Brunner, J.D., Seeger, M.A., Stahlberg, H., Hennig, M., 2022. Cryo-EM structures of a LptDE transporter in complex with Pro-macrobodies offer insight into lipopolysaccharide translocation. *Nat. Commun.* 13, 1826. <https://doi.org/10.1038/s41467-022-29459-2>
- Botte, M., Zaccai, N.R., Nijeholt, J.L. à, Martin, R., Knoops, K., Papai, G., Zou, J., Deniaud, A., Karupphasamy, M., Jiang, Q., Roy, A.S., Schulten, K., Schultz, P., Rappsilber, J., Zaccai, G., Berger, I., Collinson, I., Schaffitzel, C., 2016. A central cavity within the holo-translocon suggests a mechanism for membrane protein insertion. *Sci. Rep.* 6, 38399. <https://doi.org/10.1038/srep38399>
- Broncano-Lavado, A., Santamaría-Corral, G., Esteban, J., García-Quintanilla, M., 2021. Advances in Bacteriophage Therapy against Relevant MultiDrug-Resistant Pathogens. *Antibiotics* 10, 672. <https://doi.org/10.3390/antibiotics10060672>
- Bryant, J.A., Morris, F.C., Knowles, T.J., Maderbocus, R., Heinz, E., Boelter, G., Alodaini, D., Colyer, A., Wotherspoon, P.J., Staunton, K.A., Jeeves, M., Browning, D.F., Sevastyanovich, Y.R., Wells, T.J., Rossiter, A.E., Bavro, V.N., Sridhar, P., Ward, D.G., Chong, Z.-S., Goodall, E.C.A., Icke, C., Teo, A., Chng, S.-S., Roper, D.I., Lithgow, T., Cunningham, A.F., Banzhaf, M., Overduin, M., Henderson, I.R., 2020. Structure of dual-BON domain protein DolP identifies phospholipid binding as a new mechanism for protein localization. *eLife* 9, e62614. <https://doi.org/10.7554/eLife.62614>
- Buelow, D.R., Raivio, T.L., 2005. Cpx Signal Transduction Is Influenced by a Conserved N-Terminal Domain in the Novel Inhibitor CpxP and the Periplasmic Protease DegP. *J. Bacteriol.* 187, 6622–6630. <https://doi.org/10.1128/JB.187.19.6622-6630.2005>
- Cabelli, R.J., Dolan, K.M., Qian, L.P., Oliver, D.B., 1991. Characterization of membrane-associated and soluble states of SecA protein from wild-type and SecA51(TS) mutant strains of *Escherichia coli*. *J. Biol. Chem.* 266, 24420–24427.
- Calabrese, A.N., Schiffrin, B., Watson, M., Karamanos, T.K., Walko, M., Humes, J.R., Horne, J.E., White, P., Wilson, A.J., Kalli, A.C., Tuma, R., Ashcroft, A.E., Brockwell, D.J., Radford, S.E., 2020. Inter-domain dynamics in the chaperone SurA and multi-site binding to its outer membrane protein clients. *Nat. Commun.* 11, 2155. <https://doi.org/10.1038/s41467-020-15702-1>
- Carlson, M.L., Stacey, R.G., Young, J.W., Wason, I.S., Zhao, Z., Rattray, D.G., Scott, N., Kerr, C.H., Babu, M., Foster, L.J., Duong Van Hoa, F., 2019. Profiling the *Escherichia coli* membrane protein interactome captured in Peptidisc libraries. *eLife* 8, e46615. <https://doi.org/10.7554/eLife.46615>
- Castanié-Cornet, M.-P., Bruel, N., Genevoux, P., 2014. Chaperone networking facilitates protein targeting to the bacterial cytoplasmic membrane. *Biochim. Biophys. Acta BBA - Mol. Cell Res., Protein trafficking and secretion in bacteria* 1843, 1442–1456. <https://doi.org/10.1016/j.bbamcr.2013.11.007>
- Castanié-Cornet, M.-P., Cam, K., Jacq, A., 2006. RcsF Is an Outer Membrane Lipoprotein Involved in the RcsCDB Phosphorelay Signaling Pathway in *Escherichia coli*. *J. Bacteriol.* 188, 4264–4270. <https://doi.org/10.1128/JB.00004-06>
- Charlson, E.S., Werner, J.N., Misra, R., 2006. Differential Effects of yfgL Mutation on *Escherichia coli* Outer Membrane Proteins and Lipopolysaccharide. *J. Bacteriol.* 188, 7186–7194. <https://doi.org/10.1128/JB.00571-06>
- Chaveroche, M.-K., Ghigo, J.-M., d'Enfert, C., 2000. A rapid method for efficient gene replacement in the filamentous fungus *Aspergillus nidulans*. *Nucleic Acids Res.* 28, e97.
- Chen, X., Wei, S., Ji, Y., Guo, X., Yang, F., 2015. Quantitative proteomics using SILAC: Principles, applications, and developments. *PROTEOMICS* 15, 3175–3192. <https://doi.org/10.1002/pmic.201500108>
- Cherepanov, P.P., Wackernagel, W., 1995. Gene disruption in *Escherichia coli*: TcR and KmR cassettes with the option of Flp-catalyzed excision of the antibiotic-resistance determinant. *Gene* 158, 9–14. [https://doi.org/10.1016/0378-1119\(95\)00193-a](https://doi.org/10.1016/0378-1119(95)00193-a)
- Chin, J.W., Martin, A.B., King, D.S., Wang, L., Schultz, P.G., 2002. Addition of a photocrosslinking amino acid to the genetic code of *Escherichia coli*. *Proc. Natl. Acad. Sci.* 99, 11020–11024. <https://doi.org/10.1073/pnas.172226299>
- Chng, S.-S., Xue, M., Garner, R.A., Kadokura, H., Boyd, D., Beckwith, J., Kahne, D., 2012. Disulfide Rearrangement Triggered by Translocon Assembly Controls Lipopolysaccharide Export. *Science* 337, 1665–1668. <https://doi.org/10.1126/science.1227215>
- Cho, S.-H., Szewczyk, J., Pesavento, C., Zietek, M., Banzhaf, M., Roszczenko, P., Asmar, A., Laloux, G., Hov, A.-K., Leverrier, P., Van der Henst, C., Vertommen, D., Typas, A., Collet, J.-F., 2014. Detecting Envelope Stress by Monitoring  $\beta$ -Barrel Assembly. *Cell* 159, 1652–1664. <https://doi.org/10.1016/j.cell.2014.11.045>
- Cian, M.B., Giordano, N.P., Mettlach, J.A., Minor, K.E., Dalebroux, Z.D., 2020. Separation of the Cell Envelope for Gram-negative Bacteria into Inner and Outer Membrane Fractions with Technical Adjustments for *Acinetobacter baumannii*. *JoVE J. Vis. Exp.* e60517. <https://doi.org/10.3791/60517>
- Clavel, T., Germon, P., Vianney, A., Portalier, R., Lazzaroni, J.C., 1998. TolB protein of *Escherichia coli* K-12 interacts with the outer membrane peptidoglycan-associated proteins Pal, Lpp and OmpA. *Mol. Microbiol.* 29, 359–367. <https://doi.org/10.1046/j.1365-2958.1998.00945.x>
- Cole, G.B., Bateman, T.J., Moraes, T.F., 2021. The surface lipoproteins of gram-negative bacteria: Protectors and foragers in harsh environments. *J. Biol. Chem.* 296, 100147. <https://doi.org/10.1074/jbc.REV120.008745>
- Coleman, W.G., 1983. The rfaD gene codes for ADP-L-glycero-D-mannoheptose-6-epimerase. An enzyme required for lipopolysaccharide core biosynthesis. *J. Biol. Chem.* 258, 1985–1990. [https://doi.org/10.1016/S0021-9258\(18\)33085-0](https://doi.org/10.1016/S0021-9258(18)33085-0)
- Collinson, I., 2019. The Dynamic ATP-Driven Mechanism of Bacterial Protein Translocation and the Critical Role of Phospholipids. *Front. Microbiol.* 10. <https://doi.org/10.3389/fmicb.2019.01217>
- Combs, A.N., Silhavy, T.J., 2022. The sacrificial adaptor protein Skp functions to remove stalled substrates from the  $\beta$ -barrel assembly machine. *Proc. Natl. Acad. Sci.* 119, e2114997119. <https://doi.org/10.1073/pnas.2114997119>
- Consoli, E., Collet, J.-F., den Blaauwen, T., 2021a. The *Escherichia coli* Outer Membrane  $\beta$ -Barrel Assembly Machinery (BAM) Anchors the Peptidoglycan Layer by Spanning It with All Subunits. *Int. J. Mol. Sci.* 22, 1853. <https://doi.org/10.3390/ijms22041853>
- Consoli, E., Luirink, J., den Blaauwen, T., 2021b. The *Escherichia coli* Outer Membrane  $\beta$ -Barrel Assembly Machinery (BAM) Crosstalks with the Divisome. *Int. J. Mol. Sci.* 22, 12101. <https://doi.org/10.3390/ijms222212101>



- Cook, J., Baverstock, T.C., McAndrew, M.B.L., Stansfeld, P.J., Roper, D.I., Crow, A., 2020. Insights into bacterial cell division from a structure of EnvC bound to the FtsX periplasmic domain. *Proc. Natl. Acad. Sci.* 117, 28355–28365. <https://doi.org/10.1073/pnas.2017134117>
- Coornaert, A., Lu, A., Mandin, P., Springer, M., Gottesman, S., Guillier, M., 2010. MicA sRNA links the PhoP regulon to cell envelope stress. *Mol. Microbiol.* 76, 467–479. <https://doi.org/10.1111/j.1365-2958.2010.07115.x>
- Coppens, F., Castaldo, G., Debraekeleer, A., Subedi, S., Moonens, K., Lo, A., Remaut, H., 2018. Hop-family Helicobacter outer membrane adhesins form a novel class of Type 5-like secretion proteins with an interrupted  $\beta$ -barrel domain. *Mol. Microbiol.* 110, 33–46. <https://doi.org/10.1111/mmi.14075>
- Corpet, F., 1988. Multiple sequence alignment with hierarchical clustering. *Nucleic Acids Res.* 16, 10881–10890. <https://doi.org/10.1093/nar/16.22.10881>
- Costa, T.R.D., Felisberto-Rodrigues, C., Meir, A., Prevost, M.S., Redzej, A., Trokter, M., Waksman, G., 2015. Secretion systems in Gram-negative bacteria: structural and mechanistic insights. *Nat. Rev. Microbiol.* 13, 343–359. <https://doi.org/10.1038/nrmicro3456>
- Cowles, C.E., Li, Y., Semmelhack, M.F., Cristea, I.M., Silhavy, T.J., 2011. The free and bound forms of Lpp occupy distinct subcellular locations in *Escherichia coli*. *Mol. Microbiol.* 79, 1168–1181. <https://doi.org/10.1111/j.1365-2958.2011.07539.x>
- Crane, J.M., Randall, L.L., 2017. The Sec System: Protein Export in *Escherichia coli*. *EcoSal Plus* 7. <https://doi.org/10.1128/ecosalplus.ESP-0002-2017>
- da Mata Madeira, P.V., Zouhir, S., Basso, P., Neves, D., Laubier, A., Salacha, R., Bleves, S., Faudry, E., Contreras-Martel, C., Dessen, A., 2016. Structural Basis of Lipid Targeting and Destruction by the Type V Secretion System of *Pseudomonas aeruginosa*. *J. Mol. Biol., Molecular Mechanisms of Autophagy, Part A* 428, 1790–1803. <https://doi.org/10.1016/j.jmb.2016.03.012>
- Dadgostar, P., 2019. <p>Antimicrobial Resistance: Implications and Costs</p>. *Infect. Drug Resist.* 12, 3903–3910. <https://doi.org/10.2147/IDR.S234610>
- Danoff, E.J., Fleming, K.G., 2015. Membrane Defects Accelerate Outer Membrane  $\beta$ -Barrel Protein Folding. *Biochemistry* 54, 97–99. <https://doi.org/10.1021/bi501443p>
- Dartigalongue, C., Missiakas, D., Raina, S., 2001. Characterization of the *Escherichia coli* sigma E regulon. *J. Biol. Chem.* 276, 20866–20875. <https://doi.org/10.1074/jbc.M100464200>
- Dartigalongue, C., Raina, S., 1998. A new heat-shock gene, ppiD, encodes a peptidyl-prolyl isomerase required for folding of outer membrane proteins in *Escherichia coli*. *EMBO J.* 17, 3968–3980. <https://doi.org/10.1093/emboj/17.14.3968>
- Delhay, A., Collet, J.-F., Laloux, G., 2019a. A Fly on the Wall: How Stress Response Systems Can Sense and Respond to Damage to Peptidoglycan. *Front. Cell. Infect. Microbiol.* 9.
- Delhay, A., Laloux, G., Collet, J.-F., 2019b. The Lipoprotein NlpE Is a Cpx Sensor That Serves as a Sentinel for Protein Sorting and Folding Defects in the *Escherichia coli* Envelope. *J. Bacteriol.* 201, e00611-18. <https://doi.org/10.1128/JB.00611-18>
- Den Blaauwen, T., Aarsman, M.E.G., Vischer, N.O.E., Nanninga, N., 2003. Penicillin-binding protein PBP2 of *Escherichia coli* localizes preferentially in the lateral wall and at mid-cell in comparison with the old cell pole. *Mol. Microbiol.* 47, 539–547. <https://doi.org/10.1046/j.1365-2958.2003.03316.x>
- Derouaux, A., Wolf, B., Fraipont, C., Breukink, E., Nguyen-Distèche, M., Terrak, M., 2008. The Monofunctional Glycosyltransferase of *Escherichia coli* Localizes to the Cell Division Site and Interacts with Penicillin-Binding Protein 3, FtsW, and FtsN. *J. Bacteriol.* 190, 1831–1834. <https://doi.org/10.1128/JB.01377-07>
- Dong, C., Yang, X., Hou, H.-F., Shen, Y.-Q., Dong, Y.-H., 2012. Structure of *Escherichia coli* BamB and its interaction with POTRA domains of BamA. *Acta Crystallogr. D Biol. Crystallogr.* 68, 1134–1139. <https://doi.org/10.1107/S0907444912023141>
- Douglass, M.V., McLean, A.B., Trent, M.S., 2022. Absence of YhdP, TamB, and YdbH leads to defects in glycerophospholipid transport and cell morphology in Gram-negative bacteria. *PLOS Genet.* 18, e1010096. <https://doi.org/10.1371/journal.pgen.1010096>
- Doyle, M.T., Bernstein, H.D., 2019. Bacterial outer membrane proteins assemble via asymmetric interactions with the BamA  $\beta$ -barrel. *Nat. Commun.* 10, 3358. <https://doi.org/10.1038/s41467-019-11230-9>
- Doyle, M.T., Jimah, J.R., Dowdy, T., Ohlemacher, S.I., Larion, M., Hinshaw, J.E., Bernstein, H.D., 2022. Cryo-EM structures reveal multiple stages of bacterial outer membrane protein folding. *Cell* 185, 1143–1156.e13. <https://doi.org/10.1016/j.cell.2022.02.016>
- Du, D., Wang, Z., James, N.R., Voss, J.E., Klimont, E., Ohene-Agyei, T., Venter, H., Chiu, W., Luisi, B.F., 2014. Structure of the AcrAB–TolC multidrug efflux pump. *Nature* 509, 512–515. <https://doi.org/10.1038/nature13205>
- Duong, F., 2014. Capturing the bacterial holo-complex. *Proc. Natl. Acad. Sci. U. S. A.* 111, 4739–4740. <https://doi.org/10.1073/pnas.1402139111>
- Duong, F., Eichler, J., Price, A., Leonard, M.R., Wickner, W., 1997. Biogenesis of the Gram-Negative Bacterial Envelope. *Cell* 91, 567–573. [https://doi.org/10.1016/S0092-8674\(00\)80444-4](https://doi.org/10.1016/S0092-8674(00)80444-4)
- Egan, A.J.F., Vollmer, W., 2013. The physiology of bacterial cell division. *Ann. N. Y. Acad. Sci.* 1277, 8–28. <https://doi.org/10.1111/j.1749-6632.2012.06818.x>
- Egea, P.F., Stroud, R.M., 2010. Lateral opening of a translocon upon entry of protein suggests the mechanism of insertion into membranes. *Proc. Natl. Acad. Sci.* 107, 17182–17187. <https://doi.org/10.1073/pnas.1012556107>
- Ekiert, D.C., Bhabha, G., Isom, G.L., Greenan, G., Ovchinnikov, S., Henderson, I.R., Cox, J.S., Vale, R.D., 2017. Architectures of Lipid Transport Systems for the Bacterial Outer Membrane. *Cell* 169, 273–285.e17. <https://doi.org/10.1016/j.cell.2017.03.019>
- El Rayes, J., Szweczyk, J., Deghelt, M., Csoma, N., Matagne, A., Iorga, B.I., Cho, S.-H., Collet, J.-F., 2021. Disorder is a critical component of lipoprotein sorting in Gram-negative bacteria. *Nat. Chem. Biol.* 17, 1093–1100. <https://doi.org/10.1038/s41589-021-00845-z>
- Evans, K.L., Kannan, S., Li, G., de Pedro, M.A., Young, K.D., 2013. Eliminating a Set of Four Penicillin Binding Proteins Triggers the Rcs Phosphorelay and Cpx Stress Responses in *Escherichia coli*. *J. Bacteriol.* 195, 4415–4424. <https://doi.org/10.1128/JB.00596-13>
- Fang, J., Wei, Y., 2011. Expression, Purification and Characterization of the *Escherichia coli* Integral Membrane Protein YajC. *Protein Pept. Lett.* 18, 601–608.
- Filloux, A., 2022. Bacterial protein secretion systems: Game of types. *Microbiology* 168, 001193. <https://doi.org/10.1099/mic.0.001193>
- Fleming, K.G., 2015. A combined kinetic push and thermodynamic pull as driving forces for outer membrane protein sorting and folding in bacteria. *Philos. Trans. R. Soc. B Biol. Sci.* 370. <https://doi.org/10.1098/rstb.2015.0026>

- Fürst, M., Zhou, Y., Merfort, J., Müller, M., 2018. Involvement of PpiD in Sec-dependent protein translocation. *Biochim. Biophys. Acta BBA - Mol. Cell Res.* 1865, 273–280. <https://doi.org/10.1016/j.bbamcr.2017.10.012>
- Fürste, J.P., Pansegrau, W., Frank, R., Blöcker, H., Scholz, P., Bagdasarian, M., Lanka, E., 1986. Molecular cloning of the plasmid RP4 primase region in a multi-host-range tacP expression vector. *Gene* 48, 119–131. [https://doi.org/10.1016/0378-1119\(86\)90358-6](https://doi.org/10.1016/0378-1119(86)90358-6)
- Gallique, M., Bouteiller, M., Merieau, A., 2017. The Type VI Secretion System: A Dynamic System for Bacterial Communication? *Front. Microbiol.* 8.
- Gerding, M.A., Ogata, Y., Pecora, N.D., Niki, H., De Boer, P.A.J., 2007. The trans-envelope Tol–Pal complex is part of the cell division machinery and required for proper outer-membrane invagination during cell constriction in *E. coli*. *Mol. Microbiol.* 63, 1008–1025. <https://doi.org/10.1111/j.1365-2958.2006.05571.x>
- Gerken, H., Leiser, O.P., Bennion, D., Misra, R., 2010. Involvement and necessity of the Cpx regulon in the event of aberrant  $\beta$ -barrel outer membrane protein assembly. *Mol. Microbiol.* 75, 1033–1046. <https://doi.org/10.1111/j.1365-2958.2009.07042.x>
- Germany, E.M., Ding, Y., Imai, K., Bamert, R.S., Dunstan, R.A., Nakajima, Y., Lai, X., Webb, C.T., Stubenrauch, C.J., Hidaka, K., Thewasano, N., Tan, K.S., Shen, H.-H., Lithgow, T., Shiota, T., 2021. Discovery of a conserved rule behind the assembly of  $\beta$ -barrel membrane proteins. <https://doi.org/10.1101/2021.10.29.466387>
- Gessmann, D., Chung, Y.H., Danoff, E.J., Plummer, A.M., Sandlin, C.W., Zaccai, N.R., Fleming, K.G., 2014. Outer membrane  $\beta$ -barrel protein folding is physically controlled by periplasmic lipid head groups and BamA. *Proc. Natl. Acad. Sci.* 111, 5878–5883. <https://doi.org/10.1073/pnas.1322473111>
- Goley, E.D., Yeh, Y.-C., Hong, S.-H., Fero, M.J., Abeliuk, E., McAdams, H.H., Shapiro, L., 2011. Assembly of the Caulobacter cell division machine. *Mol. Microbiol.* 80, 1680–1698. <https://doi.org/10.1111/j.1365-2958.2011.07677.x>
- Gómez-Santos, N., Glatter, T., Koebnik, R., Świątek-Połatyńska, M.A., Søgaard-Andersen, L., 2019. A TonB-dependent transporter is required for secretion of protease PopC across the bacterial outer membrane. *Nat. Commun.* 10, 1360. <https://doi.org/10.1038/s41467-019-09366-9>
- Gorasia, D.G., Veith, P.D., Reynolds, E.C., 2020. The Type IX Secretion System: Advances in Structure, Function and Organisation. *Microorganisms* 8, 1173. <https://doi.org/10.3390/microorganisms8081173>
- Goyal, P., Krasteva, P.V., Van Gerven, N., Gubellini, F., Van den Broeck, I., Troupiotis-Tsailaki, A., Jonckheere, W., Péhau-arnaudet, G., Pinkner, J.S., Chapman, M.R., Hultgren, S.J., Howorka, S., Fronzes, R., Remaut, H., 2014. Structural and mechanistic insights into the bacterial amyloid secretion channel CsgG. *Nature* 516, 250–253. <https://doi.org/10.1038/nature13768>
- Grabowicz, M., 2019. Lipoproteins and Their Trafficking to the Outer Membrane. *EcoSal Plus* 8. <https://doi.org/10.1128/ecosalplus.ESP-0038-2018>
- Grabowicz, M., Koren, D., Silhavy, T.J., 2016. The CpxQ sRNA Negatively Regulates Skp To Prevent Mistargeting of  $\beta$ -Barrel Outer Membrane Proteins into the Cytoplasmic Membrane. *mBio* 7, e00312-16. <https://doi.org/10.1128/mBio.00312-16>
- Grabowicz, M., Silhavy, T.J., 2017a. Redefining the essential trafficking pathway for outer membrane lipoproteins. *Proc. Natl. Acad. Sci.* 114, 4769–4774. <https://doi.org/10.1073/pnas.1702248114>
- Grabowicz, M., Silhavy, T.J., 2017b. Envelope Stress Responses: An Interconnected Safety Net. *Trends Biochem. Sci.* 42, 232–242. <https://doi.org/10.1016/j.tibs.2016.10.002>
- Grijpstra, J., Arenas, J., Rutten, L., Tommassen, J., 2013. Autotransporter secretion: varying on a theme. *Res. Microbiol., Bacterial secretion systems: function and structural biology* 164, 562–582. <https://doi.org/10.1016/j.resmic.2013.03.010>
- Grinter, R., Morris, F.C., Dunstan, R.A., Leung, P.M., Kropp, A., Belousoff, M., Gunasinghe, S.D., Scott, N.E., Beckham, S., Peleg, A.Y., Greening, C., Li, J., Heinz, E., Lithgow, T., 2021. Bona from *Acinetobacter baumannii* Forms a Divisome-Localized Decamer That Supports Outer Envelope Function. *mBio* 12, e01480-21. <https://doi.org/10.1128/mBio.01480-21>
- Gu, Y., Li, H., Dong, H., Zeng, Y., Zhang, Z., Paterson, N.G., Stansfeld, P.J., Wang, Z., Zhang, Y., Wang, W., Dong, C., 2016. Structural basis of outer membrane protein insertion by the BAM complex. *Nature* 531, 64–69. <https://doi.org/10.1038/nature17199>
- Guest, R.L., Rutherford, S.T., Silhavy, T.J., 2021. Border Control: Regulating LPS Biogenesis. *Trends Microbiol.* 29, 334–345. <https://doi.org/10.1016/j.tim.2020.09.008>
- Guharajan, S., Chhabra, S., Parisutham, V., Brewster, R.C., 2021. Quantifying the regulatory role of individual transcription factors in *Escherichia coli*. *Cell Rep.* 37, 109952. <https://doi.org/10.1016/j.celrep.2021.109952>
- Gunasinghe, S.D., Shiota, T., Stubenrauch, C.J., Schulze, K.E., Webb, C.T., Fulcher, A.J., Dunstan, R.A., Hay, I.D., Naderer, T., Whelan, D.R., Bell, T.D.M., Elgass, K.D., Strugnelli, R.A., Lithgow, T., 2018. The WD40 Protein BamB Mediates Coupling of BAM Complexes into Assembly Precincts in the Bacterial Outer Membrane. *Cell Rep.* 23, 2782–2794. <https://doi.org/10.1016/j.celrep.2018.04.093>
- Hagan, C.L., Kim, S., Kahne, D., 2010. Reconstitution of Outer Membrane Protein Assembly from Purified Components. *Science* 328, 890–892. <https://doi.org/10.1126/science.1188919>
- Han, L., Zheng, J., Wang, Y., Yang, X., Liu, Y., Sun, C., Cao, B., Zhou, H., Ni, D., Lou, J., Zhao, Y., Huang, Y., 2016. Structure of the BAM complex and its implications for biogenesis of outer-membrane proteins. *Nat. Struct. Mol. Biol.* 23, 192–196. <https://doi.org/10.1038/nsmb.3181>
- Hart, E.M., Gupta, M., Wühr, M., Silhavy, T.J., 2019a. The Synthetic Phenotype of  $\Delta$ bamB  $\Delta$ bamE Double Mutants Results from a Lethal Jamming of the Bam Complex by the Lipoprotein RcsF. *mBio* 10. <https://doi.org/10.1128/mBio.00662-19>
- Hart, E.M., Mitchell, A.M., Konvalova, A., Grabowicz, M., Sheng, J., Han, X., Rodriguez-Rivera, F.P., Schwaid, A.G., Malinverni, J.C., Balibar, C.J., Bodea, S., Si, Q., Wang, H., Homsher, M.F., Painter, R.E., Ogawa, A.K., Sutterlin, H., Roemer, T., Black, T.A., Rothman, D.M., Walker, S.S., Silhavy, T.J., 2019b. A small-molecule inhibitor of BamA impervious to efflux and the outer membrane permeability barrier. *Proc. Natl. Acad. Sci.* 116, 21748–21757. <https://doi.org/10.1073/pnas.1912345116>
- Hartl, F.-U., Lecker, S., Schiebel, E., Hendrick, J.P., Wickner, W., 1990. The binding cascade of SecB to SecA to SecY E mediates preprotein targeting to the *E. coli* plasma membrane. *Cell* 63, 269–279. [https://doi.org/10.1016/0092-8674\(90\)90160-G](https://doi.org/10.1016/0092-8674(90)90160-G)
- Hayashi, Y., Tsurumizu, R., Tsukahara, J., Takeda, K., Narita, S., Mori, M., Miki, K., Tokuda, H., 2014. Roles of the Protruding Loop of Factor B Essential for the Localization of Lipoproteins (LoLB) in the Anchoring of Bacterial Triacylated Proteins to the Outer Membrane \*. *J. Biol. Chem.* 289, 10530–10539. <https://doi.org/10.1074/jbc.M113.539270>
- Heijne, G.V., 1983. Patterns of Amino Acids near Signal-Sequence Cleavage Sites. *Eur. J. Biochem.* 133, 17–21. <https://doi.org/10.1111/j.1432-1033.1983.tb07424.x>
- Heinz, E., Selkrig, J., Belousoff, M.J., Lithgow, T., 2015. Evolution of the Translocation and Assembly Module (TAM). *Genome Biol. Evol.* 7, 1628–1643. <https://doi.org/10.1093/gbe/evv097>

- Hews, C.L., Cho, T., Rowley, G., Raivio, T.L., 2019. Maintaining Integrity Under Stress: Envelope Stress Response Regulation of Pathogenesis in Gram-Negative Bacteria. *Front. Cell. Infect. Microbiol.* 9. <https://doi.org/10.3389/fcimb.2019.00313>
- Hizlan, D., Robson, A., Whitehouse, S., Gold, V.A., Vonck, J., Mills, D., Kühlbrandt, W., Collinson, I., 2012. Structure of the SecY Complex Unlocked by a Preprotein Mimic. *Cell Rep.* 1, 21–28. <https://doi.org/10.1016/j.celrep.2011.11.003>
- Höhr, A.I.C., Lindau, C., Wirth, C., Qiu, J., Stroud, D.A., Kutik, S., Guiard, B., Hunte, C., Becker, T., Pfanner, N., Wiedemann, N., 2018. Membrane protein insertion through a mitochondrial  $\beta$ -barrel gate. *Science* 359. <https://doi.org/10.1126/science.aah6834>
- Holdbrook, D.A., Burmann, B.M., Huber, R.G., Petoukhov, M.V., Svergun, D.I., Hiller, S., Bond, P.J., 2017. A Spring-Loaded Mechanism Governs the Clamp-like Dynamics of the Skp Chaperone. *Structure* 25, 1079–1088.e3. <https://doi.org/10.1016/j.str.2017.05.018>
- Holst, O., 2007. The structures of core regions from enterobacterial lipopolysaccharides – an update. *FEMS Microbiol. Lett.* 271, 3–11. <https://doi.org/10.1111/j.1574-6968.2007.00708.x>
- Horne, J.E., Brockwell, D.J., Radford, S.E., 2020. Role of the lipid bilayer in outer membrane protein folding in Gram-negative bacteria. *J. Biol. Chem.* 295, 10340–10367. <https://doi.org/10.1074/jbc.REV120.011473>
- Horne, J.E., Radford, S.E., 2022. Roll out the barrel! Outer membrane tension resolves an unexpected folding intermediate. *Cell* 185, 1107–1109. <https://doi.org/10.1016/j.cell.2022.03.001>
- Houbraken, J., Frisvad, J.C., Samson, R.A., 2011. Fleming's penicillin producing strain is not *Penicillium chrysogenum* but *P. rubens*. *IMA Fungus* 2, 87–95. <https://doi.org/10.5598/imafungus.2011.02.01.12>
- Huang, Y.M., Miao, Y., Munguia, J., Lin, L., Nizet, V., McCammon, J.A., 2016. Molecular dynamic study of MlaC protein in Gram-negative bacteria: conformational flexibility, solvent effect and protein-phospholipid binding. *Protein Sci.* 25, 1430–1437. <https://doi.org/10.1002/pro.2939>
- Huber, D., Rajagopalan, N., Preissler, S., Rocco, M.A., Merz, F., Kramer, G., Bukau, B., 2011. SecA interacts with ribosomes in order to facilitate posttranslational translocation in bacteria. *Mol. Cell* 41, 343–353. <https://doi.org/10.1016/j.molcel.2010.12.028>
- Iadanza, M.G., Higgins, A.J., Schiffrin, B., Calabrese, A.N., Brockwell, D.J., Ashcroft, A.E., Radford, S.E., Ranson, N.A., 2016. Lateral opening in the intact  $\beta$ -barrel assembly machinery captured by cryo-EM. *Nat. Commun.* 7, 1–12. <https://doi.org/10.1038/ncomms12865>
- Ieva, R., Tian, P., Peterson, J.H., Bernstein, H.D., 2011. Sequential and spatially restricted interactions of assembly factors with an autotransporter  $\beta$  domain. *Proc. Natl. Acad. Sci. U. S. A.* 108, E383–E391. <https://doi.org/10.1073/pnas.1103827108>
- Imai, Y., Meyer, K.J., Iinishi, A., Favre-Godal, Q., Green, R., Manuse, S., Caboni, M., Mori, M., Niles, S., Ghiglieri, M., Honrao, C., Ma, X., Guo, J.J., Makriyannis, A., Linares-Otaya, L., Böhringer, N., Wuisan, Z.G., Kaur, H., Wu, R., Mateus, A., Typas, A., Savitski, M.M., Espinoza, J.L., O'Rourke, A., Nelson, K.E., Hiller, S., Noinaj, N., Schäberle, T.F., D'Onofrio, A., Lewis, K., 2019. A new antibiotic selectively kills Gram-negative pathogens. *Nature* 576, 459–464. <https://doi.org/10.1038/s41586-019-1791-1>
- Inouye, S., Franceschini, T., Sato, M., Itakura, K., Inouye, M., 1983. Prolipoprotein signal peptidase of *Escherichia coli* requires a cysteine residue at the cleavage site. *EMBO J.* 2, 87–91.
- Iqbal, H., Kenedy, M.R., Lybecker, M., Akins, D.R., 2016. The TamB ortholog of *Borrelia burgdorferi* interacts with the  $\beta$ -barrel assembly machine (BAM) complex protein BamA. *Mol. Microbiol.* 102, 757–774. <https://doi.org/10.1111/mmi.13492>
- Ishida, H., Garcia-Herrero, A., Vogel, H.J., 2014. The periplasmic domain of *Escherichia coli* outer membrane protein A can undergo a localized temperature dependent structural transition. *Biochim. Biophys. Acta BBA - Biomembr.* 1838, 3014–3024. <https://doi.org/10.1016/j.bbamem.2014.08.008>
- Ishino, F., Matsuhashi, M., 1981. Peptidoglycan synthetic enzyme activities of highly purified penicillin-binding protein 3 in *Escherichia coli*: A septum-forming reaction sequence. *Biochem. Biophys. Res. Commun.* 101, 905–911. [https://doi.org/10.1016/0006-291X\(81\)91835-0](https://doi.org/10.1016/0006-291X(81)91835-0)
- Isom, G.L., Coudray, N., MacRae, M.R., McManus, C.T., Ekiert, D.C., Bhabha, G., 2020. LetB Structure Reveals a Tunnel for Lipid Transport across the Bacterial Envelope. *Cell* 181, 653–664.e19. <https://doi.org/10.1016/j.cell.2020.03.030>
- Jarchow, S., Lück, C., Görg, A., Skerra, A., 2008. Identification of potential substrate proteins for the periplasmic *Escherichia coli* chaperone Skp. *PROTEOMICS* 8, 4987–4994. <https://doi.org/10.1002/pmic.200800288>
- Jin, S., Roitsch, T., Ankenbauer, R.G., Gordon, M.P., Nester, E.W., 1990. The VirA protein of *Agrobacterium tumefaciens* is autophosphorylated and is essential for vir gene regulation. *J. Bacteriol.* 172, 525–530. <https://doi.org/10.1128/jb.172.2.525-530.1990>
- Johansen, J., Rasmussen, A.A., Overgaard, M., Valentin-Hansen, P., 2006. Conserved small non-coding RNAs that belong to the sigmaE regulon: role in down-regulation of outer membrane proteins. *J. Mol. Biol.* 364, 1–8. <https://doi.org/10.1016/j.jmb.2006.09.004>
- Joloba, M.L., Clemmer, K.M., Sledjeski, D.D., Rather, P.N., 2004. Activation of the gab Operon in an RpoS-Dependent Manner by Mutations That Truncate the Inner Core of Lipopolysaccharide in *Escherichia coli*. *J. Bacteriol.* 186, 8542–8546. <https://doi.org/10.1128/JB.186.24.8542-8546.2004>
- Jones, C.H., Danese, P.N., Pinkner, J.S., Silhavy, T.J., Hultgren, S.J., 1997. The chaperone-assisted membrane release and folding pathway is sensed by two signal transduction systems. *EMBO J.* 16, 6394–6406. <https://doi.org/10.1093/emboj/16.21.6394>
- Josts, I., Stubenrauch, C.J., Vadlamani, G., Mosbahi, K., Walker, D., Lithgow, T., Grinter, R., 2017. The Structure of a Conserved Domain of TamB Reveals a Hydrophobic  $\beta$  Taco Fold. *Struct. Lond. Engl.* 1993. <https://doi.org/10.1016/j.str.2017.10.002>
- Jumper, J., Evans, R., Pritzel, A., Green, T., Figurnov, M., Ronneberger, O., Tunyasuvunakool, K., Bates, R., Židek, A., Potapenko, A., Bridgland, A., Meyer, C., Kohl, S.A.A., Ballard, A.J., Cowie, A., Romera-Paredes, B., Nikolov, S., Jain, R., Adler, J., Back, T., Petersen, S., Reiman, D., Clancy, E., Zielinski, M., Steinegger, M., Pacholska, M., Berghammer, T., Bodenstein, S., Silver, D., Vinyals, O., Senior, A.W., Kavukcuoglu, K., Kohli, P., Hassabis, D., 2021. Highly accurate protein structure prediction with AlphaFold. *Nature* 596, 583–589. <https://doi.org/10.1038/s41586-021-03819-2>
- Kakimoto, Y., Tero, R., 2018. Supported Lipid Bilayers of *Escherichia coli* Extracted Lipids and Their Calcium Dependence. *Front. Mater.* 5.
- Kengmo Tchoupa, A., Watkins, K.E., Jones, R.A., Kuroki, A., Alam, M.T., Perrier, S., Chen, Y., Unnikrishnan, M., 2020. The type VII secretion system protects *Staphylococcus aureus* against antimicrobial host fatty acids. *Sci. Rep.* 10, 14838. <https://doi.org/10.1038/s41598-020-71653-z>
- Keramisanou, D., Biris, N., Gelis, I., Sianidis, G., Karamanou, S., Economou, A., Kalodimos, C.G., 2006. Disorder-order folding transitions underlie catalysis in the helicase motor of SecA. *Nat. Struct. Mol. Biol.* 13, 594–602. <https://doi.org/10.1038/nsmb1108>

- Kim, K.H., Paetzel, M., 2011. Crystal Structure of Escherichia coli BamB, a Lipoprotein Component of the  $\beta$ -Barrel Assembly Machinery Complex. *J. Mol. Biol.* 406, 667–678. <https://doi.org/10.1016/j.jmb.2010.12.020>
- Kim, S., Malinverni, J.C., Sliz, P., Silhavy, T.J., Harrison, S.C., Kahne, D., 2007. Structure and function of an essential component of the outer membrane protein assembly machine. *Science* 317, 961–964. <https://doi.org/10.1126/science.1143993>
- Knop, M., Siegers, K., Pereira, G., Zachariae, W., Winsor, B., Nasmyth, K., Schiebel, E., 1999. Epitope tagging of yeast genes using a PCR-based strategy: more tags and improved practical routines. *Yeast* 15, 963–972. [https://doi.org/10.1002/\(SICI\)1097-0061\(199907\)15:10B<963::AID-YEA399>3.0.CO;2-W](https://doi.org/10.1002/(SICI)1097-0061(199907)15:10B<963::AID-YEA399>3.0.CO;2-W)
- Knyazev, D.G., Kuttner, R., Zimmermann, M., Sobakinskaya, E., Pohl, P., 2018. Driving Forces of Translocation Through Bacterial Translocon SecYEG. *J. Membr. Biol.* 251, 329–343. <https://doi.org/10.1007/s00232-017-0012-9>
- Kocaoglu, O., Carlson, E.E., 2015. Profiling of  $\beta$ -Lactam Selectivity for Penicillin-Binding Proteins in Escherichia coli Strain DC2. *Antimicrob. Agents Chemother.* 59, 2785–2790. <https://doi.org/10.1128/AAC.04552-14>
- Komar, J., Alvira, S., Schulze, R.J., Martin, R., Lycklama a Nijeholt, J.A., Lee, S.C., Dafforn, T.R., Deckers-Hebestreit, G., Berger, I., Schaffitzel, C., Collinson, I., 2016. Membrane protein insertion and assembly by the bacterial holo-translocon SecYEG–SecDF–YajC–YidC. *Biochem. J.* 473, 3341–3354. <https://doi.org/10.1042/BCJ20160545>
- Konovalova, A., Kahne, D.E., Silhavy, T.J., 2017. Outer Membrane Biogenesis. *Annu. Rev. Microbiol.* 71, 539–556. <https://doi.org/10.1146/annurev-micro-090816-093754>
- Konovalova, A., Mitchell, A.M., Silhavy, T.J., 2016. A lipoprotein/ $\beta$ -barrel complex monitors lipopolysaccharide integrity transducing information across the outer membrane. *eLife* 5, e15276. <https://doi.org/10.7554/eLife.15276>
- Konovalova, A., Perlman, D.H., Cowles, C.E., Silhavy, T.J., 2014. Transmembrane domain of surface-exposed outer membrane lipoprotein RcsF is threaded through the lumen of  $\beta$ -barrel proteins. *Proc. Natl. Acad. Sci.* 111, E4350–E4358. <https://doi.org/10.1073/pnas.1417138111>
- Konovalova, A., Silhavy, T.J., 2015. Outer membrane lipoprotein biogenesis: Lol is not the end. *Phil Trans R Soc B* 370, 20150030. <https://doi.org/10.1098/rstb.2015.0030>
- Kozjak-Pavlovic, V., Ott, C., Götz, M., Rudel, T., 2011. Neisserial Omp85 Protein Is Selectively Recognized and Assembled into Functional Complexes in the Outer Membrane of Human Mitochondria \*. *J. Biol. Chem.* 286, 27019–27026. <https://doi.org/10.1074/jbc.M111.232249>
- Krojer, T., Sawa, J., Schäfer, E., Saibil, H.R., Ehrmann, M., Clausen, T., 2008. Structural basis for the regulated protease and chaperone function of DegP. *Nature* 453, 885–890. <https://doi.org/10.1038/nature07004>
- Kumazaki, K., Chiba, S., Takemoto, M., Furukawa, A., Nishiyama, K., Sugano, Y., Mori, T., Dohmae, N., Hirata, K., Nakada-Nakura, Y., Maturana, A.D., Tanaka, Y., Mori, H., Sugita, Y., Arisaka, F., Ito, K., Ishitani, R., Tsukazaki, T., Nureki, O., 2014. Structural basis of Sec-independent membrane protein insertion by YidC. *Nature* 509, 516–520. <https://doi.org/10.1038/nature13167>
- Kussell, E., Kishony, R., Balaban, N.Q., Leibler, S., 2005. Bacterial Persistence: A Model of Survival in Changing Environments. *Genetics* 169, 1807–1814. <https://doi.org/10.1534/genetics.104.035352>
- Kutik, S., Stojanovski, D., Becker, L., Becker, T., Meinecke, M., Krüger, V., Prinz, C., Meisinger, C., Guiard, B., Wagner, R., Pfanner, N., Wiedemann, N., 2008. Dissecting Membrane Insertion of Mitochondrial  $\beta$ -Barrel Proteins. *Cell* 132, 1011–1024. <https://doi.org/10.1016/j.cell.2008.01.028>
- Lasica, A.M., Ksiazek, M., Madej, M., Potempa, J., 2017. The Type IX Secretion System (T9SS): Highlights and Recent Insights into Its Structure and Function. *Front. Cell. Infect. Microbiol.* 7.
- Lauber, F., Deme, J.C., Lea, S.M., Berks, B.C., 2018. Type 9 secretion system structures reveal a new protein transport mechanism. *Nature* 564, 77–82. <https://doi.org/10.1038/s41586-018-0693-y>
- Leake, M.C., Greene, N.P., Godun, R.M., Granjon, T., Buchanan, G., Chen, S., Berry, R.M., Palmer, T., Berks, B.C., 2008. Variable stoichiometry of the TatA component of the twin-arginine protein transport system observed by in vivo single-molecule imaging. *Proc. Natl. Acad. Sci.* 105, 15376–15381. <https://doi.org/10.1073/pnas.0806338105>
- Lecker, S., Lill, R., Ziegelhoffer, T., Georgopoulos, C., Bassford Jr, P. j., Kumamoto, C. a., Wickner, W., 1989. Three pure chaperone proteins of Escherichia coli–SecB, trigger factor and GroEL–form soluble complexes with precursor proteins in vitro. *EMBO J.* 8, 2703–2709. <https://doi.org/10.1002/j.1460-2075.1989.tb08411.x>
- Lee, J., Sutterlin, H.A., Wzorek, J.S., Mandler, M.D., Hagan, C.L., Grabowicz, M., Tomasek, D., May, M.D., Hart, E.M., Silhavy, T.J., Kahne, D., 2018. Substrate binding to BamD triggers a conformational change in BamA to control membrane insertion. *Proc. Natl. Acad. Sci.* 115, 2359–2364. <https://doi.org/10.1073/pnas.1711727115>
- Lee, J., Tomasek, D., Santos, T.M., May, M.D., Meuskens, I., Kahne, D., 2019. Formation of a  $\beta$ -barrel membrane protein is catalyzed by the interior surface of the assembly machine protein BamA. *eLife* 8, e49787. <https://doi.org/10.7554/eLife.49787>
- Leo, J.C., Grin, I., Linke, D., 2012. Type V secretion: mechanism(s) of autotransport through the bacterial outer membrane. *Philos. Trans. R. Soc. B Biol. Sci.* 367, 1088–1101. <https://doi.org/10.1098/rstb.2011.0208>
- Li, C., Tan, B.K., Zhao, J., Guan, Z., 2016. In Vivo and in Vitro Synthesis of Phosphatidylglycerol by an Escherichia coli Cardiolipin Synthase \*. *J. Biol. Chem.* 291, 25144–25153. <https://doi.org/10.1074/jbc.M116.762070>
- Li, G.-W., Burkhardt, D., Gross, C., Weissman, J.S., 2014. Quantifying absolute protein synthesis rates reveals principles underlying allocation of cellular resources. *Cell* 157, 624–635. <https://doi.org/10.1016/j.cell.2014.02.033>
- Lill, R., Cunningham, K., Brundage, L.A., Ito, K., Oliver, D., Wickner, W., 1989. SecA protein hydrolyzes ATP and is an essential component of the protein translocation ATPase of Escherichia coli. *EMBO J.* 8, 961–966. <https://doi.org/10.1002/j.1460-2075.1989.tb03458.x>
- Lima, S., Guo, M.S., Chaba, R., Gross, C.A., Sauer, R.T., 2013. Dual Molecular Signals Mediate the Bacterial Response to Outer-Membrane Stress. *Science* 340, 837–841. <https://doi.org/10.1126/science.1235358>
- Liu, C., Ma, J., Wang, J., Wang, H., Zhang, L., 2020. Cryo-EM Structure of a Bacterial Lipid Transporter YebT. *J. Mol. Biol.* 432, 1008–1019. <https://doi.org/10.1016/j.jmb.2019.12.008>
- Low, H.H., Gubellini, F., Rivera-Calzada, A., Braun, N., Connery, S., Dujeancourt, A., Lu, F., Redzej, A., Fronzes, R., Orlova, E.V., Waksman, G., 2014. Structure of a type IV secretion system. *Nature* 508, 550–553. <https://doi.org/10.1038/nature13081>
- Lüke, I., Handford, J.I., Palmer, T., Sargent, F., 2009. Proteolytic processing of Escherichia coli twin-arginine signal peptides by LepB. *Arch. Microbiol.* 191, 919–925. <https://doi.org/10.1007/s00203-009-0516-5>
- Lundquist, K., Billings, E., Bi, M., Wellnitz, J., Noinaj, N., 2021. The assembly of  $\beta$ -barrel membrane proteins by BAM and SAM. *Mol. Microbiol.* 115, 425–435. <https://doi.org/10.1111/mmi.14666>
- Luther, A., Urfer, M., Zahn, M., Müller, M., Wang, S.-Y., Mondal, M., Vitale, A., Hartmann, J.-B., Sharpe, T., Monte, F.L., Kocherla, H., Cline, E., Pessi, G., Rath, P., Modaresi, S.M., Chiquet, P., Stiegeler, S., Verbree, C., Remus, T., Schmitt, M., Kolopp, C., Westwood, M.-A., Desjonquères, N., Brabet, E., Hell, S., LePoupon, K., Vermeulen, A., Jaisson, R., Rithié, V., Upert, G., Lederer, A., Zbinden, P., Wach, A., Moehle, K., Zerbe, K., Locher, H.H., Bernardini, F., Dale, G.E., Eberl, L.,

- Wollscheid, B., Hiller, S., Robinson, J.A., Obrecht, D., 2019. Chimeric peptidomimetic antibiotics against Gram-negative bacteria. *Nature* 576, 452–458. <https://doi.org/10.1038/s41586-019-1665-6>
- Malinverni, J.C., Werner, J., Kim, S., Sklar, J.G., Kahne, D., Misra, R., Silhavy, T.J., 2006. YfiO stabilizes the YaeT complex and is essential for outer membrane protein assembly in *Escherichia coli*. *Mol. Microbiol.* 61, 151–164. <https://doi.org/10.1111/j.1365-2958.2006.05211.x>
- Margolin, W., 2005. FtsZ and the division of prokaryotic cells and organelles. *Nat. Rev. Mol. Cell Biol.* 6, 862–871. <https://doi.org/10.1038/nrm1745>
- Mas, G., Thoma, J., Hiller, S., 2019. The Periplasmic Chaperones Skp and SurA. *Subcell. Biochem.* 92, 169–186. [https://doi.org/10.1007/978-3-030-18768-2\\_6](https://doi.org/10.1007/978-3-030-18768-2_6)
- Matsushashi, M., 1994. Chapter 4 Utilization of lipid-linked precursors and the formation of peptidoglycan in the process of cell growth and division: membrane enzymes involved in the final steps of peptidoglycan synthesis and the mechanism of their regulation, in: Ghuyssen, J.-M., Hakenbeck, R. (Eds.), *New Comprehensive Biochemistry, Bacterial Cell Wall*. Elsevier, pp. 55–71. [https://doi.org/10.1016/S0167-7306\(08\)60407-X](https://doi.org/10.1016/S0167-7306(08)60407-X)
- Megrian, D., Taib, N., Witwinowski, J., Beloin, C., Gribaldo, S., 2020. One or two membranes? Diderm Firmicutes challenge the Gram-positive/Gram-negative divide. *Mol. Microbiol.* 113, 659–671. <https://doi.org/10.1111/mmi.14469>
- Meng, J., Young, G., Chen, J., 2021. The Rcs System in Enterobacteriaceae: Envelope Stress Responses and Virulence Regulation. *Front. Microbiol.* 12.
- Meriläinen, G., Koski, M.K., Wierenga, R.K., 2016. The extended structure of the periplasmic region of CdsD, a structural protein of the type III secretion system of *Chlamydia trachomatis*. *Protein Sci.* 25, 987–998. <https://doi.org/10.1002/pro.2906>
- Merten, J.A., Schultz, K.M., Klug, C.S., 2012. Concentration-dependent oligomerization and oligomeric arrangement of LptA. *Protein Sci. Publ. Protein Soc.* 21, 211–218. <https://doi.org/10.1002/pro.2004>
- Meuskens, I., Saragliadis, A., Leo, J.C., Linke, D., 2019. Type V Secretion Systems: An Overview of Passenger Domain Functions. *Front. Microbiol.* 10.
- Missiakas, D., Mayer, M.P., Lemaire, M., Georgopoulos, C., Raina, S., 1997. Modulation of the *Escherichia coli*  $\sigma$  (RpoE) heat-shock transcription-factor activity by the RseA, RseB and RseC proteins. *Mol. Microbiol.* 24, 355–371. <https://doi.org/10.1046/j.1365-2958.1997.3601713.x>
- Mitchell, A.M., Silhavy, T.J., 2019. Envelope stress responses: balancing damage repair and toxicity. *Nat. Rev. Microbiol.* 17, 417–428. <https://doi.org/10.1038/s41579-019-0199-0>
- Mitra, K., Schaffitzel, C., Shaikh, T., Tama, F., Jenni, S., Brooks, C.L., Ban, N., Frank, J., 2005. Structure of the *E. coli* protein-conducting channel bound to a translating ribosome. *Nature* 438, 318–324. <https://doi.org/10.1038/nature04133>
- Morgan, J.L.W., Acheson, J.F., Zimmer, J., 2017. Structure of a Type-1 Secretion System ABC Transporter. *Structure* 25, 522–529. <https://doi.org/10.1016/j.str.2017.01.010>
- Morrison, K.L., Weiss, G.A., 2001. Combinatorial alanine-scanning. *Curr. Opin. Chem. Biol.* 5, 302–307. [https://doi.org/10.1016/S1367-5931\(00\)00206-4](https://doi.org/10.1016/S1367-5931(00)00206-4)
- Mulani, M.S., Kamble, E.E., Kumkar, S.N., Tawre, M.S., Pardesi, K.R., 2019. Emerging Strategies to Combat ESKAPE Pathogens in the Era of Antimicrobial Resistance: A Review. *Front. Microbiol.* 10. <https://doi.org/10.3389/fmicb.2019.00539>
- Murén, E.M., Suci, D., Topping, T.B., Kumamoto, C.A., Randall, L.L., 1999. Mutational Alterations in the Homotetrameric Chaperone SecB That Implicate the Structure as Dimer of Dimers. *J. Biol. Chem.* 274, 19397–19402. <https://doi.org/10.1074/jbc.274.27.19397>
- Nagamori, S., Nishiyama, K., Tokuda, H., 2002. Membrane Topology Inversion of SecG Detected by Labeling with a Membrane-Impermeable Sulphydryl Reagent that Causes a Close Association of SecG with SecA. *J. Biochem. (Tokyo)* 132, 629–634. <https://doi.org/10.1093/oxfordjournals.jbchem.a003266>
- Nakayama, T., Zhang-Akiyama, Q.-M., 2016. pqiABC and yebST, Putative mce Operons of *Escherichia coli*, Encode Transport Pathways and Contribute to Membrane Integrity. *J. Bacteriol.* 199, e00606-16. <https://doi.org/10.1128/JB.00606-16>
- Narita, S., Tokuda, H., 2009. Biochemical characterization of an ABC transporter LptBFGC complex required for the outer membrane sorting of lipopolysaccharides. *FEBS Lett.* 583, 2160–2164. <https://doi.org/10.1016/j.febslet.2009.05.051>
- New report calls for urgent action to avert antimicrobial resistance crisis [WWW Document], n.d. URL <https://www.who.int/news-room/detail/29-04-2019-new-report-calls-for-urgent-action-to-avert-antimicrobial-resistance-crisis> (accessed 4.15.20).
- Nguyen-Distèche, M., Fraipont, C., Buddelmeijer, N., Nanninga, N., 1998. The structure and function of *Escherichia coli* penicillin-binding protein 3. *Cell. Mol. Life Sci. CMLS* 54, 309–316. <https://doi.org/10.1007/s000180050157>
- Ni, D., Wang, Y., Yang, X., Zhou, H., Hou, X., Cao, B., Lu, Z., Zhao, X., Yang, K., Huang, Y., 2014. Structural and functional analysis of the  $\beta$ -barrel domain of BamA from *Escherichia coli*. *FASEB J.* 28, 2677–2685. <https://doi.org/10.1096/fj.13-248450>
- Nickerson, N.N., Mainprize, I.L., Hampton, L., Jones, M.L., Naismith, J.H., Whitfield, C., 2014. Trapped translocation intermediates establish the route for export of capsular polysaccharides across *Escherichia coli* outer membranes. *Proc. Natl. Acad. Sci.* 111, 8203–8208. <https://doi.org/10.1073/pnas.1400341111>
- Nishiyama, K., Suzuki, T., Tokuda, H., 1996. Inversion of the Membrane Topology of SecG Coupled with SecA-Dependent Preprotein Translocation. *Cell* 85, 71–81. [https://doi.org/10.1016/S0092-8674\(00\)81083-1](https://doi.org/10.1016/S0092-8674(00)81083-1)
- Nivaskumar, M., Francetic, O., 2014. Type II secretion system: A magic beanstalk or a protein escalator. *Biochim. Biophys. Acta BBA - Mol. Cell Res., Protein trafficking and secretion in bacteria* 1843, 1568–1577. <https://doi.org/10.1016/j.bbamcr.2013.12.020>
- Noinaj, N., Kuszak, A.J., Balusek, C., Gumbart, J.C., Buchanan, S.K., 2014. Lateral Opening and Exit Pore Formation Are Required for BamA Function. *Structure* 22, 1055–1062. <https://doi.org/10.1016/j.str.2014.05.008>
- Noinaj, N., Kuszak, A.J., Buchanan, S.K., 2015. Heat Modifiability of Outer Membrane Proteins from Gram-Negative Bacteria, in: Buchanan, S., Noinaj, N. (Eds.), *The BAM Complex: Methods and Protocols, Methods in Molecular Biology*. Springer, New York, NY, pp. 51–56. [https://doi.org/10.1007/978-1-4939-2871-2\\_4](https://doi.org/10.1007/978-1-4939-2871-2_4)
- Noinaj, N., Kuszak, A.J., Gumbart, J.C., Lukacik, P., Chang, H., Easley, N.C., Lithgow, T., Buchanan, S.K., 2013. Structural insight into the biogenesis of  $\beta$ -barrel membrane proteins. *Nature* 501, 385–390. <https://doi.org/10.1038/nature12521>
- Oguchi, Y., Takeda, K., Watanabe, S., Yokota, N., Miki, K., Tokuda, H., 2008. Opening and Closing of the Hydrophobic Cavity of LolA Coupled to Lipoprotein Binding and Release\*. *J. Biol. Chem.* 283, 25414–25420. <https://doi.org/10.1074/jbc.M804736200>
- Okuda, S., Tokuda, H., 2009. Model of mouth-to-mouth transfer of bacterial lipoproteins through inner membrane LolC, periplasmic LolA, and outer membrane LolB. *Proc. Natl. Acad. Sci.* 106, 5877–5882. <https://doi.org/10.1073/pnas.0900896106>
- Olatunji, S., Yu, X., Bailey, J., Huang, C.-Y., Zapotoczna, M., Bowen, K., Remškar, M., Müller, R., Scanlan, E.M., Geoghegan, J.A., Olieric, V., Caffrey, M., 2020. Structures of lipoprotein signal peptidase II from *Staphylococcus aureus* complexed with antibiotics globomycin and myxovirescin. *Nat. Commun.* 11, 140. <https://doi.org/10.1038/s41467-019-13724-y>

- Onufryk, C., Crouch, M.-L., Fang, F.C., Gross, C.A., 2005. Characterization of Six Lipoproteins in the  $\sigma$ E Regulon. *J. Bacteriol.* 187, 4552–4561. <https://doi.org/10.1128/JB.187.13.4552-4561.2005>
- Oswald, J., Njenga, R., Natriashvili, A., Sarmah, P., Koch, H.-G., 2021. The Dynamic SecYEG Translocon. *Front. Mol. Biosci.* 8.
- Özbaykal, G., Wollrab, E., Simon, F., Vigouroux, A., Cordier, B., Aristov, A., Chaze, T., Matondo, M., van Teeffelen, S., 2020. The transpeptidase PBP2 governs initial localization and activity of the major cell-wall synthesis machinery in *E. coli*. *eLife* 9, e50629. <https://doi.org/10.7554/eLife.50629>
- Paetzel, M., 2014. Structure and mechanism of *Escherichia coli* type I signal peptidase. *Biochim. Biophys. Acta BBA - Mol. Cell Res.*, Protein trafficking and secretion in bacteria 1843, 1497–1508. <https://doi.org/10.1016/j.bbamcr.2013.12.003>
- Palmer, T., Berks, B.C., 2012. The twin-arginine translocation (Tat) protein export pathway. *Nat. Rev. Microbiol.* 10, 483–496. <https://doi.org/10.1038/nrmicro2814>
- Palmer, T., Finney, A.J., Saha, C.K., Atkinson, G.C., Sargent, F., 2021. A holin/peptidoglycan hydrolase-dependent protein secretion system. *Mol. Microbiol.* 115, 345–355. <https://doi.org/10.1111/mmi.14599>
- Park, J.T., Uehara, T., 2008. How Bacteria Consume Their Own Exoskeletons (Turnover and Recycling of Cell Wall Peptidoglycan). *Microbiol. Mol. Biol. Rev.* 72, 211–227. <https://doi.org/10.1128/MMBR.00027-07>
- Parsons, J.B., Rock, C.O., 2013. Bacterial lipids: Metabolism and membrane homeostasis. *Prog. Lipid Res.* 52, 249–276. <https://doi.org/10.1016/j.plipres.2013.02.002>
- Peri, S., Steen, H., Pandey, A., 2001. GPMW – a software tool for analyzing proteins and peptides. *Trends Biochem. Sci.* 26, 687–689. [https://doi.org/10.1016/S0968-0004\(01\)01954-5](https://doi.org/10.1016/S0968-0004(01)01954-5)
- Plummer, A.M., Fleming, K.G., 2016. From Chaperones to the Membrane with a BAM! *Trends Biochem. Sci.* 41, 872–882. <https://doi.org/10.1016/j.tibs.2016.06.005>
- Prestinaci, F., Pezzotti, P., Pantosti, A., 2015. Antimicrobial resistance: a global multifaceted phenomenon. *Pathog. Glob. Health* 109, 309–318. <https://doi.org/10.1179/2047773215Y.0000000030>
- Pruden, A., 2018. Chapter 8 - Antibiotics and Antibiotic Resistance: Closing the Loop Between Hospitals and the Environment, in: Boxall, A.B.A., Kookana, R.S. (Eds.), *Health Care and Environmental Contamination, Environmental Contaminants*. Elsevier, Amsterdam, pp. 137–148. <https://doi.org/10.1016/B978-0-444-63857-1.00008-5>
- Pugsley, A.P., Kornacker, M.G., Poquet, I., 1991. The general protein-export pathway is directly required for extracellular pullulanase secretion in *Escherichia coli* k12. *Mol. Microbiol.* 5, 343–352. <https://doi.org/10.1111/j.1365-2958.1991.tb02115.x>
- Qu, J., Mayer, C., Behrens, S., Holst, O., Kleinschmidt, J.H., 2007. The Trimeric Periplasmic Chaperone Skp of *Escherichia coli* Forms 1:1 Complexes with Outer Membrane Proteins via Hydrophobic and Electrostatic Interactions. *J. Mol. Biol.* 374, 91–105. <https://doi.org/10.1016/j.jmb.2007.09.020>
- Raivio, T.L., 2014. Everything old is new again: An update on current research on the Cpx envelope stress response. *Biochim. Biophys. Acta BBA - Mol. Cell Res.*, Protein trafficking and secretion in bacteria 1843, 1529–1541. <https://doi.org/10.1016/j.bbamcr.2013.10.018>
- Raivio, T.L., Silhavy, T.J., 1997. Transduction of envelope stress in *Escherichia coli* by the Cpx two-component system. *J. Bacteriol.* 179, 7724–7733. <https://doi.org/10.1128/jb.179.24.7724-7733.1997>
- Ranava, D., Caumont-Sarcos, A., Albenne, C., Ieva, R., 2018. Bacterial machineries for the assembly of membrane-embedded  $\beta$ -barrel proteins. *FEMS Microbiol. Lett.* 365. <https://doi.org/10.1093/femsle/fny087>
- Ranava, D., Yang, Y., Orenday-Tapia, L., Roussel, F., Turlan, C., Morales, V., Cui, L., Moulin, C., Froment, C., Munoz, G., Rech, J., Marcoux, J., Caumont-Sarcos, A., Albenne, C., Bikard, D., Ieva, R., 2021. Lipoprotein DolP supports proper folding of BamA in the bacterial outer membrane promoting fitness upon envelope stress. *eLife* 10, e67817. <https://doi.org/10.7554/eLife.67817>
- Randall, L.L., Hardy, S.J., Josefsson, L.G., 1978. Precursors of three exported proteins in *Escherichia coli*. *Proc. Natl. Acad. Sci. U. S. A.* 75, 1209–1212.
- Ranjit, D.K., Jorgenson, M.A., Young, K.D., 2017. PBP1B Glycosyltransferase and Transpeptidase Activities Play Different Essential Roles during the De Novo Regeneration of Rod Morphology in *Escherichia coli*. *J. Bacteriol.* 199, e00612-16. <https://doi.org/10.1128/JB.00612-16>
- Rassam, P., Copeland, N.A., Birkholz, O., Tóth, C., Chavent, M., Duncan, A.L., Cross, S.J., Housden, N.G., Kaminska, R., Seger, U., Quinn, D.M., Garrod, T.J., Sansom, M.S.P., Piehler, J., Baumann, C.G., Kleanthous, C., 2015. Supramolecular assemblies underpin turnover of outer membrane proteins in bacteria. *Nature* 523, 333–336. <https://doi.org/10.1038/nature14461>
- Reichow, S.L., Korotkov, K.V., Hol, W.G.J., Gonen, T., 2010. Structure of the cholera toxin secretion channel in its closed state. *Nat. Struct. Mol. Biol.* 17, 1226–1232. <https://doi.org/10.1038/nsmb.1910>
- Rhodijs, V.A., Suh, W.C., Nonaka, G., West, J., Gross, C.A., 2005. Conserved and Variable Functions of the  $\sigma$ E Stress Response in Related Genomes. *PLOS Biol.* 4, e2. <https://doi.org/10.1371/journal.pbio.0040002>
- Ricci, D.P., Silhavy, T.J., 2019. Outer Membrane Protein Insertion by the  $\beta$ -barrel Assembly Machine. *EcoSal Plus.* <https://doi.org/10.1128/ecosalplus.ESP-0035-2018>
- Rice, L.B., 2008. Federal Funding for the Study of Antimicrobial Resistance in Nosocomial Pathogens: No ESKAPE. *J. Infect. Dis.* 197, 1079–1081. <https://doi.org/10.1086/533452>
- Ripoll-Rozada, J., Zunzunegui, S., de la Cruz, F., Arechaga, I., Cabezón, E., 2013. Functional Interactions of VirB11 Traffic ATPases with VirB4 and VirD4 Molecular Motors in Type IV Secretion Systems. *J. Bacteriol.* 195, 4195–4201. <https://doi.org/10.1128/JB.00437-13>
- Robert, V., Volokhina, E.B., Senf, F., Bos, M.P., Van Gelder, P., Tommassen, J., 2006. Assembly factor Omp85 recognizes its outer membrane protein substrates by a species-specific C-terminal motif. *PLoS Biol.* 4, e377. <https://doi.org/10.1371/journal.pbio.0040377>
- Rodríguez-Alonso, R., Létouart, J., Nguyen, V.S., Louis, G., Calabrese, A.N., Iorga, B.I., Radford, S.E., Cho, S.-H., Remaut, H., Collet, J.-F., 2020. Structural insight into the formation of lipoprotein- $\beta$ -barrel complexes. *Nat. Chem. Biol.* 16, 1019–1025. <https://doi.org/10.1038/s41589-020-0575-0>
- Roman-Hernandez, G., Peterson, J.H., Bernstein, H.D., 2014. Reconstitution of bacterial autotransporter assembly using purified components. *eLife* 3. <https://doi.org/10.7554/eLife.04234>
- Rouvière, P.E., Gross, C.A., 1996. SurA, a periplasmic protein with peptidyl-prolyl isomerase activity, participates in the assembly of outer membrane porins. *Genes Dev.* 10, 3170–3182. <https://doi.org/10.1101/gad.10.24.3170>
- Ruiz, N., Chng, S.-S., Hiniker, A., Kahne, D., Silhavy, T.J., 2010. Nonconsecutive disulfide bond formation in an essential integral outer membrane protein. *Proc. Natl. Acad. Sci.* 107, 12245–12250. <https://doi.org/10.1073/pnas.1007319107>
- Ruiz, N., Davis, R.M., Kumar, S., 2021. YhdP, TamB, and YdbH Are Redundant but Essential for Growth and Lipid Homeostasis of the Gram-Negative Outer Membrane. *mBio* 12, e02714-21. <https://doi.org/10.1128/mBio.02714-21>

- Ruiz, N., Kahne, D., Silhavy, T.J., 2006. Advances in understanding bacterial outer-membrane biogenesis. *Nat. Rev. Microbiol.* 4, 57–66. <https://doi.org/10.1038/nrmicro1322>
- Santajit, S., Indrawattana, N., 2016. Mechanisms of Antimicrobial Resistance in ESKAPE Pathogens. *BioMed Res. Int.* 2016. <https://doi.org/10.1155/2016/2475067>
- Sauri, A., Soprova, Z., Wickström, D., de Gier, J.-W., Van der Schors, R.C., Smit, A.B., Jong, W.S.P., Luirink, J. 2009, 2009. The Bam (Omp85) complex is involved in secretion of the autotransporter haemoglobin protease. *Microbiology* 155, 3982–3991. <https://doi.org/10.1099/mic.0.034991-0>
- Schägger, H., 2002. Respiratory chain supercomplexes of mitochondria and bacteria. *Biochim. Biophys. Acta BBA - Bioenerg.*, 12th European Bioenergetics Conference 1555, 154–159. [https://doi.org/10.1016/S0005-2728\(02\)00271-2](https://doi.org/10.1016/S0005-2728(02)00271-2)
- Schiffer, G., Höltje, J.-V., 1999. Cloning and Characterization of PBP 1C, a Third Member of the Multimodular Class A Penicillin-binding Proteins of *Escherichia coli* \*. *J. Biol. Chem.* 274, 32031–32039. <https://doi.org/10.1074/jbc.274.45.32031>
- Schiffrin, B., Brockwell, D.J., Radford, S.E., 2017a. Outer membrane protein folding from an energy landscape perspective. *BMC Biol.* 15, 123. <https://doi.org/10.1186/s12915-017-0464-5>
- Schiffrin, B., Calabrese, A.N., Devine, P.W.A., Harris, S.A., Ashcroft, A.E., Brockwell, D.J., Radford, S.E., 2016. Skp is a multivalent chaperone of outer-membrane proteins. *Nat. Struct. Mol. Biol.* 23, 786–793. <https://doi.org/10.1038/nsmb.3266>
- Schiffrin, B., Calabrese, A.N., Higgins, A.J., Humes, J.R., Ashcroft, A.E., Kalli, A.C., Brockwell, D.J., Radford, S.E., 2017b. Effects of Periplasmic Chaperones and Membrane Thickness on BamA-Catalyzed Outer-Membrane Protein Folding. *J. Mol. Biol.* 429, 3776–3792. <https://doi.org/10.1016/j.jmb.2017.09.008>
- Schiffrin, B., Machin, J.M., Karamanos, T.K., Zhuravleva, A., Brockwell, D.J., Radford, S.E., Calabrese, A.N., 2022. Dynamic interplay between the periplasmic chaperone SurA and the BAM complex in outer membrane protein folding. *Commun. Biol.* 5, 1–15. <https://doi.org/10.1038/s42003-022-03502-w>
- Schlapschy, M., Dommel, M.K., Hadian, K., Fogarasi, M., Korndörfer, I.P., Skerra, A., 2004. The periplasmic *E. coli* chaperone Skp is a trimer in solution: biophysical and preliminary crystallographic characterization 385, 137–143. <https://doi.org/10.1515/BC.2004.032>
- Seib, K.L., Haag, A.F., Oriente, F., Fantappiè, L., Borghi, S., Semchenko, E.A., Schulz, B.L., Ferlicca, F., Taddei, A.R., Giuliani, M.M., Pizza, M., Delany, I., 2019. The meningococcal vaccine antigen GNA2091 is an analogue of YraP and plays key roles in outer membrane stability and virulence. *FASEB J.* 33, 12324–12335. <https://doi.org/10.1096/fj.201900669R>
- Selkrig, J., Belousoff, M.J., Headey, S.J., Heinz, E., Shiota, T., Shen, H.-H., Beckham, S.A., Bamert, R.S., Phan, M.-D., Schembri, M.A., Wilce, M.C.J., Scanlon, M.J., Strugnell, R.A., Lithgow, T., 2015. Conserved features in TamA enable interaction with TamB to drive the activity of the translocation and assembly module. *Sci. Rep.* 5, 12905. <https://doi.org/10.1038/srep12905>
- Selkrig, J., Leyton, D.L., Webb, C.T., Lithgow, T., 2014. Assembly of  $\beta$ -barrel proteins into bacterial outer membranes. *Biochim. Biophys. Acta* 1843, 1542–1550. <https://doi.org/10.1016/j.bbamcr.2013.10.009>
- Selkrig, J., Mosbahi, K., Webb, C.T., Belousoff, M.J., Pery, A.J., Wells, T.J., Morris, F., Leyton, D.L., Totsika, M., Phan, M.-D., Celik, N., Kelly, M., Oates, C., Hartland, E.L., Robins-Browne, R.M., Ramarathnam, S.H., Purcell, A.W., Schembri, M.A., Strugnell, R.A., Henderson, I.R., Walker, D., Lithgow, T., 2012. Discovery of an archetypal protein transport system in bacterial outer membranes. *Nat. Struct. Mol. Biol.* 19, 506–510, S1. <https://doi.org/10.1038/nsmb.2261>
- Shapiro, A.B., Gu, R.-F., Gao, N., 2014. Dimerization of isolated *Pseudomonas aeruginosa* lipopolysaccharide transporter component LptA. *Biochem. Biophys. Res. Commun.* 450, 1327–1332. <https://doi.org/10.1016/j.bbrc.2014.06.138>
- Sharma, S., Zhou, R., Wan, L., Feng, S., Song, K., Xu, C., Li, Y., Liao, M., 2021. Mechanism of LolCDE as a molecular extruder of bacterial triacylated lipoproteins. *Nat. Commun.* 12, 4687. <https://doi.org/10.1038/s41467-021-24965-1>
- Shruthi, H., Madan Babu, M., Sankaran, K., 2010. TAT-Pathway-Dependent Lipoproteins as a Niche-Based Adaptation in Prokaryotes. *J. Mol. Evol.* 70, 359–370. <https://doi.org/10.1007/s00239-010-9334-2>
- Simon, S.M., 2018. Günter Blobel (1936–2018). *Cell* 173, 278–280. <https://doi.org/10.1016/j.cell.2018.03.047>
- Sklar, J.G., Wu, T., Gronenberg, L.S., Malinverni, J.C., Kahne, D., Silhavy, T.J., 2007. Lipoprotein SmpA is a component of the YaeT complex that assembles outer membrane proteins in *Escherichia coli*. *Proc. Natl. Acad. Sci.* 104, 6400–6405. <https://doi.org/10.1073/pnas.0701579104>
- Smith, V.F., Schwartz, B.L., Randall, L.L., Smith, R.D., 1996. Electrospray mass spectrometric investigation of the chaperone SecB. *Protein Sci. Publ. Protein Soc.* 5, 488–494.
- Sohlenkamp, C., Geiger, O., 2016. Bacterial membrane lipids: diversity in structures and pathways. *FEMS Microbiol. Rev.* 40, 133–159. <https://doi.org/10.1093/femsre/fuv008>
- Soltes, G.R., Martin, N.R., Park, E., Sutterlin, H.A., Silhavy, T.J., 2017. Distinctive Roles for Periplasmic Proteases in the Maintenance of Essential Outer Membrane Protein Assembly. *J. Bacteriol.* <https://doi.org/10.1128/JB.00418-17>
- Sommer, M.S., Daum, B., Gross, L.E., Weis, B.L.M., Mirus, O., Abram, L., Maier, U.-G., Kühlbrandt, W., Schleiff, E., 2011. Chloroplast Omp85 proteins change orientation during evolution. *Proc. Natl. Acad. Sci.* 108, 13841–13846. <https://doi.org/10.1073/pnas.1108626108>
- Sperandeo, P., Martorana, A.M., Polissi, A., 2017. Lipopolysaccharide biogenesis and transport at the outer membrane of Gram-negative bacteria. *Biochim. Biophys. Acta BBA - Mol. Cell Biol. Lipids, Bacterial Lipids* 1862, 1451–1460. <https://doi.org/10.1016/j.bbalip.2016.10.006>
- Steinberg, R., Knüpfner, L., Origi, A., Asti, R., Koch, H.-G., 2018. Co-translational protein targeting in bacteria. *FEMS Microbiol. Lett.* 365, fny095. <https://doi.org/10.1093/femsle/fny095>
- Stenberg, F., Chovanec, P., Maslen, S.L., Robinson, C.V., Ilag, L.L., Heijne, G. von, Daley, D.O., 2005. Protein Complexes of the *Escherichia coli* Cell Envelope. *J. Biol. Chem.* 280, 34409–34419. <https://doi.org/10.1074/jbc.M506479200>
- Storek, K.M., Vij, R., Sun, D., Smith, P.A., Koerber, J.T., Rutherford, S.T., 2019. The *Escherichia coli*  $\beta$ -Barrel Assembly Machinery Is Sensitized to Perturbations under High Membrane Fluidity. *J. Bacteriol.* 201. <https://doi.org/10.1128/jb.00517-18>
- Stubenrauch, C., Belousoff, M.J., Hay, I.D., Shen, H.-H., Lillington, J., Tuck, K.L., Peters, K.M., Phan, M.-D., Lo, A.W., Schembri, M.A., Strugnell, R.A., Waksman, G., Lithgow, T., 2016. Effective assembly of fimbriae in *Escherichia coli* depends on the translocation assembly module nanomachine. *Nat. Microbiol.* 1, 16064. <https://doi.org/10.1038/nmicrobiol.2016.64>
- Sugai, R., Takemae, K., Tokuda, H., Nishiyama, K., 2007. Topology Inversion of SecE Is Essential for Cytosolic SecA-dependent Stimulation of Protein Translocation. *J. Biol. Chem.* 282, 29540–29548. <https://doi.org/10.1074/jbc.M704716200>
- Suo, Y., Hardy, S.J.S., Randall, L.L., 2015. The Basis of Asymmetry in the SecA:SecB Complex. *J. Mol. Biol.* 427, 887–900. <https://doi.org/10.1016/j.jmb.2014.12.008>
- Szabady, R.L., Peterson, J.H., Skillman, K.M., Bernstein, H.D., 2005. An unusual signal peptide facilitates late steps in the biogenesis of a bacterial autotransporter. *Proc. Natl. Acad. Sci.* 102, 221–226. <https://doi.org/10.1073/pnas.0406055102>

- Takeda, K., Miyatake, H., Yokota, N., Matsuyama, S., Tokuda, H., Miki, K., 2003. Crystal structures of bacterial lipoprotein localization factors, LolA and LolB. *EMBO J.* 22, 3199–3209. <https://doi.org/10.1093/emboj/cdg324>
- Tan, B.K., Bogdanov, M., Zhao, J., Dowhan, W., Raetz, C.R.H., Guan, Z., 2012. Discovery of a cardiolipin synthase utilizing phosphatidylethanolamine and phosphatidylglycerol as substrates. *Proc. Natl. Acad. Sci.* 109, 16504–16509. <https://doi.org/10.1073/pnas.1212797109>
- Tanaka, Y., Sugano, Y., Takemoto, M., Mori, T., Furukawa, A., Kusakizako, T., Kumazaki, K., Kashima, A., Ishitani, R., Sugita, Y., Nureki, O., Tsukazaki, T., 2015. Crystal Structures of SecYEG in Lipidic Cubic Phase Elucidate a Precise Resting and a Peptide-Bound State. *Cell Rep.* 13, 1561–1568. <https://doi.org/10.1016/j.celrep.2015.10.025>
- Terada, M., Kuroda, T., Matsuyama, S., Tokuda, H., 2001. Lipoprotein Sorting Signals Evaluated as the LolA-dependent Release of Lipoproteins from the Cytoplasmic Membrane of *Escherichia coli* \*. *J. Biol. Chem.* 276, 47690–47694. <https://doi.org/10.1074/jbc.M109307200>
- Thong, S., Ercan, B., Torta, F., Fong, Z.Y., Wong, H.Y.A., Wenk, M.R., Chng, S.-S., 2016. Defining key roles for auxiliary proteins in an ABC transporter that maintains bacterial outer membrane lipid asymmetry. *eLife* 5, e19042. <https://doi.org/10.7554/eLife.19042>
- Tomasek, D., Rawson, S., Lee, J., Wzorek, J.S., Harrison, S.C., Li, Z., Kahne, D., 2020. Structure of a nascent membrane protein as it folds on the BAM complex. *Nature* 583, 473–478. <https://doi.org/10.1038/s41586-020-2370-1>
- Tommassen, J., 2010. Assembly of outer-membrane proteins in bacteria and mitochondria. *Microbiol. Read. Engl.* 156, 2587–2596. <https://doi.org/10.1099/mic.0.042689-0>
- Topping, T.B., Woodbury, R.L., Diamond, D.L., Hardy, S.J.S., Randall, L.L., 2001. Direct Demonstration That Homotetrameric Chaperone SecB Undergoes a Dynamic Dimer-Tetramer Equilibrium. *J. Biol. Chem.* 276, 7437–7441. <https://doi.org/10.1074/jbc.M009584200>
- Tsang, M.-J., Yakhnina, A.A., Bernhardt, T.G., 2017. NlpD links cell wall remodeling and outer membrane invagination during cytokinesis in *Escherichia coli*. *PLoS Genet.* 13, e1006888. <https://doi.org/10.1371/journal.pgen.1006888>
- Tschantz, W.R., Sung, M., Delgado-Partin, V.M., Dalbey, R.E., 1993. A serine and a lysine residue implicated in the catalytic mechanism of the *Escherichia coli* leader peptidase. *J. Biol. Chem.* 268, 27349–27354.
- Tsirigotaki, A., Geyter, J.D., Šoštarić, N., Economou, A., Karamanou, S., 2017. Protein export through the bacterial Sec pathway. *Nat. Rev. Microbiol.* 15, 21–36. <https://doi.org/10.1038/nrmicro.2016.161>
- Tsukazaki, T., Mori, H., Fukai, S., Ishitani, R., Mori, T., Dohmae, N., Perederina, A., Sugita, Y., Vassilyev, D.G., Ito, K., Nureki, O., 2008. Conformational transition of Sec machinery inferred from bacterial SecYE structures. *Nature* 455, 988–991. <https://doi.org/10.1038/nature07421>
- Typas, A., Banzhaf, M., Gross, C.A., Vollmer, W., 2012. From the regulation of peptidoglycan synthesis to bacterial growth and morphology. *Nat. Rev. Microbiol.* 10, 123–136. <https://doi.org/10.1038/nrmicro2677>
- Uehara, T., Parzych, K.R., Dinh, T., Bernhardt, T.G., 2010. Daughter cell separation is controlled by cytokinetic ring-activated cell wall hydrolysis. *EMBO J.* 29, 1412–1422. <https://doi.org/10.1038/emboj.2010.36>
- Unnikrishnan, M., Constantinidou, C., Palmer, T., Pallen, M.J., 2017. The Enigmatic Esx Proteins: Looking Beyond Mycobacteria. *Trends Microbiol.* 25, 192–204. <https://doi.org/10.1016/j.tim.2016.11.004>
- Ursell, T.S., Trepagnier, E.H., Huang, K.C., Theriot, J.A., 2012. Analysis of Surface Protein Expression Reveals the Growth Pattern of the Gram-Negative Outer Membrane. *PLOS Comput. Biol.* 8, e1002680. <https://doi.org/10.1371/journal.pcbi.1002680>
- Vermassen, A., Leroy, S., Talon, R., Provot, C., Popowska, M., Desvaux, M., 2019. Cell Wall Hydrolases in Bacteria: Insight on the Diversity of Cell Wall Amidases, Glycosidases and Peptidases Toward Peptidoglycan. *Front. Microbiol.* 10.
- Vertommen, D., Ruiz, N., Leverrier, P., Silhavy, T.J., Collet, J.-F., 2009. Characterization of the role of the *Escherichia coli* periplasmic chaperone SurA using differential proteomics. *PROTEOMICS* 9, 2432–2443. <https://doi.org/10.1002/pmic.200800794>
- Vigouroux, A., Cordier, B., Aristov, A., Alvarez, L., Özbaykal, G., Chaze, T., Oldewurtel, E.R., Matondo, M., Cava, F., Bikard, D., van Teeffelen, S., 2020. Class-A penicillin binding proteins do not contribute to cell shape but repair cell-wall defects. *eLife* 9, e51998. <https://doi.org/10.7554/eLife.51998>
- Vischer, N.O.E., Verheul, J., Postma, M., van den Berg van Saparoea, B., Galli, E., Natale, P., Gerdes, K., Luirink, J., Vollmer, W., Vicente, M., den Blaauwen, T., 2015. Cell age dependent concentration of *Escherichia coli* divisome proteins analyzed with ImageJ and ObjectJ. *Front. Microbiol.* 6.
- Vogeley, L., El Arnaout, T., Bailey, J., Stansfeld, P.J., Boland, C., Caffrey, M., 2016. Structural basis of lipoprotein signal peptidase II action and inhibition by the antibiotic globomycin. *Science* 351, 876–880. <https://doi.org/10.1126/science.aad3747>
- Vollmer, W., Bertsche, U., 2008. Murein (peptidoglycan) structure, architecture and biosynthesis in *Escherichia coli*. *Biochim. Biophys. Acta BBA - Biomembr.* Structural proteomics of the cell envelope of Gram-negative bacteria 1778, 1714–1734. <https://doi.org/10.1016/j.bbamem.2007.06.007>
- Voulhoux, R., Ball, G., Ize, B., Vasil, M.L., Lazdunski, A., Wu, L.-F., Filloux, A., 2001. Involvement of the twin-arginine translocation system in protein secretion via the type II pathway. *EMBO J.* 20, 6735–6741. <https://doi.org/10.1093/emboj/20.23.6735>
- Voulhoux, R., Bos, M.P., Geurtsen, J., Mols, M., Tommassen, J., 2003. Role of a Highly Conserved Bacterial Protein in Outer Membrane Protein Assembly. *Science* 299, 262–265. <https://doi.org/10.1126/science.1078973>
- Wall, E.A., Majdalani, N., Gottesman, S., 2020. IgaA negatively regulates the Rcs Phosphorelay via contact with the RcsD Phosphotransfer Protein. *PLoS Genet.* 16, e1008610. <https://doi.org/10.1371/journal.pgen.1008610>
- Walsh, N.P., Alba, B.M., Bose, B., Gross, C.A., Sauer, R.T., 2003. OMP Peptide Signals Initiate the Envelope-Stress Response by Activating DegS Protease via Relief of Inhibition Mediated by Its PDZ Domain. *Cell* 113, 61–71. [https://doi.org/10.1016/S0092-8674\(03\)00203-4](https://doi.org/10.1016/S0092-8674(03)00203-4)
- Wang, X., Peterson, J.H., Bernstein, H.D., 2021. Bacterial Outer Membrane Proteins Are Targeted to the Bam Complex by Two Parallel Mechanisms. *mBio*. <https://doi.org/10.1128/mBio.00597-21>
- Wang, X., Quinn, P.J., 2010. Lipopolysaccharide: Biosynthetic pathway and structure modification. *Prog. Lipid Res.* 49, 97–107. <https://doi.org/10.1016/j.plipres.2009.06.002>
- Wang, Y., Wang, R., Jin, F., Liu, Y., Yu, J., Fu, X., Chang, Z., 2016. A Supercomplex Spanning the Inner and Outer Membranes Mediates the Biogenesis of  $\beta$ -Barrel Outer Membrane Proteins in Bacteria \*. *J. Biol. Chem.* 291, 16720–16729. <https://doi.org/10.1074/jbc.M115.710715>
- Wang, Z., Fan, G., Hryc, C.F., Blaza, J.N., Serysheva, I.I., Schmid, M.F., Chiu, W., Luisi, B.F., Du, D., 2017. An allosteric transport mechanism for the AcrAB-TolC multidrug efflux pump. *eLife* 6, e24905. <https://doi.org/10.7554/eLife.24905>
- Webb, C.T., Selkrig, J., Perry, A.J., Noinaj, N., Buchanan, S.K., Lithgow, T., 2012. Dynamic Association of BAM Complex Modules Includes Surface Exposure of the Lipoprotein BamC. *J. Mol. Biol.* 422, 545–555. <https://doi.org/10.1016/j.jmb.2012.05.035>



- Wells, T.J., Tree, J.J., Ulett, G.C., Schembri, M.A., 2007. Autotransporter proteins: novel targets at the bacterial cell surface. *FEMS Microbiol. Lett.* 274, 163–172. <https://doi.org/10.1111/j.1574-6968.2007.00833.x>
- Welte, W., Nestel, U., Wacker, T., Diederichs, K., 1995. Structure and function of the porin channel. *Kidney Int.* 48, 930–940. <https://doi.org/10.1038/ki.1995.374>
- Werner, J., Misra, R., 2005. YaeT (Omp85) affects the assembly of lipid-dependent and lipid-independent outer membrane proteins of *Escherichia coli*. *Mol. Microbiol.* 57, 1450–1459. <https://doi.org/10.1111/j.1365-2958.2005.04775.x>
- Wilkinson, S.G., 1996. Bacterial lipopolysaccharides—Themes and variations. *Prog. Lipid Res.* 35, 283–343. [https://doi.org/10.1016/S0163-7827\(96\)00004-5](https://doi.org/10.1016/S0163-7827(96)00004-5)
- Wolfe, P.B., Wickner, W., Goodman, J.M., 1983. Sequence of the leader peptidase gene of *Escherichia coli* and the orientation of leader peptidase in the bacterial envelope. *J. Biol. Chem.* 258, 12073–12080.
- Wu, R., Bakelar, J.W., Lundquist, K., Zhang, Z., Kuo, K.M., Ryoo, D., Pang, Y.T., Sun, C., White, T., Klose, T., Jiang, W., Gumbart, J.C., Noinaj, N., 2021. Plasticity within the barrel domain of BamA mediates a hybrid-barrel mechanism by BAM. *Nat. Commun.* 12, 7131. <https://doi.org/10.1038/s41467-021-27449-4>
- Wu, R., Stephenson, R., Gichaba, A., Noinaj, N., 2020. The big BAM theory: An open and closed case? *Biochim. Biophys. Acta BBA - Biomembr., Molecular biophysics of membranes and membrane proteins* 1862, 183062. <https://doi.org/10.1016/j.bbmem.2019.183062>
- Wu, T., Malinverni, J., Ruiz, N., Kim, S., Silhavy, T.J., Kahne, D., 2005. Identification of a Multicomponent Complex Required for Outer Membrane Biogenesis in *Escherichia coli*. *Cell* 121, 235–245. <https://doi.org/10.1016/j.cell.2005.02.015>
- Xiao, L., Han, L., Li, B., Zhang, M., Zhou, H., Luo, Q., Zhang, X., Huang, Y., 2021. Structures of the  $\beta$ -barrel assembly machine recognizing outer membrane protein substrates. *FASEB J.* 35, e21207. <https://doi.org/10.1096/fj.202001443RR>
- Xu, X., Wang, S., Hu, Y.-X., McKay, D.B., 2007. The Periplasmic Bacterial Molecular Chaperone SurA Adapts its Structure to Bind Peptides in Different Conformations to Assert a Sequence Preference for Aromatic Residues. *J. Mol. Biol.* 373, 367–381. <https://doi.org/10.1016/j.jmb.2007.07.069>
- Yamaguchi, K., Yu, F., Inouye, M., 1988. A single amino acid determinant of the membrane localization of lipoproteins in *E. coli*. *Cell* 53, 423–432. [https://doi.org/10.1016/0092-8674\(88\)90162-6](https://doi.org/10.1016/0092-8674(88)90162-6)
- Yamamoto, K., Ishihama, A., 2006. Characterization of Copper-Inducible Promoters Regulated by CpxA/CpxR in *Escherichia coli*. *Biosci. Biotechnol. Biochem.* 70, 1688–1695. <https://doi.org/10.1271/bbb.60024>
- Yan, Z., Hussain, S., Wang, X., Bernstein, H.D., Bardwell, J.C.A., 2019. Chaperone OsmY facilitates the biogenesis of a major family of autotransporters. *Mol. Microbiol.* 112, 1373–1387. <https://doi.org/10.1111/mmi.14358>
- Yeats, C., Bateman, A., 2003. The BON domain: a putative membrane-binding domain. *Trends Biochem. Sci.* 28, 352–355. [https://doi.org/10.1016/S0968-0004\(03\)00115-4](https://doi.org/10.1016/S0968-0004(03)00115-4)
- Yeow, J., Chng, S.-S., 2022. Of zones, bridges and chaperones – phospholipid transport in bacterial outer membrane assembly and homeostasis. *Microbiology* 168, 001177. <https://doi.org/10.1099/mic.0.001177>
- Yeow, J., Tan, K.W., Holdbrook, D.A., Chong, Z.-S., Marzinek, J.K., Bond, P.J., Chng, S.-S., 2018. The architecture of the OmpC–MlaA complex sheds light on the maintenance of outer membrane lipid asymmetry in *Escherichia coli*. *J. Biol. Chem.* 293, 11325–11340. <https://doi.org/10.1074/jbc.RA118.002441>
- Young, T.S., Ahmad, I., Yin, J.A., Schultz, P.G., 2010. An Enhanced System for Unnatural Amino Acid Mutagenesis in *E. coli*. *J. Mol. Biol.* 395, 361–374. <https://doi.org/10.1016/j.jmb.2009.10.030>
- Zhang, S., Cheng, Y., Ma, J., Wang, Y., Chang, Z., Fu, X., 2019. Degp degrades a wide range of substrate proteins in *Escherichia coli* under stress conditions. *Biochem. J.* 476, 3549–3564. <https://doi.org/10.1042/BCJ20190446>
- Zimmermann, R., Watts, C., Wickner, W., 1982. The biosynthesis of membrane-bound M13 coat protein. Energetics and assembly intermediates. *J. Biol. Chem.* 257, 6529–6536.

# Lipoprotein DolP supports proper folding of BamA in the bacterial outer membrane promoting fitness upon envelope stress

David Ranava<sup>1†</sup>, Yiyang Yang<sup>1†</sup>, Luis Orenday-Tapia<sup>1†</sup>, François Rousset<sup>2</sup>, Catherine Turlan<sup>1</sup>, Violette Morales<sup>1</sup>, Lun Cui<sup>2</sup>, Cyril Moulin<sup>1</sup>, Carine Froment<sup>3</sup>, Gladys Munoz<sup>1</sup>, Jérôme Rech<sup>1</sup>, Julien Marcoux<sup>3</sup>, Anne Caumont-Sarcos<sup>1</sup>, Cécile Albenne<sup>1</sup>, David Bikard<sup>2</sup>, Raffaele Ieva<sup>1\*</sup>

<sup>1</sup>Laboratoire de Microbiologie et Génétique Moléculaires (LMGM), Centre de Biologie Intégrative (CBI), Université de Toulouse, CNRS, UPS, Toulouse, France; <sup>2</sup>Synthetic Biology Group, Microbiology Department, Institut Pasteur, Paris, France; <sup>3</sup>Institut de Pharmacologie et de Biologie Structurale (IPBS), Université de Toulouse, CNRS, UPS, Toulouse, France

**Abstract** In Proteobacteria, integral outer membrane proteins (OMPs) are crucial for the maintenance of the envelope permeability barrier to some antibiotics and detergents. In Enterobacteria, envelope stress caused by unfolded OMPs activates the sigmaE ( $\sigma^E$ ) transcriptional response.  $\sigma^E$  upregulates OMP biogenesis factors, including the  $\beta$ -barrel assembly machinery (BAM) that catalyses OMP folding. Here we report that DolP (formerly YraP), a  $\sigma^E$ -upregulated and poorly understood outer membrane lipoprotein, is crucial for fitness in cells that undergo envelope stress. We demonstrate that DolP interacts with the BAM complex by associating with outer membrane-assembled BamA. We provide evidence that DolP is important for proper folding of BamA that overaccumulates in the outer membrane, thus supporting OMP biogenesis and envelope integrity. Notably, mid-cell recruitment of DolP had been linked to regulation of septal peptidoglycan remodelling by an unknown mechanism. We now reveal that, during envelope stress, DolP loses its association with the mid-cell, thereby suggesting a mechanistic link between envelope stress caused by impaired OMP biogenesis and the regulation of a late step of cell division.

\*For correspondence: raffaele.ieva@univ-tlse3.fr

†These authors contributed equally to this work

**Competing interests:** The authors declare that no competing interests exist.

**Funding:** See page 21

**Received:** 24 February 2021

**Accepted:** 04 April 2021

**Published:** 13 April 2021

**Reviewing editor:** Bavesh D Kana, University of the Witwatersrand, South Africa

© Copyright Ranava et al. This article is distributed under the terms of the [Creative Commons Attribution License](https://creativecommons.org/licenses/by/4.0/), which permits unrestricted use and redistribution provided that the original author and source are credited.

## Introduction

The outer membrane (OM) of Gram-negative bacteria forms a protective barrier against harmful compounds, including several antimicrobials. This envelope structure surrounds the inner membrane and the periplasm that contains the peptidoglycan, a net-like structure made of glycan chains and interconnecting peptides. During cell division, the multi-layered envelope structure is remodelled by the divisome machinery (*den Blaauwen et al., 2017*). At a late step of division, septal peptidoglycan synthesized by the divisome undergoes splitting, initiating the formation of the new poles of adjacent daughter cells. Finally, remodelling of the OM barrier completes formation of the new poles in the cell offspring. The mechanisms by which cells coordinate OM remodelling with peptidoglycan splitting, preserving the permeability barrier of this protective membrane, are ill-defined (*Egan et al., 2020*).

Integral outer membrane proteins (OMPs) are crucial to maintain the OM permeability barrier. OMPs fold into amphipathic  $\beta$ -barrel structures that span the OM and carry out a variety of tasks. Porins are OMPs that facilitate the diffusion of small metabolites. Other OMPs function as cofactor transporters, secretory channels, or machineries for the assembly of proteins and lipopolysaccharide

(LPS), a structural component of the external OM leaflet that prevents the diffusion of noxious chemicals (Calmettes et al., 2015; Nikaido, 2003). The  $\beta$ -barrel assembly machinery (BAM) is a multi-subunit complex that mediates the folding and membrane insertion of OMPs transiting through the periplasm (Ranava et al., 2018; Schiffrin et al., 2017). The essential and evolutionarily conserved BamA insertase subunit is an OMP consisting of an amino (N)-terminal periplasmic domain made of polypeptide transport-associated (POTRA or P) motifs and a carboxy (C)-terminal 16-stranded  $\beta$ -barrel membrane domain that catalyses OMP biogenesis (Ranava et al., 2018). The flexible pairing of  $\beta$ -strands 1 and 16 of the BamA  $\beta$ -barrel controls a lateral gate connecting the interior of the barrel towards the surrounding lipid bilayer (Bakelar et al., 2016; Gu et al., 2016; Iadanza et al., 2016; Noinaj et al., 2013). Conformational dynamics of the BamA  $\beta$ -barrel region proximal to the lateral gate is thought to locally increase the entropy of the surrounding lipid bilayer (Doerner and Sousa, 2017; Noinaj et al., 2013) and to assist the insertion of nascent OMPs into the OM (Doyle and Bernstein, 2019; Gu et al., 2016; Tomasek et al., 2020). The N-terminal periplasmic portion of BamA from the enterobacterium *Escherichia coli* contains five POTRA motifs that serve as a scaffold for four lipoproteins, BamBCDE, which assist BamA during OMP biogenesis (Kim et al., 2007; Sklar et al., 2007; Wu et al., 2005). The N-terminal POTRA motif is also the docking site for the periplasmic chaperone SurA (Bennion et al., 2010). Together with the chaperones Skp and DegP, SurA contributes to monitor unfolded OMPs transported into the periplasm by the inner membrane general secretory (Sec) apparatus (Crane and Randall, 2017; Rizzitello et al., 2001).

Defective OMP assembly causes periplasmic accumulation of unfolded protein transport intermediates. This envelope stress is signalled across the inner membrane to induce the sigmaE ( $\sigma^E$ )-mediated transcriptional response (Walsh et al., 2003). In the absence of a stress,  $\sigma^E$  is sequestered by the inner membrane-spanning RseA factor. By-products of misfolded OMP turnover activate degradation of RseA, liberating  $\sigma^E$  (Ades, 2008). The  $\sigma^E$  response copes with stress (i) by upregulating genes involved in OMP biogenesis, such as the *bam* genes (Rhodius et al., 2006), and (ii) by lowering the OMP biogenesis burden via a post-transcriptional mechanism (Guillier et al., 2006). Whereas  $\sigma^E$  is essential (De Las Peñas et al., 1997a), a tight control of cytosolic  $\sigma^E$  availability is necessary for optimal cell fitness and to prevent a potentially detrimental effect on the envelope (De Las Peñas et al., 1997b; Missiakas et al., 1997; Nicoloff et al., 2017). Remarkably, the functions of a number of genes upregulated by  $\sigma^E$  remain unknown. Among those, *dolP/yraP* (recently renamed division and OM stress-associated lipid-binding protein) encodes an ~20 kDa OM-anchored lipoprotein largely conserved in  $\gamma$  and  $\beta$  proteobacteria that is crucial for OM integrity and pathogenicity (Bos et al., 2014; Bryant et al., 2020; Morris et al., 2018; Onufryk et al., 2005; Seib et al., 2019). DolP consists of two consecutive BON (bacterial OsmY and nodulation) domains, a family of conserved folding motifs named after the osmotic stress-induced periplasmic protein OsmY (Yeats and Bateman, 2003). During a late step of cell division, DolP localizes at the mid-cell where it contributes to the regulation of septal peptidoglycan splitting by an unknown mechanism (Tsang et al., 2017). A recent structural analysis of DolP reveals a phospholipid-binding site in the C-terminal BON domain (Bryant et al., 2020). It remains unclear, however, why DolP is upregulated in response to  $\sigma^E$  activation and how this lipoprotein helps coping with envelope stress.

By using a genome-wide synthetic-defect screen, we show that DolP is particularly important when the BAM complex is defective and under envelope stress conditions. We demonstrate that DolP interacts with the BAM complex in the OM and supports the proper folding and functioning of the BamA subunit. Taken together our results indicate that DolP functions as a fitness factor during activation of the  $\sigma^E$  response and that BamA is a molecular target of the fitness role of DolP. We also reveal that, upon envelope stress, DolP loses its association with the mid-cell, thus suggesting a possible link between the envelope stress response and septal peptidoglycan hydrolysis during a late step of cell division.

## Results

### A genome-wide synthetic-defect screen identifies *dolP* genetic interactions

The mutant allele  $\Delta dolP::kan$  (Baba et al., 2006) was introduced into *E. coli* BW25113 by P1 transduction. The resulting  $\Delta dolP$  strain grew normally on LB medium, but was highly susceptible to

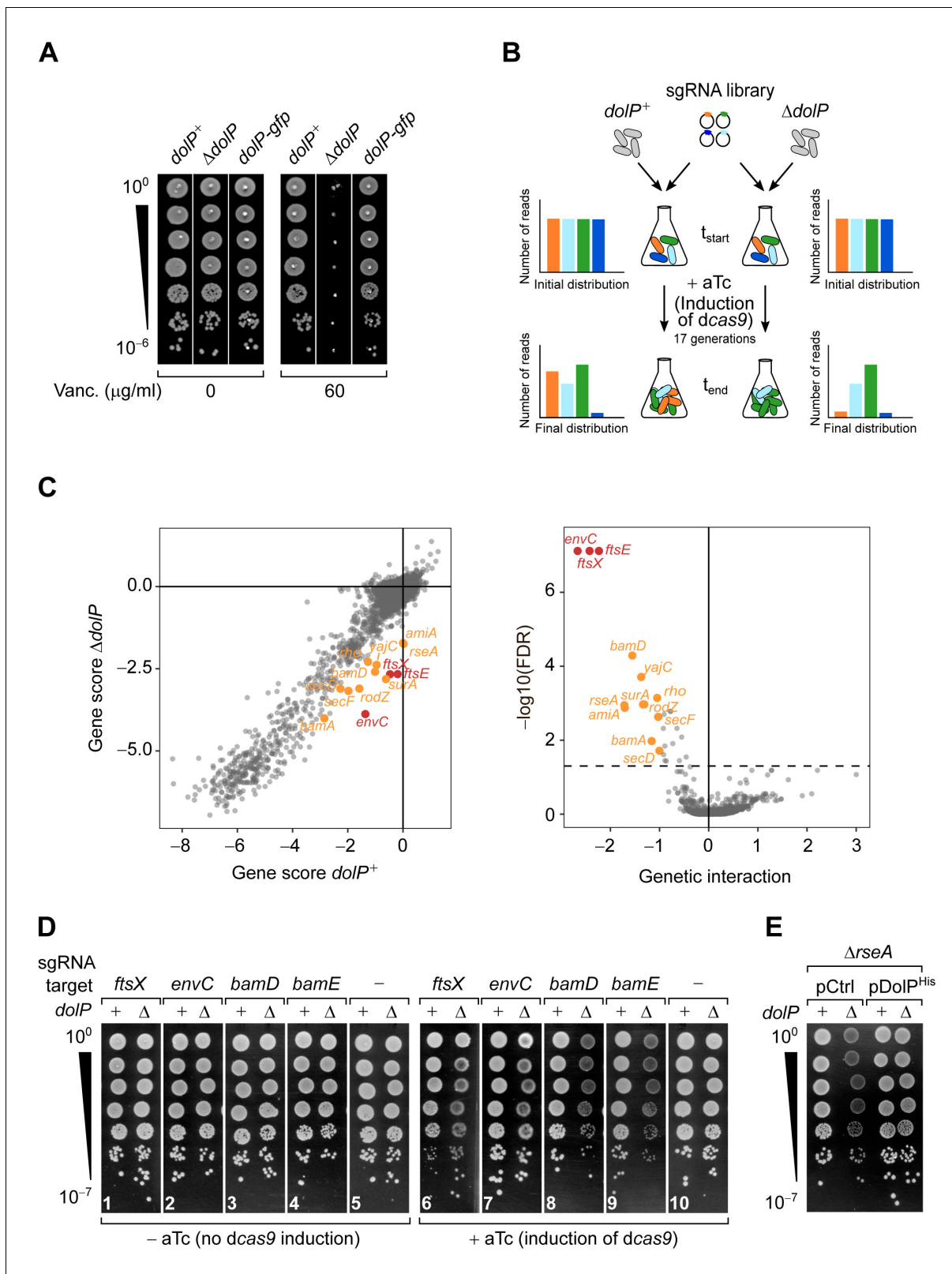


**Figure 1.** Genome-wide screen of *doIP* genetic interactions. (A) The deletion of *doIP* impairs OM integrity. The indicated strains were serially diluted and spotted onto LB agar plates lacking or supplemented with 60  $\mu$ g/ml vancomycin as indicated. (B) Schematic representation of the CRISPR-based gene silencing approach. LC-E75 (*doIP*<sup>+</sup>) or its  $\Delta$ *doIP* derivative strain, both carrying *dcas9* under the control of an anhydrotetracycline (aTc)-inducible promoter in their chromosome were transformed with a library of plasmids encoding gene-specific sgRNAs. The library covers any *E. coli* MG1655

Figure 1 continued on next page

Figure 1 continued

genetic features with an average of five sgRNAs per gene. Pooled transformed cells were cultured to early exponential phase prior to plasmid extraction and quantitative Illumina sequencing to assess the initial distribution of sgRNA constructs in each culture ( $t_{\text{start}}$ ). Upon addition of 1  $\mu\text{M}$  aTc to induce sgRNA-mediated targeting of *dcas9* for approximately 17 generations, samples of cells from each culture were newly subjected to plasmid extraction and Illumina sequencing to determine the final distribution of sgRNA constructs ( $t_{\text{end}}$ ). (C) Left: Comparison of gene scores obtained in *dolP*<sup>+</sup> and  $\Delta dolP$  screens. The log<sub>2</sub> fold-change (log<sub>2</sub>FC) between  $t_{\text{end}}$  and  $t_{\text{start}}$  calculated for each sgRNAs (Figure 1—figure supplement 2B) was grouped by gene target, and their median was used to derive fitness gene scores (see also Figure 1—source data 1 and 2). Right: Volcano plot of the *dolP* genetic interaction scores. The x-axis shows a genetic interaction score calculated for each gene based on the minimum hypergeometric (mHG) test conducted on the ranked difference of sgRNA-specific log<sub>2</sub>FC values between the  $\Delta dolP$  and the *dolP*<sup>+</sup> screens. The y-axis shows the log<sub>10</sub> of the false discovery rate (FDR) of the test. The dashed line shows FDR = 0.05. In both panels, genes highlighted in orange have FDR < 0.05 and GI > 1 whereas genes highlighted in red have FDR < 0.05 and GI > 2. (D and E) Validation of the genetic interactions determined in (C). (D) LC-E75 (*dolP*<sup>+</sup>) or its  $\Delta dolP$  derivative strain expressing sgRNAs that target the indicated genes were serially diluted and spotted on LB agar lacking or supplemented with aTc to induce expression of *dcas9*, as indicated. (E) BW25113 derivative cells deleted of *rseA* or both *rseA* and *dolP* were transformed with an empty vector (pCtrl) or a plasmid encoding DolP (pDolP<sup>His</sup>). Ectopic expression of DolP<sup>His</sup> was driven by the leaky transcriptional activity of P<sub>trc</sub> in the absence of IPTG. (D and E) Ten-fold serial dilutions of the indicated transformants were spotted on LB agar.

The online version of this article includes the following source data and figure supplement(s) for figure 1:

**Source data 1.** Log<sub>2</sub>FC values of sgRNAs in the screens conducted with wild-type or  $\Delta dolP$  cells.

**Source data 2.** Genetic interaction scores.

**Figure supplement 1.** The deletion of *dolP* severely impairs growth in the presence of vancomycin.

**Figure supplement 2.** Reproducibility of the CRISPRi screens and ontology analysis of gene hits.

vancomycin (Figure 1A and Figure 1—figure supplement 1A). This antibiotic is normally excluded from the OM of wild-type cells but inhibits growth of cells lacking OMP biogenesis factors such as *skp* and *surA* (Figure 1—figure supplement 1B). The expression of C-terminally tagged DolP protein variants in place of its wild-type form restored vancomycin resistance (Figure 1A and Figure 1—figure supplement 1C). This result supports the notion that DolP is important for envelope integrity (Bos et al., 2014; Onufryk et al., 2005; Seib et al., 2019; Tsang et al., 2017). However, the role of DolP during envelope stress remains poorly understood.

To gain insights into the role of DolP, we subjected  $\Delta dolP$  cells to a genome-wide synthetic-defect screen exploiting a Clustered Regularly Interspaced Short Palindromic Repeat interference (CRISPRi) approach. Targeting of the catalytically inactive dCas9 nuclease by gene-specific single guide RNAs (sgRNAs) enables gene repression (Figure 1B; Cui et al., 2018). The EcoWG1 sgRNA library targeting the entire genome of *E. coli* MG1655 (Calvo-Villamañán et al., 2020) was introduced into isogenic  $\Delta dolP$  or *dolP*<sup>+</sup> MG1655-derivative strains. The fitness of each knockdown was then compared in these backgrounds by deep-sequencing of the sgRNA library after ~17 growth generations. The outputs obtained from two independent tests were highly reproducible (Figure 1—figure supplement 2A). A strong fitness defect in the  $\Delta dolP$  strain was caused by the targeting of *envC*, followed by the targeting of *ftsX* and *ftsE* (Figure 1C, Figure 1—figure supplement 2B, Figure 1—source data 1 and 2). A validation growth test showed that the synthetic fitness defect observed for  $\Delta dolP$  cells was caused by dCas9-dependent silencing of *ftsX* and *envC* (Figure 1D, panels 6 and 7). The ABC transporter-like complex FtsE/FtsX has multiple roles in organizing the cell divisome, including the recruitment of periplasmic EnvC, a LytM domain-containing factor required for the activation of amidases that hydrolyse septal peptidoglycan (Pichoff et al., 2019). This peptidoglycan remodelling reaction is mediated by two sets of highly controlled and partially redundant amidases, AmiA/AmiB and AmiC (Heidrich et al., 2001; Uehara et al., 2009). Whereas AmiA and AmiB are activated at the inner membrane/peptidoglycan interface by the coordinated action of FtsE/FtsX and EnvC, activation of AmiC requires the OM-anchored LytM domain-containing lipoprotein NlpD (Uehara et al., 2010; Yang et al., 2011). Under laboratory conditions, the activity of only one of these two pathways is sufficient for septal peptidoglycan splitting, whereas inhibition of both pathways leads to the formation of chains of partially divided cells, i.e., cells that have begun to divide but that are blocked at the step of septal peptidoglycan splitting (Uehara et al., 2010). A recent report showed that *dolP* is necessary for completion of septal peptidoglycan splitting and cell separation when the AmiA/AmiB pathway is inactive, somehow linking DolP to AmiC activation (Tsang et al., 2017). Thus, the reduced fitness caused by silencing of *envC*, *ftsE*, or *ftsX* in  $\Delta dolP$  cells (Figure 1C) can be explained by the impaired cell separation when both the AmiA/AmiB and

the AmiC pathways are not active. In keeping with this notion, *amiA* itself was found among the negative fitness hits of the CRISPRi screen (**Figure 1C**). The *amiB* gene was not a hit (**Figure 1—source data 2**) probably because AmiA is sufficient to split septal peptidoglycan in the absence of other amidases (**Chung et al., 2009**).

Most importantly, the CRISPRi approach identified novel *dolP*-genetic interactions that had a score similar to that obtained for *amiA* (**Figure 1C**). These included an interaction with *rseA*, encoding the inner membrane  $\sigma^E$ -sequestering factor, as well as with *bamD*, encoding an essential subunit of the BAM complex (**Malinverni et al., 2006; Onufryk et al., 2005**). In accordance with the screen output, a serial dilution assay confirmed that CRISPRi reducing the levels of BamD or of its stoichiometric interactor BamE (**Figure 1—figure supplement 2D**) causes a fitness defect in cells lacking DolP (**Figure 1D**, panels 8 and 9). In addition, the interaction of *dolP* with *rseA* was confirmed in the genetic background of a BW25113 strain (**Figure 1E**). Further genes, involved in OMP biogenesis and more generally in protein secretion, had a lower interaction score (**Figure 1—source data 2 and Figure 1—figure supplement 2C**) and are highlighted in **Figure 1C**. These comprise *bamA*, the OMP chaperone-encoding gene *surA*, as well as the genes encoding the Sec ancillary complex SecDF-YajC that contributes to efficient secretion of proteins including OMPs (**Crane and Randall, 2017**) and that was shown to interact with the BAM complex (**Alvira et al., 2020; Carlson et al., 2019**). Collectively, the results of the CRISPRi screen indicate that the function of DolP is particularly critical for cell fitness upon inactivation of septal peptidoglycan hydrolysis by AmiA, as well as when the BAM complex is defective or the assembly of proteins in the OM is impaired.

### DolP improves cell fitness when the OM undergoes stress

The newly identified genetic interaction between *dolP* and *bamD* (**Figure 1C and D**) points to a possible role of DolP in OM biogenesis. However, the overall protein profile of the crude envelope fraction was not affected by the deletion of *dolP* (**Figure 2—figure supplement 1A**, lanes 1–4). OMPs such as the abundant OmpA and OmpC (**Li et al., 2014**) can be recognized by the characteristic heat-modifiable migration patterns of their  $\beta$ -barrel domains when separated by SDS-PAGE (**Figure 2—figure supplement 1A–C; Nakamura and Mizushima, 1976**). The envelope protein profiles were not affected also when *dolP* was deleted in cells lacking one of the OMP periplasmic chaperones Skp or DegP (**Figure 2—figure supplement 1A**, lanes 5–12). Furthermore, the levels of BamA and BamE, which are susceptible of  $\sigma^E$ -mediated regulation, were not increased in  $\Delta dolP$  cells (**Figure 2A**). Taken together, these observations suggest that if DolP plays a role in OM biogenesis, this would probably be indirectly related to the process of OMP assembly.

To further test the role of DolP under envelope stress conditions, we deleted *dolP* in a strain lacking *bamB*, which was identified with a lower genetic score by the CRISPRi approach (**Figure 1—source data 2**). In  $\Delta bamB$  cells, the  $\sigma^E$  response is partially activated (**Charlson et al., 2006; Wu et al., 2005**), causing the upregulation of *bam* genes (**Figure 2B**). A strain carrying the simultaneous deletion of *dolP* and *bamB* was viable but growth-defective. Normal growth was restored by ectopic expression of a C-terminally polyhistidine tagged DolP protein variant (**Figure 2C**). As expected, the  $\Delta bamB$  envelope protein profile presented a marked reduction of the major heat-modifiable OMPs, OmpA and OmpC. The concomitant lack of DolP had no additional effect on the levels of these OMPs (**Figure 2—figure supplement 1A**, lanes 13–18). However, we noticed that the levels of BamA, which presents the typical heat modifiable behaviour of OMPs, were reduced in this strain (**Figure 2D**). Furthermore, phase-contrast microscopy analysis of the same  $\Delta dolP \Delta bamB$  strain revealed a number of cells with altered morphology (**Figure 2E**). Taken together, these results corroborate the importance of DolP when the BAM complex is defective and point to a possible role of DolP in maintaining BamA levels during envelope stress.

### DolP supports proper folding and function of BamA

In part because we found DolP to be critical in cells with an impaired BAM complex and in part because the BAM complex is upregulated upon activation of the  $\sigma^E$  response, we wished to explore the effect of BAM overproduction in *dolP*<sup>+</sup> and  $\Delta dolP$  cells. To this end, the genes encoding wild-type BamABCD and a C-terminally polyhistidine-tagged BamE protein variant were ectopically expressed via the isopropylthiogalactoside (IPTG)-inducible *trc* promoter ( $P_{trc}$ ) as a transcriptional unit, adapting a previously established method (**Roman-Hernandez et al., 2014**). With 400  $\mu$ M

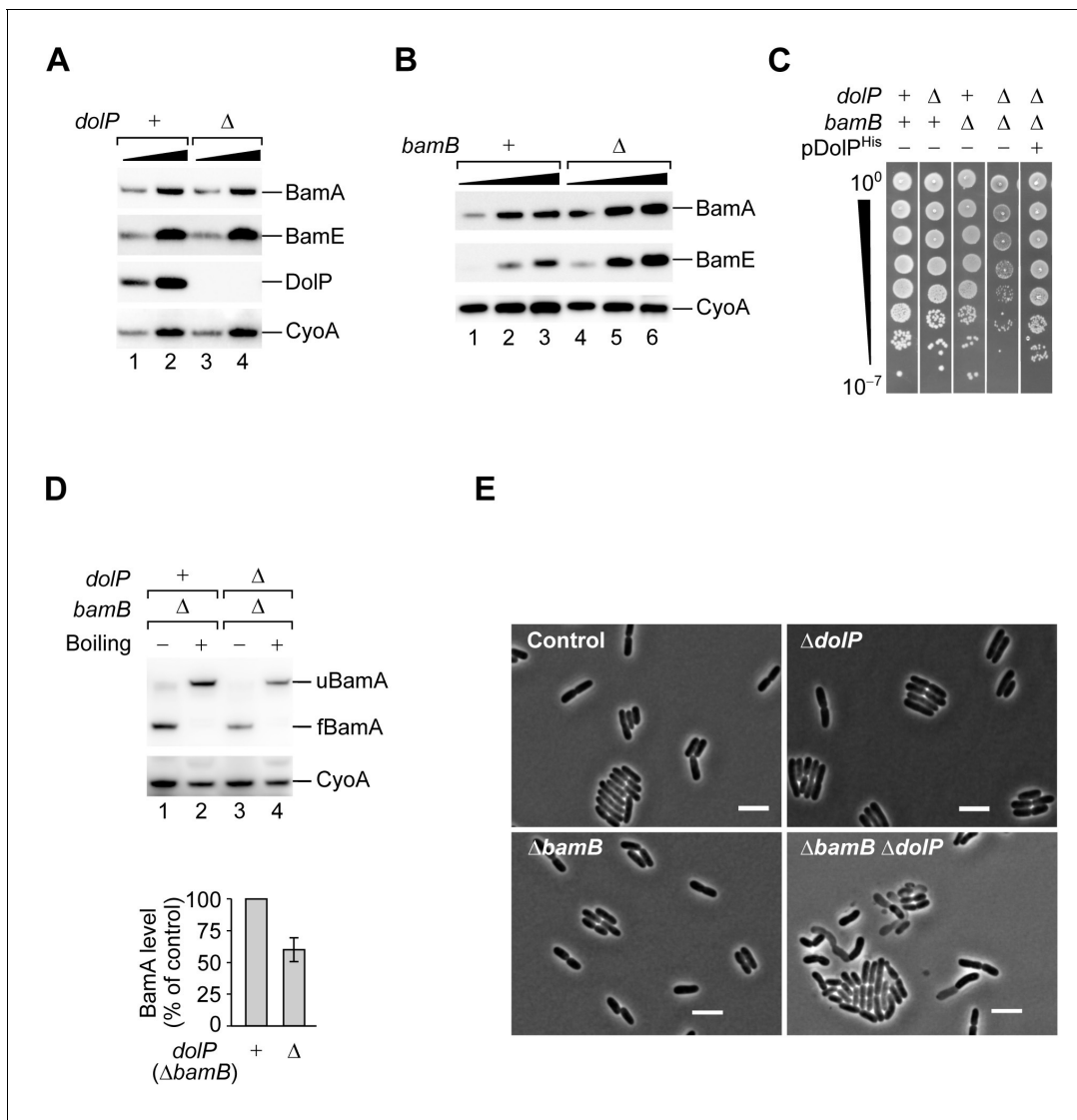


**Figure 2.** DolP promotes fitness in cells that undergo envelope stress. (A) One- and three-fold amounts of the total cell lysate fractions obtained from a BW25113 (*dolP*<sup>+</sup>) strain and a derivative  $\Delta$ *dolP* strain were analysed by SDS-PAGE and immunoblotting using the indicated antisera. (B) One-, two-, and three-fold amounts of the total cell lysate fractions obtained from a BW25113 (*bamB*<sup>+</sup>) strain and a derivative  $\Delta$ *bamB* strain were analysed by SDS-PAGE and immunoblotting using the indicated antisera. (C) BW25113 and derivative cells deleted of *dolP*, *bamB*, or both genes were cultured, serially diluted, and spotted on LB agar. Cells deleted of both *dolP* and *bamB* and transformed with pDolP<sup>His</sup> were cultured, serially diluted, and spotted on LB agar supplemented with ampicillin. (D) The envelope fractions of the indicated strains were analysed by SDS-PAGE and immunoblotting. Prior to gel loading, samples were incubated at 25°C (Boiling –) or 99°C (Boiling +). The total amounts of BamA in  $\Delta$ *bamB* *dolP*<sup>+</sup> and  $\Delta$ *bamB*  $\Delta$ *dolP* strains were quantified, normalized to the amount of the inner membrane protein CyoA, and expressed as percentage of the value obtained for the  $\Delta$ *bamB* *dolP*<sup>+</sup> sample. Data are reported as means  $\pm$  standard error of the mean (SEM, N = 3). u, unfolded; f, folded. (E) Overnight cultures of BW25113 (control),  $\Delta$ *dolP*,  $\Delta$ *bamB*, and  $\Delta$ *dolP*  $\Delta$ *bamB*, were freshly diluted in LB medium and re-incubated at 30°C until OD<sub>600</sub> = 0.3. Cells were visualized on 1% (w/v) agarose pads by phase contrast microscopy. Bar = 5  $\mu$ m.

The online version of this article includes the following figure supplement(s) for figure 2:

**Figure supplement 1.** DolP does not play a direct role in OMP biogenesis.

IPTG, the amounts of BAM subunits that accumulated in the cell membrane fraction were roughly similar to those of the major OMPs OmpA or OmpC (Figure 3A, lane 2). Importantly, we noticed that BAM overproduction caused a partial detrimental effect in the wild-type BW25113 strain (Figure 3B). The detrimental effect was more severe in a  $\Delta$ *dolP* strain (Figure 3B). This difference was particularly noticeable with 200  $\mu$ M IPTG, which had a minor inhibitory effect on the growth of wild-type cells but strongly impaired the growth of a  $\Delta$ *dolP* strain. Similar to *dolP*, *skp* is upregulated

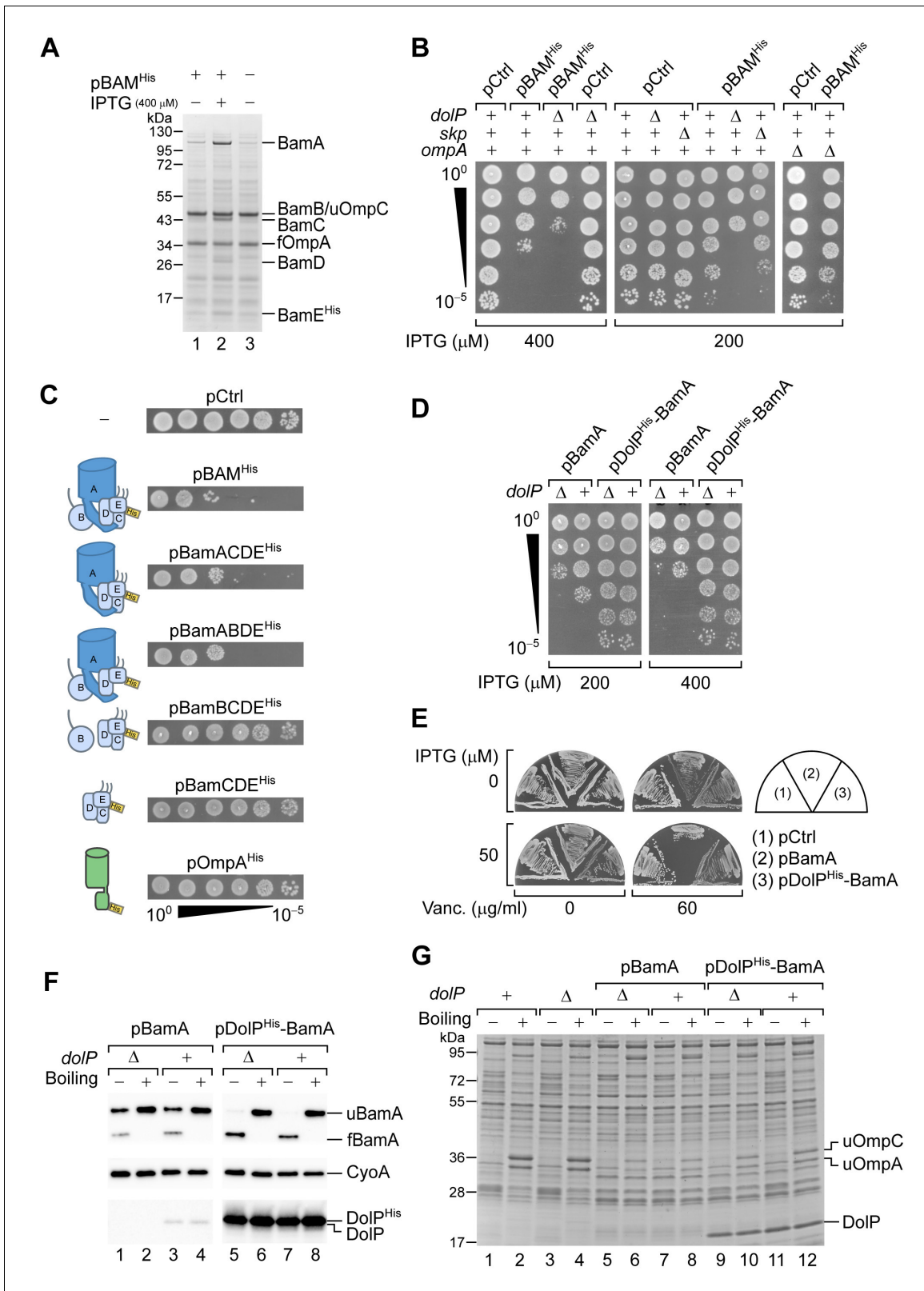


**Figure 3.** DolP opposes an envelope detrimental effect caused by BamA overaccumulation in the OM. (A) BW25113 cells harbouring pBAM<sup>His</sup> where indicated were cultured and supplemented with no IPTG or 400 μM IPTG for 1 hr prior to collecting cells. The protein contents of the envelope fractions were analysed by SDS-PAGE and coomassie staining. Prior to loading, samples were heated for 5 min at 90°C, a temperature which is not sufficient to fully denature OmpA (folded OmpA, fOmpA). The band of BamB overlaps with the band of the major porin unfolded OmpC (uOmpC). (B) Figure 3 continued on next page



## Figure 3 continued

The BW25113 and the derivative  $\Delta dolP$ ,  $\Delta skp$ , or  $\Delta ompA$  strains carrying an empty control vector (pCtrl) or pBAM<sup>His</sup> were serially diluted and spotted onto LB agar supplemented with IPTG as indicated. (C) BW25113 cells carrying a control empty vector (pCtrl), or the indicated plasmids for ectopic overproduction of BAM, or subsets of BAM subunits, or OmpA<sup>His</sup> were serially diluted and spotted onto LB agar containing 400  $\mu$ M IPTG. The diagrams depict the overproduced proteins. (D) BW25113 and derivative  $\Delta dolP$  cells carrying the indicated plasmids for ectopic overproduction of either BamA alone or both DolP<sup>His</sup> and BamA were serially diluted and spotted onto LB agar supplemented with IPTG as indicated. (E) BW25113 cells carrying the indicated plasmids were cultured overnight and streaked onto LB agar containing IPTG and vancomycin as indicated. (F) Heat-modifiability of BamA in wild-type and  $\Delta dolP$  cells carrying the indicated plasmids. When the cultures reached the mid-exponential phase, the expression of BamA was induced for 2 hr with 200  $\mu$ M IPTG. Total cell proteins were incubated at 25°C (Boiling –) or at 99°C (Boiling +), separated by SDS-PAGE and analysed by immunoblotting using the indicated antisera. u, unfolded; f, folded. (G) Heat modifiability of the protein contents of the envelope fraction of BW25113 ( $dolP^+$ ) or  $\Delta dolP$  cells carrying no vector or transformed with pBamA or pDolP<sup>His</sup>-BamA. Plasmid-borne genes were induced with 200  $\mu$ M IPTG for 2 hr prior to collecting cells. The envelope fractions were mixed with SDS-PAGE loading buffer, incubated at 25°C (Boiling –) or 99°C (Boiling +) for 10 min, and analysed by SDS-PAGE and coomassie staining. u, unfolded.

The online version of this article includes the following figure supplement(s) for figure 3:

**Figure supplement 1.** The detrimental effect of BAM overproduction is caused by the overaccumulation of BamA in the OM.

by  $\sigma^E$  and its deletion causes sensitivity to vancomycin (**Figure 1—figure supplement 1B**). In contrast to  $\Delta dolP$ , a  $\Delta skp$  strain harbouring the same BAM overproduction plasmid could grow as efficiently as the wild-type reference (**Figure 3B**). Similarly, cells lacking OmpA, which is downregulated by  $\sigma^E$  activation, could tolerate BAM overproduction (**Figure 3B**). These results suggest a specific effect of DolP in supporting cell fitness when BAM is overproduced.

The excess of BamA alone was responsible for the observed growth defect, as the excess of different subsets of BAM subunits that did not include BamA or an excess of OmpA obtained using a similar overproduction plasmid (see also the subsequent description of **Figure 5—figure supplement 3C**) had no detectable effects in our growth tests (**Figure 3C**). The detrimental effect of BAM overproduction was caused by the overaccumulation of BamA in the OM, as the overproduction of an assembly-defective BamA variant, BamA<sup>AP1</sup>, that lacks the N-terminal POTRA1 motif and that largely accumulates in the periplasm (**Bennion et al., 2010**), did not impair growth to the same extent (**Figure 3—figure supplement 1A–1C**). Strikingly, the growth defect caused by the overproduction of BamA was fully rescued by the concomitant overproduction of DolP (**Figure 3D**), indicating a dose-dependent positive-fitness effect of DolP. Most importantly, we noticed that a lower induction of BamA expression (50  $\mu$ M IPTG) did not cause any major growth defect but determined a marked sensitivity of wild-type cells to vancomycin (**Figure 3E**). Even under these conditions, the concomitant overproduction of DolP was beneficial and restored growth, thus revealing that DolP contributes to rescue an OM integrity defect caused by increased BamA levels (**Figure 3E**).

To better understand this phenotype, we analysed the levels of heat-modifiable (properly folded) versus non-heat-modifiable (improperly folded) BamA in cells overproducing equal amounts of BamA and lacking or expressing different levels of DolP. A large fraction of overproduced BamA in wild-type or  $\Delta dolP$  cells was non-heat-modifiable (**Figure 3F**, lanes 1–4). Given that overproduced BamA did not accumulate in the periplasm (**Figure 3—figure supplement 1D**), we deduce that improperly folded BamA is associated with the OM. In contrast to BamA, OmpA that was overproduced with a similar plasmid and the same amount of inducer was quantitatively heat-modifiable (**Figure 3—figure supplement 1E**), indicating that this degree of protein expression did not saturate the OMP biogenesis machinery. We noticed that cells overproducing BamA had reduced OMP levels (**Figure 3G**, lanes 5–8), suggesting that improperly folded BamA may interfere with the OMP biogenesis activity of the endogenous BAM complex. Strikingly, when DolP was concomitantly overproduced with BamA, virtually all BamA was found to be heat-modifiable, suggesting that it could properly fold (**Figure 3F**, lanes 5–8). The overproduction of DolP partially rescued the wild-type level of OMPs (**Figure 3G**, lanes 9–12), indicating some degree of restoration of the BamA function. The fact that the wild-type OMP levels were not fully restored probably owes to the lack of stoichiometric amounts of the BAM lipoproteins compared to the amount of BamA in these cells. Taken together these results suggest that the detrimental effects inherent to incremental BamA expression correlate well with the observed BamA folding defect. Most importantly, DolP can restore proper folding of BamA rescuing OM integrity. We could not detect the non-heat-modifiable form of BamA produced at endogenous levels in a  $\Delta dolP$  genetic background (**Figure 3—figure supplement 1E**).

It is possible that low levels of improperly folded BamA would be promptly degraded (*Narita et al., 2013*), whereas when BamA is produced at higher levels, the larger fraction of improperly folded BamA may not be degraded as efficiently and is thus detected. Overall, these results indicate that DolP supports proper folding and functioning of BamA.

### DolP interacts with BamA assembled in the OM

We wished to investigate whether DolP physically interacts with the BAM complex. In a first set of pull-downs, we exploited the specificity of staphylococcal protein A-IgG binding to investigate a possible BAM–DolP association. A construct encoding C-terminally protein A-tagged DolP was ectopically expressed in  $\Delta dolP$  cells. The envelope of cells expressing DolP<sup>ProtA</sup> was solubilized using digitonin as main mild-detergent component prior to IgG-affinity chromatography (**Figure 4A**, Coomassie staining). Site-specific enzymatic cleavage of an amino acid linker between DolP and the protein A tag was used for protein elution. Notably, BamA, BamC, BamD, and BamE were immunodetected in the elution fraction of protein A-tagged DolP (**Figure 4A**, lane 3). In contrast, the membrane proteins OmpA and CyoA, and cytosolic RpoB were not detected. Next, BAM<sup>ProtA</sup> (consisting of wild-type BamABCD and a C-terminally protein A-tagged BamE protein variant) was ectopically overproduced to isolate the BAM complex via IgG-affinity purification (**Figure 4—figure supplement 1A**, Coomassie staining). Along with the BamE bait and other subunits of the BAM complex, DolP was also immunodetected in the elution fraction (**Figure 4—figure supplement 1A**, lane 3). Other proteins of the bacterial envelope (Skp, LamB, OmpA, and F<sub>1</sub>β of the F<sub>1</sub>F<sub>0</sub> ATP synthase) or cytosolic RpoB were not detected. Taken together, our native pull-down analysis indicates that DolP and BAM have affinity for each other.

To explore whether the central BAM subunit, BamA, is a critical determinant of the BAM–DolP interaction, we performed Ni-affinity purification using the solubilized envelope fraction obtained from cells overproducing BamA and C-terminally polyhistidine-tagged DolP. Under these conditions, BamA was efficiently co-eluted together with DolP<sup>His</sup>, demonstrating that BamA and DolP can interact even in the absence of stoichiometric amounts of the BAM lipoproteins (**Figure 4B**, Coomassie staining). To assess if the interaction of DolP and BAM takes place at the OM, DolP<sup>His</sup> was overproduced together with the assembly-defective form BamA<sup>AP1</sup>. When expressed together with DolP<sup>His</sup>, assembly-defective BamA<sup>AP1</sup> was highly depleted in the corresponding eluate (**Figure 4B**, lane 7), even though BamA<sup>AP1</sup> was only marginally reduced in the crude envelope fraction with respect to wild-type BamA (**Figure 4B**, lane 3). In contrast to BamA<sup>AP1</sup>, the BamA<sup>AP2</sup> variant, which is efficiently assembled into the OM (**Figure 3—figure supplement 1C**), was co-eluted to a similar extent as wild-type BamA (**Figure 4B**, lane 8). We conclude that DolP has affinity for OM-assembled BamA.

To verify the proximity of DolP to BamA in living cells, we performed in vivo site-directed photocrosslinking. A photo-activatable amino acid analog, p-benzoyl-L-phenylalanine (Bpa), was introduced by amber suppression (*Chin et al., 2002*) at 17 distinct positions in DolP, three in the linker between the N-terminal lipid-modified cysteine residue and the first BON domain (BON1), eight in BON1, and six in the second BON domain (BON2). Bpa can crosslink with other amino acids at a distance of 3–4 Å, possibly revealing direct protein–protein interactions. Upon UV irradiation and Ni-affinity purification of DolP, several crosslink products were identified by immunoblotting (**Figure 4C** and **Figure 4—figure supplement 1B**). Using both anti-DolP and anti-BamA antibodies, a crosslink product of approximately 115 kDa was detected with samples containing Bpa at positions V52, V72 and, to a lower extent, V101. Notably, positions V52, V72, and V101 are proximal in the three-dimensional structure of DolP with their side chains exposed on the surface of BON1 and oriented away from BON2 (**Figure 4C**). Thus, these results identify in BON1 a site of interaction of DolP with BamA. In addition, a major crosslink product with an apparent molecular weight of 55 kDa was detected with Bpa at several DolP positions, and most prominently V52, I64, V72, and V101 of BON1. This product is approximately 35 kDa larger than the mass of DolP. When analysed by MALDI-TOF mass spectrometry, tryptic peptides of DolP and OmpA (37 kDa) were identified in the 55 kDa crosslink products obtained with Bpa at position V41 and V52 (**Figure 4—figure supplement 2A–C**). LC-MS/MS analysis further identified a peptide of the C-terminal domain of OmpA, which localizes in the periplasm (*Ishida et al., 2014*), to be crosslinked by Bpa at position V52 of DolP (**Figure 4—figure supplement 2D–2F**). Thus, whereas OmpA could not be detected in native pull-downs of affinity-tagged DolP, it was efficiently crosslinked. Compared to  $\Delta dolP$ , cells lacking OmpA are not susceptible to vancomycin treatment (**Figure 4—figure supplement 1D**) and can tolerate

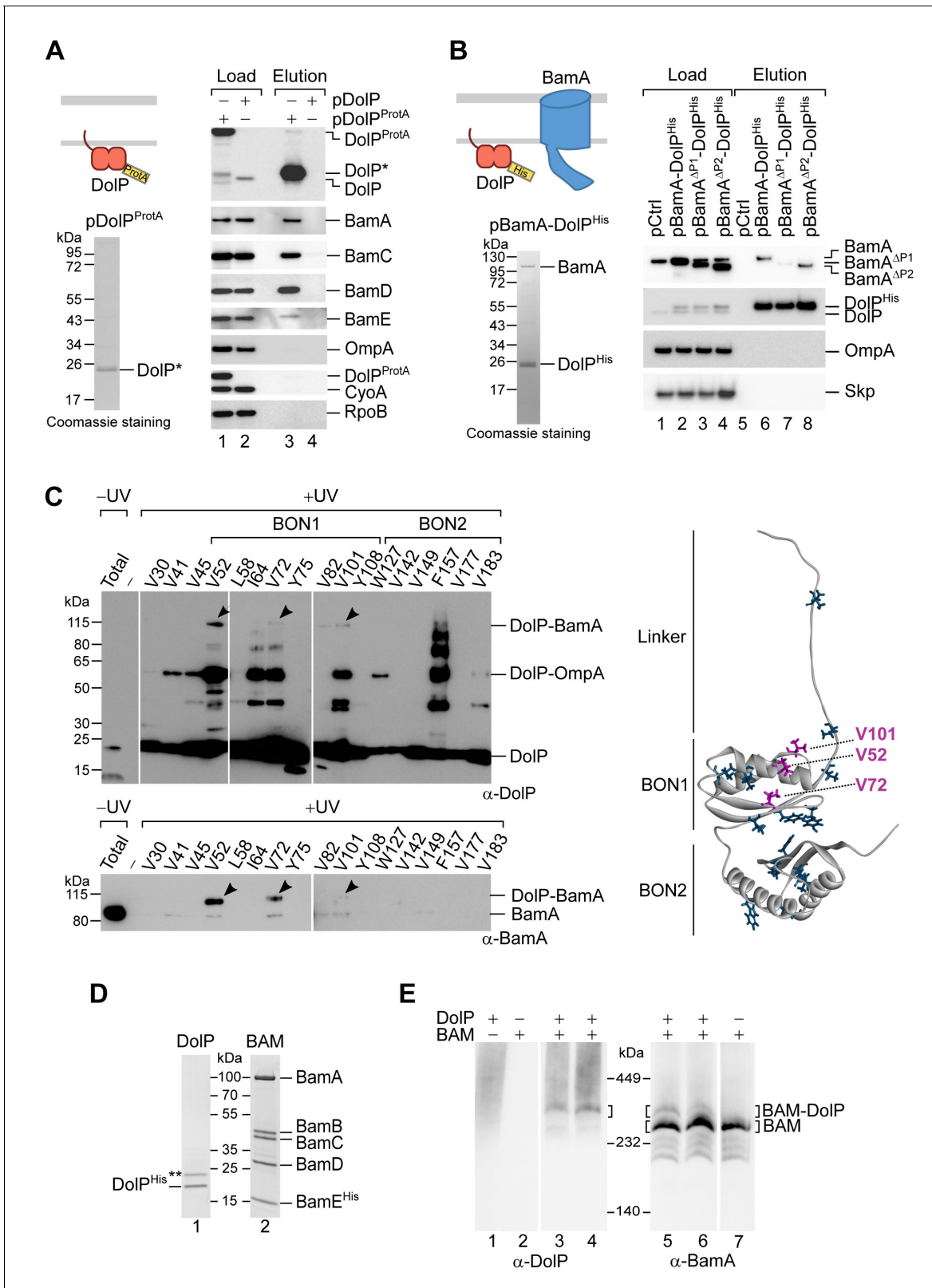


**Figure 4.** DolIP associates with the BAM complex via an interaction with BamA. (A) The envelope fractions of BW25113 cells carrying the indicated plasmids were solubilized with 1% (w/v) digitonin and 0.1% (w/v) DDM and subjected to IgG affinity purification of protein A-tagged DolIP. The load and elution fractions were analysed by SDS-PAGE. The coomassie staining of the elution of protein A-tagged DolIP is shown below the diagrams representing the overproduced protein. Blotted proteins from load and elution fractions were detected by immunolabelling using the indicated antibodies. (B) Co-purification of BamA-DolIP<sup>His</sup> with BamA. (C) UV cross-linking of DolIP with BamA and OmpA. Mass spectrometry identified residues V101, V52, and V72. (D) Co-solubilization of DolIP<sup>His</sup> and BamA. (E) Cross-linking of BamA and DolIP.

Figure 4 continued on next page

Figure 4 continued

antisera. Load 0.5%; Elution 100%. The asterisk indicates the TEV-digestion product of DoIP<sup>ProtA</sup>. (B) The envelope fractions of BW25113 cells carrying the plasmids overproducing His-tagged DolP and the indicated BamA protein variants (deleted of POTRA1 or of POTRA2) were solubilized with 1% (w/v) digitonin and 0.1% (w/v) DDM and subjected to Ni-affinity purification. The load and elution fractions were analysed by SDS-PAGE. The coomassie staining of the elution of His-tagged DolP overproduced together with wild-type BamA is shown below the diagram representing the overproduced proteins. Blotted protein from load and elution fractions were detected by immunolabelling using the indicated antisera. Load 2%; Elution 100%. The amount of BamA co-isolated with DolP<sup>His</sup> was normalized to the amount of BamA detected in the load fraction. The value obtained for the pBamA-DolP<sup>His</sup> sample was set to 100%. The average of the relative amounts of co-isolated BamA<sup>ΔP1</sup> and BamA<sup>ΔP2</sup> are as follows: BamA<sup>ΔP1</sup>, 16.5% (N = 2; 1st exp. 23.6%; 2nd exp. 9.3%); BamA<sup>ΔP2</sup>, 81.2% (N = 2; 1st exp. 101.8%; 2nd exp. 60.6%). (C) UV photo-crosslinking of  $\Delta dolP$  cells transformed with pEVOL-pBpF and pBamA-DolP<sup>His</sup> harbouring an amber codon at the indicated position of the *dolP* ORF. Upon Ni-affinity chromatography of DolP<sup>His</sup>, eluates obtained from UV irradiated samples were separated by SDS-PAGE and analysed by immunoblotting using the indicated antisera. The total envelope fraction of cells expressing DolP<sup>His</sup> with Bpa at position V52 (non-irradiated) is shown in the first lane and serves as a reference for the migration of non-crosslinked DolP and BamA. Arrowheads indicate crosslinked products detected with both DolP and BamA antisera. Analysis of eluates obtained from non-irradiated samples are shown in **Figure 4—figure supplement 1B**. The amino acid residues replaced with Bpa are indicated on the structure of DolP, PDB: 7A2D (Bryant et al., 2020). In purple are the positions crosslinked to BamA. (D) The envelope fraction of BW25113 cells overproducing DolP<sup>His</sup> or the BAM complex containing C-terminally His-tagged BamE was subjected to protein extraction with 1% (w/v) DDM, Ni-affinity purification, and gel filtration chromatography. The elution fractions were analysed by SDS-PAGE and coomassie staining. The double asterisk indicates a contaminant protein in the elution of DolP. (E) Roughly equimolar quantities of purified His-tagged BAM complex and DolP were incubated alone for 1 hr at 4°C (lanes 1, 2, and 7), or together for 1 hr at 4°C (lanes 3 and 6) or for 30 min at 25°C (lanes 4 and 5), prior to blue native-PAGE and immunoblotting using the indicated antisera.

The online version of this article includes the following figure supplement(s) for figure 4:

**Figure supplement 1.** Analysis of the DolP–BamA interaction.

**Figure supplement 2.** Mass spectrometry analyses of the DolP–OmpA crosslink product.

the overproduction of BamA (**Figure 3B**), suggesting that OmpA is not required for DolP function. Finally, a series of crosslink products with molecular weights approximately two to six times the mass of DolP were detected with anti-DolP antibodies when Bpa was introduced at position F157 (**Figure 4C**), suggesting that DolP can form oligomers.

In seeking a detergent that would interfere with the interaction of BAM and DolP, and allow their purification as separate components, we solubilized the envelope fraction with increasing amounts of n-dodecyl  $\beta$ -D-maltoside (DDM), a detergent previously used to isolate the native BAM complex (Roman-Hernandez et al., 2014). At concentrations of DDM between 0.3% (w/v) and 1% (w/v), we observed a drastic reduction in the amounts of BAM subunits that were co-eluted with DolP<sup>His</sup> (**Figure 4—figure supplement 1C**), indicating that the BAM–DolP interaction is sensitive to DDM. We thus used 1% (w/v) DDM to extract and purify His-tagged DolP or His-tagged BAM as separate components (**Figure 4D**). When analysed by blue native-PAGE and immunoblotting, purified DolP gave rise to a diffused signal at around 450 kDa (**Figure 4E**, lane 1), suggesting a dynamic multimeric organization of this protein. Purified BAM migrated as expected at 250 kDa (**Figure 4E**, lane 7). When roughly equimolar amounts of purified BAM and DolP were pre-incubated in the presence of a low DDM concentration and subsequently resolved by blue native-PAGE, a complex with an apparent molecular weight higher than that of the BAM complex was detected with both anti-BamA- and anti-DolP-specific antibodies (**Figure 4E**, lanes 3–6), suggesting that DolP can associate with the penta-subunit BAM complex. Taken together our results demonstrate that DolP can interact with the BAM complex, making direct contacts with OM-assembled BamA.

### BamA overaccumulation in the OM reduces DolP mid-cell localization

In light of our observation that DolP interacts with BAM, we asked whether the envelope localization patterns of DolP and BAM are reciprocally linked. First, we monitored the effect of DolP expression on the localization of the chromosomally encoded BamD<sup>mCherry</sup> subunit of the BAM complex. This protein generated a fluorescence signal throughout the envelope that was not affected by the lack or the overproduction of DolP (**Figure 5—figure supplement 1**). Next, we checked the effect on DolP localization of BAM overaccumulation in the OM. DolP associates with the OM and accumulates at mid-cell during a late step of cell division (Tsang et al., 2017). To monitor the localization of DolP, we used a strain harbouring a chromosomal *dolP-gfp* fusion (**Figure 1A**). The localization of the DolP<sup>GFP</sup> fusion protein (**Figure 5—figure supplement 2A**) was analysed concomitantly with two other chromosomally encoded markers of the division septum, ZipA<sup>mCherry</sup> or NlpD<sup>mCherry</sup>. ZipA is

involved in an early step of divisome assembly and accumulates at division sites before, as well as, during envelope constriction (**Figure 5—figure supplement 2B**; Hale and de Boer, 1997). Instead, NlpD is a late marker of cell division involved in the activation of AmiC and accumulates at septa that are already undergoing constriction (**Figure 5—figure supplement 2C**; Uehara et al., 2009; Uehara et al., 2010). DolP<sup>GFP</sup> accumulated at mid-cell sites where the envelope appeared invaginated, showing a localization pattern similar to that of NlpD<sup>mCherry</sup> (**Figure 5—figure supplement 2C**; Tsang et al., 2017). We investigated the effect of short-lived (1 hr) BAM overproduction on DolP<sup>GFP</sup> localization. Strikingly, we found that BAM overproduction depleted DolP<sup>GFP</sup> from mid-cell sites (**Figure 5A**, plot, and **Figure 5—figure supplement 3A**, left). In contrast, no obvious effects on cell division nor on mid-cell recruitment of ZipA<sup>mCherry</sup> and NlpD<sup>mCherry</sup> were observed (**Figure 5—figure supplement 3B**). The overproduction of BamA alone was sufficient to alter the distribution of the DolP<sup>GFP</sup> fluorescence signal in constricting cells, with its intensity being reduced at constriction sites but enhanced at decentred positions along the cell axis (**Figure 5—figure supplement 3A**). In contrast, the overproduction of only the four BAM lipoproteins (**Figure 5—figure supplement 3A**, right) as well as the overproduction of OmpA (**Figure 5—figure supplement 3C**) had no obvious effects on DolP mid-cell localization.

As BAM catalyses OMP assembly, we asked whether this activity interferes with DolP mid-cell localization. To address this question, we made use of an inactive BamA mutant form (**Figure 5—figure supplement 4A**) harbouring a polyhistidine peptide extension at its C-terminal  $\beta$ -strand (Hartmann et al., 2018). Similar to the overaccumulation of the BAM complex or BamA, the overaccumulation of BamA<sup>His</sup> interfered with DolP mid-cell localization (**Figure 5—figure supplement 4B and C**), without affecting ZipA<sup>mCherry</sup> and NlpD<sup>mCherry</sup> (**Figure 5—figure supplement 3D**), indicating that the cellular localization of DolP does not depend on the OMP-assembly activity of BamA. In contrast, the ability of BamA to assemble into the OM was a critical determinant of the observed septal depletion of DolP. In fact, the periplasm-accumulating BamA <sup>$\Delta$ P1/His</sup> variant (**Figure 5—figure supplement 4D**) did not impair DolP<sup>GFP</sup> mid-cell localization (**Figure 5—figure supplement 4B**, centre), whereas the OM-overaccumulating BamA <sup>$\Delta$ P2/His</sup> did (**Figure 5—figure supplement 4B**, right, 4C and 4D). Taken together, these results suggest that the overaccumulation of BamA in the OM interferes with the recruitment of DolP at mid-cell sites.

### DolP mid-cell localization is impaired under envelope stress conditions

Given that DolP is critical for fitness under envelope stress conditions, we wished to know whether envelope stress would influence the localization of DolP<sup>GFP</sup>. To this end, first we analysed the localization of DolP<sup>GFP</sup> in strains lacking either the OMP chaperone SurA or the lipoprotein BamB. Both  $\Delta$ surA and  $\Delta$ bamB strains are defective in OMP biogenesis and produce higher levels of BAM complex due to activation of the  $\sigma^E$  response (Charlson et al., 2006; Rouvière and Gross, 1996; Vertommen et al., 2009; Wu et al., 2005). Importantly, the frequency of mid-cell labelling by DolP<sup>GFP</sup> was reduced in  $\Delta$ surA cells both in minimal (**Figure 5—figure supplement 5A**, centre) and LB (**Figure 5B**) culture media. In contrast, lack of SurA did not affect septal recruitment of the late cell division marker NlpD (**Figure 5—figure supplement 5B**). The analysis of the fluorescence plot profiles of constricted cells clearly showed a marked reduction of the DolP<sup>GFP</sup> signal at mid-cell sites and higher fluorescence levels at decentred positions along the cell axis (**Figure 5B**, right plot). As for the  $\Delta$ surA strain, DolP<sup>GFP</sup> accumulated at the mid-cell with a lower frequency when bamB was deleted (**Figure 5—figure supplement 5A**, bottom). Together, these results indicate that, during envelope stress, DolP is depleted at mid-cell sites.

Because the levels of OmpA and OmpC are reduced under envelope stress conditions, we investigated if these OMPs are required for the mid-cell localization of DolP. In both ompA or ompC deletion strains, we observed marked DolP<sup>GFP</sup> intensities at cell constriction sites, indicating that neither OmpA nor OmpC are crucial for DolP mid-cell localization (**Figure 5C** and **Figure 5—figure supplement 5C**). Nevertheless, the plot collective profile of DolP<sup>GFP</sup> in  $\Delta$ ompA showed a marginal reduction of fluorescence intensity at the mid-cell and a similarly small increment at non-septal positions. Like BamA, OmpA was crosslinked with DolP at position V52. By monitoring this crosslink reaction, we found that the DolP-BamA association is enhanced in the absence of OmpA (**Figure 5D**), suggesting that OmpA competes with BamA for an interaction with DolP. Hence, the depletion of OmpA in stressed cells might favour the interaction of DolP with BamA.

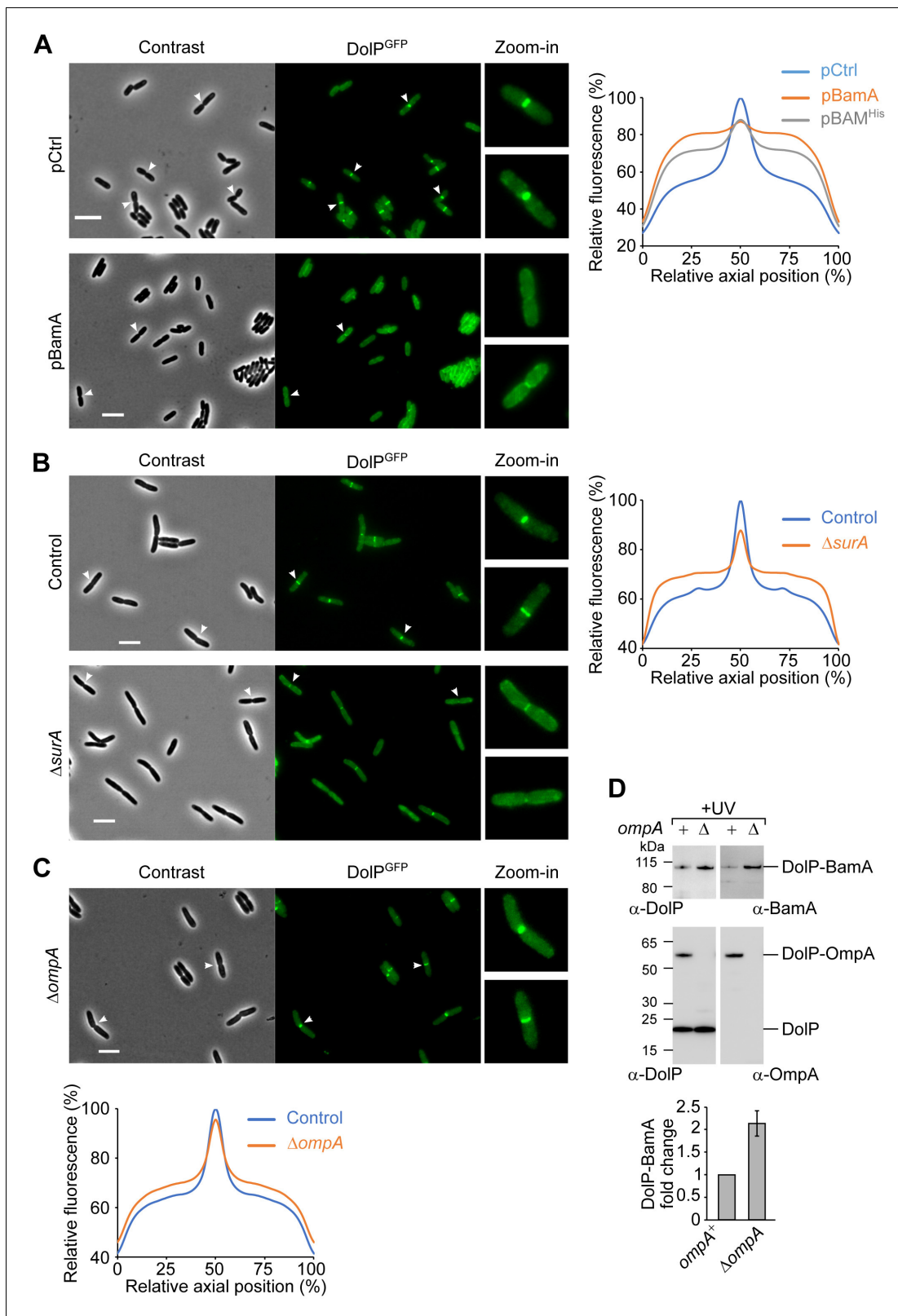


**Figure 5.** BamA overaccumulation in the OM and envelope stress interfere with the mid-cell localization of DoIP. (A) Overnight cultures of BW25113 cells harbouring the chromosomal fusion *doIP-gfp* and transformed with either pCtrl (empty vector) or pBamA were freshly diluted in minimal M9 medium, incubated at 30°C until OD<sub>600</sub> = 0.1 and supplemented with 400  $\mu$ M IPTG for 1 hr. Cell samples were visualized on 1% (w/v) agarose pads by phase contrast and fluorescence microscopy. Arrowheads indicate envelope constriction sites between forming daughter cells. Bar = 5  $\mu$ m. The Figure 5 continued on next page

Figure 5 continued

collective profiles of fluorescence distribution versus the relative position along the cell axis were plotted: pCtrl, blue; pBamA, orange; pBAM<sup>His</sup>, grey (images of cells transformed with pBAM<sup>His</sup> are shown in **Figure 5—figure supplement 3A**). Only cells with a constriction (N = 361, pCtrl; N = 187, pBamA; N = 187, pBAM<sup>His</sup>) were taken into account for the collective profile plots. Fluorescence intensities were normalized to the mid-cell value obtained for the control sample. (B) Overnight cultures of BW25113 (control) or  $\Delta surA$  derivative cells carrying the *dolP-gfp* chromosomal fusion were freshly diluted in LB medium and incubated at 30°C until OD<sub>600</sub> = 0.3. Cell samples were visualized as in (A). Bar = 5  $\mu$ m. The collective profiles of fluorescence distribution versus the relative position along the cell axis is shown for  $\Delta surA$  cells (orange) and *surA*<sup>+</sup> control cells (blue). Only cells with a constriction (N = 318, Control; N = 320,  $\Delta surA$ ) were taken into account for the collective profile plots. Fluorescence intensities were normalized to the mid-cell value obtained for the control sample. (C) Overnight cultures of  $\Delta ompA$  cells carrying the *dolP-gfp* chromosomal fusion were cultured and visualized as in (B). Bar = 5  $\mu$ m. The collective profiles of fluorescence distribution versus the relative position along the cell axis is shown for  $\Delta ompA$  cells (orange) and an *ompA*<sup>+</sup> (control) strain that was cultured and visualized in a parallel experiment (blue). Only cells with a constriction (N = 287, Control; N = 193,  $\Delta ompA$ ) were taken into account for the collective profile plots. Fluorescence intensities were normalized to the mid-cell value obtained for the control sample. (D) UV photo-crosslinking of  $\Delta dolP$  and  $\Delta dolP \Delta ompA$  cells transformed with pBamA-DolP<sup>His</sup> harbouring an amber codon at position V52 of the *dolP* ORF. Signals obtained with the anti-BamA antiserum were quantified and showed in the histogram. The amount of DolP-BamA crosslink product obtained with samples lacking OmpA is expressed as fold change of the amount of the same product obtained in samples expressing OmpA. Data are reported as mean  $\pm$  SEM (N = 3).

The online version of this article includes the following figure supplement(s) for figure 5:

**Figure supplement 1.** Effect of the lack or the overproduction of DolP on BAM localization.

**Figure supplement 2.** DolP<sup>GFP</sup>, NlpD<sup>mCherry</sup>, and ZipA<sup>mCherry</sup> mid-cell localization patterns.

**Figure supplement 3.** Overproduction of BAM influences septal recruitment of DolP<sup>GFP</sup> but not NlpD<sup>mCherry</sup> or ZipA<sup>mCherry</sup>.

**Figure supplement 4.** BamA overaccumulation in the OM impairs mid-cell localization of DolP<sup>GFP</sup>.

**Figure supplement 5.** Envelope stress influences the localization of DolP<sup>GFP</sup>.

## Discussion

Upon envelope stress, the BAM complex and other OM biogenesis factors are upregulated to meet the cellular demand for OMP assembly. The role of DolP, which is also upregulated by the envelope stress response, was unclear. In our study, we uncover that DolP supports cell fitness under envelope stress conditions and we demonstrate that the BAM complex, in particular its central catalytic subunit BamA, is a direct target of such fitness function.

First we have shown that in cells that lack BamB and undergo envelope stress, DolP is important to maintain the levels of BamA. Next, we have exploited the observation that, when overproduced, BamA impairs OM integrity, causing a detrimental effect dependent on its accumulation in the OM. Under these conditions, a significant portion of membrane-embedded BamA is improperly folded and OMP biogenesis is reduced. We have shown that an increment of DolP expression rescues proper folding of BamA and, to some extent, efficient OMP biogenesis. Finally, we have demonstrated that DolP directly interacts with the BAM complex in the OM, making contacts to BamA. Taken together, these results strongly suggest that DolP contributes to preserve the OM integrity by supporting the function of BamA, thus shedding some light on how DolP copes with envelope stress.

In addition to promoting efficient OMP biogenesis, proper folding of BamA may be necessary to regulate the dynamics of this protein in the OM. As part of the mechanism by which BAM functions in OMP biogenesis, BamA is predicted to interfere with the organization of the surrounding lipid bilayer and to generate an energetically favourable environment for the insertion of nascent OMPs in the OM (Fleming, 2015; Horne et al., 2020). BamA-mediated destabilization of a lipid bilayer was shown by molecular dynamics simulations, as well as by reconstituting both BamA into proteoliposomes and the BAM complex into nanodiscs (Iadanza et al., 2020; Noinaj et al., 2013; Sinnige et al., 2014). Furthermore, when reconstituted into a lipid bilayer, BamA can form pores characterized by variable conductance (Stegmeier and Andersen, 2006). With an improperly folded conformation, these features of BamA may be uncontrolled and potentially detrimental for OM integrity. The finding that DolP supports proper folding of BamA provides an explanation as to how DolP helps preserving OM integrity. This role of DolP is reminiscent of the chaperone function attributed to a different dual BDN-domain protein, OsmY, which promotes the folding of a specific subclass of OMPs (Yan et al., 2019). We speculate that, by associating with BamA, DolP directly contributes to its folding in the OM. The evidence that DolP associates but does not form a stoichiometric complex with BAM is consistent with the hypothesis that DolP may transiently act on BamA

similar to a chaperone. Notably, although the chaperone SurA is not required for BamA assembly in the OM, it was shown that in the absence of this factor a portion of BamA is proteolytically degraded (Bennion *et al.*, 2010; Narita *et al.*, 2013). It is thus tempting to explain the quasi-lethal phenotype of a double *surA* and *dolP* deletion strain (Onufryk *et al.*, 2005) with a scenario where at least SurA or DolP must be expressed to maintain BamA in a properly folded conformation. Further studies will be warranted to determine in detail the molecular bases of how DolP helps preserving the proper folding of BamA in the OM.

The observation that DolP binds anionic phospholipids, such as phosphatidylglycerol and cardiolipin (Bryant *et al.*, 2020), is particularly interesting in the context of the BAM–DolP interaction. Phospholipid binding is mediated by residues in BON2 of DolP, away from to the site of interaction with BamA that we have identified in BON1. Conceivably, the binding of BamA may not interfere with the ability of DolP to interact with phospholipids. However, whether phospholipid binding by DolP plays a role in supporting proper folding and activity of BamA remains to be determined. In an *in vitro* experimental set-up, the OMP-assembly activity of BamA is only marginally dependent on the surrounding lipid content (Hussain and Bernstein, 2018). It is intriguing however that amino acid residues of the BamA POTRA domains can make contact with the lipid head-groups on the periplasmic surface of the OM and that BamE interacts with an anionic phospholipid (Fleming *et al.*, 2016; Knowles *et al.*, 2011). Thus, two non-mutually exclusive scenarios should be considered: (i) enriching the BAM sites with negatively charged phospholipids may be part of the mechanism by which DolP contributes to maintain BamA in a properly folded conformation; (ii) DolP may interact with phospholipids in proximity of the BAM complex and form a structure that helps preserving the integrity of these sites. Of note, we have obtained some evidence that DolP can form oligomers, but it remains to be established whether these DolP structures form in proximity of the BAM complex.

Whereas we have shown that DolP restores an OM integrity defect inherent to BamA expression, we cannot exclude that also other OM features determined by the activation of the envelope stress response require the activity of DolP. In any event, a key finding of our study is that DolP mid-cell localization is sensitive to envelope stress conditions. During envelope stress, the OM undergoes a significant alteration of its protein composition, with a marked downregulation of porins and OmpA (Rhodius *et al.*, 2006). OMPs are largely arranged in clusters (Gunasinghe *et al.*, 2018; Jarosławski *et al.*, 2009; Rassam *et al.*, 2015) embedded by highly organized LPS molecules in the external leaflet of the OM (Nikaido, 2003) and the rigidity of their  $\beta$ -barrel structures contributes to the mechanical stiffness of the OM (Lessen *et al.*, 2018). Downregulation targets of  $\sigma^E$  also include the lipoproteins Pal and Lpp (Gogol *et al.*, 2011; Guo *et al.*, 2014), which are critical for OM integrity (Asmar and Collet, 2018; Cascales *et al.*, 2002). Importantly, we have shown that the overaccumulation of BAM in the OM influences DolP localization, suggesting that during stress the upregulation of BamA contributes to deplete DolP from cell constriction sites. We have also obtained evidence that OmpA competes with BamA for an interaction with DolP. A role of OmpA in buffering the function of an envelope stress factor has been reported (Dekoninck *et al.*, 2020). We propose that during envelope stress, the depletion of OmpA might enhance the interaction of DolP with BamA.

Distinct biogenesis and surveillance pathways are required to maintain the protective function of the multi-layered envelope of Gram-negative bacteria (Egan *et al.*, 2020). The hits of our CRISPRi synthetic-defect screen in  $\Delta dolP$  cells include mainly genes involved in efficient transport and assembly of OMPs or in the activation of the  $\sigma^E$ -mediated envelope stress response, which is consistent with the notion that DolP supports the high demand for OMP biogenesis during stress. In addition, genes involved in the activation of the AmiA pathway of septal peptidoglycan splitting were identified. This result is in line with the conclusions of a previous study implicating DolP in the regulation of the NlpD-mediated activation of AmiC (Tsang *et al.*, 2017). Cells lacking both NlpD and AmiC have reduced OM integrity, which contributes to explain the vancomycin sensitivity of  $\Delta dolP$  cells (Tsang *et al.*, 2017). Intriguingly, our observation that mid-cell localization of DolP is reduced under envelope stress conditions points to a possible role of DolP in linking envelope stress to septal peptidoglycan hydrolysis. Reduced levels of DolP at mid-cell sites, and thus impaired AmiC activation (Tsang *et al.*, 2017), could play an important role in coping with envelope stress, for instance by regulating the window of time available to restore efficient OMP biogenesis prior to completing the formation of the new poles in the cell offspring.



In summary, our results reveal an unprecedented function for DolP in supporting the correct folding of BamA, providing an explanation as to how DolP promotes OM integrity and why this factor is upregulated during envelope stress. The identified role of DolP in supporting the BamA function represents a potentially exploitable target in the development of alternative antibacterial therapies. The re-localization of DolP during stress points to a mechanistic link between activation of the envelope stress response and a late step of cell division that will be interesting to investigate in future studies.

## Materials and methods

### Bacterial strains and growth conditions

All *E. coli* strains used in this study are listed in **Supplementary file 1**. Strains newly generated for this study derive from BW25113 [ $\Delta(\text{araD-araB})567 \Delta(\text{rhaD-rhaB})568 \Delta\text{lacZ4787} (::\text{rrnB-3}) \text{ hsdR514 rph-1}$ ] (**Grenier et al., 2014**) or MG1655 ( $F^- \lambda^- \text{ ilvG}^- \text{ rfb-50 rph-1}$ ) (**Blattner et al., 1997**). Deletions of *dolP*, *rseA*, *surA*, *bamB*, *degP*, *skp*, *ompA*, or *ompC* were achieved by P1 transduction of the  $\Delta\text{dolP}::\text{kan}$ ,  $\Delta\text{rseA}::\text{kan}$ ,  $\Delta\text{surA}::\text{kan}$ ,  $\Delta\text{bamB}::\text{kan}$ ,  $\Delta\text{degP}::\text{kan}$ ,  $\Delta\text{skp}::\text{kan}$ ,  $\Delta\text{ompA}::\text{kan}$ , or  $\Delta\text{ompC}::\text{kan}$  alleles, respectively, obtained from the corresponding Keio collection strains (**Baba et al., 2006**). BW25113 derivative strains harbouring chromosomal fusions of constructs encoding superfolder GFP downstream of *dolP* or mCherry downstream of *nlpD*, *zipA*, and *bamD* were obtained by  $\lambda$ -red recombination as previously described (**Datsenko and Wanner, 2000**). Briefly, a kanamycin-resistance cassette was amplified from plasmid pKD4 using oligonucleotides carrying extensions of approximately 50 nucleotides homologous to regions immediately upstream or downstream the stop codon of the interested genes. *DpnI*-digested and purified PCR products were electroporated into the BW25113 or derivative strains. Recombinant clones were selected at 37°C on LB agar plates containing kanamycin. When necessary, the kanamycin-resistance cassette inserted into a mutated locus (gene deletion or fusion) was removed upon transformation with the heat-curable plasmid pCP20 (**Datsenko and Wanner, 2000**). The MG1655 derivative strain LC-E75, harbouring a dCas9-encoding construct under the control of the  $P_{\text{tet}}$  promoter, has been described (**Cui et al., 2018**). Cells were cultured in home-made lysogeny broth (LB) medium (1% (w/v) tryptone, 0.5% (w/v) yeast extract, 5 mg/ml (NaCl), commercially available Miller LB Broth (Sigma) or M9 minimal medium containing M9 salts (33.7 mM  $\text{Na}_2\text{HPO}_4$ , 22 mM  $\text{KH}_2\text{PO}_4$ , 8.55 mM NaCl, 9.35 mM  $\text{NH}_4\text{Cl}$ ) and supplemented with 0.2% w/v glycerol and all the amino acids. Antibiotics were used at the following concentrations: ampicillin 100  $\mu\text{g/ml}$ , kanamycin 50  $\mu\text{g/ml}$ , and vancomycin 60  $\mu\text{g/ml}$ . For spot tests, cells were cultured to mid-log phase, washed with M9 salts, and serially diluted in ice-cold M9 salts prior to spotting on agar plates.

### Plasmid construction

All plasmids used in this study are listed in **Supplementary file 2**. Plasmids for the ectopic expression of BAM subunits, DolP, or OmpA are derived from a pTrc99a vector. The plasmid pBAM<sup>His</sup> (pJH114), which harbours a  $P_{\text{trc}}$  promoter followed by the sequences of the *E. coli* K12 *bamA* ribosome-binding site, the *bamABCDE* open reading frames, and an octahistidine tag fused downstream of *bamE*, was described (**Roman-Hernandez et al., 2014**). The region of pBAM<sup>His</sup> comprising the segment that spans from the *bamA* start codon to the *bamE* stop codon was deleted by site-directed mutagenesis, generating pCtrl. Plasmids pBamA<sup>His</sup> was generated by restriction-free cloning, inserting the *bamA* ORF without its stop codon downstream of the  $P_{\text{trc}}$  promoter and upstream of the octahistidine encoding region in pCtrl. pBamA<sup>His</sup> was subjected to site-directed mutagenesis to generate pBamA, encoding wild-type, non-tagged BamA. The *dolP* ORF amplified from the BW25113 genomic DNA was used to replace the *bamABCDE* ORFs in pJH114 by restriction-free cloning, generating pDolP<sup>His</sup>. The plasmid pBamA-DolP<sup>His</sup> was generated by restriction-free cloning of the *bamA* ORF between the  $P_{\text{trc}}$  promoter and *dolP* in pDolP<sup>His</sup>. Where indicated, site-directed mutagenesis on pBamA-DolP<sup>His</sup> or pDolP<sup>His</sup> was used to replace specific *dolP* codons with an amber codon. pDolP<sup>His</sup>-BamA was built in two steps starting from pDolP<sup>His</sup>. First, the sequence of the *E. coli* K12 *bamA* ribosome-binding site was deleted positioning the *dolP* ORF eight nucleotides downstream of the ribosome-binding site of the pTrc99a multiple cloning site. The resulting plasmid was

then used to insert a segment of pJH114 containing the entire *bamA* ORF including the *E. coli* *bamA* ribosome-binding site.

Site-directed mutagenesis was conducted on pBAM<sup>His</sup> (pJH114) to obtain pBamACDE<sup>His</sup>, pBamABDE<sup>His</sup>, pBamBCDE<sup>His</sup>, and pBamCDE<sup>His</sup>. A sequence encoding the tobacco etch virus protease cleavage site (TEV site) followed by a tandem Protein A tag was amplified from pYM10 (Knop *et al.*, 1999) and fused by restriction-free cloning with the last codon of the *bamE* gene in pBAM<sup>His</sup> to generate pBAM<sup>ProtA</sup>. A stop codon was introduced downstream of the *bamE* last codon to generate pBAM. Plasmids encoding the  $\Delta$ P1 and  $\Delta$ P2 BamA variant were obtained by site-directed mutagenesis deleting the portion of *bamA* ORFs corresponding to residues E22-K89 or P92-G172, respectively. The TEV site and the tandem Protein A construct amplified from pYM10 were inserted by restriction-free cloning downstream of the *dolP* last codon in pDolP<sup>His</sup>, generating pDolP<sup>ProtA</sup>. pDolP was derived from pDolP<sup>ProtA</sup> using site-directed mutagenesis to introduce a stop codon immediately downstream of the *dolP* ORF. The *ompA* ORF was amplified from the BW25113 genomic DNA and inserted by restriction-free cloning between P<sub>trc</sub> and the His-tag encoding construct of pCtrl to generate pOmpA<sup>His</sup>. The sgRNAs plasmids are derived from psgRNAcos (Cui *et al.*, 2018). To generate sgRNA-encoding plasmids the DNA sequences AGCTGCACCTGCTGCGAATA (*bamD* sgRNA, plasmid pCAT187), GTAAACCACTCGCTCCAGAG (*bamE* sgRNA, plasmid pCAT189), CTCATCCGCG TGGGCGGAAA (*envC* sgRNA, plasmid pCAT191), and CTGAGCCGCCGACCGATTTA (*ftsX* sgRNA, pCAT193) were inserted into a *BsaI* site of the psgRNAcos.

### CRISPRi screen and data analysis

Strain LC-E75 (*dolP*<sup>+</sup>) and its  $\Delta$ *dolP* derivative were transformed with the EcoWG1 library which contains five guides per gene as previously described (Calvo-Villamañán *et al.*, 2020). After culturing pooled transformant cells in LB at 37°C to early exponential phase (optical density at 600 nm [OD<sub>600</sub>] = 0.2), a sample was withdrawn for plasmid isolation (t<sub>start</sub>). Subsequently, cultures were supplemented with 1  $\mu$ M anhydrotetracycline (aTc) to induce dCas9 expression and further incubated at 37°C. When cultures reached an OD<sub>600</sub> of 2 they were diluted 1:100 into LB supplemented with 1  $\mu$ M aTc and incubated at the same temperature until an OD<sub>600</sub> of 2. This step was repeated one more time prior to withdrawing a sample for isolation of plasmid DNA (t<sub>end</sub>). Sequencing indexes were used to assign reads to each sample. Illumina sequencing samples were prepared and analysed as previously described (Cui *et al.*, 2018). Briefly, a two-step PCR was performed with Phusion polymerase (Thermo Scientific) using indexed primers. The first PCR adds the first index and the second PCR adds the second index and flow-cell attachment sequences. Pooled PCR products were gel-purified. Sequencing was performed on a NextSeq550 machine (Illumina). The total number of reads obtained for each sample was used to normalize raw reads by sample size. Replicates were pooled to increase depth before another normalization by sample size. Guides with less than 100 normalized read counts in initial time points were discarded. For each screen, sgRNA fitness was calculated as the log<sub>2</sub>-transformed ratio of normalized reads counts between the final and the initial time point:

$$\log_2FC = \log_2 \left( \frac{\text{Normalized reads}_{\text{final}} + 1}{\text{Normalized reads}_{\text{initial}} + 1} \right)$$

For each sample, log<sub>2</sub>FC values were centred by subtracting the median log<sub>2</sub>FC of non-targeting control guides. We then calculated for each sgRNA the difference of log<sub>2</sub>FC value between the  $\Delta$ *dolP* screen and the *dolP*<sup>+</sup> screen. Guides were ranked from the lowest negative values (negative fitness effect in  $\Delta$ *dolP* compared to *dolP*<sup>+</sup>) to the highest positive values (positive fitness effect in  $\Delta$ *dolP* compared to *dolP*<sup>+</sup>) and the significance of the interaction between *dolP* and each gene was evaluated by performing a minimum hypergeometric (mHG) test on the ranked list for each gene using the mHG R package (v. 1.1) (McLeay and Bailey, 2010). False-discovery rate (FDR) was used to correct p-values for multiple testing. For each gene, the median difference of log<sub>2</sub>FC between  $\Delta$ *dolP* and *dolP*<sup>+</sup> screens was used as a measure of the genetic interaction.

### Cell fractionation

To prepare whole-cell lysates, cells were cultured to early exponential phase (OD<sub>600</sub> = 0.2–0.3) in LB medium at 37°C and collected. Where indicated, IPTG was added 1 or 2 hr prior to cell collection, as indicated. Cells were pelleted by centrifugation, washed once with M9 salt, and lysed with Laemmli

Sample Buffer (Bio-Rad) (69 mM Tris-HCl, pH 6.8, 11.1% [v/v] glycerol, 1.1% [w/v] lithium dodecyl sulphate [LDS], 0.005% [w/v] bromophenol blue, supplemented with 357 mM  $\beta$ -mercaptoethanol and 2 mM phenylmethylsulfonyl fluoride [PMSF]). The whole-cell lysates were heat-denatured at 98°C for 5 min prior SDS-PAGE analysis.

To obtain spheroplasts cells were cultured to early exponential phase, collected by centrifugation, resuspended in 33 mM Tris-HCl, pH 8, 40% (w/v) sucrose to an  $OD_{600}$  of 1. The cell suspension was then supplemented with 0.1 mg/ml lysozyme (Sigma), 2 mM EDTA, and incubated on ice for 20 min to induce lysis. After addition of 10 mM  $MgSO_4$ , the spheroplast fraction was collected by centrifugation at  $16,000 \times g$ . The supernatant was further centrifuged at  $100,000 \times g$  to remove any residual membrane fraction, which was discarded. The obtained soluble (periplasm) fraction was subjected to protein precipitation by adding 10% (w/v) trichloroacetic acid (TCA). TCA precipitates were solubilized in Laemmli Sample Buffer (Bio-Rad) prior to SDS-PAGE analysis. A similar procedure, with a cell resuspension buffer lacking sucrose, was used to lyse cells and obtain the membrane and soluble fractions.

The crude envelope fractions directly analysed by SDS-PAGE or used for native affinity purification of affinity tagged BAM complex or DolP were prepared from cells that were cultured in LB until early exponential phase and, where indicated, supplemented with 400  $\mu$ M IPTG for 1 or 2 hr (as reported in the figure legends) to induce ectopic protein expression. Cells were collected by centrifugation at  $6000 \times g$  at 4°C, resuspended in 20 mM Tris-HCl pH 8, and mechanically disrupted using a Cell Disruptor (Constant Systems LTD) set to 0.82 kPa. The obtained cell lysate fractions were clarified by centrifugation at  $6000 \times g$  and 4°C. The supernatant was then subjected to ultracentrifugation at  $100,000 \times g$  at 4°C to collect the envelope fraction.

### Protein heat-modifiability

Whole-cell lysates or the crude envelope fractions diluted in Laemmli Sample Buffer were incubated at different temperatures (as indicated in figures and figure legends) prior to analysis by SDS-PAGE and immunoblotting. For the analysis of BamA heat-modifiability, samples were incubated either at 25°C or at 99°C for 10 min and gel electrophoresis was conducted at 4°C.

### Isolation of native protein complexes by IgG- or nickel-affinity chromatography

The envelope fraction was resuspended at a concentration of approximately 10 mg/ml in solubilization buffer (20 mM Tris-HCl pH 7.4, 100 mM NaCl, 0.1 mM EDTA, 2 mM PMSF) supplemented with EDTA-free protease inhibitor cocktail (Roche), and 1.1% (w/v) of a mild detergent component corresponding to digitonin (Merck) and DDM (Merck) as indicated in figure legends. To facilitate extraction of membrane proteins, samples were subjected to mild agitation for 1 hr at 4°C. Insoluble material was removed by centrifugation at  $16,000 \times g$  at 4°C. To perform IgG affinity purification, membrane-extracted proteins were incubated for 1.5 hr at 4°C with purified human IgG (Sigma) that had been previously coupled with CNBr-activated Sepharose beads (GE Healthcare). After extensive washes of the resin with solubilization buffer containing 0.3% (w/v) digitonin and 0.03% (w/v) DDM, bound proteins were eluted by incubation with AcTEV protease (ThermoFisher) overnight at 4°C under mild agitation. To perform nickel (Ni)-affinity purification, membrane-extracted proteins were supplemented with 20 mM imidazole and incubated with Protino Ni-NTA agarose beads (Macherey-Nagel) for 1 hr at 4°C. After extensive washes of the resin with solubilization buffer supplemented with 50 mM imidazole, 0.3% (w/v) digitonin, 0.03% (w/v) DDM, and the EDTA-free protease inhibitor cocktail (Roche), bound proteins were eluted using the same buffer supplemented with 500 mM imidazole.

### In vitro reconstitution of the BAM–DolP interaction and BN-PAGE analysis

Envelope fractions were obtained from cells carrying pBAM<sup>His</sup> or pDolP<sup>His</sup> and cultured until early exponential phase in LB medium at 37°C and subsequently supplemented with 400  $\mu$ M IPTG for 1.5 hr to induce the expression of the BAM complex genes or *dolP*. The envelope fractions were solubilized and purified by Ni-affinity and size exclusion chromatography, adapting a previously published protocol. Briefly, after membrane solubilization with 50 mM Tris-HCl pH 8.0, 150 mM NaCl, and 1%

(w/v) DDM, and removal of insoluble material by ultracentrifugation at  $100,000 \times g$ ,  $4^{\circ}\text{C}$ , soluble proteins were loaded onto a Ni-column (HisTrap FF Crude, GE Healthcare) pre-equilibrated with 50 mM Tris-HCl pH 8.0, 150 mM NaCl, and 0.03% (w/v) DDM (equilibration buffer), using an ÄKTA Purifier 10 (GE Healthcare) at  $4^{\circ}\text{C}$ . The column containing bound proteins was washed with equilibration buffer supplemented with 50 mM imidazole. Proteins were eluted in equilibration buffer, applying a gradient of imidazole from 50 mM to 500 mM and further separated by gel filtration using an HiLoad 16/600 Superdex 200 (GE Healthcare) in equilibration buffer. Eluted proteins were concentrated using an ultrafiltration membrane with a 10 kDa molecular weight cutoff (Vivaspin 6, Sartorius). To reconstitute the BAM–DolP complex *in vitro*, equimolar concentrations of purified BAM and DolP were used. Purified proteins were mixed in equilibration buffer for 1 hr at  $4^{\circ}\text{C}$  or for 30 min at  $25^{\circ}\text{C}$  as indicated in figure legends. The reaction was further diluted 1:4 times in ice-cold blue native buffer (20 mM Tris-HCl pH 7.4, 50 mM NaCl, 0.1 mM EDTA, 1% [w/v] digitonin, 10% w/v glycerol) and ice cold blue native loading buffer (5% coomassie brilliant blue G-250, 100 mM Bis-Tris-HCl, pH 7.0, 500 mM 6-aminocaproic acid) prior to loading onto home-made 5–13% blue native polyacrylamide gradient gels. Resolved protein complexes were blotted onto a PVDF membrane and immunolabelled. Where non-relevant gel lanes were removed, a white space was used to separate contiguous parts of the same gel.

### Site-directed photo-crosslinking

Cells harbouring pEVOL-pBpF (*Chin et al., 2002*) and pBamA-DolP<sup>His</sup> or pDolP<sup>His</sup> with single amber codon substitutions in the *dolP* open reading frame were cultured in minimal media until early exponential phase, supplemented with 1 mM Bpa (Bachem) and 400  $\mu\text{M}$  IPTG for 1.5 hr. Cultures were divided into two equal parts, one left on ice and one subjected to UV irradiation for 10 min on ice, using a UV-A LED light source (Tritan 365 MHB, Spectroline). Harvested cells were mechanically disrupted to obtain the envelope fraction as described above. Envelope fractions were solubilized in 200 mM Tris-HCl, pH 8, 12% (w/v) glycerol, 4% (w/v) SDS, 15 mM EDTA, and 2 mM PMSF. After a clarifying spin, the supernatants were diluted 20-fold in RIPA buffer (50 mM Tris/HCl, pH 8, 150 mM NaCl, 1% [v/v] NP-40, 0.5% [w/v] sodium deoxycholate, 0.1% [w/v] SDS) supplemented with 20 mM imidazole and subjected to Ni-affinity chromatography. After extensive washing with RIPA buffer containing 50 mM imidazole, proteins were eluted with the same buffer containing 500 mM imidazole. Equal portions of the elution fractions were separated by SDS-PAGE and subjected to immunoblotting.

### Antibodies and western blotting

Proteins separated by SDS-PAGE or blue native-PAGE were transferred onto PVDF membranes (Merck). After blocking with skim milk, membranes were immunolabelled using epitope-specific rabbit polyclonal antisera, with the exception of RpoB that was labelled using a mouse monoclonal antibody (NeoClone Biotechnology). The  $F_1\beta$  subunit of the ATP  $F_1F_0$  synthase was detected using a rabbit polyclonal antiserum raised against an epitope of the homologous protein of *Saccharomyces cerevisiae* (Atp2). The secondary immunodecoration was conducted using anti-rabbit or anti-mouse antibodies conjugated to horseradish peroxidase produced in goat (Sigma). Protein signals were generated using a Clarity Western ECL blotting substrate (Bio-Rad) and detected using a LAS-4000 (Fujifilm) system. The signal intensities of protein bands were quantified using a Multi Gauge (Fujifilm) software.

### Mass spectrometry analyses

MALDI-TOF MS: Coomassie-stained bands of interest were excised from SDS-polyacrylamide gels and cut into pieces. Samples were washed twice with 100  $\mu\text{l}$  of 25 mM ammonium bicarbonate, 50% (v/v) acetonitrile for 10 min under agitation.

After drying, the gel pieces were rehydrated with 10  $\mu\text{l}$  of 10  $\mu\text{g}/\text{ml}$  modified trypsin (Promega) in 25 mM ammonium bicarbonate and digested overnight at  $37^{\circ}\text{C}$ . Acetonitrile was added to the digest to a final concentration of 10% (v/v). After 5 min sonication, 1  $\mu\text{l}$  of the extracted peptide mixture was spotted on the sample plate of the mass spectrometer with 1  $\mu\text{l}$  of the matrix solution (6 mg/ml of  $\alpha$ -cyano-4-hydroxycinnamic acid in 50% [v/v] acetonitrile and 0.1% [v/v] trifluoroacetic acid). The analysis was performed using a MALDI-TOF/TOF mass spectrometer (Voyager 5800,

Applied Biosystems/MDS, Sciex) in positive reflectron mode with the following parameters: accelerating voltage, 20 kV; grid voltage, 68%; extraction delay time, 200 ns; shoot number, 1000. Acquisition range was between 750 and 3000 *m/z*. Spectra were treated using the Data Explorer software (Applied Biosystems).

NanoLC-MS/MS: 70 µg of eluted proteins from each sample (+ UV or – UV) were digested with trypsin (Promega) using S-Trap Micro spin columns (Protifi) according to the manufacturer's instruction (*HaileMariam et al., 2018*). Digested peptide extracts were analysed by online nanoLC using an UltiMate 3000 RSLCnano LC system (ThermoScientific) coupled with an Orbitrap Fusion Tribrid mass spectrometer (Thermo Scientific) operating in positive mode. Five microliters of each sample (5 µg) were loaded onto a 300 µm ID × 5 mm PepMap C18 pre-column (Thermo Scientific) at 20 µl/min in 2% (v/v) acetonitrile, 0.05% (v/v) trifluoroacetic acid. After 3 min of desalting, peptides were online separated on a 75 µm ID × 50 cm C18 column (in-house packed with Reprosil C18-AQ Pur 3 µm resin, Dr. Maisch; Proxeon Biosystems) equilibrated in 90% buffer A (0.2% [v/v] formic acid), with a gradient of 10–30% buffer B (80% [v/v] acetonitrile, 0.2% [v/v] formic acid) for 100 min, then 30–45% for 20 min at 300 nl/min. The instrument was operated in data-dependent acquisition mode using a top-speed approach (cycle time of 3 s). Survey scans MS were acquired in the Orbitrap over 375–1800 *m/z* with a resolution of 120,000 (at 200 *m/z*), an automatic gain control (AGC) target of 4e5, and a maximum injection time (IT) of 50 ms. Most intense ions (2+ to 7+) were selected at 1.6 *m/z* with quadrupole and fragmented by Higher Energy Collisional Dissociation (HCD). The monoisotopic precursor selection was turned on, the intensity threshold for fragmentation was set to 25,000, and the normalized collision energy (NCE) was set to 30%. The resulting fragments were analysed in the Orbitrap with a resolution of 30,000 (at 200 *m/z*), an AGC target of 1e5, and a maximum IT of 100 ms. Dynamic exclusion was used within 30 s with a 10 ppm tolerance. The ion at 445.120025 *m/z* was used as lock mass. The dipeptides were searched manually in Xcalibur using ms2 reporter ions of the modified peptide (*m/z* 159.11; 187.11; 244.13) and MSMS spectra of the crosslinked peptides were annotated manually using GPMaw (*Peri et al., 2001*).

## Epifluorescence microscopy and analysis

Overnight cultures of *E. coli* BW25113 and its derivative strains were diluted into fresh M9 medium containing 0.2% glycerol or LB medium and grown at 30°C to OD<sub>600</sub> = 0.2–0.3. When indicated, cultures were supplemented with 400 µM of IPTG to induce ectopic expression of plasmid-borne genes for 1 hr prior to collecting samples for microscopy analysis. Culture volumes of 0.6 µl were deposited directly onto slides coated with 1% (w/v) agarose in a phosphate-buffered saline solution and visualized by epifluorescence microscopy. Cells were imaged at 30°C using an Eclipse TI-E/B Nikon wide field epifluorescence inverted microscope with a phase contrast objective (Plan APO LBDA 100X oil NA1.4 Phase) and a Semrock filter mCherry (Ex: 562BP24; DM: 593; Em: 641BP75) or FITC (Ex: 482BP35; DM: 506; Em: 536BP40). Images were acquired using a CDD OrcaR2 (Hamamatsu) camera with illumination at 100% from a HG Intensilight source and with an exposure time of 1–3 s, or using a Neo 5.5 sCMOS (Andor) camera with illumination at 60% from a LED SPECTRA X source (LumenCor) with an exposure time of 2 s. Nis-Elements AR software (Nikon) was used for image capture. Image analysis was conducted using the Fiji and ImageJ software. The fraction of cells with DoIP<sup>GFP</sup> signals at mid-cell sites was estimated using the Fiji Cell Counter plugin. Collective profiles of fluorescence distribution versus the relative position along the cell axis were generated using the Coli-Inspector macro run in ImageJ within the plugin ObjectJ (*Vischer et al., 2015*), selecting only cells with a constriction (80% of cell diameter) as qualified objects. Fluorescence intensities were normalized to the mid-cell intensity measured for a control reference strain harbouring the chromosomal *dolP-gfp* fusion.

## Acknowledgements

We thank Harris Bernstein (NIDDK/NIH, Bethesda, MD) for providing key reagents and for comments on the manuscript. We thank Tanneke den Blaauwen (University of Amsterdam) and Nathalie Dautin (IBPC/CNRS, Paris) for discussion. We thank the Light Imaging Toulouse CBI (LITC) platform for assistance with and maintenance of the microscopy instrumentation. We thank Odile Burlet-Schiltz (IPBS/CNRS, Toulouse) for support and access to the Toulouse Proteomics Infrastructure. Further financial support was provided by: the Fondation pour la Recherche Médicale to DR; the Chinese Scholarship

Council as part of a joint international PhD program with Toulouse University Paul Sabatier to YY; the French Ministry of Higher Education and Research to LO-T; the Ecole Normale Supérieure to FR; the European Research Council (Europe Union's Horizon 2020 research and innovation program, grant agreement No 677823), the French governmental Investissement d'Avenir program and the Laboratoire d'Excellence 'Integrative Biology of Emerging Infectious Diseases' (ANR-10-LABX-62-IBED) to DB; the Centre National de la Recherche Scientifique and the ATIP-Avenir program to RI.

## Additional information

### Funding

| Funder   | Grant reference number | Author             |
|--|------------------------|--------------------|
| Centre National de la Recherche Scientifique             | ATIP-Avenir            | Raffaele Ieva      |
| Agence Nationale de la Recherche                         | ANR-10-LABX-62-IBED    | David Bikard       |
| Fondation pour la Recherche Médicale                     | PostDoc Fellowship     | David Ranava       |
| European Research Council                                | 677823                 | David Bikard       |
| École Normale Supérieure                                 |                        | François Rousset   |
| Chinese Scholarship Council                              |                        | Yiyang Yang        |
| Ministère de l'Enseignement Supérieur et de la Recherche |                        | Luis Orenday-Tapia |

The funders had no role in study design, data collection and interpretation, or the decision to submit the work for publication.

### Author contributions

David Ranava, Conceptualization, Supervision, Validation, Investigation, Visualization, Methodology, Writing - review and editing; Yiyang Yang, Luis Orenday-Tapia, Conceptualization, Validation, Investigation, Visualization, Methodology, Writing - review and editing; François Rousset, Software, Formal analysis, Validation, Investigation, Writing - review and editing; Catherine Turlan, Methodology, Validation, Investigation, Writing - review and editing; Violette Morales, Supervision, Validation, Investigation, Methodology, Writing - review and editing; Lun Cui, Cyril Moulin, Carine Froment, Gladys Munoz, Investigation; Jérôme Rech, Investigation, Methodology; Julien Marcoux, Supervision, Validation, Methodology, Writing - review and editing; Anne Caumont-Sarcos, Methodology, Supervision, Validation, Investigation, Visualization, Writing - review and editing; Cécile Albenne, Conceptualization, Supervision, Investigation, Visualization, Writing - review and editing; David Bikard, Conceptualization, Software, Formal analysis, Supervision, Funding acquisition, Methodology, Writing - review and editing; Raffaele Ieva, Conceptualization, Supervision, Funding acquisition, Validation, Investigation, Methodology, Writing - original draft, Project administration, Writing - review and editing


### Author ORCIDs

David Ranava  <http://orcid.org/0000-0002-5841-7699>

Luis Orenday-Tapia  <https://orcid.org/0000-0002-1134-0823>

Julien Marcoux  <https://orcid.org/0000-0001-7321-7436>

David Bikard  <http://orcid.org/0000-0002-5729-1211>

Raffaele Ieva  <https://orcid.org/0000-0002-3405-0650>

### Decision letter and Author response

Decision letter <https://doi.org/10.7554/eLife.67817.sa1>

Author response <https://doi.org/10.7554/eLife.67817.sa2>

## Additional files

### Supplementary files

- Supplementary file 1. List of strains used in this study.
- Supplementary file 2. List of plasmids used in this study.
- Transparent reporting form

### Data availability

All data generated and analysed during this study are available in the manuscript and supporting files. Source data related to the CRISPRi screen are provided in the supporting files.

## References

- Ades SE. 2008. Regulation by destruction: design of the sigmaE envelope stress response. *Current Opinion in Microbiology* **11**:535–540. DOI: <https://doi.org/10.1016/j.mib.2008.10.004>, PMID: 18983936
- Alvira S, Watkins DW, Troman L, Allen WJ, Lorrinan JS, Degliesposti G, Cohen EJ, Beeby M, Daum B, Gold VA, Skehel JM, Collinson I. 2020. Inter-membrane association of the sec and BAM translocons for bacterial outer-membrane biogenesis. *eLife* **9**:e60669. DOI: <https://doi.org/10.7554/eLife.60669>, PMID: 33146611
- Ashburner M, Ball CA, Blake JA, Botstein D, Butler H, Cherry JM, Davis AP, Dolinski K, Dwight SS, Eppig JT, Harris MA, Hill DP, Issel-Tarver L, Kasarskis A, Lewis S, Matese JC, Richardson JE, Ringwald M, Rubin GM, Sherlock G. 2000. Gene ontology: tool for the unification of biology. The gene ontology consortium. *Nature Genetics* **25**:25–29. DOI: <https://doi.org/10.1038/75556>, PMID: 10802651
- Asmar AT, Collet J-F. 2018. Lpp, the braun lipoprotein, turns 50—major achievements and remaining issues. *FEMS Microbiology Letters* **365**:199. DOI: <https://doi.org/10.1093/femsle/fny199>
- Baba T, Ara T, Hasegawa M, Takai Y, Okumura Y, Baba M, Datsenko KA, Tomita M, Wanner BL, Mori H. 2006. Construction of *Escherichia coli* K-12 in-frame, single-gene knockout mutants: the keio collection. *Molecular Systems Biology* **2**:2006.0008. DOI: <https://doi.org/10.1038/msb4100050>, PMID: 16738554
- Bakelar J, Buchanan SK, Noinaj N. 2016. The structure of the  $\beta$ -barrel assembly machinery complex. *Science* **351**:180–186. DOI: <https://doi.org/10.1126/science.aad3460>, PMID: 26744406
- Bennion D, Charlson ES, Coon E, Misra R. 2010. Dissection of  $\beta$ -barrel outer membrane protein assembly pathways through characterizing BamA POTRA 1 mutants of *Escherichia coli*. *Molecular Microbiology* **77**:1153–1171. DOI: <https://doi.org/10.1111/j.1365-2958.2010.07280.x>, PMID: 20598079
- Blattner FR, Plunkett G, Bloch CA, Perna NT, Burland V, Riley M, Collado-Vides J, Glasner JD, Rode CK, Mayhew GF, Gregor J, Davis NW, Kirkpatrick HA, Goeden MA, Rose DJ, Mau B, Shao Y. 1997. The complete genome sequence of *Escherichia coli* K-12. *Science* **277**:1453–1462. DOI: <https://doi.org/10.1126/science.277.5331.1453>, PMID: 9278503
- Bos MP, Grijpstra J, Tommassen-van Boxtel R, Tommassen J. 2014. Involvement of *Neisseria meningitidis* lipoprotein GNA2091 in the assembly of a subset of outer membrane proteins. *Journal of Biological Chemistry* **289**:15602–15610. DOI: <https://doi.org/10.1074/jbc.M113.539510>, PMID: 24755216
- Bryant JA, Morris FC, Knowles TJ, Maderbocus R, Heinz E, Boelter G, Alodaini D, Colyer A, Wotherspoon PJ, Staunton KA, Jeeves M, Browning DF, Sevastyanovich YR, Wells TJ, Rossiter AE, Bavro VN, Sridhar P, Ward DG, Chong ZS, Goodall EC, et al. 2020. Structure of dual BON-domain protein DolP identifies phospholipid binding as a new mechanism for protein localisation. *eLife* **9**:e62614. DOI: <https://doi.org/10.7554/eLife.62614>, PMID: 33315009
- Calmettes C, Judd A, Moraes TF. 2015. Structural aspects of bacterial outer membrane protein assembly. *Advances in Experimental Medicine and Biology* **883**:255–270. DOI: [https://doi.org/10.1007/978-3-319-23603-2\\_14](https://doi.org/10.1007/978-3-319-23603-2_14), PMID: 26621472
- Calvo-Villamañán A, Ng JW, Planel R, Ménager H, Chen A, Cui L, Bikard D. 2020. On-target activity predictions enable improved CRISPR-dCas9 screens in Bacteria. *Nucleic Acids Research* **48**:e64. DOI: <https://doi.org/10.1093/nar/gkaa294>, PMID: 32352514
- Carlson ML, Stacey RG, Young JW, Wason IS, Zhao Z, Rattray DG, Scott N, Kerr CH, Babu M, Foster LJ, Duong Van Hoa F. 2019. Profiling the *Escherichia coli* membrane protein interactome captured in peptidic libraries. *eLife* **8**:e46615. DOI: <https://doi.org/10.7554/eLife.46615>, PMID: 31364989
- Cascales E, Bernadac A, Gavioli M, Lazzaroni JC, Lloubes R. 2002. Pal lipoprotein of *Escherichia coli* plays a major role in outer membrane integrity. *Journal of Bacteriology* **184**:754–759. DOI: <https://doi.org/10.1128/JB.184.3.754-759.2002>, PMID: 11790745
- Charlson ES, Werner JN, Misra R. 2006. Differential effects of yfgL mutation on *Escherichia coli* outer membrane proteins and lipopolysaccharide. *Journal of Bacteriology* **188**:7186–7194. DOI: <https://doi.org/10.1128/JB.00571-06>, PMID: 17015657
- Chin JW, Martin AB, King DS, Wang L, Schultz PG. 2002. Addition of a photocrosslinking amino acid to the genetic code of *Escherichia coli*. *PNAS* **99**:11020–11024. DOI: <https://doi.org/10.1073/pnas.172226299>, PMID: 12154230

- Chung HS**, Yao Z, Goehring NW, Kishony R, Beckwith J, Kahne D. 2009. Rapid beta-lactam-induced lysis requires successful assembly of the cell division machinery. *PNAS* **106**:21872–21877. DOI: <https://doi.org/10.1073/pnas.0911674106>, PMID: 19995973
- Crane JM**, Randall LL. 2017. The sec system: protein export in *Escherichia coli*. *EcoSal Plus* **7**:2017. DOI: <https://doi.org/10.1128/ecosalplus.ESP-0002-2017>
- Cui L**, Vigouroux A, Rousset F, Varet H, Khanna V, Bikard D. 2018. A CRISPRi screen in *E. coli* reveals sequence-specific toxicity of dCas9. *Nature Communications* **9**:1912. DOI: <https://doi.org/10.1038/s41467-018-04209-5>, PMID: 29765036
- Datsenko KA**, Wanner BL. 2000. One-step inactivation of chromosomal genes in *Escherichia coli* K-12 using PCR products. *PNAS* **97**:6640–6645. DOI: <https://doi.org/10.1073/pnas.120163297>, PMID: 10829079
- De Las Peñas A**, Connolly L, Gross CA. 1997a. SigmaE is an essential sigma factor in *Escherichia coli*. *Journal of Bacteriology* **179**:6862–6864. DOI: <https://doi.org/10.1128/JB.179.21.6862-6864.1997>, PMID: 9352942
- De Las Peñas A**, Connolly L, Gross CA. 1997b. The sigmaE-mediated response to extracytoplasmic stress in *Escherichia coli* is transduced by RseA and RseB, two negative regulators of sigmaE. *Molecular Microbiology* **24**:373–385. DOI: <https://doi.org/10.1046/j.1365-2958.1997.3611718.x>, PMID: 9159523
- Dekoninck K**, Létoquart J, Laguri C, Demange P, Bevernaegie R, Simorre JP, Dehu O, Iorga BI, Elias B, Cho SH, Collet JF. 2020. Defining the function of OmpA in the rcs stress response. *eLife* **9**:e60861. DOI: <https://doi.org/10.7554/eLife.60861>, PMID: 32985973
- den Blaauwen T**, Hamoen LW, Levin PA. 2017. The divisome at 25: the road ahead. *Current Opinion in Microbiology* **36**:85–94. DOI: <https://doi.org/10.1016/j.mib.2017.01.007>, PMID: 28254403
- Doerner PA**, Sousa MC. 2017. Extreme dynamics in the BamA  $\beta$ -Barrel seam. *Biochemistry* **56**:3142–3149. DOI: <https://doi.org/10.1021/acs.biochem.7b00281>, PMID: 28569500
- Doyle MT**, Bernstein HD. 2019. Bacterial outer membrane proteins assemble via asymmetric interactions with the BamA  $\beta$ -barrel. *Nature Communications* **10**:3358. DOI: <https://doi.org/10.1038/s41467-019-11230-9>, PMID: 31350400
- Egan AJF**, Errington J, Vollmer W. 2020. Regulation of peptidoglycan synthesis and remodelling. *Nature Reviews Microbiology* **18**:446–460. DOI: <https://doi.org/10.1038/s41579-020-0366-3>, PMID: 32424210
- Fleming KG**. 2015. A combined kinetic push and thermodynamic pull as driving forces for outer membrane protein sorting and folding in Bacteria. *Philosophical Transactions of the Royal Society B: Biological Sciences* **370**:20150026. DOI: <https://doi.org/10.1098/rstb.2015.0026>, PMID: 26370938
- Fleming PJ**, Patel DS, Wu EL, Qi Y, Yeom MS, Sousa MC, Fleming KG, Im W. 2016. BamA POTRA domain interacts with a native lipid membrane surface. *Biophysical Journal* **110**:2698–2709. DOI: <https://doi.org/10.1016/j.bpj.2016.05.010>, PMID: 27332128
- Gogol EB**, Rhodius VA, Papenfort K, Vogel J, Gross CA. 2011. Small RNAs endow a transcriptional activator with essential repressor functions for single-tier control of a global stress regulon. *PNAS* **108**:12875–12880. DOI: <https://doi.org/10.1073/pnas.1109379108>, PMID: 21768388
- Grenier F**, Matteau D, Baby V, Rodrigue S. 2014. Complete genome sequence of *Escherichia coli* BW25113. *Genome Announcements* **2**:e01038-14. DOI: <https://doi.org/10.1128/genomeA.01038-14>, PMID: 25323716
- Gu Y**, Li H, Dong H, Zeng Y, Zhang Z, Paterson NG, Stansfeld PJ, Wang Z, Zhang Y, Wang W, Dong C. 2016. Structural basis of outer membrane protein insertion by the BAM complex. *Nature* **531**:64–69. DOI: <https://doi.org/10.1038/nature17199>, PMID: 26901871
- Guillier M**, Gottesman S, Storz G. 2006. Modulating the outer membrane with small RNAs. *Genes & Development* **20**:2338–2348. DOI: <https://doi.org/10.1101/gad.1457506>, PMID: 16951250
- Gunasinghe SD**, Shiota T, Stubenrauch CJ, Schulze KE, Webb CT, Fulcher AJ, Dunstan RA, Hay ID, Naderer T, Whelan DR, Bell TDM, Elgass KD, Strugnell RA, Lithgow T. 2018. The WD40 protein BamB mediates coupling of BAM complexes into assembly precincts in the bacterial outer membrane. *Cell Reports* **23**:2782–2794. DOI: <https://doi.org/10.1016/j.celrep.2018.04.093>, PMID: 29847806
- Guo MS**, Updegrove TB, Gogol EB, Shabalina SA, Gross CA, Storz G. 2014. MicL, a new  $\sigma$ E-dependent sRNA, combats envelope stress by repressing synthesis of lpp, the major outer membrane lipoprotein. *Genes & Development* **28**:1620–1634. DOI: <https://doi.org/10.1101/gad.243485.114>, PMID: 25030700
- HaileMariam M**, Eguez RV, Singh H, Bekele S, Ameni G, Pieper R, Yu Y. 2018. S-Trap, an ultrafast Sample-Preparation approach for shotgun proteomics. *Journal of Proteome Research* **17**:2917–2924. DOI: <https://doi.org/10.1021/acs.jproteome.8b00505>, PMID: 30114372
- Hale CA**, de Boer PA. 1997. Direct binding of FtsZ to ZipA, an essential component of the septal ring structure that mediates cell division in *E. coli*. *Cell* **88**:175–185. DOI: [https://doi.org/10.1016/S0092-8674\(00\)81838-3](https://doi.org/10.1016/S0092-8674(00)81838-3), PMID: 9008158
- Hartmann JB**, Zahn M, Burmann IM, Bibow S, Hiller S. 2018. Sequence-Specific solution NMR assignments of the  $\beta$ -Barrel insertase BamA to monitor its conformational ensemble at the atomic level. *Journal of the American Chemical Society* **140**:11252–11260. DOI: <https://doi.org/10.1021/jacs.8b03220>, PMID: 30125090
- Heidrich C**, Templin MF, Ursinus A, Merdanovic M, Berger J, Schwarz H, de Pedro MA, Höltje JV. 2001. Involvement of N-acetylmuramyl-L-alanine amidases in cell separation and antibiotic-induced autolysis of *Escherichia coli*. *Molecular Microbiology* **41**:167–178. DOI: <https://doi.org/10.1046/j.1365-2958.2001.02499.x>, PMID: 11454209
- Horne JE**, Brockwell DJ, Radford SE. 2020. Role of the lipid bilayer in outer membrane protein folding in Gram-negative Bacteria. *Journal of Biological Chemistry* **295**:10340–10367. DOI: <https://doi.org/10.1074/jbc.REV120.011473>, PMID: 32499369



- Hussain S**, Bernstein HD. 2018. The bam complex catalyzes efficient insertion of bacterial outer membrane proteins into membrane vesicles of variable lipid composition. *Journal of Biological Chemistry* **293**:2959–2973. DOI: <https://doi.org/10.1074/jbc.RA117.000349>, PMID: 29311257
- Iadanza MG**, Higgins AJ, Schiffrin B, Calabrese AN, Brockwell DJ, Ashcroft AE, Radford SE, Ranson NA. 2016. Lateral opening in the intact  $\beta$ -barrel assembly machinery captured by cryo-EM. *Nature Communications* **7**: 12865. DOI: <https://doi.org/10.1038/ncomms12865>, PMID: 27686148
- Iadanza MG**, Schiffrin B, White P, Watson MA, Horne JE, Higgins AJ, Calabrese AN, Brockwell DJ, Tuma R, Kalli AC, Radford SE, Ranson NA. 2020. Distortion of the bilayer and dynamics of the BAM complex in lipid nanodiscs. *Communications Biology* **3**:766. DOI: <https://doi.org/10.1038/s42003-020-01419-w>, PMID: 33318620
- Ishida H**, Garcia-Herrero A, Vogel HJ. 2014. The periplasmic domain of *Escherichia coli* outer membrane protein A can undergo a localized temperature dependent structural transition. *Biochimica Et Biophysica Acta (BBA) - Biomembranes* **1838**:3014–3024. DOI: <https://doi.org/10.1016/j.bbamem.2014.08.008>, PMID: 25135663
- Jaroslowski S**, Duquesne K, Sturgis JN, Scheuring S. 2009. High-resolution architecture of the outer membrane of the Gram-negative Bacteria *roseobacter denitrificans*. *Molecular Microbiology* **74**:1211–1222. DOI: <https://doi.org/10.1111/j.1365-2958.2009.06926.x>, PMID: 19843216
- Kim S**, Malinverni JC, Sliz P, Silhavy TJ, Harrison SC, Kahne D. 2007. Structure and function of an essential component of the outer membrane protein assembly machine. *Science* **317**:961–964. DOI: <https://doi.org/10.1126/science.1143993>, PMID: 17702946
- Knop M**, Siegers K, Pereira G, Zachariae W, Winsor B, Nasmyth K, Schiebel E. 1999. Epitope tagging of yeast genes using a PCR-based strategy: more tags and improved practical routines. *Yeast* **15**:963–972. DOI: [https://doi.org/10.1002/\(SICI\)1097-0061\(199907\)15:10B<963::AID-YEA399>3.0.CO;2-W](https://doi.org/10.1002/(SICI)1097-0061(199907)15:10B<963::AID-YEA399>3.0.CO;2-W)
- Knowles TJ**, Browning DF, Jeeves M, Maderbocus R, Rajesh S, Sridhar P, Manoli E, Emery D, Sommer U, Spencer A, Leyton DL, Squire D, Chaudhuri RR, Viant MR, Cunningham AF, Henderson IR, Overduin M. 2011. Structure and function of BamE within the outer membrane and the  $\beta$ -barrel assembly machine. *EMBO Reports* **12**:123–128. DOI: <https://doi.org/10.1038/embor.2010.202>, PMID: 21212804
- Lessen HJ**, Fleming PJ, Fleming KG, Sodt AJ. 2018. Building blocks of the outer membrane: calculating a general elastic energy model for  $\beta$ -Barrel membrane proteins. *Journal of Chemical Theory and Computation* **14**:4487–4497. DOI: <https://doi.org/10.1021/acs.jctc.8b00377>, PMID: 29979594
- Li GW**, Burkhardt D, Gross C, Weissman JS. 2014. Quantifying absolute protein synthesis rates reveals principles underlying allocation of cellular resources. *Cell* **157**:624–635. DOI: <https://doi.org/10.1016/j.cell.2014.02.033>, PMID: 24766808
- Malinverni JC**, Werner J, Kim S, Sklar JG, Kahne D, Misra R, Silhavy TJ. 2006. YfiO stabilizes the YaeT complex and is essential for outer membrane protein assembly in *Escherichia coli*. *Molecular Microbiology* **61**:151–164. DOI: <https://doi.org/10.1111/j.1365-2958.2006.05211.x>, PMID: 16824102
- McLeay RC**, Bailey TL. 2010. Motif enrichment analysis: a unified framework and an evaluation on ChIP data. *BMC Bioinformatics* **11**:165. DOI: <https://doi.org/10.1186/1471-2105-11-165>, PMID: 20356413
- Missiakas D**, Mayer MP, Lemaire M, Georgopoulos C, Raina S. 1997. Modulation of the *Escherichia coli* sigmaE (RpoE) heat-shock transcription-factor activity by the RseA, RseB and RseC proteins. *Molecular Microbiology* **24**:355–371. DOI: <https://doi.org/10.1046/j.1365-2958.1997.3601713.x>, PMID: 9159522
- Morris FC**, Wells TJ, Bryant JA, Schager AE, Sevastyanovich YR, Squire DJP, Marshall J, Isom GL, Rooke J, Maderbocus R, Knowles TJ, Overduin M, Rossiter AE, Cunningham AF, Henderson IR. 2018. YraP contributes to cell envelope integrity and virulence of *Salmonella enterica* Serovar Typhimurium. *Infection and Immunity* **86**: e00829-17. DOI: <https://doi.org/10.1128/IAI.00829-17>, PMID: 30201701
- Nakamura K**, Mizushima S. 1976. Effects of heating in dodecyl sulfate solution on the conformation and electrophoretic mobility of isolated major outer membrane proteins from *Escherichia coli* K-12. *The Journal of Biochemistry* **80**:1411–1422. DOI: <https://doi.org/10.1093/oxfordjournals.jbchem.a131414>, PMID: 828162
- Narita S**, Masui C, Suzuki T, Dohmae N, Akiyama Y. 2013. Protease homolog BepA (YfgC) promotes assembly and degradation of  $\beta$ -barrel membrane proteins in *Escherichia coli*. *PNAS* **110**:E3612–E3621. DOI: <https://doi.org/10.1073/pnas.1312012110>, PMID: 24003122
- Nicoloff H**, Gopalkrishnan S, Ades SE. 2017. Appropriate regulation of the  $\sigma^E$ -Dependent Envelope Stress Response Is Necessary To Maintain Cell Envelope integrity and Stationary-Phase survival in *Escherichia coli*. *Journal of Bacteriology* **199**:e00089-17. DOI: <https://doi.org/10.1128/JB.00089-17>, PMID: 28373273
- Nikaido H**. 2003. Molecular basis of bacterial outer membrane permeability revisited. *Microbiology and Molecular Biology Reviews* **67**:593–656. DOI: <https://doi.org/10.1128/MMBR.67.4.593-656.2003>, PMID: 14665678
- Noinaj N**, Kuszak AJ, Gumbart JC, Lukacik P, Chang H, Easley NC, Lithgow T, Buchanan SK. 2013. Structural insight into the biogenesis of  $\beta$ -barrel membrane proteins. *Nature* **501**:385–390. DOI: <https://doi.org/10.1038/nature12521>, PMID: 23995689
- Onufryk C**, Crouch ML, Fang FC, Gross CA. 2005. Characterization of six lipoproteins in the sigmaE regulon. *Journal of Bacteriology* **187**:4552–4561. DOI: <https://doi.org/10.1128/JB.187.13.4552-4561.2005>, PMID: 15968066
- Peri S**, Steen H, Pandey A. 2001. GPMW—a software tool for analyzing proteins and peptides. *Trends in Biochemical Sciences* **26**:687–689. DOI: [https://doi.org/10.1016/S0968-0004\(01\)01954-5](https://doi.org/10.1016/S0968-0004(01)01954-5), PMID: 11701329
- Pichoff S**, Du S, Lutkenhaus J. 2019. Roles of FtsEX in cell division. *Research in Microbiology* **170**:374–380. DOI: <https://doi.org/10.1016/j.resmic.2019.07.003>, PMID: 31376483

- Ranava D**, Caumont-Sarcos A, Albenne C, Ieva R. 2018. Bacterial machineries for the assembly of membrane-embedded  $\beta$ -barrel proteins. *FEMS Microbiology Letters* **365**:087. DOI: <https://doi.org/10.1093/femsle/fny087>
- Rassam P**, Copeland NA, Birkholz O, Tóth C, Chavent M, Duncan AL, Cross SJ, Housden NG, Kaminska R, Seger U, Quinn DM, Garrod TJ, Sansom MS, Piehler J, Baumann CG, Kleantous C. 2015. Supramolecular assemblies underpin turnover of outer membrane proteins in Bacteria. *Nature* **523**:333–336. DOI: <https://doi.org/10.1038/nature14461>, PMID: 26061769
- Rhodium VA**, Suh WC, Nonaka G, West J, Gross CA. 2006. Conserved and variable functions of the sigmaE stress response in related genomes. *PLOS Biology* **4**:e2. DOI: <https://doi.org/10.1371/journal.pbio.0040002>, PMID: 16336047
- Rizzitello AE**, Harper JR, Silhavy TJ. 2001. Genetic evidence for parallel pathways of chaperone activity in the periplasm of *Escherichia coli*. *Journal of Bacteriology* **183**:6794–6800. DOI: <https://doi.org/10.1128/JB.183.23.6794-6800.2001>, PMID: 11698367
- Roman-Hernandez G**, Peterson JH, Bernstein HD. 2014. Reconstitution of bacterial autotransporter assembly using purified components. *eLife* **3**:e04234. DOI: <https://doi.org/10.7554/eLife.04234>, PMID: 25182416
- Rouvière PE**, Gross CA. 1996. SurA, a periplasmic protein with peptidyl-prolyl isomerase activity, participates in the assembly of outer membrane porins. *Genes & Development* **10**:3170–3182. DOI: <https://doi.org/10.1101/gad.10.24.3170>, PMID: 8985185
- Schiffirin B**, Brockwell DJ, Radford SE. 2017. Outer membrane protein folding from an energy landscape perspective. *BMC Biology* **15**:123. DOI: <https://doi.org/10.1186/s12915-017-0464-5>, PMID: 29268734
- Seib KL**, Haag AF, Oriente F, Fantappiè L, Borghi S, Semchenko EA, Schulz BL, Ferlicca F, Taddei AR, Giuliani MM, Pizza M, Delany I. 2019. The meningococcal vaccine antigen GNA2091 is an analogue of YraP and plays key roles in outer membrane stability and virulence. *The FASEB Journal* **33**:12324–12335. DOI: <https://doi.org/10.1096/fj.201900669R>, PMID: 31442078
- Sinnige T**, Weingarth M, Renault M, Baker L, Tommassen J, Baldus M. 2014. Solid-state NMR studies of full-length BamA in lipid bilayers suggest limited overall POTRA mobility. *Journal of Molecular Biology* **426**:2009–2021. DOI: <https://doi.org/10.1016/j.jmb.2014.02.007>, PMID: 24530687
- Sklar JG**, Wu T, Gronenberg LS, Malinverni JC, Kahne D, Silhavy TJ. 2007. Lipoprotein SmpA is a component of the YaeT complex that assembles outer membrane proteins in *Escherichia coli*. *PNAS* **104**:6400–6405. DOI: <https://doi.org/10.1073/pnas.0701579104>, PMID: 17404237
- Stegmeier JF**, Andersen C. 2006. Characterization of pores formed by YaeT (Omp85) from *Escherichia coli*. *The Journal of Biochemistry* **140**:275–283. DOI: <https://doi.org/10.1093/jb/mvj147>, PMID: 16829683
- Tomasek D**, Rawson S, Lee J, Wzorek JS, Harrison SC, Li Z, Kahne D. 2020. Structure of a nascent membrane protein as it folds on the BAM complex. *Nature* **583**:473–478. DOI: <https://doi.org/10.1038/s41586-020-2370-1>, PMID: 32528179
- Tsang MJ**, Yakhnina AA, Bernhardt TG. 2017. NlpD links cell wall remodeling and outer membrane invagination during cytokinesis in *Escherichia coli*. *PLOS Genetics* **13**:e1006888. DOI: <https://doi.org/10.1371/journal.pgen.1006888>, PMID: 28708841
- Uehara T**, Dinh T, Bernhardt TG. 2009. LytM-domain factors are required for daughter cell separation and rapid ampicillin-induced lysis in *Escherichia coli*. *Journal of Bacteriology* **191**:5094–5107. DOI: <https://doi.org/10.1128/JB.00505-09>, PMID: 19525345
- Uehara T**, Parzych KR, Dinh T, Bernhardt TG. 2010. Daughter cell separation is controlled by cytokinetic ring-activated cell wall hydrolysis. *The EMBO Journal* **29**:1412–1422. DOI: <https://doi.org/10.1038/emboj.2010.36>
- Vertommen D**, Ruiz N, Leverrier P, Silhavy TJ, Collet JF. 2009. Characterization of the role of the *Escherichia coli* periplasmic chaperone SurA using differential proteomics. *Proteomics* **9**:2432–2443. DOI: <https://doi.org/10.1002/pmic.200800794>, PMID: 19343722
- Vischer NO**, Verheul J, Postma M, van den Berg van Saparoea B, Galli E, Natale P, Gerdes K, Luirink J, Vollmer W, Vicente M, den Blaauwen T. 2015. Cell age dependent concentration of *Escherichia coli* divisome proteins analyzed with ImageJ and ObjectJ. *Frontiers in Microbiology* **6**:586. DOI: <https://doi.org/10.3389/fmicb.2015.00586>, PMID: 26124755
- Walsh NP**, Alba BM, Bose B, Gross CA, Sauer RT. 2003. OMP peptide signals initiate the envelope-stress response by activating DegS protease via relief of inhibition mediated by its PDZ domain. *Cell* **113**:61–71. DOI: [https://doi.org/10.1016/S0092-8674\(03\)00203-4](https://doi.org/10.1016/S0092-8674(03)00203-4), PMID: 12679035
- Wu T**, Malinverni J, Ruiz N, Kim S, Silhavy TJ, Kahne D. 2005. Identification of a multicomponent complex required for outer membrane biogenesis in *Escherichia coli*. *Cell* **121**:235–245. DOI: <https://doi.org/10.1016/j.cell.2005.02.015>, PMID: 15851030
- Yan Z**, Hussain S, Wang X, Bernstein HD, Bardwell JCA. 2019. Chaperone OsmY facilitates the biogenesis of a major family of autotransporters. *Molecular Microbiology* **112**:1373–1387. DOI: <https://doi.org/10.1111/mmi.14358>, PMID: 31369167
- Yang DC**, Peters NT, Parzych KR, Uehara T, Markovski M, Bernhardt TG. 2011. An ATP-binding cassette transporter-like complex governs cell-wall hydrolysis at the bacterial cytokinetic ring. *PNAS* **108**:E1052–E1060. DOI: <https://doi.org/10.1073/pnas.1107780108>, PMID: 22006326
- Yeats C**, Bateman A. 2003. The BON domain: a putative membrane-binding domain. *Trends in Biochemical Sciences* **28**:352–355. DOI: [https://doi.org/10.1016/S0968-0004\(03\)00115-4](https://doi.org/10.1016/S0968-0004(03)00115-4), PMID: 12878000